

33rd International Gemmological Conference IGC

October 2013
Hanoi, Vietnam

33rd International Gemmological Conference IGC

October, 2013

Hanoi, Vietnam

Distinguished Participants of the 33rd IGC Conference in Hanoi, Vietnam

On behalf of Vietnam National University, Hanoi (VNU), I am pleased to extend my warmest welcome to all of you to the 33rd International Gemmological Conference (IGC).

Following the great success of the 32nd IGC which was co-organized by Swiss Gemmological Institute (SSEF) in 2011, VNU is honored to cooperate with DOJI Gold & Gems Group to host this year's conference in the thousand-year-old capital city of Hanoi in its most beautiful season.

As you may know, Vietnam is endowed with a diversity of gem minerals thanks to its geologic position along the margins of two cratons. However, Vietnam's mining and pearl farming sectors are still relatively small and undeveloped, leaving many potential resources unexploited. While being the leading university in Vietnam with an important role in scientific development, VNU finds this both an opportunity and responsibility in promoting the studies on gemmology, contributing to develop this potential industry of the country. Besides, we also need the practical experiences and support from other countries around the world, especially those with developed gemstone industries and research. For those reasons, we find the great necessity to hold this important event in Vietnam.

Aiming at going to the heart of all matters relating to gemstones and endeavoring to exchange every knowledge and experience in gemmology, this year's conference will bring together the leading scientists, researchers, practitioners, managers and elite businessmen from around the world. I expect that you can gain lots of gemological inputs for your own gemological research and work as well as unforgettable experiences during your time in Vietnam.

On behalf of my co-chairman, Dr. Do Minh Phu – President of DOJI Gold & Gems Group, I wish you a memorable and enriching conference.

August 2013

Phung Xuan Nha, Prof. Dr
President of Vietnam National University, Hanoi

About the organising Committee for the 33rd IGC Conference:

International Organisers

Phung Xuan Nha, Vietnam National University, Hanoi: Chairman
 Do Minh Phu, DOJI Gold & Gems Group: Co-chairman
 Nguyen Ngoc Khoi, Vietnam National University, Hanoi; and DOJI Gold & Gems Group
 Le Thi Thu Huong, Vietnam National University, Hanoi
 Michael S. Krzemnicki, Swiss Gemmological Institute SSEF
 Laurent E. Cartier, Swiss Gemmological Institute SSEF
 Jayshree Panjekar, Panjekar Gem Research & Tech Institute
 IGC Executive Committee

Local Organisers

Nguyen Huu Duc, Vietnam National University, Hanoi: Chairman
 Do Vu Phuong Anh, DOJI Gold & Gems Group: Co-chairlady
 Le Thi Thu Huong, Vietnam National University, Hanoi
 Nguyen Ngoc Khoi, Vietnam National University, Hanoi; and DOJI Gold & Gems Group
 Duong Anh Tuan, DOJI Gold & Gems Group
 Bui Duy Cam, Vietnam National University, Hanoi
 Nguyen Anh Thu, Vietnam National University, Hanoi
 Dinh Van Huong, Vietnam National University, Hanoi
 Nguyen Van Vuong, Vietnam National University, Hanoi
 Nguyen Thanh Quang, DOJI Gold & Gems Group

Local planning & Social programme

Le Thi Thu Huong, Vietnam National University, Hanoi
 Do Vu Phuong Anh, DOJI Gold & Gems Group

Abstract Review Board

Urich Henn, German Gemmological Institute
 Hanco Zwaan, Netherland Gemmological Institute
 Emmanuel Fritsch, University of Nantes

Layout & Editing & Website

Laurent Cartier, Swiss Gemmological Institute SSEF

Special thanks to

- IGC Executive Boards for giving us the opportunity to hold the conference
- Abstract review board for their tremendous work finalizing and reviewing the abstracts.
- Michael Krzemnicki, SSEF for his advices and Laurent Cartier, SSEF, Le Thi Thu Huong, VNU for layout and editing the website and Conference proceedings.

August 2013, Phung Xuan Nha

About the IGC Executive Board



Photo of the IGC Executive Board, taken in July 2011 in Interlaken (Switzerland):

(From left to right) John Koivula, Hanco Zwaan, Emmanuel Fritsch, Gamini Zoysa, Henry A. Hänni, Jayshree Panjekar, Tay Thye Sun, John Saul, George Bosshart (†), Michael S. Krzemnicki. Long-standing Board members Dr. Jan Kanis, Mr. Alan Jobbins are also on this picture.

Pre-conference excursion: 10-12 October 2013. Hanoi – Halong Bay – Catba archipelago – Hanoi

Conference: 12-16 October 2013. Hanoi, Vietnam.

Post-conference excursion: 17-19 October 2013. Gem Mining Areas in Yen Bai Province

Guest programme: 12-16 October 2013. Hanoi, Vietnam

About the venue

Hanoi

Hanoi is the crowded capital city of Vietnam. The site where Hanoi stands today has been inhabited since the Neolithic period. Emperor Ly Thai To moved his capital here in AD1010 naming it Thang Long meaning Soaring Dragon. Spectacular celebrations in honour of the 1000th birthday of the city had taken place 2010.

The elegant heart of Hanoi is centred on the Hoan Kiem lake. Just north to this lake is the Old Quarter which is characterised by narrow streets.

Participants visiting Hanoi may discover Vietnam not only in its modern life but also its past.



Hoan Kiem lake is the most centred and one of the major scenic spots of Hanoi and serves as a focal point for its public life.

The Conference Venue

The Conference is held at the Lake Side hotel. We choose Lake Side hotel to host the conference because it is a beautiful and peaceful hotel beside the romantic sight of Giang Vo lake. The location is convenient not only for visitor but also for transportation. With 02 high standard restaurant system (Royal Vietnamese restaurant & Azuma Japanese restaurant), peaceful space, beside serving coffee during coffee breaks the hotel will offer lunch during lunch breaks.



About the Sponsors

Vietnam National University, Hanoi

Vietnam National University, Hanoi (VNU) is the first modern university ever establish in the country and one of the two national universities in Vietnam. VNU has undergone various stage of development: the University of Indochina established on 16 May 1906; Vietnam National University (November, 1945); the University of Hanoi (June, 1956). In December 1993, VNU was reorganized on the basis of amalgamating the University of Hanoi and other leading universities in Hanoi.

VNU holds a special position in Vietnam's higher education system, operating according to special regulation promulgated by the Prime Minister. VNU has its Headquarter at Xuan Thuy street, 3 old campuses inside Hanoi centre and a new one which is 30 km far from the centre of Hanoi.



Hoa Lac – the new campus with an area of 1000 hectares in Thach That district which is 40 km far from the centre of Hanoi



One of old campuses of VNU inside Hanoi old town – Le Thanh Tong campus



DOJI Gold and Gems Group

Originally known as TTD Technology and Trading Development Company, DOJI Gold & Gems Group has spectacularly expanded its business not only in Gold & Gems mining, Gems cutting & processing, Jewelry manufacturing, Gold bar trade, Gold import & export and Jewelry boutiques & shops nationwide network, Invest in service industry, real estate, banking and finance. Up to now, DOJI Gold & Gems Group has owned six member subsidiaries, five association companies and twelve branches. DOJI Group established its own DOJI Institute & Laboratory For Gemology And Jewelry (DOJILAB) reputed in Vietnam. DOJILAB has been equipped with the latest advanced analytical and testing instruments. Besides its qualified gemologists, DOJILAB is also collaborated with the top grading labs and scientists from national and international universities and institutes.

As the only Vietnamese representative of the International Colored Gemstone Association (ICA) and being honored as “the King of Star Ruby” for its Vietnam Star Ruby (VSR), DOJI Gold & Gems Group has launched its distinguished products to international markets such as Japan, Thailand, India, Hong Kong and Taiwan. DOJI Gold & Gems Group has remarkably contributed to pinpoint Vietnam on the gemstone world map.

The Group is proud to be the owner of the most precious stones exploited in Vietnamese mines, namely Dai Lam Ngoc – a 15-ton giant blue sapphire, Bao Hong Ngoc – the most precious natural rough Star Ruby of 18.88 kg and notably the Emperor Star Ruby well known in Vietnam and the world.

DOJI Gold & Gems Group has been strongly developed to reach the goal of becoming a leading Group in Vietnam and further, a prestigious brand in the world.

IGC 2013 Programme

Interlaken, Switzerland 12-16 October 2013

Saturday 12 October

- 18.00-20.30 IGC Welcome reception in Hanoi at the Lake Side Hotel
- 20.30-22.00 Executive Committee (EXCO) reunion

Sunday 13 October

- 9.00-9.15 Opening Ceremony and Announcements
- 9.15-9.30 Greeting speech by VNU president
- 9.30-9.45 Greeting speech by DOJl president
- 9.45-10.00 Speech from IGC EXCO
- 10.00-10.15 Conference photo
- 10.15-10.30 Coffee Break

Corundums (Chairman Emmanuel Fritsch)

- 10.30-10.50 J.C. (Hanco) Zwaan, Eric Buter, Robert E. Kane: Mineral inclusions in alluvial sapphires from Montana - an update
- 10.50-11.10 M.A. Viktorov, A. D. Semina, M. I. Pshenichny: Sapphires from Koltashi deposits (Ural Mountains, Russia)
- 11.10-11.30 Dietmar Schwarz, Stefanos Karampelas, Lu Taijin, Claudio C. Milisenda: Kenya, Tanzania: ruby and sapphire – an update/review
- 11.30-11.50 Nguyen Ngoc Khoi, Christoph A. Hauzenberger, Chakkaphan Sutthirat, Duong Anh Tuan, Nguyen Thi Minh Thuyet, Nguyen Thuy Duong, Nguyen Van Nam, Chu Van Lam: The characteristics of gneiss-hosted corundum deposits of Tan Huong-Truc Lau area, Northern Vietnam

- 11.50-12.10 Pornsawat Wathanakul, Prayath Nantasin, Kachane Kraisittipong, Prakarn Buenkoontod, Marute Lekkean: New deposit style concept and characteristics of gem corundum, Phrae Province, Northern Thailand
- 12.10-13.30 Lunch (Lake Side hotel: Azuma Japanese Restaurant)
- Diamonds (Chairman Michael Krzemnicki)**
- 13.30-13.50 Emmanuel Fritsch, Aurélien Delaunay, Benjamin Rondeau, Ichiro Sunagawa, Moreton Moore, Thomas Hainschwang: The morphology of natural and synthetic diamonds: Remaining challenges
- 13.50-14.10 Thomas Hainschwang, Emmanuel Fritsch, Franck Notari, Benjamin Rondeau, Andrey Katrusha: The origin of colour and correlated properties of natural type Ib diamonds
- 14.10-14.30 Hiroshi Kitawaki, Mio Hisanaga, Masahiro Yamamoto: Identification of gem diamonds using high-energy UV luminescence imaging
- 14.30-14.50 James E. Shigley: Observations on CVD-grown synthetic diamonds
- 15.00 Meeting point at Lake Side hotel lobby to go on bus to visit Ruby Plaza (DOJI)
- 15.30-18.30 Ruby Plaza tour, Gems show and Auction
- 18.30-21.00 GALA DINNER (Invited by VNU and DOJI presidents)
- 21.00 Meeting point at Ruby Plaza lobby to go on bus back to Lake Side hotel

Monday 14 October

Corundums/Pearls

- 8.00-8.45 EXCO reunion

Corundum (Chairman Karl Schmetzer)

- 9.00-9.20 Jayshree Panjekar, Aatish Panjekar: Yellow blue bicoloured sapphires from Chinnadharapuram, South India
- 9.20-9.40 Hpone-Phyo Kan-Nyunt, Lore Kiefert, Stefanos Karampelas: Characteristics of sapphires from the Kyat Pyin area, West Mogok, Burma (Myanmar)
- 9.40-10.00 Shane McClure: The potential for Co-diffusion in sapphire

- 10.00-10.20 Kentaro Emori, Hiroshi Kitawaki, Makoto Okano: The present situation of Beryllium diffusion corundum
- 10.20-10.40 Coffee Break
- 10.40-11.00 Y. Shelementiev, R. Serov, E. Altunina, M. Pshenichnyy: Alteration of the mineral inclusions behavior in corundum during heat treatment process
- 11.00-11.20 Hai An Nguyen Bui, Emmanuel Fritsch, Franck Notari, Alexandre Droux, Aurélien Delaunay, Benjamin Rondeau: Kashmir sapphires: geographical origin determination of top-quality blue sapphires versus science

Pearls (Chairman Henry Hänni)

- 11.20-11.40 Shigeru Akamatsu: Cultured pearl – Present situation and future prospect
- 11.40-12.00 Terrence S. Coldham: Observations of natural pearls within freshly opened *Pinctada maculata* from Tongavera atoll, Cook Islands
- 12.00-13.30 Lunch (Lake Side hotel: Royal Restaurant)
- 13.30-13.50 Laurent E. Cartier, Michael S. Krzemnicki, John Rere: Pearl or gemstone? *Galatea* pearls: a “new” pearl product from French Polynesia
- 13.50-14.10 Stefanos Karampelas, Enrique Arizmendi, Douglas McLaurin, Manuel Nava, Pierre Hardy, Lore Kiefert: Current situation of the pearl cultivation at Guaymas (Sonora) Mexico
- 14.10-14.30 Steve Kennedy: The pearl of Asia: examination of the pearl, a review of its history, and conjecture on its origin
- 14.30-14.50 Kenneth Scarratt: Additional data collected on natural and cultured pearls from *P. maxima* in Australian waters
- 14.50-15.10 Sutas Singbamroong, Nazar Ahmed: Digital SLR camera applied to investigation of X-ray luminescence of pearl
- 15.10-15.30 Abeer Tawfeeq Al-Alawi, Stefanos Karampelas, Osama Taqi: Comparison of “cavities” in saltwater natural pearls and saltwater cultured pearls without bead
- 15.30-15.50 Coffee Break
- 15.50-17.00 Poster Session 1 (See below)
- 18.00 Meeting point at Lake Side hotel lobby to go on bus to dinner
- 19-21.00 Dinner at POTOMAC restaurant (a boat on West lake)
- 21.00 Meeting point at the restaurant entrance to go on bus to Lake Side hotel

Tuesday 15 October

Beryl, chrysoberyl, spinel, garnet (Chairman Ken Scarratt)

- 9.00-9.20 Jorgen Schnellrath, Ricardo Scholz, Dietmar Schwarz, Stefanos Karampelas, Ariadne Senna Azzaro: Itatiaia mine: a new emerald occurrence near Conselheiro Pena, Minas Geras, Brazil
- 9.20-9.40 Jean Marie Dereppe, Claudette Moreaux: Identification of Maxixe beryls by EPR
- 9.40-10.00 Le Thi-Thu Huong, Tobias Häger, Wolfgang Hofmeister, Stefanos Karampelas, Nguyen-Duc Trung-Kien: New features to identify natural and synthetic emerald by vibrational spectroscopy
- 10.00-10.20 Karl Schmetzer, Michael S. Krzemnicki, Thomas Hainschwang, Heinz-Jürgen Bernhardt: The role of vanadium and titanium in natural and synthetic chrysoberyl and alexandrite – coloration, chatoyancy and asterism
- 10.20-10.40 Coffee Break
- 10.40-11.00 Edward Boehm: A comparative overview of inclusions in spinel
- 11.00-11.20 Tobias Häger, Christoph A. Hauzenberger, D. Zimmer, Nguyen Ngoc Khoi, Duong Anh Tuan, Le Thi-Thu Huong, Wolfgang Hofmeister: Causes of colour of natural untreated spinels from Vietnam in comparison to flame fusion and flux grown synthetics
- 11.20-11.40 Henry A. Hänni: Rare Earth Elements in mint green grossular garnet from Merelani, Tanzania
- 11.40-12.00 Jaroslav Hyrsl: Spectroscopic study of chrome pyropes from different sources
- 12.00-13.30 Lunch (Lake Side hotel: Azuma Japanese Restaurant)

Topaz, zoisite, feldspar, quartz, jade, optical effect (Chairman Hanco Zwaan)

- 13.30-13.50 Masaki Furuya: Spectroscopic study of electron-irradiated OH-type topaz
- 13.50-14.10 Claudio C. Milisenda, Kathrin Wehr, Michael Wild: Zoisite from Pakistan
- 14.10-14.30 Willow Weight: Canadian labradorite – classic colour
- 14.30-14.50 Ulrich Henn, Rainer Schultz-Güttler: Special features in quartz colours
- 14.50-15.10 Mimi C. M. Ouyang, Miro F. Y. Ng: The zonal texture and isomorphic series in Fei Cui minerals
- 15.10-15.30 Michael S. Krzemnicki, W. Zhou, J. Maizlan: Colour change effects in gemstones: causes and perception
- 15.30-15.50 Coffee Break

- 15.50-17.00 Poster session 2 (see below)
- 18.00 Meeting point at the Lake Side hotel lobby to go on bus to dinner
- 19.00-21.00 Dinner at Phu Son restaurant in Bac Ninh province
- 21.00 Meeting point at the entrance of the restaurant to go on bus back to Lake Side hotel

Wednesday 16 October

- 8.00-8.45 EXCO Meeting
- Glass, historic jewelry, occurrence, application (Chairman Ulrich Henn)**
- 9.00-9.20 Karen E. Fox: Optical spectroscopy of iron in sodium silicate glasses
- 9.20-9.40 Elisabeth Strack, Ruslan I. Kostov: Gemmological examination of jewellery objects from the Veliki Preslav treasure in Bulgaria
- 9.40-10.00 Anette Clausen: Gemstones of Greenland
- 10.00-10.20 Michael Gray: Gemstone mining in the United States in the previous decade
- 10.20-10.40 Coffee Break
- 10.40-11.00 Menahem Sevdermish: Further research into digital color analysis and communication of color in gems
- 11.00-11.20 Yuri Shelementiev, Sergey Sivovolenko: Digital Microscopy applications in gemology
- 11.20-12.00 Announcements
- 12.00-13.30 Lunch (Lake Side hotel: Royal Restaurant)
- 13.30 Meeting point at the Lake Side hotel lobby to go on bus to visit Presidential Palace
- 15.30 Back to the Lake Side hotel
- 16.00-17.00 Conference closing ceremony
- 17.00 Conference ends

POSTERS

5 min presentation per author

Monday 14 October

- 15.50 Chakkrich Boonmee, Natthapong Monarumit , Sermrak Ingavanija, Somruedee Satitkune, Pornsawat Wathanakul: Structural and chemical analysis of Thai ivory from Lampang Province using SEM/EDS and LA-ICP-MS
- 15.55 Gagan Choudhary, Shyamala Fernandes: Inclusions in Indian rubies
- 16.00 Christoph A. Hauzenberger, Nguyen Ngoc Khoi, Chakkaphan Sutthirat, Tobias Häger, Pornsawat Wathanakul, Duong Anh Tuan: Genesis of corundum with spinel corona from Truc Lau and Kinh La, North Vietnam
- 16.05 Arunas Kleismantas: XVII – XVIII century garnet-garnet doublets imitating rubies
- 16.10 Liu-Shang-I, George Bosshart†, Peng Ming-sheng: Causes of colour in natural and irradiated green spodumene
- 16.15 Gamini Zoysa: Sapphire deposits of Sri Lanka – past & present
- 16.20 Natthapong Monarumit, Thitinun Chantrakul, Pongsakorn Jantaratana, Pornsawat Wathanakul: Application of dielectric constant values for identifying ruby samples from Myanmar and Mozambique
- 16.25 Nguy Tuyet Nhung, Le Thi Thu Huong, Nguyen Thi Le Ouyen, Tran Thi Duyen, Dinh Thi Hue, Tran Thi Lan: Gemstones from the Luc Yen pegmatite in Vietnam
- 16.30 Aumaparn Phlayrahan, Natthapong Monarumit, Lucksika Loetwanitsakul, Somruedee Satitkune, Pornsawat Wathanakul: The alteration of structural OH group in FTIR spectra on ruby samples from Mong Hsu, Myanmar and Montepeuz, Mozambique

Tuesday 15 October

- 15.50 Somruedee Satitkune, Bhuwadol Wanthanachaisaeng, Krit Won-in, Wiwat Wongkokau, Pongsakorn Chantararat, Thanong Leelawattanasuk, Pornsawat Wathanakul: Heat treatment of zircon samples from Kanchanaburi, Thailand and Ratanakiri, Cambodia
- 15.55 Chanikarn Sanguanphun, Natthapong Monarumit, Thanapong Lhuaamporn, Wiwat Wongkokua, Somruedee Satitkune, Pornsawat Wathanakul: Effect of electron irradiation on diamond surfaces using Atomic Force Microscope
- 16.00 John M. Saul: Gemstone occurrences, “organic” odors, and a circular structure in the collision zone between East and West Gondwana
- 16.05 S. Sivovolenko, R. Serov, Y. Shelementiev: Fancy colored diamonds cut optimization technology

- 16.10 Elizabeth Su: Classification of jadeite
- 16.15 Sora Shin, Jingyo Seo, Yongkil Ahn, U. Tin Hlaing, Jongwan Park: Differentiation of the colourless gemstones: phenakite, petalite, pollucite and goshenite
- 16.20 Panjawan Thanasuthipitak, Chawalit Chankhantha, Theerapongs Thanasuthipitak: Heat treatment of coloured beryl from Madagascar
- 16.25 Nguyen Thi Minh Thuyet, Nguyen Ngoc Khoi, Christoph Hauzenberger, Nguyen Hoang, Duong Anh Tuan: Some gemological characteristics of peridot from South Vietnam
- 16.30 U. Wehrmeister, T. M. Gluhak, H. Götz, D. E. Jacob: Differentiation of African and Asian elephant dentine by FT-Raman spectroscopy and chemometric methods

Mineral inclusions in alluvial sapphires from Montana - an update

J.C. (Hanco) Zwaan¹, Eric Buter¹, Robert E. Kane²

¹ Netherlands Gemmological Laboratory, Naturalis Biodiversity Center, Darwinweg 2, 2333 CR Leiden, the Netherlands; e-mail: Hanco.Zwaan@naturalis.nl

² Fine Gems International, P.O. Box 1710, Helena, Montana 59624, USA

Mineral inclusions in sapphires, mainly from Rock Creek, Montana, were identified and compared with existing data. While Yogo Gulch is Montana's only primary sapphire deposit, Rock Creek, or Gem Mountain as it is popularly known, is the most important of the Montana secondary, alluvial deposits (Kane, 2004). Study of inclusions in sapphires from secondary deposits may give clues on their original source, and ultimately contribute in understanding the genesis of corundum deposits.

Materials and methods

A parcel of faceted sapphires, with a total weight of 702.63 carats, has been studied with a focus on mineral inclusions. The sapphires were mostly brilliant-cut, of variable size (mainly between ~1 to 2.6 ct) and colour (Figure 1), mostly dark blue, but also pale to medium blue, yellow to orange, colourless to pale green, and bicoloured stones (blues and greens with yellow to orange parts). Although the parcel mainly contains sapphires from Rock Creek, also a few stones from Dry Cottonwood Creek and even fewer stones from the Eldorado Bar deposit on the Missouri River could be included, due to mixing of sapphires from those deposits, by the American Gem Corporation (AGC). During the mid-1990s, AGC mined more than 3.5 million carats from Rock Creek and 500,000 carats from Dry Cottonwood Creek. A test-mining program at the Eldorado Bar deposit produced several kilograms of rough. All the stones were routinely heat treated.



Figure 1. A selection of sapphires from Rock Creek, Montana, used for this study. Stones ranged between ~1 and 2.6 ct, and the total weight of the parcel studied is 702.63 ct. Photo by Dirk van der Marel.

After selecting sapphires that contained recognizable mineral inclusions, 98 dark blue samples and in total 27 samples with other colours were analyzed with a Thermo DXR micro-Raman spectrometer, using 532 nm laser excitation. Raman spectra were collected at room temperature in confocal mode, which is necessary for analysis of individual

inclusions on a micron scale (1-2 μm). A grating of 1800 grooves/mm and a pinhole size of 25 μm was used which, combined with the optical path length, yields a spectral resolution of 1.0 cm^{-1} . The generated Raman spectra were interpreted with help of the RUFF Raman database of minerals (ruff.info) and other sources (e.g., Wang et al., 2004).

Results

Among the large number of negative crystals, often with characteristic corroded-like surfaces, rutile was the dominant mineral inclusion. Ca-rich plagioclase (spectral matches with anorthite and bytownite) and alkali feldspar (most spectral matches closest to orthoclase) were occasionally encountered. In alphabetic order, other mineral inclusions that were found are allanite, aluminite ($\text{Al}_2\text{SO}_4(\text{OH})_4 \cdot 7\text{H}_2\text{O}$), anatase, anhydrite, apatite, barite, chalcopyrite, cristobalite (SiO_2), hematite, ilmenite, magnetite, monazite, muscovite/lithian mica, nahcolite (NaHCO_3), phlogopite, spinel, topaz and uranpyrochlore. Topaz was only found in one sapphire (Figure 2), but two isolated subhedral grains could be identified in it. Raman spectra of some mica's were difficult to interpret; spectral matches could be attributed to muscovite - $\text{KAl}_2(\text{AlSi}_3\text{O}_{10})(\text{OH})_2$, but also, and often with a slightly better match, to the closely related, but Li-bearing, trilithionite - $\text{K}(\text{Li,Al})_3(\text{AlSi}_3\text{O}_{10})(\text{F,OH})_2$. For monazite, the spectral match was closest to monazite-Ce. The encountered spinel group mineral is difficult to characterize correctly due to existing solid solution series; comparing spectra with Wang et al. (2004), it can be either magnesiochromite or a Fe-Cr spinel, with a hercynite and chromite component. Many atoll-like inclusions with a central mineral surrounded by a discoid stress halo, did not show clear mineral shapes, but showed indistinct ovoid, roundish, or elongated shapes. These inclusions did not reveal clear Raman spectra and were interpreted to be of amorphous nature, probably as a result of heat treatment.

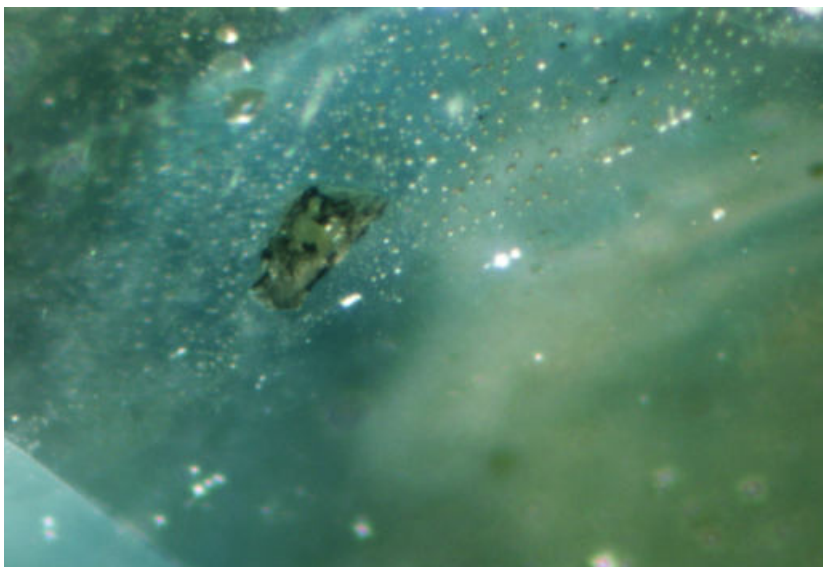


Figure 2. Topaz was found as a mineral inclusion in an alluvial Montana sapphire. Another grain of topaz was found in the same stone. Topaz was never reported before as an inclusion in Montana sapphire. Width of view 1.2 mm. Photomicrograph by J.C. Zwaan.

EPR, eventually combined with FTIR spectroscopy or colorimetry, can help to differentiate similar materials and imitations from turquoise. Figure 3 shows the Mn^{2+} EPR spectrum characteristic of magnesite and carbonates.

Discussion

Identification - The inclusions are listed and compared with previously published data in Table 1. Our study shows the presence of allanite, anatase, chalcopyrite, monazite and topaz (Figure 2), which were not reported before. Orthoclase and Ca-rich plagioclase (anorthite-bytownite) are comparable with earlier reported alkali feldspar and labradorite, respectively, whereas phlogopite is consistent with the earlier mention of biotite.

Dominance of rutile (in many cases the only mineral present) appears to confirm Rock Creek as the most important sample location (compare e.g., Guo et al., 1996; Gübelin and Koivula, 2008). However, the frequent absence of the typical hexagonal zoning enhanced by exsolved rutile needles, which according to Gübelin and Koivula (2008) are the most evident inclusions in alluvial Montana sapphires, combined with the presence of blue haloes around small rutile crystals (compare Emmett & Douthit, 1993) indicated and confirmed that most examined stones were heat-treated. The heat treatment routine demands further caution when interpreting the results. Aluminite, a clay-like hydrated/hydroxylated aluminium sulphate and nahcolite (NaHCO₃), which appeared as a captured phase in a fluid inclusion, were both found in partially healed fissures reaching the surface, and are interpreted as products of heat treatment as well. Cristobalite was detected in relation to the described atoll-like inclusions as ovoid or snowball-like features and is therefore also seen as a result of heat-treatment, either due to crystallisation out of a molten flux, when cooling is not too rapid (compare Emmett et al., 2003), or simply by heating natural glass inclusions, which were described in unheated Rock Creek sapphires by Gübelin & Koivula (2008).

Implications for the original source of corundum – the combination of mineral inclusions and features found in this preliminary study indicate that a complex geologic history must have led to the formation and deposition of sapphire. Topaz, barite, apatite, monazite, uranpyrochlore, anatase, allanite, and K-feldspar suggest the involvement of pegmatites and related veins, and/or an environment rich in incompatible elements and volatiles (such as in alkali magmas, Giuliani et al., 2007, and carbonatites, Guo et al., 1996). Opposedly, chromite-spinel and Ca-rich plagioclase would indicate an ultramafic to mafic igneous source. Phlogopite is often present associated with ultramafic intrusions, as a result of metasomatism. Metasomatism is critical to the genesis of many gem corundum deposits and desilication of an intrusive pegmatite in ultramafic/mafic rock by contact metasomatism is described as a corundum

Table 1. Mineral inclusions in Montana sapphires

Minerals	Localities								
	Data from literature*								
	Yogo Gulch	Rock Creek	Dry Cottonwood	Silver Bow	French Bar	Browns Gulch	Eldorado Bar	Montana unspecified	This study (mainly Rock Creek)
albite				Y		Y		Y	
alkalifeldspar								Y	Y
allanite									Y
almandine garnet	Y		Y				Y		
aluminite									Y
analcime	Y	Y					Y	Y	
anatase									Y
andesine								Y	
anhydrite			Y					Y	Y
anorthite									Y
apatite			Y			Y		Y	Y
baddeleyite								Y	
barite								Y	Y
biotite	Y							Y	
boehmite							Y		
bytownite									Y
calcite	Y	Y	Y				Y	Y	
carbon (amorphous)			Y						
chalcopyrite									Y
clinozoisite		Y	Y				Y	Y	
cristobalite									Y
diaspore		Y	Y						
diopside								Y	
epidote		Y							
ferro-columbite								Y	
fuchsite			Y						
gibbsite		Y							
graphite		Y							
hematite		Y						Y	Y
hercynite		Y					Y	Y	
ilmenite		Y	Y	Y		Y		Y	Y
labradorite	Y	Y	Y						
magnetite		Y						Y	Y
monazite									Y
muscovite*/lithian mica		Y	Y					Y	Y
nahcolite									Y
orthoclase			Y						Y
phlogopite	Y		Y	Y		Y	Y	Y	Y
plagioclase							Y	Y	Y
pyrite	Y							Y	
pyrochlore								Y	
pyroxene								Y	
pyrrhotite			Y						
rutile	Y	Y	Y	Y		Y	Y	Y	Y
sphalerite			Y						
spinel	Y			Y		Y		Y	Y
topaz									Y
uraninite								Y	
uranpyrochlore								Y	Y
zircon	Y				Y	Y		Y	
zoisite		Y							

*Berger & Berg 2006, Garland, 2002; Giuliani et al., 2007; Gübelin & Koivula, 1996; Gübelin & Koivula, 2008; Williams & Walters 2004.

forming process (e.g., Giuliani et al., 2007; Simonet et al., 2008). This would be in line with the discovery of a pebble of plumasite at the Silver Bow sapphire occurrence (Berger & Berg, 2006).

Additionally, the corroded-like inside surfaces of negative crystals strongly resembled the surfaces of basaltic corundum megacrysts from the Lava Plains, Queensland Australia, which Guo et al (1996) described as an irregular high-temperature corrosion pattern resulting from corundum-basalt interaction. This is in line with transportation of the corundum to the Earth's surface by extrusives, as advocated by Berg (2011), who argues that rhyolitic volcanic rocks are the bedrock source of sapphires in the Rock Creek area.

Obviously, more (chemical) work needs to be done to constrain a possible mode or modes of formation, and to discuss presented models on the formation of the alluvial sapphire deposits in Montana (Berger & Berg, 2006, Garland, 2002).

Conclusion

Topaz is a remarkable find in sapphire and together with the other identified minerals may reflect a metasomatic origin of the alluvial sapphires from Montana.

References

- Berg, R.B., 2011. Bedrock source of sapphires in alluvial deposits in the Rock Creek, Sapphire District, Western Montana. Geological Society of America, Abstracts with Programs, 34 (4), 9.
- Berger A.L., Berg R., 2006. The Silver Bow Sapphire Occurrence, Montana: Evidence for a Volcanic Bedrock Source for Montana's Alluvial Sapphire Deposits. *Econ. Geology*, 101, 679-684.
- Emmett J.L., Douthit T.R (1993) Heat Treating the Sapphires of Rock Creek, Montana. *Gems & Gemology*, 29 (4), 250-272.
- Emmett, J.L., Scarratt, K., McClure, S.F., Moses, T., Douthit, T.R., Hughes, R., Novak, S., Shigley, J.E., Wang, W., Bordelon, O., Kane, R.E., 2003. Beryllium Diffusion of Ruby and Sapphire. *Gems & Gemology*, 39 (2), 84–135.
- Garland M.A. (2002) The Alluvial Sapphire Deposits of Western Montana. PhD thesis, University of Toronto, Canada, p. 343.
- Giuliani G., Ohnenstetter, D., Garnier, V., Fallick, A.E., Rakotondrazafy, M., Schwarz, D., 2007. The Geology and Genesis of Gem Corundum Deposits. *Min. Assoc. Canada, Short Course Ser.* 37, 23-78.
- Gübelin E.J., Koivula J.I., 1986. Photoatlas of inclusions in Gemstones. ABC Edition, Zurich, Switzerland.
- Gübelin E.J. & Koivula J.I., 2008. Photoatlas of inclusions in Gemstones. Vol.3, Opinio Publishers, Basel, Switzerland.
- Guo J., O'Reilly S.Y. & Griffin W.L., 1996. Corundum from basaltic terrains: a mineral inclusion approach to the enigma. *Contributions to Mineralogy and Petrology*, 122, 368-386.
- Kane R.E. (2004) The Sapphires of Montana - A Rainbow of Color. *Gem Market News*, 22 (1-1), 1-8.
- Simonet C., Fritsch, E., Lasnier, B., 2008. A classification of gem corundum deposits aimed towards gem exploration, *Ore Geology Reviews*, 34, 127-133.
- Wang A., Kuebler K.E. Bradley L., Haskin L.A. (2004). Raman spectroscopy of Fe-Ti-Cr-oxides, case study: Martian meteorite EETA 79001, *American Mineralogist*, vol. 89, pp. 665-680.
- Williams T.J., Walters, L. (2004) Mineral Inclusions in Alluvial Sapphires from Browns Gulch, Southwestern Montana; Implications for the Origin of Montana Alluvial Sapphires, *Geol. Soc. of America, Abstracts with Programs*, 36 (5), 225.

Acknowledgements

Fine Gems International, kindly loaned the sapphires for this study.

Sapphires from Koltashi deposits (Ural Mountains, Russia)

M.A.Viktorov, A.D. Semina, M.I. Pshenichny

Gemmological Center of Moscow State University, Moscow, Russia, email: viktorov@geol.msu.ru

Alluvial deposits of the Rezh region (Ural Mountains, Ekaterinburg region) are known since the end of nineteenth century. Most of the deposits are situated along the Poloziha river which is no more than 2 km long. This river is flowing through schists in its upper part and through dolomitic limestones in its lower part. The richest layers are concentrated in the lower part of the river where local miners extract different kinds of gemstones such as multi-colored sapphires, colorless sapphires, yellow sapphires, purplish rubies, rare crystals of topaz, beryl, garnet and quartz. They use a simple sand washing technique. It is interesting that here are also known findings of diamond crystals along with colored gemstones. Despite such a long mining period gem alluvial deposits are not exhausted yet and local mining is still active.

The main tasks of this work are the investigation of corundum properties in conjunction to genesis and also evaluation of perspectives of mining in this area. For this purpose we made a special field trip in June 2012 in Rezh region (near Koltashi village) and got samples of sapphire crystals and associated rocks. We collected sapphire samples of gray-blue and pink color from a vermiculite schist forming lens-shaped bodies of several meter in size.



Figure 1. Gray-blue sapphire sample.



Figure 2. Pink sapphire samples.

Sapphire samples presented themselves as crystals and crystal fragments up to 1.5 cm in diameter of tabular hexagonal prism shape with a deep blue color in the central part and a gray layer at the rim (Figure 1) and also small pink crystals of irregular shape (Figure 2). Samples contain a lot of rutile needles and cracks filled with mica.

We used several analytical methods for sample characterization including Raman micro-spectroscopy, microprobe analysis, FTIR-spectroscopy, UV-VIS-spectroscopy. Gray-blue samples also underwent heat treatment (with different red-ox conditions at 1600°C during 2 hours). Samples were characterized by UV-VIS and IR spectroscopy before and after treatment.

During our research we found liquid and mineral inclusions in our samples. Mineral inclusions identified by means of visual observation and Raman micro-spectroscopy were found to be rutile, ilmenite, feldspar (Figure 3), fluorite, spinel, and diaspore.

Table 1. Microprobe analysis data for pink and gray-blue sapphires.

	W%(Ti)	W%(V)	W%(Cr)	W%(Fe)	W%(Ga)
Pink	n.d.	n.d.	0,04 - 0,1	0,07 - 0,12	n.d.
Blue	0,17 - 0,96	n.d.	n.d.	0,09 - 0,24	0,2 - 0,63

Gray-blue samples were subjected to heat treatment in different red-ox conditions at 1600 °C during 2 hours with rapid cooling. Some samples were heated under oxidizing and other under reducing conditions.

We saw several kinds of changes in sapphires during heating in both conditions: 1) intensification of the blue color, 2) changing of gray color to blue color and 3) increase of transparency (Figure 3). All these processes are due to dissolution of rutile inclusions (silk) and dissolution of Ti content in the sapphire structure.

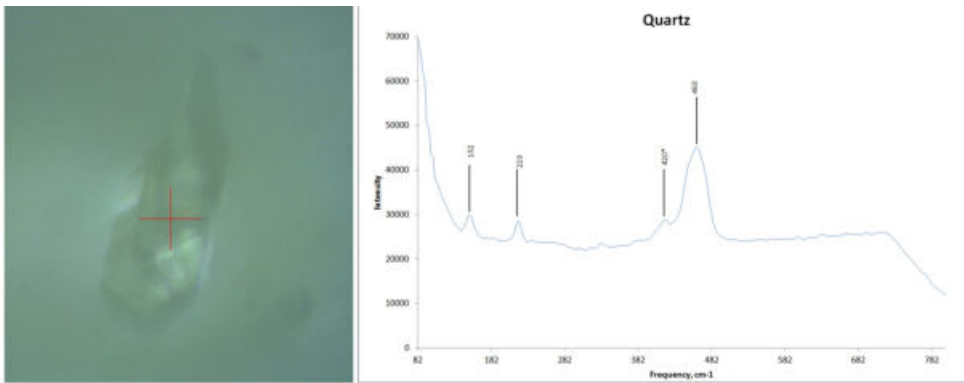


Fig. 3. Feldspar inclusion (left) identified by Raman spectra (right).

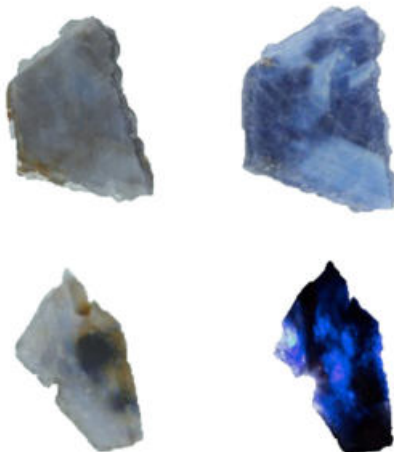


Figure 4. Gray-blue sapphires before (left) and after (right) heat treatment under oxidizing and reducing conditions.

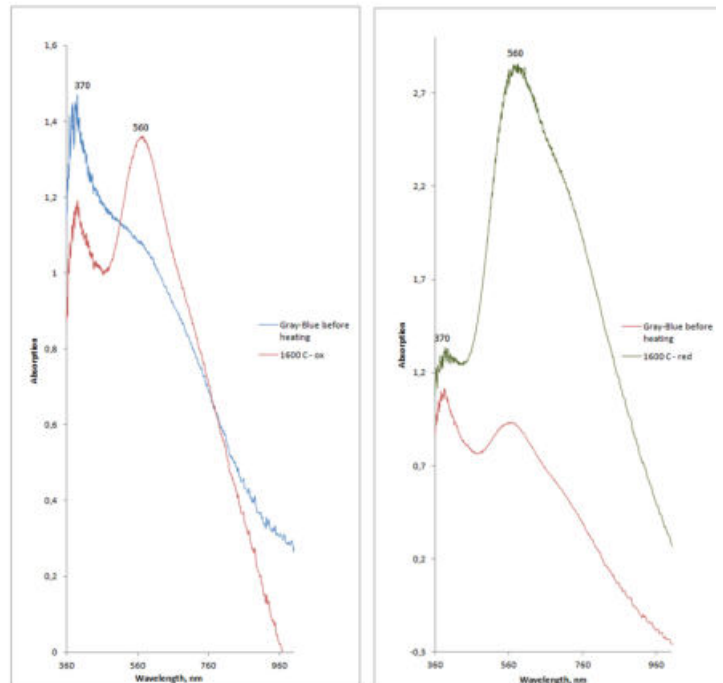


Figure 5. UV-VIS-spectra of sapphires before and after heat treatment under oxidizing (left) and reducing (right) conditions

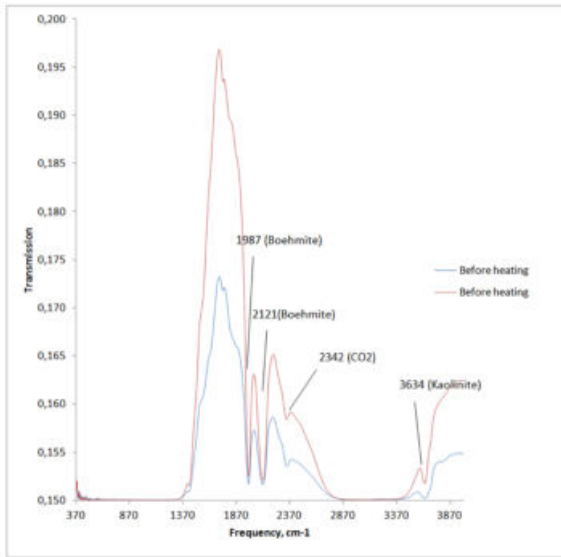


Figure 6. IR-spectra of sapphires before heat treatment.

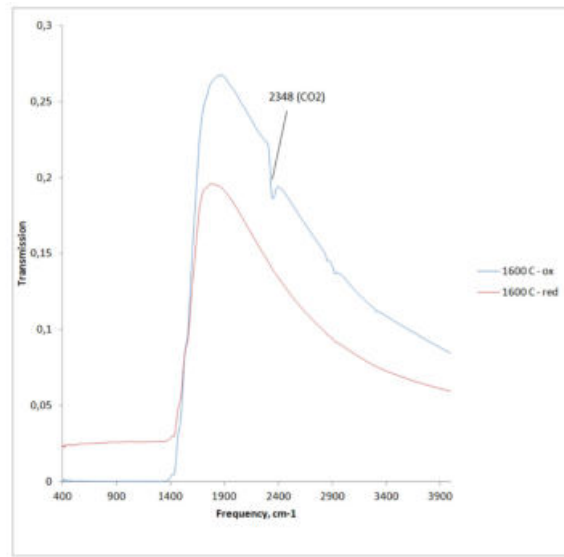


Figure 7. IR-spectra of sapphires after heat treatment under reducing and oxidizing conditions.

UV-VIS and IR-spectra before and after heat treatment were acquired from thin parallel polished plates, prepared from gray-blue sapphires. UV-VIS-spectra show increasing absorption of Fe-Ti charge transfer at about 560 nm after heating (Figure 5). IR-spectra show almost full elimination of hydroxyl absorption after heating (Figure 6-7).

Our research allows us to assume that sapphire-bearing rocks in this region has complex genesis connected with metasomatic and metamorphic processes. Heating experiments showed the perspective for sapphires from Koltashi deposits as potential gem quality material.

References

- Ahmetshin E.A., Bagasheva T.V., 2010. Changing the color of natural sapphire by heat treatment. Nauchny Vestnik of MSMU,9, 9-15. <http://vestnik.msmu.ru/archive/index9.html>
- Gubelin E.J., Koivula. J.I., 2008. Photoatlas of Inclusions in Gemstones. Volume 3. Opinio Verlag, Basel, 672 pp.
- Orlov R.Yu., Viganina M.F., Uspenskaya M.E., 2007. Atlas of Raman spectra of natural minerals. GEOC Москва, 142 pp.
- Hughes R.W., 1997. Ruby & Sapphire. RWH Publishing Boulder, CO, 512 pp.
- Themelis T., 2010. The heat treatment of Ruby and Sapphire, second edition, 384 pp.
- Thirangoon K., 2009. Ruby and pink sapphire from Aappaluttoq Greenland. http://www.giathai.net/pdf/Greenland_Ruby_March_2009.pdf

Kenya, Tanzania: ruby and sapphire - an update/review

Dietmar Schwarz¹, Stefanos Karamelas¹, Lu Taijin², Claudio C. Milisenda³

¹ Gübelin Gem Lab, Maihofstrasse 102, 6006 Lucerne, Switzerland drdietmarschwarz@hotmail.com

² NGTC, National Gemstone Testing Center, Beijing, 100013, China

³ DSEF – Geman Gem Lab, Prof.-Schlossmacher-Str. 1, 55743 Idar-Oberstein, Germany

Colored gemstone deposits in East Africa are associated with Upper Cenozoic to Pleistocene volcanics, specifically alkaline basalts related to the East African Rift or they are found in the so-called Proterozoic Mozambique Metamorphic Belt. The Mozambique Belt (also referred to as the «East African gemstone belt») is a mobile belt of high-grade metamorphic rocks, formed by the collision of the east and west Gondwana continental plates. It underwent several phases of folding and metamorphism before its final stage of regional metamorphism, some 600 million years ago at the end of the Precambrian. The belt contains the most important East African gemstone countries (e.g. Kenya, Tanzania, Mozambique) and can also be found in Sri Lanka and Madagascar.

Kenya

In the Mangari region in southern Kenya, ruby mineralizations are associated with serpentinites formed during the main tectonic Pan-African event (700-600 Ma) of the Mozambique belt. Corundum is found in micaceous lenses and pockets or in veins that crosscut the serpentinites («desilicated pegmatites»). Corundum deposits formed in the granulite facies and they are associated with shear zones (Giuliani et al., 2007); their formation goes back to hydrothermal alteration reactions (Mercier et al., 1999).

The Baringo rubies/pink sapphires are found in basaltic rocks. Their mineralogical-gemological properties indicate a metamorphic formation. Such rubies originate from mafic-ultramafic rocks in the subcontinental lithosphere; they were brought to the surface by the alkali basalts that host now the secondary deposits.

Mineral inclusions in rubies from the Mangari region are rutiles in the form of iridescent pinpoints/platelets/oriented needles and grey or brown pinpoints/particles/short needles that concentrated in well-developed growth bands and -sectors. Other solid inclusions are colorless-transparent to grayish white, irregular shaped crystals and colorless-transparent, brown or green, compact masses (often present as fissures fillings) that are mainly composed of different phyllo-silicates (e.g. mica, chlorite). Also present are healed fissures, growth structures, twin planes and intersection tubules.

Solid inclusions are very rare in Baringo rubies. Most striking inclusion feature is the presence of innumerable small planar, disk-like healed fissures, which are composed of tiny reflective (iridescent) fluid films. These inclusions remind the so-called «rosettes» known from Thai/Cambodian rubies; they are all oriented parallel to each other.

The chemical fingerprinting of Mangari rubies is characterized by generally low titanium contents (up to ca. 0.02 wt % TiO₂), variable V₂O₃ contents (mostly ca. 0.01-0.04 wt %), chromium in the range of ca. 0.3-0.7 wt % Cr₂O₃, normally low iron contents (up to ca. 0.02 wt % Fe₂O₃) and commonly high gallium concentrations (mostly ca. 0.025 to 0.04 wt % Ga₂O₃).

Rubies from the Baringo area show a relatively constant chemical fingerprinting. They have only low titanium contents, the vanadium concentration is generally below the EDXRF detection limit, chromium varies from ca. 0.05 to 0.3 wt % Cr₂O₃ (including pink stones). Iron contents are always high (from ca. 0.4 to 0.8 wt % Fe₂O₃), gallium is always low (< 0.01 wt % Ga₂O₃).

Tanzania

For some time, the Uмба Valley in northern Tanzania was one of the most important sources for fancy coloured sap-

phires (and less important for blue sapphires and rubies). Gem-quality sapphire in a large range of colours and ruby are confined to desilicated pegmatites that crosscut serpentinite rocks. Two types of corundum veins have been described (Giuliani et al., 2007): (1) veins with calcic plagioclase, vermiculite-actinolite-chlorite containing fancy coloured sapphires; and (2) veins with vermiculite that contain orange and yellow-brown sapphire.

Umba sapphires contain a large variety of mineral inclusions (see, e.g., Hughes, 1997): rutile, zircon, apatite, calcite, feldspar, graphite, hematite, mica (vermiculite), monazite, pyrrhotite, spinel, boehmite. Other inclusion features are twin planes (+ intersection tubules).

The chemical fingerprinting of Umba sapphires shows some interesting features. The titanium contents are always low, independent of their body colour (also including rubies): generally < 0.015 wt % TiO₂. Mostly, Umba sapphires (and rubies) have Ga₂O₃ contents of ca. 0.005 to 0.020 wt %. Vanadium is normally below the detection limit of the EDXRF analytical technique in blue and green sapphires; on the other hand, in «V-rich» purple to reddish purple Umba sapphires V₂O₃ contents in the range of ca. 0.05-0.15 wt % were measured. Umba sapphires of different colors distinguish themselves when comparing their iron and chromium contents. Chromium is low (or below the detection limit) in most «green» and «blue» stones, the highest Cr-contents were found in «purple» sapphires (ca. 0.1-0.3 wt % Cr₂O₃). Iron is the element that shows the highest contents of all «impurities» observed in Umba sapphires: it varies from ca. 0.2-0.5 wt % Fe₂O₃ in «purple» stones, goes up to 0.7 wt % in blue sapphires, is approx. 1 wt % in yellow sapphires, varies from ca. 0.8-1.5 in green sapphires and from ca. 1.5-2 wt % Fe₂O₃ in (orange-) brown stones. Umba rubies (mostly purplish red, orangy red or brownish red) have relatively low chromium contents (mostly ca. 0.1-0.3 wt % Cr₂O₃); their iron concentration is distinctly higher: ca. 0.5-1.3 wt % Fe₂O₃.

Since late 2007 rubies and sapphires have been mined by hand methods from both eluvial and primary deposits at Winza in Central Tanzania. The gem corundum is related to dikes of amphibolitic rocks that belong to the Paleoproterozoic Usagaran Belt (Schwarz et al., 2008). Both rubies and sapphires from Winza commonly show colour zoning (mostly bluish violet layers parallel to the prism and basal pinacoid). Top quality vivid red rubies are generally very homogeneous in colour, but they may contain small areas of narrow blue zones. The most distinctive features observed in high quality Winza rubies are long tube-, fibre-, needle-, or hair-like inclusions that are filled with an orange-brown (probably polycrystalline) solid material. Mineral inclusions have been identified as: amphibole, garnet, apatite, monazite, spinel, and various OH-bearing minerals. Other inclusions features are growth planes parallel to the dominant crystal faces, twin planes and «intersection tubules»; also present are slightly milky domains as well as healed and unhealed fissures (Schwarz et al., 2008).



The Winza mining area after the great rush in autumn 2009.

The chemical fingerprinting of Winza rubies and sapphires is characterized by a relatively uniform chemical composition. The chromophores Cr and Fe are present in significant concentrations. Chromium varies from ca. 0.1-0.6 wt % Cr_2O_3 in ruby and can be as high as 0.1-0.3 wt % in blue to purplish blue sapphires. Iron contents are ca. 0.3-0.4 wt % Fe_2O_3 in high quality rubies and ca. 0.6-0.95 wt % Fe_2O_3 in blue and purplish blue sapphires. Winza rubies of the best colour contain little or no titanium, the highest TiO_2 concentration in blue sapphires was about 0.045 wt %. Vanadium and gallium contents in Winza rubies and sapphires are generally low.

Especially during the 1990s, various mining areas around the town of Songea (limited in the south by the Ruvuma river), the region east and south-east of the town of Tunduru along the rivers Muhuwesi, Mtetesi, and Lumesule (e.g. Ngapa), as well as in the Liwale area produced a large variety of gemstones.



Mining activities in the river sediments of the Tunduru region in 1996.

A large number of inclusion minerals were identified in rubies/sapphires from the Songea mining area, most common are: zircon, apatite, rutile, feldspar (plagioclase), mica (biotite-phlogopite), xenotime, monazite, uraninite, epidote, garnet (spessartite), diaspore, pyrrhotite. Different types of fissures (healed and unhealed) are common. Growth structures and colour zoning are only poorly developed in Songea sapphires; Songea rubies, however, often show pronounced and regular, straight growth structures. Also present are twin planes; diffuse, cloud-like formations composed of pinpoint inclusions and/or reflective «particles»; tube-like inclusions.

The following minerals belong to the internal association observed in Tunduru sapphires: zircon, apatite, rutile, feldspar, mica (biotite), xenotime, monazite, calcite/magnesite, shungite, quartz, uraninite, goethite. Sometimes, mineral inclusions are accompanied by comet tail-like formations which are composed of tiny reflective «particles». A common inclusion type in Tunduru corundums are negative crystals (+ fluid fillings), these display a large variation regarding size and shape. Growth structures are often distinct; they are normally observed as straight/angular and regular (fairly equidistant) growth bands. Depending on the viewing direction, the growth bands appear sharp or they display a slightly diffuse aspect (rarely, nearly swirl-like appearance). Different types of fissures are common. Other inclusion types are stringer formations with delicate, reflective platelets, 'pinpoints/particles', and short grayish needles; tube- or channel-like inclusions; grey flake-like formations; lamellar twinning parallel to the positive rhombohedron r. Rubies and sapphires from Songea, generally have low-to-moderate contents of titanium, vanadium, and gallium -often below the EDXRF detection limit. The chromium concentration in rubies normally varies from ca. 0.2-0.7 wt %

Cr_2O_3 , Songea rubies (and sapphires of different colours) distinguish themselves by very high iron contents: ca. 0.8-2 wt % Fe_2O_3 . Tunduru sapphires commonly contain ca. 0.01-0.1 wt % TiO_2 , very high titanium concentrations (up to 0.4 wt % TiO_2) were measured in some brownish blue and purplish grey stones. Vanadium is low (often below detection limit) in most blue Tunduru sapphires, in violetish-blue or pink/purple/red Tunduru corundums, however, vanadium may show contents up to ca. 0.15 wt % V_2O_5 . The chromium contents show a large variation in Tunduru sapphires - depending on their colour. In blue stones chromium is generally low, fancy coloured sapphires may show up to ca. 0.25 wt % Cr_2O_3 , in pink/purple/purplish red corundums the Cr concentration varies a lot: ca. 0.05-0.3 wt % Cr_2O_3 (rarely up to ca. 0.6 wt % in intense red rubies). Gallium contents in Tunduru sapphires are mostly in the range of ca. 0.005-0.04 wt % Ga_2O_3 .

References

- Giuliani G., Ohnenstetter D., Garnier V., Fallick A.E., Rakotondrazafy M., Schwarz D., 2007. The geology and genesis of gem corundum deposits. In: Geology of gem deposits. L. Groat (Ed.), Short Course Series, Vol. 37. Mineralogical Association of Canada, Quebec, 23-78.
- Hughes R., 2007. Ruby and Sapphire. RWH Publishing, Boulder, CO.
- Mercier A., Debat P., Saul J.M., 1999. Exotic origin of the ruby deposits in the Mangari area in SE Kenya. Ore Geology Reviews, Vol. 14, 83-104.
- Schwarz D., Pardieu V., Saul J.M., Schmetzer K., Laurs B.M., Giuliani G., Klemm L., Malsy A.K., Erel E., Hauzenberger C., DuToit G., Fallick A.E., Ohnenstetter D. 2008. Rubies and sapphires from Winza, central Tanzania. Gems & Gemology, Vol. 44(4), 322-347.

The characteristics of gneiss-hosted corundum deposits of Tan Huong-Truc Lau area, Northern Vietnam

**Nguyen Ngoc Khoi^{1, 2}, Hauzenberger C. A.⁴, Sutthirat C.⁵, Duong Anh Tuan²,
Nguyen Thi Minh Thuyet¹, Nguyen Thuy Duong¹, Nguyen Van Nam³, Chu Van Lam³**

¹ Hanoi University of Science, 334 Nguyen Trai str., Thanh Xuan dist., Hanoi, Vietnam, e-mail: khoinn@vnu.edu.vn

² DOJI Gold & Gems Group, 44 Le Ngoc Han, Hanoi, Vietnam

³ Vietnam Institute of Geosciences and Mineral Resources, Chien Thang road, Hanoi, Vietnam.

⁴ Karl-Franzens-University of Graz, A – 8010, Graz, Austria.

⁵ Department of Geology, Faculty of Science, Chulalongkorn University Patumwan, Bangkok 10330, Thailand.

Introduction

Deposits and occurrences of gneiss-hosted type of corundum deposits are much rarer than other types (marble-hosted, basalt-related, etc.) and yields gem material (mainly corundum, spinel) with their typical gemological properties. On the territory of Vietnam they have been found in some areas such as Tan Huong-Truc Lau in North Vietnam (Long et al., 2004), and Phuoc Hiep in Central Vietnam. Detailed investigation of the typical deposits and occurrences allowed us to establish the attributes of this type. This is the basis for modeling this deposit type in the future.

Geological characteristics

Tectonic and geological settings

Corundum-bearing lithologies of Tan Huong-Truc Lau area around the Con Voi mountain range (Red River Shear Zone), are mainly hosted by partly migmatized, plagioclase-rich gneiss, diopside gneiss, biotite-garnet gneiss, and quartz-sillimanite-garnet gneiss intercalated with biotite-sillimanite schist and lenses of amphibolite and marble of the Nui Voi Formation. These rocks lie underneath the Ngoi Chi Formation, which comprises quartz-mica schist, sillimanite schist, and garnet schist (Fig. 1). Corundum occurs as porphyroblasts or idiomorphic, xenomorphic or skeletal crystals within high-grade (mainly amphibolites-granulite facies), regionally metamorphosed belts. It is confined to specific metamorphic layers and concordant lenses of alumina-rich gneisses and schists. Corundum is considered to be syn-metamorphic (22.17-24.52 Ma), while the protolith is Precambrian.

Deposit form, ore texture/ structure

Corundum-bearing, stratabound and discontinuous layers and lenses in gneisses measure ten centimetres to a few metres in thickness and may be traced for tens to hundreds of metres along their strike. These layers are commonly strongly deformed, with coarse-grained «sweat outs» which may cut across the gneissic texture. Gneissosity and schistosity is generally parallel to the compositional layering and corundum mineralization; however, if migmatization or granitization was involved, corundum zones may be irregular or vein-like. The texture of corundum-bearing rocks varies from fine-grained, equigranular to coarse-grained (approaching pegmatitic), locally displaying pseudo-orbicular texture.

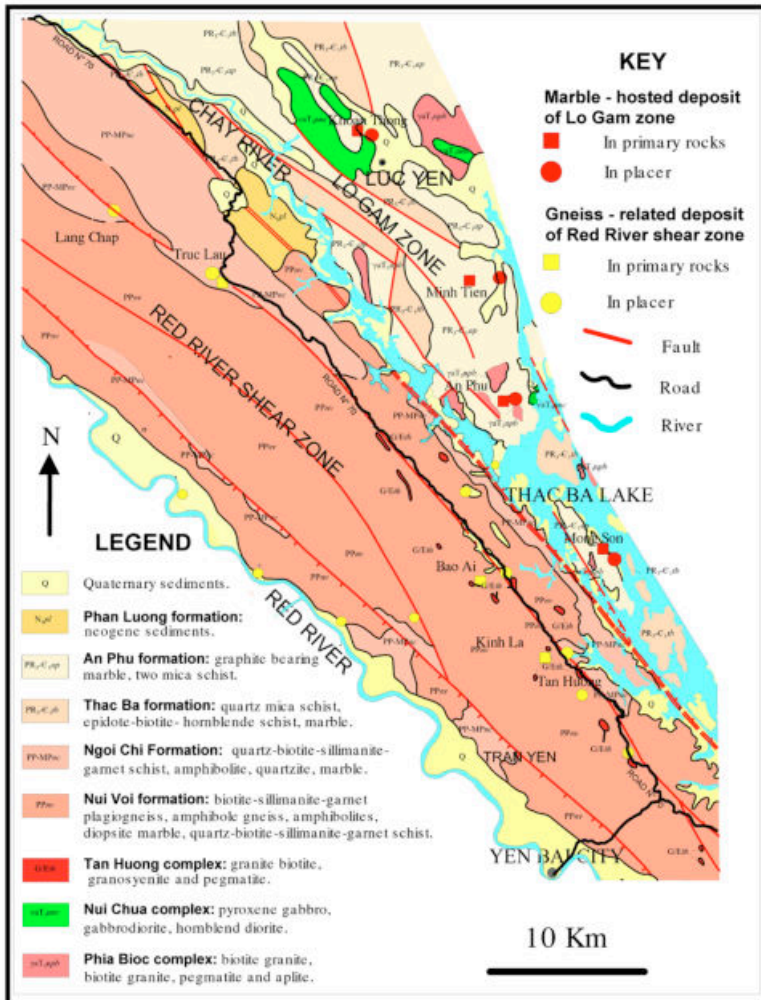


Figure 1. Simplified geologic map showing the locations and rock formations of the gneiss-hosted corundum occurrences in Con Voi mountain range of the Red River shear zone (in yellow) and marble-hosted occurrences in the Lo Gam zone (in red). (Modified after Geological and Mineral Resources Map of Vietnam, scale 1:200.000, sheet Bac Quang, 2000, ed. Tran Xuyen, and sheet Yen Bai, 2005, ed. Nguyen Vinh).

Mineralogy (Principal and subordinate)

Corundum is a dominant constituent of the corundum-bearing gneiss (20 to 40% in mass). The same gneiss may contain specimen quality material and exceptionally near-gem quality stones.

The primary corundum of Tan Huong-Truc Lau area can be grouped into two main types which are found in two different kinds of host rock and at different locations (see Fig. 1):

- Type I: Gray, grayish white to bluish, and yellowish gray sapphires, with little pinkish sapphires, embedded in gneisses and migmatized gneisses.
- Type II: Dark red to pinkish, sometimes big to very big, ruby crystals in weathered feldspathic (pegmatoid) rocks, developed in gneisses. Ruby crystals of tens kilograms have been found (Fig 2).

Corundum of Type I is more widespread than that of Type II, though its economic importance is lower due to lower quality of gem material.

The gneisses hosting Type I corundum are characterized by 3 different types of mineral assemblages: (1) Sillimanite + corundum + K-feldspar + biotite, (2) Sillimanite + garnet + spinel + corundum + biotite + K-feldspar + plagioclase + ilmenite, and (3) Sillimanite + garnet + spinel + corundum + pyroxene + ilmenite, while feldspathic rocks hosting Type II corundum is found in only one mineral assemblage: Garnet + biotite + plagioclase + K-feldspar + corundum.

Corundum crystals sometimes alter to muscovite along fractures and twinning planes. Retrograde corundum alteration to diaspore and margarite is also known. Vermiculite-rich layers may form at the contact between corundum-bea-

ring and mafic rocks or marbles.



Figure 2. Ruby crystals of Type II from Tan Huong-Truc Lau area

Ore controls and genetic models

The principal controls are the chemical composition (high alumina and low silica content) of the protolith and a high regional metamorphic grade, typically granulite facies.

Post-depositional exposure of rocks to intense weathering produces high-alumina protolith required to form isochemical metamorphic emery and corundum deposits. Corundum is resistant to chemical and mechanical weathering. Weathering facilitates crystal recovery from the hardrock deposits. Corundum may be enriched in residual soils or eroded and deposited as placer-type deposits. A large proportion of alluvial gem corundum (Tan Huong and Truc Lau placer mines) is interpreted to be derived from corundum layers within garnet-sillimanite-biotite gneisses (Dahanayake and Ranasinghe, 1981).

Corundum from gneisses in Tan Huong-Truc Lau appear to be of polygenic origin. Sapphire in gneisses (Type I) was formed in solid state during isochemical regional metamorphism, whereas ruby in feldspathic rocks (Type II) probably formed at the contact of migmatized pegmatoid bodies with surrounding mafic/ultramafic rocks (amphibolites, marbles) known for their desilicizing impact.

Gemmological properties of corundum

Morphology and Appearance

Corundum crystals in gneisses may be idiomorphic, xenomorphic or skeletal and may vary from near gem quality to those with abundant solid inclusions and/or fractures. Short prismatic and sometimes tabular morphologies with granular spinel coating are most prominent. In general, the crystals are much larger than those from the other types. Corundum from gneiss-hosted deposits of Tan Huong-Truc Lau area shows a color variation from gray, white and yellowish, to dark red, pink to purplish or brownish pink. Color zoning is uncommon. Diaphaneity is semitransparent to translucent or opaque because of fracturing and the abundance of inclusions.

Internal Features

Corundum from gneiss-hosted deposits contains a different diversity of mineral inclusions, such as ilmenite, magnetite, rutile, plagioclase, muscovite, biotite, apatite, zircon, and boehmite. Straight and angular growth structures are

quite common, while color zoning is rare. Trappiche rubies and pink sapphires also occur in this region. In general, primary ruby and pink sapphire from gneiss-hosted deposit type contains more Fe and less Cr than their counterpart from marble-hosted deposits. Provide an analysis

Exploration guides

Corundum and associated minerals, such as spinel, sillimanite, \pm garnet are frequently found as heavy mineral concentrates in streams, lakes, tills and residual soils. Other important exploration guides are:

- Aluminous lithologies within metasedimentary sequences in high-grade metamorphic belts, commonly containing high-alumina silicate assemblages
- contact of migmatized pegmatoid bodies with surrounding mafic ultramafic rocks (amphibolites, marbles)

Conclusions

Most of the gneiss-hosted primary deposits in Con Voi mountain range contain only industrial grade corundum (Type I) with little or no high gem-quality stones. Nevertheless, corundum from feldspathic rocks (Type II) has higher gem-quality and has been sporadically mined from host rocks in some places of Con Voi mountain range. Moreover, residual and placer deposits are not only less expensive to exploit, but typically contain a higher proportion of gem-quality material due to the break-up of micro-fractured stones during stream transport. Many placer deposits in Con Voi mountain range were exploited from 1996-1998 period, and until now, small-scale gem mining is still active in some locations.

References

- Dahanayake, K. and Ranasinghe, A.P., 1981. Source Rocks of Gem Minerals A case Study from Sri Lanka. *Mineralium Deposita*, Volume 16, pp. 103-111.
- Golani, P.R., 1989. Sillimanite-Corundum Deposits of Sonapahar, Meghalaya, India: A Metamorphosed Precambrian Paleosol. *Precambrian Research*, Volume 43, pp. 175-189.
- Long P.V., Vinh H.Q., Garnier V., Giuliani G., Ohnenstetter D., Lhomme T., Schwarz D., Fallick A., Dubessy J., Trinh P.T., 2004. Gem corundum deposits in Vietnam. *Journal of Gemmology*, Vol. 29, No. 3, pp. 129–147.
- Khoi N.N., Sutthirat C., Tuan D.A., Nam N.V., Thuyet N.T.M., Nhung N.T., 2010. Comparative study of rubies and fancy sapphires from two different deposit types in Yen Bai Province, Vietnam. *Proceedings of the 5th International Conference "Provenance and Properties of Gems and Geo – Materials,"* Hanoi, October 17–24, pp. 212–223.
- Nguy Tuyet Nhung, Nguyen Van Nam, Nguyen Ngoc Khoi, Phan Van Quynh, Nguyen Thi Minh Thuyet, Vu Van Tich, 2006. Characteristics of Corundum from Primary Deposit in Truc Lau Area, Northern Vietnam. *The 1st International Gem and Jewelry Conference GIT 2006*. Bangkok, 6-9 December, 2006.
- Nguyen Ngoc Khoi, Chakaphan Sutthirat, Duong Anh Tuan, Nguyen Van Nam, Nguyen Thi Minh Thuyet & Nguy Tuyet Nhung, 2011. Ruby and Sapphire from Tan Huong-Truc Lau Area, Yen Bai Province, Vietnam. *Gems & Gemology*, Vol. 47, No. 3, pp. 182-195.
- Nguyen Thi Minh Thuyet, Nguy Tuyet Nhung, Nguyen Ngoc Khoi, 2011. Genesis and formation conditions of corundums in gneisses from Truc Lau mine, Luc Yen district, Yen Bai province. *J. Earth Sciences*, T.33 (1), pp. 55-62.
- Simandl, G.J., Paradis, S., 1999. Corundum in alumina-rich metasediments. In G. J. Simandl Z. D. Hora, and D. V. LeFebvre, Eds., *Selected British Columbia Mineral Deposit Profiles*, Vol. 3, Industrial Minerals. British Columbia Ministry of Energy and Mines, Open File 1999-10.

Acknowledgements

This research is funded by Vietnam National Foundation for Science and Technology Development (NAFOSTED) under grant number 105.02-2012.08.

New deposit style concept and characteristics of gem corundum, Phrae Province, Northern Thailand

**Pornsawat Wathanakul^{1*}, Prayath Nantasin², Kachane Kraissittipong²,
Prakarn Buenkoontod², and Marute Lekkean²**

¹ The Gems and Jewelry Institute of Thailand (Public Organization), ITF-Tower, Silom Road, Bangkok 10500, Thailand

*pwathanakul2@gmail.com

² Department of Earth Sciences, Kasetsart University, Bangkok 10900, Thailand

Thailand is known as one of the main localities of corundum deposits though the productivity of most gem fields was declined in recent years. However, mining activity in some localities are still active i.e. Bo Phloi at Karnchanaburi, Chantaburi-Trat, and Phrae Province, northern Thailand.

The detail geology of the Den Chai basalt suite, Phrae Province has been reported in many previous works (e.g., Charoenprawat, 1967; Piyasin, 1975; Vichit et al, 1978; Vichit, 1992; Barr & Macdonald, 1978, 1979; Thayapink & Sutthirat, 1992; Sutthirat, 2001). The Denchai basalt was designated to be 7 layers with the K/Ar age of 5.64 ± 0.28 Ma (Barr & Macdonald, 1979). However, we divide the Den Chai basalt into 3 main layers based on field evidences, textural and mineralogical characteristics (Wathanakul et al., 2004). Although the above depositional style was widely accepted but many doubts are existing. The distribution of basalts in the Phrae Province is shown in Figure 1. Therefore, this paper was aimed to synthesize a new depositional style of the Den Chai sapphire deposit which has been believed that the upper most basaltic layer is only one carrier which brought up sapphire to the earth's surface in the study area.

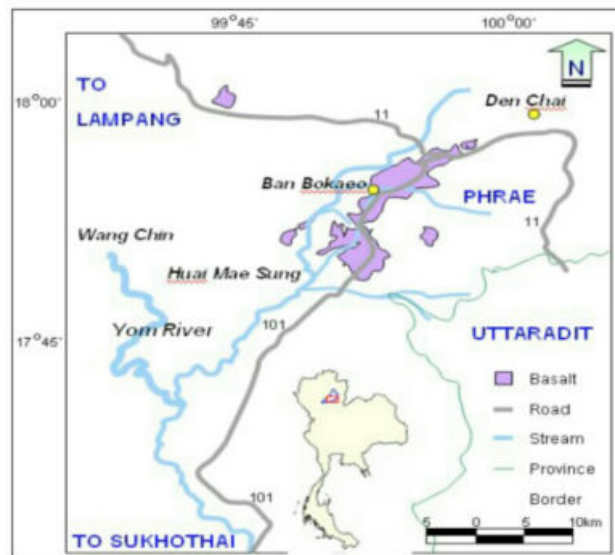


Figure 1. Map of the Ban Bo Kaeo sapphire deposit, Phrae Province, and the related basaltic areas.

Gem corundum deposit style

The occurrence of inter-basaltic layers gravel under burden gravel beds found in Ban Bo Kaeo sapphire reveal a new concept on depositional style of Denchai corundum. However, those corundum-bearing gravel beds show different relation to adjacent rocks. In pitting holes, firstly, most corundum-bearing gravel bed overlay the bedrock, shale and some of these holes were dug through a basaltic layer. Secondly, there are two dipping gravel beds found in digging pond. These gravel beds contain numerous considerable black spinel, the common related mineral of corundum. Thirdly, at Ban Bo Kaeo, there is a distinctive gravel layer between two basaltic layers. This gravel bed which exposes perpendicularly to the waterfall and thick approximately 50 cm shows very poor sorting and contains corundum therein (Figure 2). Therefore, on the basis of field witnesses, the concept of corundum depositional style and episode of Denchai corundum might be changed. The new concept probably is multiple episodes of corundum-related basalt and multiple depositional styles instead of single episode and only alluvial deposits.

The relationship between basaltic layers and the gravel bed which contains spinel and corundum was clearly evidenced in a vicinity (Figure 2). The upper basaltic layer which shows a horizontal configuration is a dark, dense, olivine basalt (Figure 2). Numerous vesicular formed on its upper part. While the lower basaltic layer is well-developed columnar joints and its lower part exhibits flagged fracture. The inter-layered gravel bed is very poor-sorted and composed of 1-12 cm rounded sediments of tuff, sandstone, basalt and chert (Wathanakul et al., 2002). The bed contains spinel, zircon, olivine and corundum.



Figure 2. Relationship between basaltic layers and a corundum-bearing gravel bed at Bo Kaeo village, Den Chai District.

Gem corundum characteristics

For this study rough blue sapphire samples were collected from the area related to the basaltic host rock.

The sapphire samples range from 0.33-10.88 carat. Broken hexagonal crystals are common. Some are similar to the trapiche-like ones. A minor amount of greenish-blue and brown stones was observed. The largest stone reported was 257 carat. Most of them are saturated blue in colour. Among blue sapphires a few ruby grains were also found. Black spinel, zircon, garnet and olivine are found as indicators of sapphires.

The internal features are typically full of liquid CO₂ inclusions, some of which having necked with exsolved melt phases. Mineral inclusions include rutile, ilmenite, zircon, spinel, bronzite, magnetite, mica (?) and unidentified crystals (Wathanakul et al., 2004).

Chemical analyses by LA-ICPMS (Table 1) of blue sapphire samples from Phrae Province were detected in ppm by weight and show high Fe contents with affinities of rare metals and high field strength elements (HFSE) such as Be, Sn, Ce, Zr, Nb and Ta.

H₂O and CO₂ molecules are also incorporated in channel positions and are further raising the physical data (Cerni & Hawthorne, 1967; Goldman et al., 1978). The beryl structure as described by Bragg & West (1926), has seen a number of refinements (Gibbs et al., 1968; Artioli et al., 1993). Spectroscopic investigations have shown the relationship between chromophore trace elements and absorption spectrum, as well as traces and channel constituents in the infrared spectrum (Wood & Nassau, 1968). Water molecules in alkali-free emeralds have their dipole axis parallel to the channel (Type I water). The rotation of H₂O molecules with their axes perpendicular to the c-axis of the beryl molecules is a consequence of the presence of channel constituents such as Na⁺ or Li⁺ (Type II water). Flux grown synthetic emeralds are water free and contain no alkalis. A rich display of beryl characteristics, origins and individual features has been given by Sinkankas (1981). A modern alternative to the FTIR identification of natural and synthetic emeralds is possible by Raman spectroscopy (Huong et al., 2010).

Chromophore trace element or solid solution admixture

The colour of emeralds has always been attributed to traces of Cr and/or V. A typical Colombian emerald could thus contain 6842 ppm Cr and 4079 ppm V. These contents correspond to concentrations of 1 wt% of Cr₂O₃ and 0.6 wt% V₂O₃ (Cr/V ratios < 1 are known as well).

One could postulate new end-members with beryl structure, such as Be₃Cr₂Si₆O₁₈ or Be₃V₂Si₆O₁₈. The content of 1.0 wt% Cr₂O₃ and 0.6 wt% V₂O₃ correspond to 5.6 Be₃Cr₂Si₆O₁₈ and 4.4 Be₃V₂Si₆O₁₈ molecules, the rest being 90 Be₃Al₂Si₆O₁₈ of 100.

The Colombian emerald cited above could hence be plotted in a triangular concentration diagram, same as mineralogists are doing for other minerals in complex solid solution situations. (Fig.3).

Table 1: The chemical result by using LA-ICPMS of blue sapphire samples from Phrae compared with those from other sources (detected in ppm by weight).

Element (ppm)	Phrae	Phrae	Kanchanaburi	Chanthaburi
Be	357	6	1	<1
B	41	22	19	14
P	66	47	35	28
Ca	359	2071	460	1116
Ti	279	253	874	181
V	1	1	1	13
Cr	1	8	0	<1
Mn	8	44	1	4
Fe	4637	7942	4014	10741
Ga	204	205	130	224
Nb	36	89	14	20
Sn	7	6	4	4
Ta	40	238	24	52

Concluding remarks

Deposit style: The research investigation shows that the small individual sapphire deposits were commonly found and scattered along the Huay Mae Sung and its tributaries (note: Huay =stream). The deposition of sapphires indicates 2 styles as placer and as residual from basaltic weathering.

Based on field evidences mentioned above it can be concluded that at least two basaltic episodes exist which brought the Den Chai corundum up to the surface at different time. Therefore, the depositional style of corundum at Phrae Province should be multi episode rather than a single episode as previous concept.

References

- Charoenprawat, A., 1967. Geological investigation report of Wang Chin Map sheet and Ban Bo Kaeo Map sheet, scale 1:50,000. Geological survey Section, Department of Mineral Resources, 70 pp (in Thai).
- Piyasin, S., 1975. Geological Map of Utradit Province, scale 1:250,000. Geological survey Section, Department of Mineral Resources, 68 pp (in Thai).
- Vichit, P., Vudhichativanich, S., and Hansawek, R., 1978. The Distribution and some Characteristic of Corundum-bearing Basalt in Thailand. *Jour. Geol. Soc. Thailand., Special Issue for III GEOSEA, November, 14-16, 3(1), M4-1-M4-38.*
- Vichit, P., 1992. Gemstone inn Thailand, in *Proceedings of a National Conference on Geologic Resources of Thailand: Potential for Future Development, 17-24 November.* Department of Mineral Resources, Bangkok, Thailand, Supplementary volume, 124-150.
- Bar, S.M. and Macdonald, A.S., 1978. Geochemistry and petrogenesis of late Cenozoic alkaline basalts of Thailand. *Geol. Soc. Malaysia Bull., 10 : 25-52.*
- Bar, S.M. and Macdonald, A.S., 1979. Paleomagnetism age, and geochemistry of the Denchai Basalt, northern Thailand . *Earth and Planetary Science Letters, 46, 113-124.*
- Thayapink, S., Sutthirat, C., 1992. Geological survey of corundum deposits at Wang Chin District and Long District area, Phrae Province. *Economic geology report no. 36/1992, 173 pp (in Thai).*
- Sutthirat, 2001. *Petrogenesis of Mantle and Crustal Xenoliths and Xenocrysts in Basaltic Rocks Associated with Corundum Deposits in Thailand.* Unpublished Ph.D. thesis, University of Manchester.
- Wathanakul, P., Kraisittipong, K., Buenkoontod, P. and Lekkean, M., 2002. Final report on the survey of corundum deposit style of Ban Bo Kaeo, Den Chai District, Phrae Province (in Thai), Kasetsart University Research and Development Institute, 259p.
- Wathanakul, P., Thongvijit, B., Suanburi, D., Lamjuan, A., Nantasin, P., Cheudee, N., and Jenjitphaibun, K., 2004. Spectacular geological feature related to Agro-Eco-Geo Tourism Project, Phrae Province (in Thai), Kasetsart University Research and Development Institute, 105p.

Acknowledgements

The Ministry of Education and Kasetsart University Research and Development Institute (KURDI) are thanked for grant provided. The LA-ICPMS analysis facility was provided by the Gem and Jewelry Institute of Thailand – GIT.

The morphology of natural and synthetic diamonds: remaining challenges

Emmanuel Fritsch¹, Aurélien Delaunay², Benjamin Rondeau³, Ichiro Sunagawa†⁴, Moreton Moore⁵, Thomas Hainschwang⁶

¹ Institut des Matériaux Jean Rouxel (I.M.N.) University of Nantes, Nantes, France; emmanuel.fritsch@cncrs-imn.fr

² LFG, Paris, France. a.delaunay@bjop.fr

³ University of Nantes, Nantes, France. benjamin.rondeau@univ-nantes.fr

⁴ Tokyo, Japan

⁵ Royal Holloway University of London, Egham, Surrey, United Kingdom M.Moore@rhul.ac.uk

⁶ GGTL, Liechtenstein. thomas.hainschwang@ggtl-lab.org

With detailed studies dedicated to the morphological differences between natural and synthetic diamonds, one would think everything is known on the subject. Yet, some remaining challenges appear through the careful observation of rough crystals and the study of rare colored diamonds. In addition, the daily practice of the DiamondView with “normal” near-colorless gem diamonds reveals sometimes unexpected internal morphologies.

We propose a quick overview of diamond morphology before dwelling into what we believe are current challenges. This is in part based on the Sunagawa diagram (Figure 1, after Sunagawa, 2005), detailing the kinds of growth mechanisms found in natural or synthetic crystals, as a function of the growth rate and driving force of crystallization.

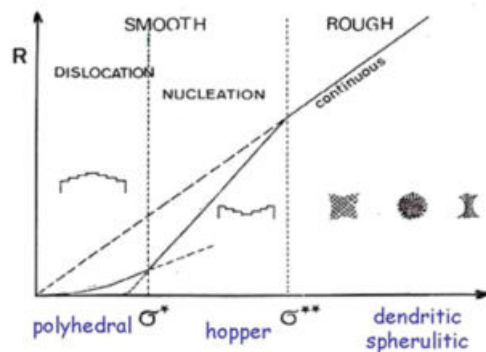


Figure 1. The Sunagawa diagram indicates growth mechanism and “driving force” of crystallization as a function of growth rate (R). after Sunagawa, 2005.

As it is well-known, most gem diamonds experience a regular (111), octahedral growth. Although there are some exceptions, in general, high-quality, high-colour stones show such a regular concentric growth, with only average or little luminescence contrast. This relates to a dislocation-driven, slow growth in a stable environment.

But what about fibrous growth? It is also a (111) growth, however with a fast rate, under an elevated driving force. When it forms the well known cubes from the Democratic Republic of Congo, it could be more adequately called dendritic growth. For balas, the spherical variety of boart, fast growth is spherulitic.

Cube and cuboid growth are very different. Regarding now (100) growth sectors, only cuboid growth is found in the external morphology of natural gem diamonds. These are not true cube faces, with flat, smooth surfaces and straight edges. Rather, they are hummocky or undulating, not flat, and the edges are rounded and curved, not sharp and straight (Figure 2). So (100) growth may be an ambiguous term. A diamond showing exclusively cuboid growth is rare in nature.

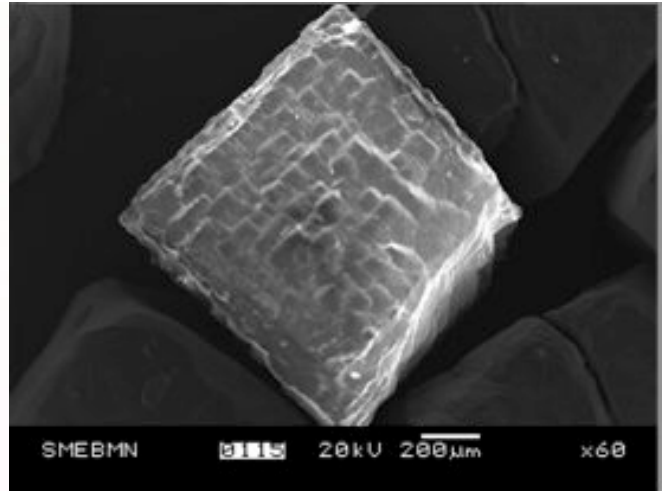
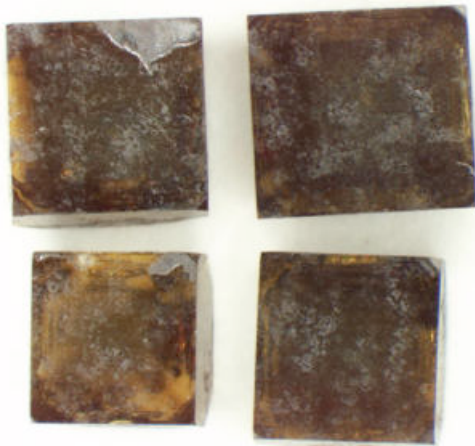


Figure 2. True cubes and cuboids are very different. a) Large true cube sectors are seen only in synthetics, with smooth surface and sharp straight edges. b) Cuboid sectors are undulating - not flat - with only an average (100) orientation, and rounded edges, seen here in a secondary electrons micrograph.

Daily examination of gem diamonds proves also the great importance of mixed octahedral and cuboid growth. It is very common in gems, and can manifest itself in a number of scenarios, in which they alternate or coexist. Alternate octahedral and cuboid growth is most often observed in relatively short successive spurts, sometimes the start is cuboid but octahedral growth takes over, and rarely does the morphology begins octahedral to finish with dominant cuboid features.

Simultaneous octahedral and cuboid growth leads to spectacular asteriated diamonds, but is seen more often than thought in regular gem diamonds of moderate quality and can be followed by octahedral growth. Cuboid sectors contain high concentration of nitrogen, hydrogen and traces of nickel. However, conditions leading to cuboid growth remain a mystery, and it has never been duplicated in the laboratory. Furthermore, there is no equivalent in other materials.

Are there only cuboid sectors in natural diamonds, or could there be also growth on true cube faces as well in natural diamonds? There has been several reports of small cube faces in natural diamonds, but all samples coming from a single mine. We have observed a few more, again in "normal" diamonds. We believe true cube faces may be found very rarely in natural diamonds, as long as they remain very small, typically less than one millimetre in maximum dimension (Figure 3a).

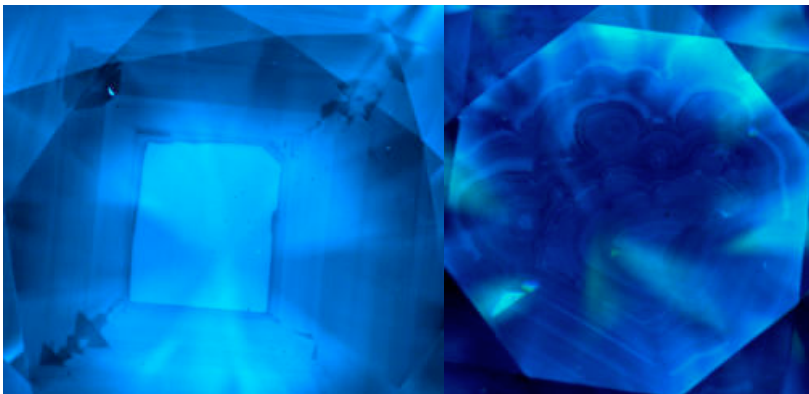


Figure 3. Unusual internal morphologies seen in DiamondView™. left: small true cube faces in a natural diamond, between more luminescent octahedral sectors; right) concretion-like growth.

Looking now at synthetics, grown either by HPHT or CVD, their potential growth sectors are well-known. They develop smooth faces with sharp edges in the octahedral, cubic (Figure 2), dodecahedral and trapezohedral sectors. What would happen if the growth driving force was slightly higher? Could hopper crystals be produced? It appears that hopper crystals are produced in conditions at the limit of the parameter space (for example 1315°C and 5.5 GPa), therefore leading to very low quality crystals, which are typically not documented, even thrown away. So if hopper crystals can be found in synthetics, why have they never been observed in natural crystals? Is it that they would appear in such a small parameter field that it only very rarely occurs, or would they dissolve before reaching the surface?

Finally, some features observed cannot be interpreted using the previous schemes of growth, and reveal generally complex growth phenomena, with exotic events.

Among the most striking are concretion-like growth features (Figure 3b), which do not seem to relate to fibrous growth as they are found in gem-quality, micro inclusion-free diamonds.

References:

Sunagawa I. (2005) Crystals: growth, morphology and perfection. Cambridge University Press, Cambridge UK, 295 p.

The origin of colour and correlated properties of natural type Ib diamonds

Thomas Hainschwang¹, Emmanuel Fritsch², Franck Notari¹, Benjamin Rondeau³, Andrey Katrusha⁴

¹ GGTL Laboratories - GEMLAB (Liechtenstein)/GemTechLab, Liechtenstein and Switzerland
thomas.hainschwang@ggtl-lab.org

² Université de Nantes – CNRS Institut des Matériaux Jean Rouxel (IMN), Nantes, France

³ Université de Nantes – CNRS Laboratoire de Planétologie et Géodynamique de Nantes (LPGN), Nantes, France

⁴ Bakul Institute for Superhard Materials, National Academy of Sciences of Ukraine, Kiev, Ukraine

Single substitutional nitrogen (N0) has a very strong colouring effect in diamonds due to its electron donor properties and the resulting energy level in the band gap at about 1.7 eV. It is common perception that such diamonds are always “canary” yellow, i.e. of strong yellow colouration.

During the study of several hundreds so-called type Ib diamonds (i.e. diamonds with isolated nitrogen – or C centre-detectable via infrared spectroscopy) it became rapidly clear that natural diamonds with dominating C centres are only rarely of pure yellow colour and that the vast majority of purely yellow diamonds are type IaA>>Ib with far higher total nitrogen content than the typical Ib material. By far most natural type Ib diamonds with dominating C centres are mixed colours such as various combinations of yellow, brown, grey and green (“olive”) and combinations of yellow, orange and brown. The rarest colour for such diamonds is “dull” brown, followed by pure yellow. The type Ib stones studied can be subdivided into two basic groups, those of octahedral growth and those of mixed cuboid-octahedral growth. The octahedrally grown diamonds are mostly of very low to moderate nitrogen content (i.e. from about 1 to 100 ppm) and very rarely contain more than 150 ppm of nitrogen. The diamonds of mixed growth generally contain much more nitrogen with the aggregated nitrogen strongly dominating the C centres; the lowest nitrogen content for such diamonds was found at about 100 ppm, and the highest, about 1900 ppm.

In the octahedrally grown type Ib diamonds deformation-related defects are very common while they are virtually absent in mixed growth diamonds that contain C centres. The slip caused by post-growth plastic deformation is directly observable under crossed polarizing filters: strong strain along (111) is evident in most octahedral type Ib diamonds and the more deformed the more distinct the amber centre absorptions in the infrared spectrum. The amber centre infrared absorptions are good indicator for extended defects caused by plastic deformation in type Ia diamonds; it was found to be even more consistently present in deformed type Ib diamonds. Olive and brown type Ib diamonds show the strongest strain under crossed polarizing filters and in consequence the infrared spectra of “olive” and brown type Ib diamonds exhibit far stronger amber centre absorption than orange to yellow samples (Figure 1).

Strain in the mixed growth type Ib diamonds was limited to that created by the mixed growth itself; such growth results in cross-like strain, just like the one known in synthetic diamonds of mixed cubo-octahedral growth. No deformation-related strain could be observed and some of the samples were practically free of strain, just like some synthetic diamonds. It is thus not surprising that none of the mixed growth type Ib diamonds exhibited amber centres in their infrared spectra (Figure 2).

It seems that the vast majority of high nitrogen mixed-growth type Ib diamonds are so-called “re-entrant cubes”; a collection of such re-entrant cube crystals showed very uniform properties and always practically identical infrared spectra such as the ones shown in figure 2. Most bright yellow type Ib diamonds show the “re-entrant cube” type of spectra and properties.

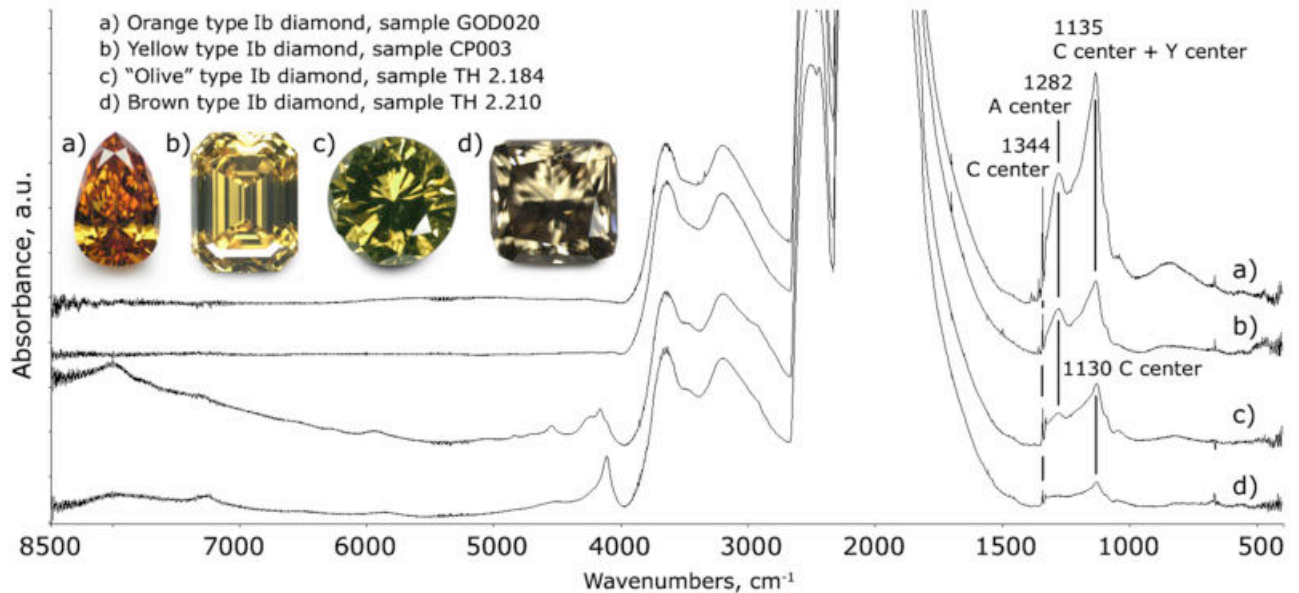


Figure 1. Representative infrared spectra of the different color groups of type Ib diamonds (with C center strongly dominating). Typically the spectra of yellow and orange diamonds (traces a and b) are characterized by one phonon absorption due mainly to C centers with minor A and Y centers, while olive and brown type Ib diamonds (traces c and d) generally lack the Y center and often have lower nitrogen content. The amber center absorption (ranging from about 3400 to 8500 cm^{-1}) is most prominent in olive and brown type Ib diamonds while it is only weak to very weak in orange diamonds and practically absent in yellow samples. The spectra are shifted vertically for clarity.

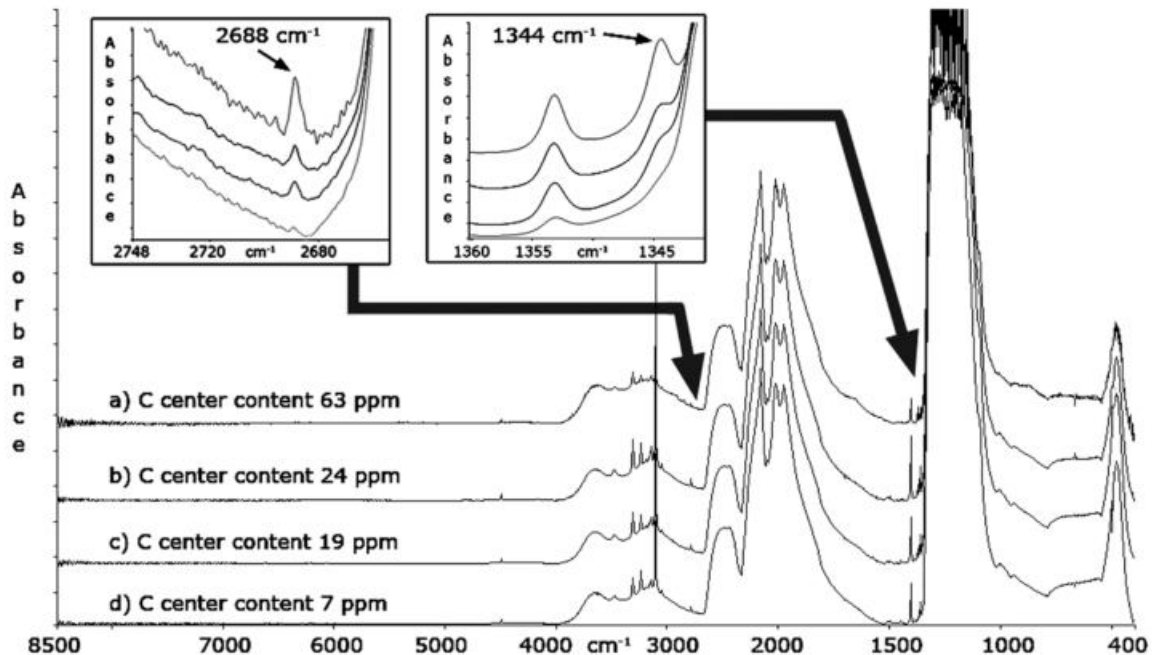


Figure 2. The infrared spectra of four strongly yellow colored re-entrant cube diamonds (resolution 1 cm^{-1}). The spectra show that these diamonds are all extremely similar being type IaA>>Ib with significant concentrations of hydrogen. Additionally the hydrogen signature of all stones are practically identical. The C center content of such stones varies and can sometimes only be determined via the overtone of the 1344 cm^{-1} line at 2688 cm^{-1} since in low C center samples the strong A center absorption hides the 1344 cm^{-1} line. The spectra are shifted vertically for clarity.

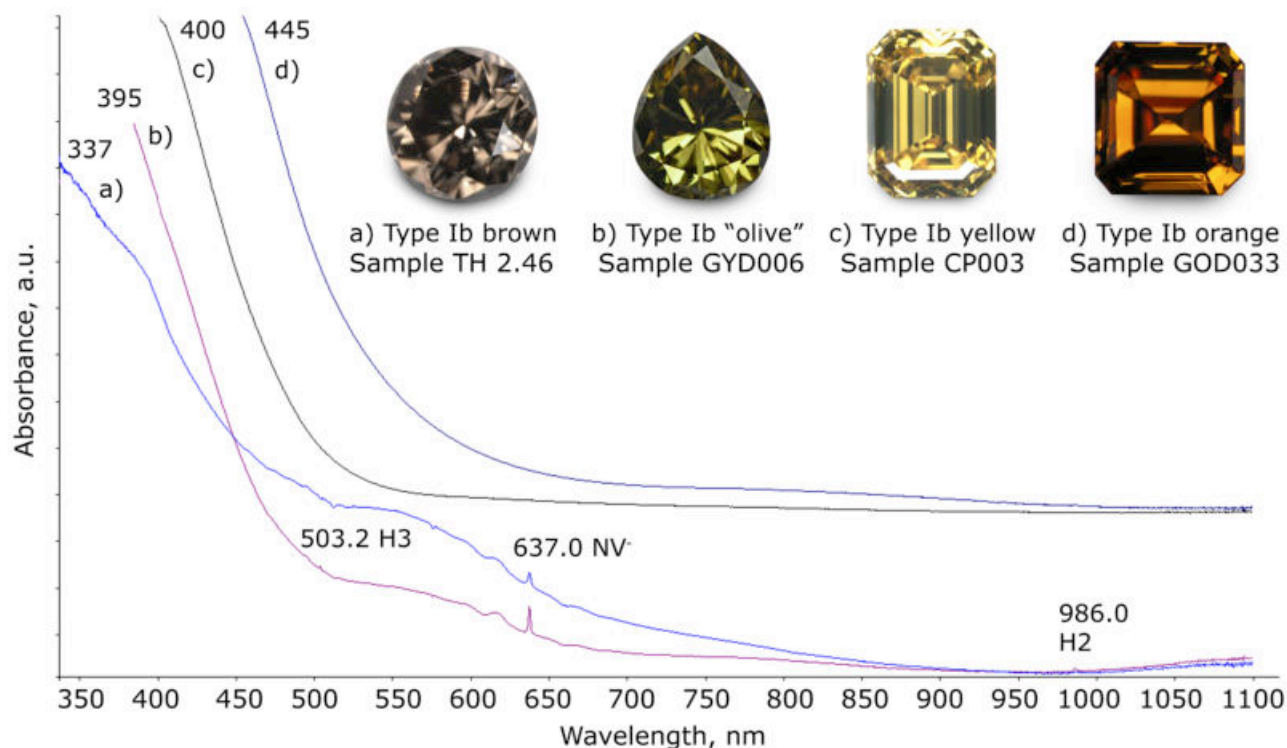


Figure 3. Representative UV-Vis-NIR spectra of the different color groups of type Ib diamonds. It can be seen that the different colors are caused by variations in absorbance of the continuum plus overlaid broad band absorption mainly from the NV- center.

The UV-Vis-NIR spectra of the differently coloured type Ib diamonds all showed a continuum absorption with the cut-off ranging from 450 to 307 nm; yellow to orange diamonds showed no additional colour-causing features while “olive” and brown diamonds all had NV- centre absorption overlaying the continuum (Figure 3). This NV- centre absorption was generally more distinct in the spectra of “olive” diamonds and furthermore most “olive” and brown diamonds also showed some H3 absorption. The spectra of the brown and the olive diamonds had a less steep slope and their cut-off was generally shifted towards the UV, because of their often particularly low nitrogen content. This combination results in their lower colour saturation (brownish appearance); the distinct NV- centre absorptions in the spectra of olive diamonds are responsible for the greenish tint of these stones: a weak, shallow relative transmission window appears in the green, one side due to the continuum, the other due to the NV- centre

In conclusion this study shows that the colours other than yellow in type Ib diamonds are caused by related defects, in combination with the variable C centre content. While many of the colour causing defects could be explained, there still are cases which remain mysterious, such as strongly yellow coloured diamonds with very low C centre content, saturated yellow samples with undetectable C centres (what we call “type Ib character”) and last but not least strongly yellow coloured diamonds defined as type IIa (thus virtually nitrogen-free) by infrared spectroscopy. These diamonds all appear to indicate that there are colour-causing defects that are currently unknown and that cause distinct yellow colouration.

Identification of gem diamonds using high-energy UV luminescence imaging

Hiroshi Kitawaki, Mio Hisanaga, Masahiro Yamamoto

Central Gem Laboratory Tokyo, Japan; kitawaki@cgl.co.jp

Introduction

Diamond has been produced for various industrial uses as it possesses extreme chemical stability and superlative physical properties, and its synthesis is actively ongoing. For the gem uses, commercial production of synthetic diamonds by HPHT and CVD method started in 1990s and 2000s respectively, and soon after that these materials appeared in routine identification work in gem laboratories. In mid-2012, one of the international diamond grading laboratories in Antwerp reported undisclosed CVD synthetic diamond, causing a stir in the diamond industry (Even-Zohar, 2012). Most of such CVD synthetic diamonds were in the range of 0.3 and 0.7 ct in weight initially, but recently larger stones, over 1 ct, are appearing. The procedure for diamond synthesis has dramatically improved recently. Therefore, establishment of identification criteria as well as definite information disclosure is strongly required in the jewellery market.

Samples and Methods

Natural and synthetic diamonds show different crystal morphologies due to their different growth environment. This gives important clues to the distinction between natural and synthetic stones. However, gem diamonds have been already cut and polished thus observation of external form or crystal surface is not possible, and to understand growth history of the crystal, inhomogeneity that has been remaining inside should be investigated. Inhomogeneity in diamond has been studied by various techniques, and non-destructive methods such as cathodoluminescence (CL) analysis or high-energy UV luminescence analysis are effective for gem-quality diamonds (Welbourn et al., 1996). In this study, UV luminescence images observed with DTC DiamondView™ on more than 10,000 natural diamonds and over 500 synthetic diamonds that were submitted to CGL for identification are systematically summarised for the purpose of refining identification criteria for natural/synthetic origin of diamonds (Shigley et al., 1995).

Morphology in Diamond

The morphologies of crystals are controlled both by internal structural factors and by external factors. Theoretically, if one entirely neglects the effect of external factors, morphology is determined by the internal chemical bonding and crystal structure. According to PBC analysis of a diamond crystal, {111} is an F face and grows in spiral growth mechanism under the condition of small driving force to become relatively larger than other faces such as {100} and {110}. Therefore, a typical form of a diamond inferred from the crystal structure is an octahedron surrounded by smooth {111}. Practically, however, natural diamond crystals are often rounded due to dissolution and occasionally show mixed-habit growth in which smooth {111} faces and rough {100} faces coexist (Sunagawa, 1995). In natural diamonds, {100} faces are not cubic faces, but cuboid faces, because they are always rugged, and never appear as flat crystallographic faces.

By contrast, HPHT-grown synthetic diamonds commonly show cubo-octahedral habit in which {111} and {100} are well developed, and they may be accompanied by {110} or {113}. These morphologies are commonly known to vary depending on a number of parameters, but notably on the growth temperature (Yamaoka et al., 1977) and metal solvent. It is also known that, in CVD grown synthetic crystals, {100} behaves as the most stable face morphologically, presumably due to atomic hydrogen which induces a reversal of surface free energy of {111} and {100} (Sunagawa, 2004).

Results and Discussion

Most of colourless to near colourless natural diamonds are formed only of $\{111\}$ faces, and this, together with observation of growth bands, confirms that the crystal growth took place under small driving force and near equilibrium conditions. Nearly all samples show blue-white luminescence due to N3 centre. These images are unique to each stone and can be applied to fingerprint (individual identification) of diamonds (Figure 1).

Natural diamonds showing mixed-habit growth have straight growth bands on $\{111\}$, implying that the crystal had grown with smooth interfaces. However, $\{100\}$ faces are always hummocky and this indicates that they behaved as rough interfaces (Figure 2). From $\{100\}$ sectors, the peaks derived from C-H are typically detected in infrared spectrophotometry, thus presumably a defect containing hydrogen atom was involved in forming the $\{100\}$ sector.

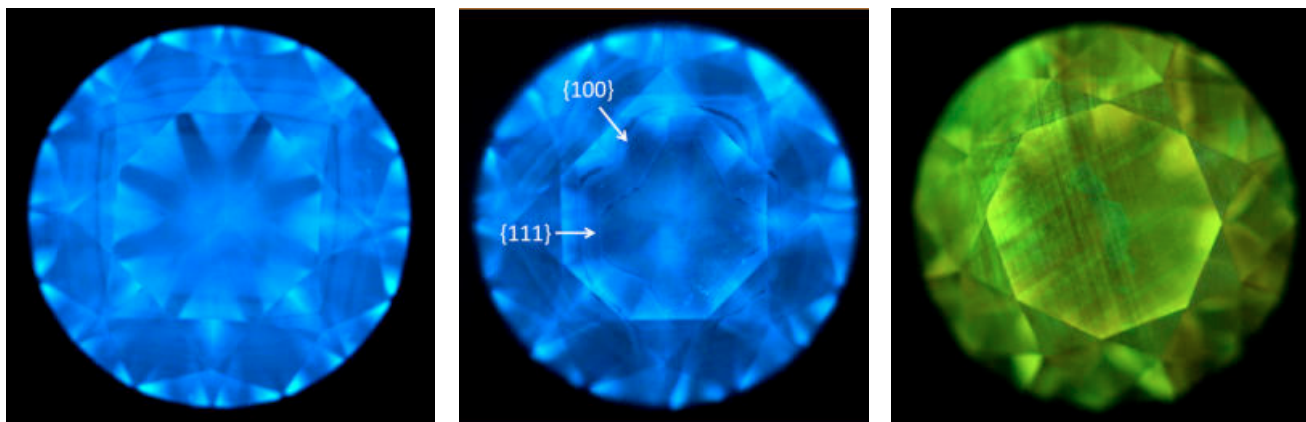


Figure 1 (left): Polygonal growth banding can be seen in type I colourless diamonds. Figure 2 (centre): $\{100\}$ sectors appear always hummocky in mixed-habit growth diamond. Figure 3 (right): Slip lines on 2 intersecting set of $\{111\}$ due to plastic deformation typically seen in type Ib diamonds

In type Ib natural yellow diamonds, slip lines on 2 or 3 intersecting sets of $\{111\}$ planes as well as bright luminescence colour of H3 centre (503,2 nm) are observed (Figure 3). This is thought that diamonds containing small concentration of nitrogen tend to receive the stress of plastic deformation after its growth (Sunagawa, 2001).

Luminescence images of type II natural diamond hardly show growth bands parallel to $\{111\}$ and dot-like or mosaic-like network assumedly formed by plastic deformation are observed. Among them, distinct mosaic patterns are more often observed in the samples with higher colour-grades such as D or E. Type II diamonds also show blue luminescence due to band A in general.

Growth sectors of $\{111\}$ and $\{100\}$ are clearly observed in HPHT-grown synthetic diamonds, and they are often associated with $\{110\}$ and $\{113\}$ sectors. In natural diamonds, $\{100\}$ sectors appear as hummocky (non-straight) growth bands, whereas straight growth bands are observed in $\{100\}$ sectors of HPHT-grown synthetic stones (Figure 4). It is assumed that on the $\{100\}$ surface of a HPHT-grown diamond, reconstruction occurs among carbon atoms and the face changes from K-face to F-face, which grows as a smooth interface (Sunagawa 1995).

In CVD-grown synthetic diamonds, straight or curved striations are observed (Figure 5). These are due to so called Step bunching, which are thought to be formed under the influence of its growth from a seed crystal in $\{100\}$ orientation with off angle as well as its high growth rate by employing nitrogen gas (Tallaire et al., 2006).

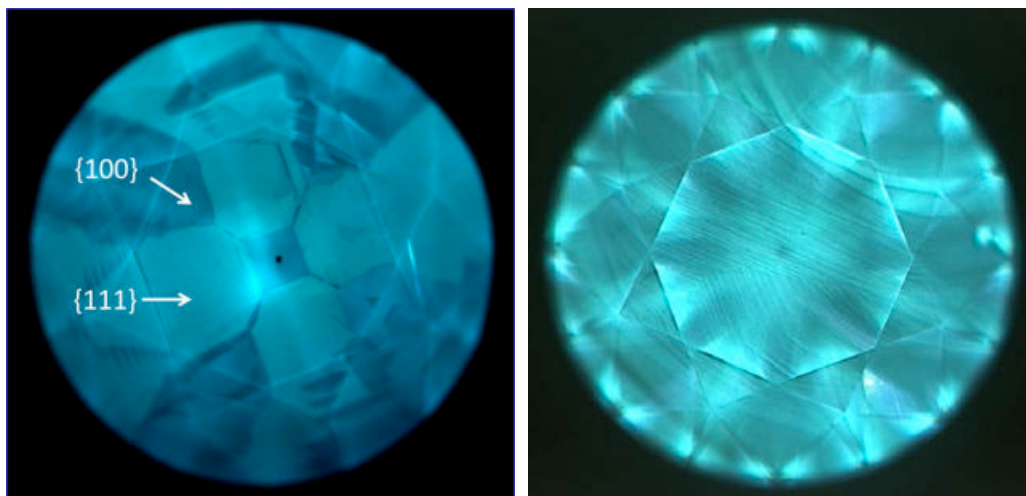


Figure 4 (left): Growth sectors of $\{111\}$ and $\{100\}$ typically seen in HPHT-grown synthetic diamonds (type IIb blue stones).
 Figure 5 (right): Curved striation typically seen in CVD-grown synthetic diamonds (near colourless).

Conclusion

Even in small amount, synthetic diamonds now have been circulated in the gem and jewellery market, and establishment of identification criteria as well as definite information disclosure is strongly required. Although synthetic diamonds are identical with natural diamonds as a material, they have fairly different growth histories. In this study, it has been confirmed that Observation of UV luminescence images is quite effective to find out these differences. Each of natural and synthetic diamond shows unique luminescence images, which give important clues to distinction between them. However, distinct images may not be obtained or their images may closely resemble to each other in some cases, therefore a large number of luminescence images should be observed to establish precise identification criteria on the basis of a theoretical background of crystal growth.

References

- Even-Zohar, C., 2012. Synthetic specifically “made to defraud”. *Diamond Intelligence Briefs*, 27 (709), 7281–7290.
- Song, Z., Lu, T., Lan, Y., Shen, M., Ke, J., Liu, J., Zhang, Y., 2012. The identification features of undisclosed loose and mounted CVD synthetic diamonds which have appeared recently in the NGTC laboratory. *Journal of Gemmology*, 33(1-4), 45-48.
- Shigley, J. E., Fritsch, E., Reinitz, I., Moses, T. M., 1995. A Chart for the separation of natural and synthetic diamonds. *Gems & Gemology*, 31(4), 256-264.
- Sunagawa, I., 1995. The distinction of natural from synthetic diamond. *Journal of Gemmology*, 24(7), 485-499.
- Sunagawa, I., 2001. A discussion on the origin of irregular shapes of type diamonds. *Journal of Gemmology*, 27(7), 417-425.
- Sunagawa, I., 2004. The Morphology of Diamond. *Journal of the Japanese Association for Crystal Growth*, 31(4), 4-10.
- Tallaire, A., Collins, A.T., Charles, D., Achard, J., Sussmann, R., Gicquel, A., Newton, A.M., Cruddace, R.J. M.E., Edmonds, 2006. Characterisation of high-quality thick single-crystal diamond grown by CVD with a low nitrogen addition. *Diamond and Related Materials*, 9, 1439-1449.
- Welbourn, C.M., Cooper, M., Spear P.M., 1996. De Beers natural versus synthetic diamond verification instruments. *Gems & Gemology*, 32(3), 156-169.
- Yamaoka, S., Komatsu, H., Kanda, H., Setaka N., 1977. Growth of diamond with rhombic dodecahedral faces. *Journal of Crystal Growth*, 37, 349-352.

Observations on CVD-grown synthetic diamonds

James E. Shigley

GIA Research, Gemological Institute of America, Carlsbad, California, USA; jshigley@gia.edu

Over the past decade, GIA researchers have examined 193 polished CVD-grown synthetic diamonds as well as a limited number of tabular crystals. The faceted gems were either obtained on loan directly from the manufacturers (Apollo Diamond [now Scio Diamond] and Gemesis Corporation), or were submitted by these same manufacturers (or in a few instances by clients) to the GIA Laboratory for quality grading reports.

“Colorless to Near-Colorless” Samples

Of the 193 samples, 101 (52%) were assigned color grades within the “D-to-Z” color grading system (colorless [D-F] – 29, near colorless [G-J] – 61, faint color [K-M] – 8, and very light color [N-R] – 3, with the sample with the lowest color grade being Q-R). All were type IIa by standard infrared spectroscopy. The samples varied in weight from 0.18 to 1.05 ct (only 2 weighed more than 1 ct), and most were fashioned as round brilliants. The majority of samples were assigned VVS or VS clarity grades (highest clarity grade IF, and lowest I1), with the lower grades usually being the result of the presence of tiny black inclusions of non-diamond carbon. Of the samples, 42 exhibited fluorescence to either standard long- or short-wave ultraviolet lamps with very weak-to-moderate yellow (17), orange (8), or green (17) reactions. In instances of luminescence reactions to both ultraviolet lamps, the intensity of fluorescence was stronger to the short-wave than to the long-wave lamp. 11 of the samples displayed very weak-to-weak yellow phosphorescence after the short-wave ultraviolet lamp was turned off. 54 of the samples were examined with the DiamondView™ instrument, and they exhibited moderate-intensity fluorescence in various colors (red, reddish orange, orange, yellowish or bluish green, greenish blue, or blue). In many cases, this luminescence exhibited a pattern of growth bands parallel to the upper surface of the original tabular crystal. Weak-to-strong, evenly distributed blue phosphorescence was observed using this instrument in 27 of these samples. There was no correlation between fluorescence color or intensity and the color grades of these samples.

Certain spectral features seem to be indicative of colorless to near-colorless CVD synthetic diamonds. In the near-infrared region, they include absorption bands at 5562, 6425, 6855 and 7353 wavenumbers, and photoluminescence emission bands at 534, 543, 546, the 596/597 and 736.6/736.9 doublets, 946 and 951 nanometers. Some of these features have been recorded in the spectra of occasional natural diamonds. The responsible lattice defects for these spectral features are known in some cases but not in others.

“Fancy Color” Samples

The remaining 92 samples (48%) displayed stronger face-up colors. In terms of color hue, 60 were pink (including purplish pink and orangy pink, and 1 that was red), 15 were yellow (including greenish yellow and orangy yellow), 13 were brown (including yellowish brown and orangy brown), and 2 were orange (2 were also gray). Under magnification, their coloration appeared to be evenly distributed with no zoning. Among these samples, the pink, orange and red colors were the result of post-growth HPHT annealing followed by irradiation and low-temperature annealing treatments. Of these 92 samples, 26 were assigned Fancy or Fancy Light grades, and the remainder had Fancy Deep, Fancy Intense, or Fancy Vivid grades. All were type IIa except for the yellow ones most of which were type IIb. They varied in weight from 0.008 to 3.01 ct (with 6 weighing more than 1 ct). Among them, 60 were fashioned as round brilliants and the remainder as one of several fancy shapes. Clarity grades ranged from SI2 to VVS1. Of the samples, 72 exhibited fluorescence to either standard long- or short-wave ultraviolet lamps with very weak-to-very strong orange (51), yellow (13), or red (8) reactions that were often turbid or cloudy in appearance. The pink samples displayed the strongest fluorescence reactions. No phosphorescence was noted. When examined with the DiamondView™ instrument, the

pink samples that were tested displayed moderate-to-strong orange or red luminescence; the other samples displayed weaker luminescence reactions with the same or yellowish green to green colors. Again in many cases, this luminescence exhibited a pattern of parallel growth banding. In a few instances, a second luminescence color (typically blue) was seen as irregular lines or areas that appeared to originate from a pattern of dislocation networks.

Spectral features seen in various pink CVD synthetic diamonds include absorption bands at 1295, 1332, 1344, 1352, 1362, 1371, 1405, 1450, 1502, 3107, 3123, 4337, 4672, 4888, 5219, 6963, 7353, 7533 and 7804 wavenumbers in the infrared and near-infrared, as well as photoluminescence bands 389, 415, 503, 540, 575, 637, the 736.6/736.9 doublet, 850, 875 and 946 nanometers.

Conclusion

The identification of CVD-grown synthetic diamonds presents more difficulties for gemologists because of the absence of diagnostic visual features that can be observed with the microscope, and the more limited amount of published information because fewer samples have been available for detailed study. Nonetheless, the strong and often banded luminescence colors such as orange, red and green, combined with distinctive infrared and photoluminescence spectral features, provide means for their detection by gemological laboratories that have a database of information on the corresponding properties of natural diamonds.

Yellow blue bicoloured sapphires from Chinnadharapuram, South India

Jayshree Panjekar, Aatish Panjekar

Pangem Testing Laboratory, Pune, PANGEMTECH – Panjekar Gem Research & Tech Institute, Pune, India
jayshreepanjekar@gmail.com

Introduction

Yellow blue bicoloured sapphires are regularly found in Chinnadharapuram (10085':77085') in the Karur district of Tamil Nadu. The state of Tamil Nadu formerly known as Madras state lies on the southern tip of the Indian Peninsula. Numerous deposits of corundum in this region are the *raison d'être* for the fact that the term "corundum" originates from the word "kuruntam" in the Tamil language. Corundum occurs in definite bands of anorthosites which border the serpentinised dunite. Bi-colored yellow-blue, blue green corundum transparent crystals (Figure 1 and 2) as well as faceted specimen (Figure 3) were personally collected by the first author from source in Chinnadharapuram and the results of the investigation carried out on these corundum have been reported.



Figure 1. Bi-coloured sapphire 28.6ct.



Figure 2. Rough material 386 carats.



Figure 3. Blue-yellow sapphire 6.78carats.

Materials and methods

Specimens with inclusions were selected and examined by standard gemmological methods to determine their optical properties (refractive indices, birefringence and pleochroism, specific gravity, UV fluorescence etc). In depth study of the internal features was done using gemmological microscopes. Laser Raman Spectroscopy was used and the microscopic inclusions near surface were investigated. Qualitative chemical analyses were performed on faceted samples using an EDXRF to determine the elements. Quantitative electron microprobe analyses carried out on some of the selected samples on 4 points for each color. Un-polarized spectroscopic measurements over the near-infrared ($9000\text{--}4000\text{ cm}^{-1}$) and mid-infrared ($4000\text{--}1500\text{ cm}^{-1}$) ranges were carried out on using a Nicolet Nexus Fourier transform infrared (FTIR) spectrometer equipped with a diffuse reflectance accessory (DRIFT) and operating with a resolution of 4 cm^{-1} . Polarized ultraviolet-visible-near infrared (UV-VIS-NIR) spectroscopic measurements covering the $250\text{--}3300\text{ nm}$ range were performed with a Perkin Elmer Lambda 950 spectrometer on all samples. Sapphires were analyzed by LIBS to check if they contained any beryllium. All faceted stones were checked with SSEF Diamond Spotter to see whether they transmitted UV light.

Results

Visual Appearance

The Chinnadharapuram yellow-blue bicoloured sapphire typically ranges from bright yellow blue to light greenish yellow blue of low to moderate saturation with a light to medium-dark tone.

Gemmological Properties

Specific Gravity was found to be in the range of 3.92 to 4.01, refractive indices fell in the range n_o 1.766 to 1.772 and n_e 1.758-1.764 with a negative birefringence of 0.008. All samples were inert to both LWUV and SWUV.

Microscopic Observation

The natural yellow-blue sapphires in this study had a wide variety of internal features indicative of their metamorphic origin: silk, crystals of zircon (Figure 4), mica flakes (Figure 5), ilmenite (Figure 6), feldspar (Figure 7), apatite (Figure 8), corundum-daughter crystals, liquid-filled feathers, various patterns of healed feathers, feathers around crystalline inclusions, feathers with liquid films, feathers with two phase inclusions, color zoning (Figure 9) and growth structures. Electron microprobe analyses results showed that the Fe_2O_3 weight% content was high 0.68 to 1.10 weight% for the blue portion, about 0.43 to .86 weight % for the yellow to yellow green portion. Titanium was also detected in all of the samples in the range of 0.10 to 0.15 weight %. The vanadium and gallium concentrations were very low about 0.02% and 0.03 weight % respectively.

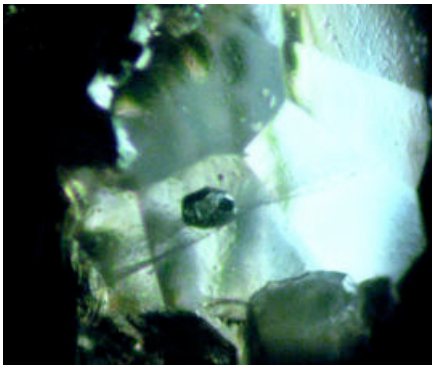


Figure 4. Zircon Crystal.

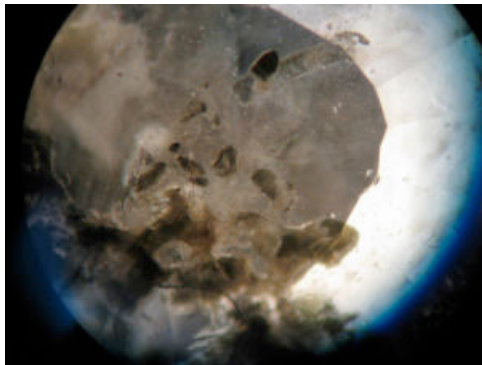


Figure 5. Mica Crystals.

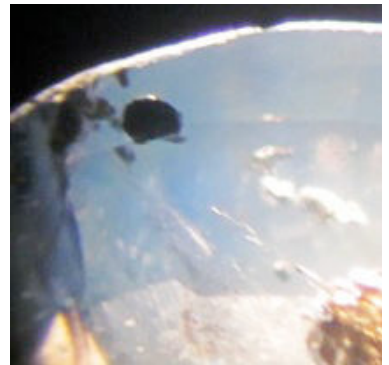


Figure 6. Ilmenite Crystals.



Figure 7. Feldspar Crystal.



Figure 8. Apatite crystals.

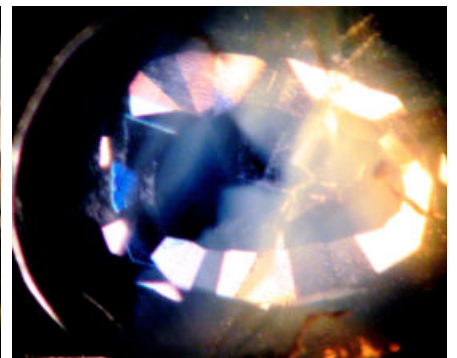


Figure 9. Bi-colour distinct zones.

Spectroscopy

The Chinnadharapuram yellow-blue sapphires exhibit characteristic UV-Vis-NIR absorption spectra in both blue and the yellow portions dominated by the three essential absorption mechanisms Fe^{3+} bands at 376nm, 387nm, and in the visible region at 451nm. The Fe^{2+} - Ti^{4+} IVCT broad-bands centered at 584nm and the Fe^{2+} - Fe^{3+} IVCT in the infrared region from 700nm to 800nm (Figure 10). Unlike the basaltic sapphires the Fe^{2+} - Fe^{3+} IVCT in the infrared region are not very pronounced indicating a metamorphic origin. The FTIR spectra in the mid-infrared region between 4000 and 1500 cm^{-1} show the prominent OH peak positioned at 3309 cm^{-1} and other major peak at 3232 cm^{-1} and a combination of peaks at 3395 cm^{-1} and 3185 cm^{-1} which are of unknown phases. A small peak at 2340 cm^{-1} generally assigned to CO_2 was also detected.

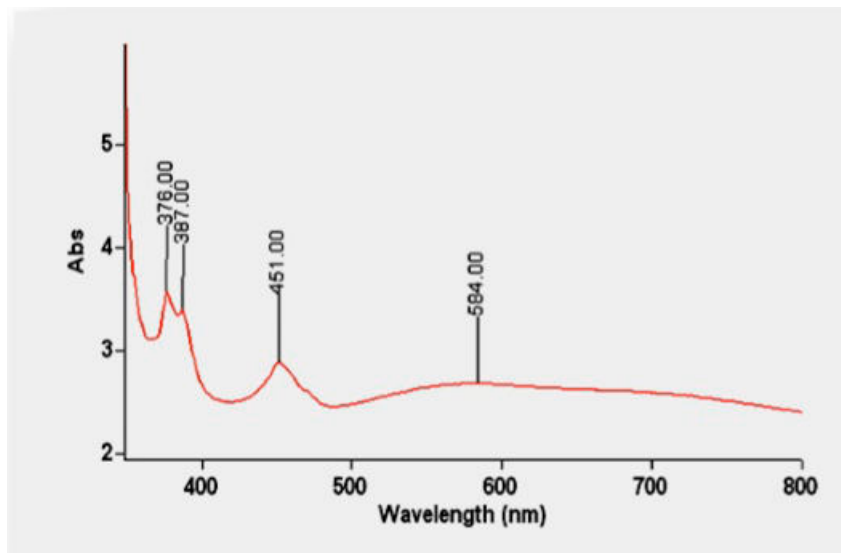


Figure 10. UV-Vis-NIR spectrum of Chinnadharapuram yellow-blue sapphires

Discussion

The bicoloured corundum are found in the anorthosite which were emplaced during the Archaean eon (ca 3,800-2,400 Ma), although most have been dated between 3,200 and 2,800 Ma. Their most characteristic feature is the presence of megacrysts of feldspars surrounded by a fine-grained mafic groundmass. These Archean anorthosites have large amounts of aluminium substituting for silicon which give rise to yellow crystals of corundum. The bi-colouration in the corundum results from the presence of titanium in the titanium-bearing oxide ilmenite in anorthosite bodies. The bi-coloured yellow blue sapphires occur in two types as intergrowths representing two distinct growth phases separated by sharp demarcation in their internal features and secondly as single crystals with clear yellow colour slowly grading into yellowish green to blue. Although both types are found in the same area there may have been time lapse between their emplacements.

Conclusions

Natural yellow-blue sapphires from Chinnadharapuram in South India have characteristic inclusions and features. They may be readily distinguished using a combination of gemmological, chemical and spectroscopic features. UV-VIS and FTIR spectroscopy, chemical analysis, can provide clear proof of their metamorphic origin.

References

- Balmer, W., Leelawatanasuk, T., Atichat, W., Wathanakul, P., Somboon, C., 2006. Update on FTIR characteristics of heated and unheated yellow sapphire. GIT2006 Conference, Bangkok, December 6–7, p. 91.
- Peucat, J.J., Ruffault, P., Fritsch, E., Bouhnik-Le Coz, M., Simonet, C., Lasnier, B., 2007. Ga/Mg ratio as a new geochemical tool to differentiate magmatic from metamorphic blue sapphires. *Lithos*, 98, 261–274.
- Ramakrishnan, M., Vaidyanadhan, R., 2010. *Geology of India*, Vol. 1, Geological Society of India publication, 376-379.
- Schmetzer, K., Bosshart, G., Haenni, H. A., 1983. Naturally coloured and treated yellow and orange brown sapphires. *Journal of Gemmology*, 18(76), 607-622.
- Schmetzer, K., Medenbach, O. 1988. Examination of three-phase inclusions in colorless, yellow and blue sapphires from Sri Lanka. *Gems & Gemology* 24(2) 107-111.
- Smith C.P., Van der Bogert C. 2006. Infrared spectra of gem corundum. *Gems and Gemology*, 42, (3), 92–93.
- Thanasuthipitak, P., Kulsrisuwan, P., Zoysa, G., Thanasuthipitak, T. 2013. Bi coloured sapphires from basaltic and metamorphic affiliations. Abstract Proceedings IGC 2011, Switzerland 188-191.

Acknowledgements

Authors thank Ms Nirmala, of Mettupalayam for the invaluable help to visit the location and collect samples. Authors express their gratitude to Indian Diamond Institute, National Chemical Laboratory, Dept. of Geology, University of Pune and their scientists for carrying out the analyses.

Characteristics of sapphires from the Kyat Pyin area, West Mogok, Burma (Myanmar)

Hpone-Phyo Kan-Nyunt¹, Lore Kiefert², Stefanos Karamelas²

¹Gübelin Gem Lab Ltd., Room 1005, 10/F, Aon China Building, 29 Queen's Road, Central, Hong Kong

²Gübelin Gem Lab Ltd., Maihofstrasse 102, Lucerne 6006, Switzerland l.kiefert@gubelingemlab.ch

The area of the Mogok stone tract, famous for its rubies and sapphires for centuries, spreads over nearly 100 km from east to west and 30 km from north to south. The Mogok stone tract can be divided into 4 areas: 1. Thabeik Kyin Township situated to the far west of Mogok, 2. Kyat Pyin located west of Mogok, 3. Mogok itself, and 4. the Momeik mining area, which is situated to the east of Mogok. Each of these large areas can be subdivided into several smaller mining areas, which contain numerous artisanal to larger scale mines producing various types of gemstones, mainly ruby and sapphire. The Kyat Pyin area, to the west of Mogok, contains one of the currently most active mining areas for Burma blue sapphire (Baw Mar mining area). While for years this mining area was worked by several artisanal operations, they are recently combined to one large operation.

Thirty unheated rough and faceted blue sapphires of gem quality, ranging from 0.03 to 2.3 cts, from this region, directly purchased at the mine, at the end of 2012, were selected for this preliminary work. The internal features and luminescence of all samples were studied using a gemological microscope and a short wave- and long wave-UV lamp (6 watt), respectively. Polarized UV-Vis-NIR (from 280 to 1400 nm; SBW/DI: 0.5, scan rate: 100 nm/min), and FTIR spectra (from 400 to 6000 cm⁻¹; resolution: 4 cm⁻¹, 60 scans) as well as EDXRF analysis using various energies were acquired on all samples.

Besides the «classic» inclusions in sapphires from Burma (see some examples in Gübelin & Koivula, 1986; Smith, 2010), some sapphires from the Baw Mar mine are marked by a relatively «clean» appearance, with twinning in 2-3 directions as the most frequent feature (Figure 1). At the intersections of twin planes, boehmite «needles» parallel to each other (Figure 2), or forming a three-dimensional pattern, are observed. In addition to healed fissures and rutile needles, which are rather infrequently observed in the studied samples, the sapphires often show rutile platelets (Figure 3). Generally, they have a high transparency with good saturation and medium to dark tone. All samples were inert both to long wave and short wave UV light.



Figure 1. Twin planes in a sapphire from the Kyat Pyin area, Mogok, Burma. - Magnification 5x. Photo: Hpone-Phyo Kan-Nyunt, Gübelin Gem Lab Ltd.



Figure 2. At the intersection of perpendicular twin planes, these intersection «needles», most likely of boehmite (not identified), can be found. - 45x. Photo: Hpone-Phyo Kan-Nyunt, Gübelin Gem Lab

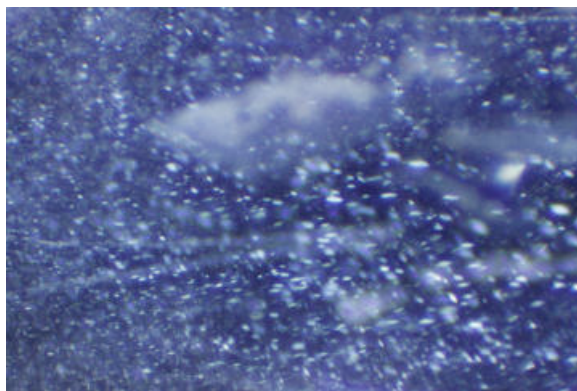


Figure 3. Small reflective platelets, most likely of rutile (not identified), in a sapphire from the Kyat Pyin area, Mogok, Burma. - 65x. Photo: Hpone-Phyo Kan-Nyunt, Gübelin Gem Lab Ltd.

EDXRF analysis of the sapphires from the Baw Mar mine show a chemical composition which resembles that of sapphires from a basaltic source with high Fe_2O_3 contents between 0.4 and 1%, with an average of 0.6-0.7%. Ga_2O_3 contents are between 60 and 250 ppm, with an average of 150-160 ppm. All other relevant trace elements are below the detection limit (Cr_2O_3 , V_2O_5 , TiO_2), with only TiO_2 occasionally showing values up to 80 ppm; preliminary LA-ICP-MS data confirm these results.

In contrast to the «classic» Burma sapphires (Hänni, 1994), the UV-Vis spectra of samples from Baw Mar give «intense» Fe^{3+} attributed absorption peak series at around 380 and 450 nm (Figure 4 and 5). Some samples also do not show a shoulder in the UV region when normalized, meaning the shoulder is much more intense than in the «classic» samples (see again some examples in Hänni, 1994). The area in the near infrared (NIR) where absorptions attributed to $\text{Fe}^{2+}/\text{Fe}^{3+}$ pairs are located varies greatly (see again Figure 4 and 5) and can in some cases be mistaken for spectra of basaltic sapphires (Kiefert, 1987).

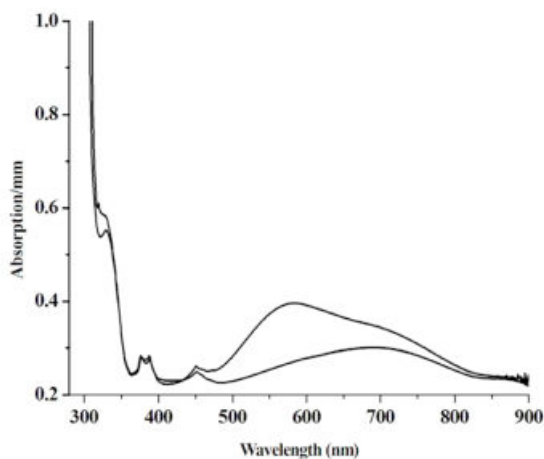


Figure 4. UV-Vis-NIR spectrum of a sapphire from the Kyat Pyin area, Mogok, Burma. The spectrum shown resembles the «classic» sapphire spectra of Burmese sapphires, except for the «intense» Fe^{3+} related absorption series around 380 and 450 nm.

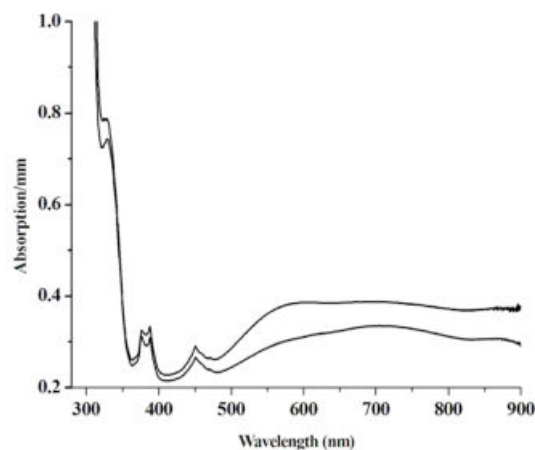


Figure 5. UV-Vis-NIR spectrum of a sapphire from the Kyat Pyin area, Mogok, Burma. This spectrum shows strong absorptions in the near infrared, probably due to $\text{Fe}^{2+}/\text{Fe}^{3+}$, which resembles that of a basaltic sapphire.

The FTIR spectra of sapphires from the Baw Mar mine mainly reflect the inclusions found within the stones. The most frequent absorption bands encountered are situated at the «water region» (3800 to 3000 cm^{-1}) and are most likely derived from hydroxyl related vibrations in boehmite, which is present in samples with intersecting twin planes. In addition, goethite and kaolinite hydroxyl related absorption bands could be observed either in conjunction or as isolated features.

Sapphires from the Baw Mar mine in the Kyat Pyin area west of Mogok will most likely be seen more and more in the trade, as this mine is becoming one of the largest mining operations with an auction every 3 months taking place in the Baw Mar Company in the Mogok area. The last auction took place in June 2013. Sometimes, the inclusion scene and appearance are consistent with classic Burmese sapphires. However, several sapphires from the Baw Mar mine show features that are not observed in those, such as a high Fe_2O_3 content, a dearth of inclusions, and UV-Vis spectra sometimes resembling the ones from basaltic sources. These characteristics sometimes make their identification difficult. Our research team is currently studying a larger sampling to compare it with samples from other mines in different countries and geological environments, in order to better understand the differences, when present.

References

Gübelin, E.J., Koivula, J.I., 1986: Photoatlas of Inclusions in Gemstones, Vol. 1. - Opinio Verlag, Basel, Switzerland, 532 pp.

Hänni H.A., 1994.: Origin determination for gemstones: Possibilities, restrictions, and reliability. - J.Gemm., 24(3), 139-148.

Kiefert L., 1987: Mineralogische Untersuchungen zur Charakterisierung und Unterscheidung natürlicher und synthetischer Saphire. - Diplomarbeit, Mineralogisch-Petrographisches Institut der Universität Heidelberg, 203 pp.

Smith, Christopher P. 2010: Inside sapphires. Rapaport Diamond Report, pp. 123-132.

The potential for Co-diffusion in sapphire

Shane McClure

GIA Laboratory, Carlsbad California, USA; smcclure@gia.edu

Titanium diffusion of sapphire to create blue color has been known in the gemstone industry since the 1980's (Kane et al, 1990). Once recognized, identification criteria were quickly formed and recognizing these treated stones was not difficult to informed gemologists. The layer of blue color was typically very shallow and necessary repolishing after treatment often produced a patchy facet related color. Immersion in methylene iodide also revealed color reinforcement of facet junctions and unusual high relief compared to untreated stones, all of which served to identify the treatment (Nassau, 1981).

Identification became a bit more difficult in the early 1990's with the advent of what was referred to as "deep diffusion". Much longer heating times allowed the titanium to diffuse farther into a stone. The deeper layer eliminated the patchy facet related color caused by recutting. It became necessary to immerse such stones in methylene iodide to see the artificial color layer. Without such immersion the treatment was almost impossible to detect (Kane et al, 1990). In the 1990's titanium diffused sapphires largely disappeared from the market. This changed recently and many have been seen over the last three years. Large sizes have been common with the largest we have seen being over 70 carats. The diffused color layer of the majority of these stones was very thin, making the identification of the treatment simple (figure 1). However, many of these stones were very clean – even large ones – which would be extremely rare in natural sapphires.



Figure 1. These new synthetic diffused sapphires showed distinct patchy coloration in immersion, making the fairly easy to identify. Mag. 10X, Photomicrograph by Shane McClure.

One point that was always an issue with titanium diffused sapphires was determining whether the starting material was natural or synthetic. Diffused synthetic sapphires have been reported as early as 1982 (Fryer et al., 1982) but in our experience there was never a lot of them on the market. If a stone had no inclusions or color zoning it became very difficult to make the separation. Other methods of identification of colorless sapphire, such as ultraviolet fluorescence and short wave ultraviolet transparency, did not work very well because of the layer of diffused titanium, which tended to affect these properties. For those who knew how, looking of Plato lines was effective but this technique was often not remembered and not easy to master. Plato lines are a type of polysynthetic twinning that in our experience only occurs in synthetic corundum. To see these lines it is necessary to view the stone under crossed polaroid filters down the optic axis while immersed in methylene iodide (Plato, 1952).

In such cases laboratories would often resort to EDXRF, looking for chemistry that was indicative of a natural stone. Titanium levels would obviously be elevated, but the presence of trace elements such as gallium, vanadium, chromium or higher levels of iron were considered to be indicative of a natural stone. The chemistry of synthetic colorless sapphire is typically very simple, with no trace elements present except perhaps small amounts of iron. A study done by Elen and Fritsch (1999) on the identification of colorless sapphire lists EDXRF chemistry for a large group of natu-

ral and synthetic samples using electron microprobe. The study shows V, Cr, and Ga to be below detection limits on almost all the synthetic stones, whereas all of these elements were present to some degree in the natural stones. Fe was either below detection limits or up to approximately 50 ppmw in the synthetics.

One stone in particular drew our attention. The stone weighed 8.66 carats, was obviously titanium diffused and had no inclusions or color zoning. The presence of Plato lines indicated the stone was synthetic, but chemistry in the EDXRF and subsequently in the LA-ICP-MS using our standard testing procedures (three spots along the girdle approximately 50 microns in diameter by 20 microns deep) indicated the stone was natural. It had high levels of Fe and low but distinct concentrations of Ga and V along with several other elements. In our experience, Plato lines are not found in natural stones and we know that large flawless colorless natural sapphires are rare. When the chemistry seemed contradict the synthetic conclusion we felt there must be something wrong. The stone was put back in the LA-ICP-MS, but this time an analysis was performed up to four times on the same spot, in effect penetrating approximately 60 microns into the stone in three steps.

The concentration of the elements in question dropped off significantly with depth, indicating these concentrations were related to the diffused layer. Iron concentrations dropped from a high of approximately 2800ppmw to zero or nearly zero by the fourth spot (figure 2). At the same time, gallium concentrations dropped from a high of approximately 21ppmw to 2-3ppmw by the fourth spot. Beryllium was also detected but only to a maximum of 10ppmw in one stone and all dropped off to zero by the third spot. We subsequently acquired some samples of Ti diffused synthetic sapphires (represented as such) in Bangkok and cut a slice out of the middle of one (figure 3). A depth profile run on the LA-ICP-MS once again confirmed that all of these elements were related to the diffused layer.

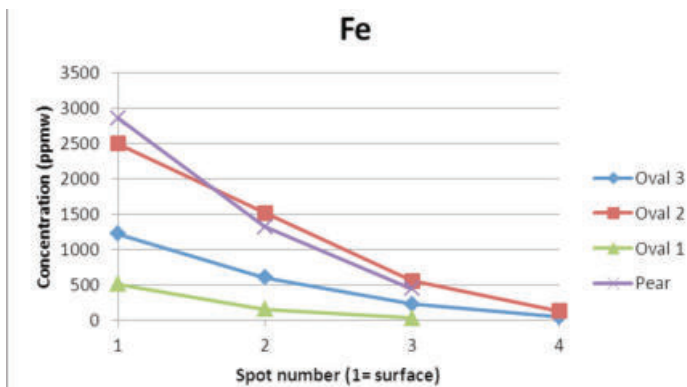


Figure 2. A graph of the Fe content of four samples in relation to the number of times the analysis was taken in the same spot clearly shows a relationship to the surface diffused layer.



Figure 3. Ti diffused synthetic sapphires (represented as such) were acquired in Bangkok, from which a slice was cut out of the middle of one.

Subsequently we had the opportunity to examine another Ti diffused sapphire with somewhat different characteristics. This stone had a much deeper diffusion layer comparable to the "deep diffused" stones described earlier (figure 4). This stone however was also clearly beryllium diffused. Sapphires diffused with both Be and Ti have been reported before (Dutoit, 2009) but this was in stones that were clearly natural. This stone had a much higher concentration of Be compared to the other synthetic stones mentioned earlier.

The typical reinforcement of facet junctions one expects to see in immersion was almost not present and there was no patchy color because the color layer was too deep (figure 5). Close observation in immersion revealed what could have been a very thin colorless layer at the surface but it was too thin to be certain of its presence.

So what is going on here? We have elements diffusing far enough into sapphire to fool an XRF that we have not typically thought of as diffusible. In addition, we have one example of titanium diffusing many times farther into a stone when beryllium was diffused at the same time.

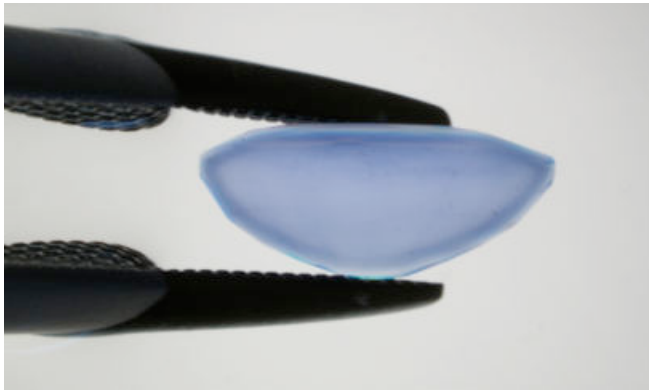


Figure 4. This stone that was submitted to the laboratory clearly showed a much deeper diffusion layer in immersion, Mag. 10X, photomicrograph by Nathan Renfro.

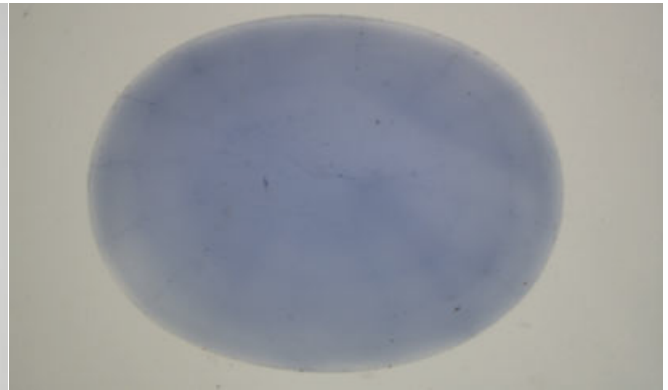


Figure 5. The sapphire with the deeper layer showed almost none of the typical identification features such as patchy color or reinforcement of facet junctions. Mag. 10X, photomicrograph by Nathan Renfro

A likely explanation is a mechanism called co-diffusion, meaning the diffusion of one element facilitating the diffusion of another. A search of the literature has shown that very little research has been done on the subject and we could find none pertaining to corundum. What there is refers to erbium-titanium co-diffusion into lithium niobate (Caccavale et al, 1998; Gill et al, 1992).

Can diffusing Ti into sapphire help elements such as Fe, Ga, Cr and V diffused farther into the stone than they would have otherwise? Can diffusion of Be at the same time as Ti cause the Ti to travel farther into the stone? At this point we don't know. At the time of this writing experiments are being started to try and answer these questions. This is clearly a question we should try to answer, not only from the standpoint of the identification issues it raises for gemological laboratories and therefore also the jewelry industry.

References

- Caccavale F., Segato F., Mansour I., Almeida J., Leite A., 1998. Secondary ion mass spectrometry study of erbium diffusion in lithium niobate crystals. *Journal of Materials Research*, Vol. 13 (6), 1672-1678.
- Dutoit G., 2009. Lab Notes: Blue sapphires diffusion treated with both titanium and beryllium. *Gems & Gemology*, 45 (4), 293-294.
- Elen S., Fritsch E., 1999. The separation of natural from synthetic colorless sapphire. *Gems & Gemology*, 35 (1), 30-41.
- Fryer C.W., Crowningshield R., Hurwit K., Kane R., 1982. Gem Trade Lab Notes: Treated synthetic sapphire. *Gems & Gemology*, 18 (2), 107.
- Gill D., Aaron J., McCaughan L., Wright J., 1992. Method for the local incorporation of Er into LiNbO₃ guided wave optic devices by Ti co-diffusion. *Applied Physics Lett.* 60 (9), 1067-1069.
- Kane R.E., Kammerling R.C., Koivula J.I., Shigley J.E., Fritsch E., 1990. The identification of blue diffusion – treated sapphires. *Gems & Gemology*, 26 (2), 115-133.
- Nassau K., 1981. Heat treating ruby and sapphire: technical aspects. *Gems & Gemology*, 17 (3), 121-131.
- Plato W., 1952. Oriented lines in synthetic corundum. *Gems and Gemology*, 7 (7), 223-224 (translated from the German and originally published in *Edelsteine und Schmuck*).

Acknowledgements

The author would like to thank Dr. Andy Shen for his invaluable help with the chemical data, Nathan Renfro for his help with sample acquisition and preparation and Dr. John Emmett for his help and advice.

The present situation of Beryllium diffused corundum

Kentaro Emori, Hiroshi Kitawaki, Makoto Okano

Central Gem Laboratory, Tokyo, Japan, emori@cgl.co.jp

Since September 2001, some vivid color of orangey red, orange, pink and yellow sapphires appeared on the market. It was the concern of the jewelry branch that many orangey pink to pinkish orange (“padparadscha”-like) sapphires are distributed that have a surface-conformed layer which is not caused by the conventional heat treatment. Intense research by the international laboratories elucidated that this layer is made by a new heating process called Be-diffusion treatment in which the light element beryllium (Be) diffuses into the sapphires from surrounding chrysoberyl crystals in the crucible (Emmett et al., 2003). Nowadays this Be-diffusion treatment is also applied to some violet, green and blue sapphires. Identification of the Be-diffusion treated corundum requires sophisticated methods of chemical analysis such as secondary ion mass spectroscopy (SIMS) or laser ablation-inductively coupled plasma-mass spectrometry (LA-ICP-MS) to detect the trace levels of Be that are indicative of this treatment. Beryllium is a light element that is not detectable by standard analytical methods used in gemological laboratories. In recent years, LA-ICP-MS has been introduced as a tool in advanced laboratories, and is utilized in daily work (Abduriyim & Kitawaki, 2006). Since the beryllium diffused corundum became apparent, the presence of beryllium in corundum has been evidence of a Be-diffusion treatment. But in recent studies, trace amounts of natural beryllium are sometimes detected in untreated corundum. In this study, we measured more than 1000 corundum samples submitted to CGL in 2012 and report the present situation of Be-diffusion treated corundum and untreated corundum containing trace amounts of natural beryllium.

To measure beryllium, we used the LA-ICP-MS system, Laser ablation as NEW WAVE UP-213 and ICP-MS as Agilent 7500a. Analysis conditions were as follows: Laser ablation setting: laser wavelength 213 nm, crater size 15 μm (sometimes use 30 μm), laser power 0.025 mJ, laser frequency 10 Hz, ICP-MS setting: ICP 27.15 MHz, RF Power 1200 W, Plasma gas (Ar) 14.93 l/min, Auxiliary gas (Ar) 0.89 l/min, Carrier gas (Ar) 1.44 l/min.

The color variations of corundum submitted to the Central Gem Laboratory (CGL) in 2012 were blue 30.5%, yellow or golden 3.5%, pink to orange 22.6%, red (including ruby) 40.8% and others 2.5%. This ratio was almost the same as the one of corundum circulated in Japan. At CGL, the LA-ICP-MS measurements were done on corundum, other stones were clearly judged by standard identification methods such as FT-IR. There were corundum samples which were not measured by LA-ICP-MS because the customer did not agree or difficulties in sample settings occurred. In the result, 2.2% of the measured corundum could not be determined as Be-diffusion treated or not. The color variation of the unidentified corundum is blue 35.9%, yellow or golden 38.8%, pink to orange 12.9%, red (including ruby) 8.0% and others 4.4%. Be-treated corundum which was determined by standard identification methods or LA-ICP-MS is 1.5%, and color variation is as follows: blue 4.3%, yellow or golden 26.1%, pink to orange 58.6%, red (including ruby) 10.9% and others 0% (Figure 1).

In the result of LA-ICP-MS analysis, the average of beryllium concentrations in Be-treated blue sapphires is 9.23 ppm, yellow or golden 0.42 ppm, pink to orange 10.27 ppm and red (including ruby) 11.42 ppm. In Be-treated corundum, the beryllium concentration is 10 ppm on an average regardless of color variation. This is almost identical with Be-treated corundum obtained directly from the treating company in Thailand (Bangkok) in 2007.

There were some sapphires in which beryllium was detected by LA-ICP-MS, but its origin was determined to be natural by color-zoning and other identification methods. It is reported that niobium (Nb), tantalum (Ta) and thorium (Th) are detected along with beryllium in natural blue sapphire, and zirconium (Zr), hafnium (Hf) and tungsten (W) are detected along with beryllium in natural yellow sapphire (Shen et al., 2009). For example, in golden sapphire (16.949

ct, oval mixed cut), 8 spots around the girdle of this stone were analyzed by LA-ICP-MS and beryllium was present in 8 of these; beryllium concentrations were 1.42 ppm to 7.14 ppm and there were proportional relationships between beryllium, zirconium, and hafnium in each spot (Figure 2).

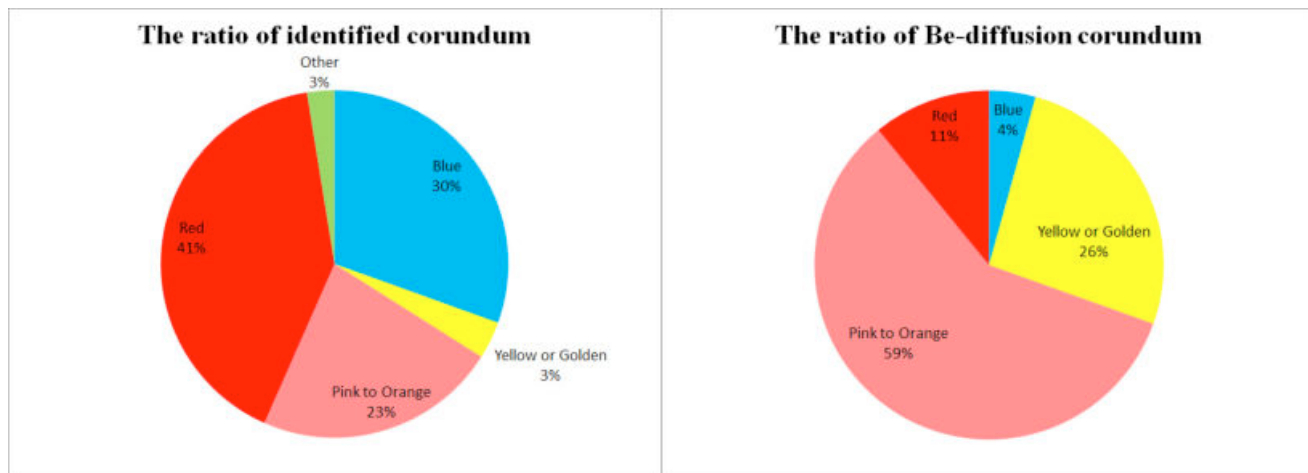


Figure 1. Ratio of identified corundum and Be-diffused treated corundum.

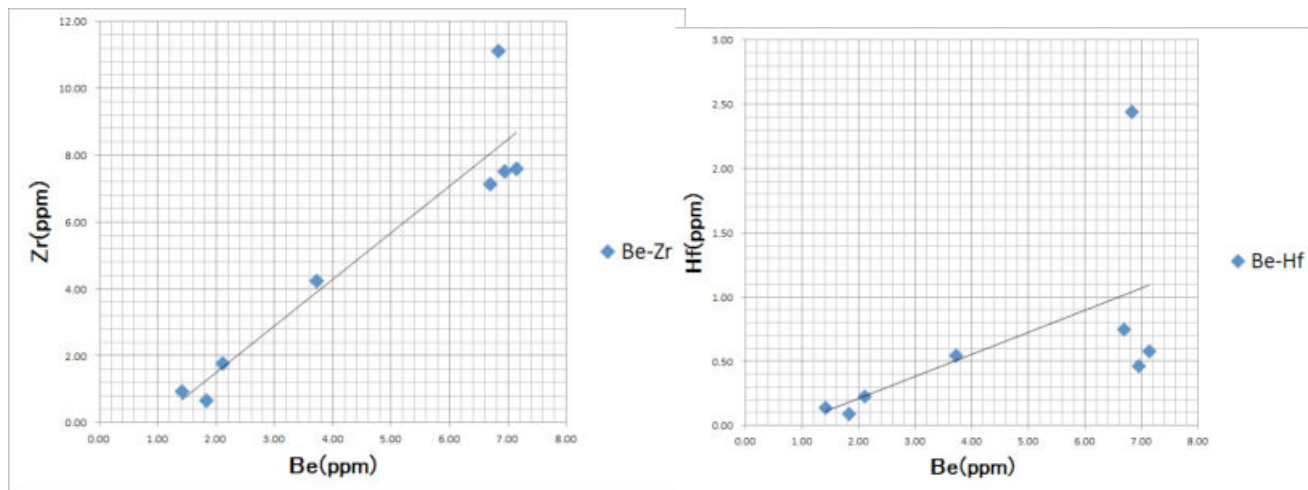


Figure 2. Plots of Be vs Zr and Be vs Hf in the golden sapphire.

Although it was thought trace elements detected along with natural origin beryllium are derived from micro inclusions in the cloud (Shen et al., 2012), beryllium was sometimes detected in inclusion free regions.

Niobium (Nb), tantalum (Ta), hafnium (Hf) and tungsten (W) were detected with beryllium (Be) in basaltic blue sapphire from Huai-Sai, Laos, Pailin, Cambodia and Mabira, Nigeria. Those were collected in the project of geographic origin determination at CGL. Those elements are called HFSE (High Field Strength Elements), that culminate in the liquid phase when the solid mantle partially melts, and suggest the corundum being of magmatic origin.

Beryllium is sometimes detected in corundum without any trace elements. For example, in a 5.55 ct yellow sapphire, 6 spots around the girdle of this stone were analyzed by LA-ICP-MS and beryllium concentrations were measured at 0.47 to 1.29 ppm but no trace elements were detected. In general very low concentrations of beryllium like in this corundum do not affect the color (Emmett & Wang, 2007). Evidence of heating was observed under the microscope but a surface-conformed layer was not observed. In this case, the origin of beryllium was the contamination from reusing the crucible for heating.

Even if beryllium is detected in corundum by LA-ICP-MS, we cannot identify definitely that it results from Be-diffusion treatment. It is necessary to measure related trace elements in many spots and to identify them carefully.

References

- Abduriyim, A., Kitawaki, H., 2006. Applications of Laser Ablation-Inductively Coupled Plasma-Mass Spectrometry (LA-ICP-MS) to Gemology. *Gems & Gemology*, 42(2), 98-118.
- Emmett, J.L., Scarrat, K., McClure, S.F., Moses, T., Douthit, T.R., Hughes, R., Novak, S., Shigley, J.E., Wang, W., Bordelon, O., Kane, R.E., 2003. Beryllium diffusion of Ruby and Sapphire. *Gems & Gemology*, 39(2), 84-135.
- Emmett, J.E., Wang, W., 2007. The Corundum group, Memo to the Corundum Group: How much beryllium is too much in blue sapphire – the role of quantitative spectroscopy. 26 August 2007.
- Shen, A., McClure, S., Breeding, C. M., Scarratt, K., Wang, W., Smith, C., Shigley, J., 2007. Beryllium in Corundum: The Consequences for Blue Sapphire. *GIA Insider*, Vol.9, Issue 2 (January 26, 2007).
- Shen, A., McClure, S., Scarratt, K., 2009. Beryllium in Pink and Yellow Sapphires. *News from Research* (April 3, 2009).
- Shen, A., Wirth, R., 2012. Beryllium-bearing nano-inclusions identified in untreated Madagascar sapphire. *Gems & Gemology*, 48(2), 150-151.

Digital Microscopy applications in gemmology

Yuri Shelementiev¹, Sergey Sivovolenko²

¹ MSU Gemmological Center, Moscow, Russia; yuri@gem-center.ru

² OctoNus Software, Tampere, Finland; sivovolenko@octonus.com

Binocular microscope is the common tool used by gemologists worldwide to solve a number of problems, including challenges of gemstone identification, distinguishing natural and synthetic stones, identifying indications of treatment and color origin, etc. Conventional binoculars offer a way to witness beautiful and exciting interior scenes in gemstones.

In order to record an image observed under such microscope, nowadays photo and video cameras are applied. Apart from the certain advantages, such cameras also have the certain limitations, and one of them is mono image: only a single photo or single movie is obtained while recording an initial stone.

Stereo image has some advantages in comparison with mono: on the base of stereo human brain divides objects by the depth of their location, for example, it easily distinguishes a scratch on the stone's surface from inclusions under the surface. In some cases a stereo image provides a qualitatively different and critical information for making a decision than its equivalent mono image.

For receiving stereo information, Octonus Software Company developed Digital Microscope (DM), enabling to record images by using two video cameras, respectively for the left eye and for the right eye. It makes possible to record real time immersive 3D movies with high image quality. Independent video signals are compressed and transmitted for the left and right eyes, so that high-resolution 3D images can be recorded and viewed on 3D-capable TVs or 3D computer monitors. Using special software for stereo films viewing one can watch movies in 3D-version, and these movies have the same properties as the images observed under a binocular microscope.

Technical parameters and possibilities of DM:

- controlling and monitoring the microscope by multi-button computer «mouse»
- regulating the gemstone's position by using a manipulator.
- observing internal "pictures" on the monitor by using stereo glasses.
- a Leica microscope head, providing the optical zoom up to 115 X magnification.
- real-time recording of movies,
- various types of lighting, automatic adjustment of brightness when enlargement (zoom) changes.
- 3D viewing software with the function of distant simultaneity (synchronization)

After recording several dozens of movies with gems (colored gemstones and faceted diamonds) we've learn that this technology can be a useful teaching tool for gemologists and jewelers, because it has the following properties and features:

1. 3D effect mentioned above.
2. Recording of internal features in gemstones, which passed through a laboratory and were returned back to their owners.
3. Demonstration of the process of gemstones observation and examination, as gemstones are usually seen and observed by a well-experienced, skilled specialist. It helps to avoid the stage of training the newcomers (non-skilled users) in installing and tuning the microscope, lighting, image (image properties and conditions) and looking for the necessary details and focusing on them.

4. The possibility of simultaneous viewing (watching) a certain movie by two or more observers, located in different countries (the observer can play it manually – moving it by the computer “mouse”- and point to the discussed area by the “mouse”). Each participant can see the “mouse” cursors of all the observers.

Demonstration movies, produced by us, enable to learn how to analyze inclusions, to identify natural or synthetic origin of colored gemstones, indications of treatment, and also to observe luminescence. Recording of internal features for cut diamonds allows creating a database of various clarity grades, with various schemes of inclusions in diamonds. Such database doesn't require buying a great amount of real diamonds, and makes it possible to reduce subjectivity in clarity grading, and also to provide training in clarity grading of polished diamonds.

Such stereo movies can make the educational process (process of teaching and process of learning) significantly more effective. A database of such movies, classified and systematized properly, makes it possible to improve effectiveness of distance education.

A remote operator may control and monitor the microscope at a distance, and that enables to observe a stone, located in another place, under the microscope. We see the potential of such a technology: in fact it is a new method of cooperative shared work and learning, as gemologists can share 3D scenes, details and excitement with others.

As imaging technologies are developing from year to year, stereo images technology and 3D movies viewing will become more available in the future. Nowadays it is already available, for example, on the stereo computer monitors with the certain video cards (display cards), 3D projectors (projection devices) and 3D TV-s.

Kashmir sapphires: geographical origin determination of top-quality blue sapphires versus science

HaiAn Nguyen Bui¹, Emmanuel Fritsch¹, Franck Notari², Alexandre Droux³, Aurélien Delaunay³, Benjamin Rondeau⁴

¹ Institut des Matériaux Jean Rouxel (IMN-CNRS) & University of Nantes, Nantes, France; haianguyenbui@hotmail.com; emmanuel.fritsch@cnrs-imn.fr

² GGTL Laboratories - GEMLAB (Liechtenstein)/GemTechLab, Liechtenstein and Switzerland; franck.notari@ggtl-lab.org

³ LFG, Paris, France

⁴ LPGN-CNRS & University of Nantes, Nantes, France. benjamin.rondeau@univ-nantes.fr

The geographical origin of gemstones has had an important impact on value for some gem varieties, coming from some specific provenances. Arguably the most spectacular difference in value is found for Kashmir sapphire versus other localities (Figure 1).



Figure 1. The price per carat of about 3 ct blue sapphires from Kashmir is about three times higher than that of other natural sapphires, even though the latter are much larger. Photo taken at the 2011 Tucson show.

Kashmir sapphires are characterized by a highly saturated blue color, believed unique, and that should therefore also translate in an equally unique UV-Visible absorption spectrum: it is characterized by a total absorption in the range 325-330 nm, low Fe³⁺-related absorptions, a dominating Fe²⁺-Ti⁴⁺ charge transfer, and no Fe²⁺-Fe³⁺ charge transfer (Figure 2).

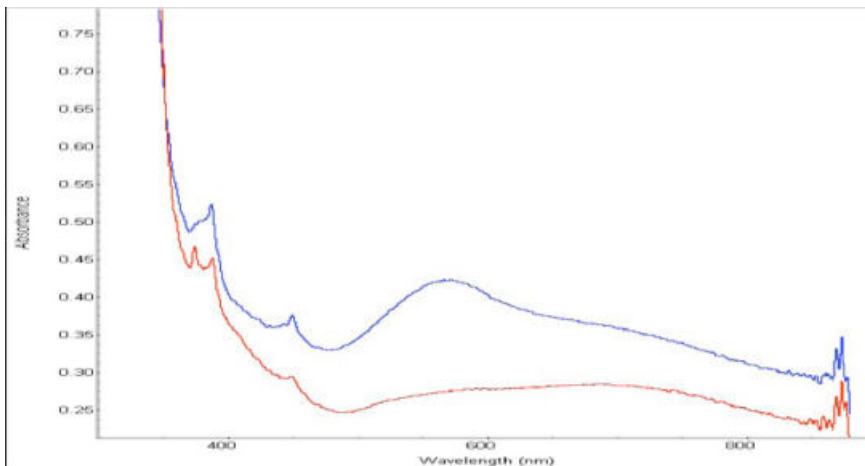


Figure 2. The typical absorption spectrum in polarized light of a Kashmir sapphire collected at the historical mines.

The color appearance of Kashmir sapphires is also caused in part by light scattering on tiny whitish inclusions believed to be rutile. In terms of internal characteristics, several inclusions are presented as characteristic of Kashmir sapphires, in particular tourmaline, pargasite, and “corroded” zircons. Also, blue to near-colorless color zoning in parallel bands, the later sometimes fluorescing red, are often associated with this locality.

However, other localities share some of these characteristics, most notably Elahera, in central Sri Lanka, and Andranomdambo in southern Madagascar. The best Andranomdambo blue sapphires show a similar absorption spectrum and, for example, comparable red-luminescing near-colorless bands. For this reason, recent articles describe the UV-Visible spectrum as simply typical of metamorphic blue sapphires, and not unique to Kashmir sapphires.

Furthermore, any deposit produces a range of qualities, only the top one being considered for locality of origin determination. Therefore, a small number of crystals from one specific origin may contain surprising inclusions: Kashmir sapphires collected at the mine captured for example hematite, and also green spinel – an inclusion deemed typical of Sri Lankan blue sapphires (Figure 3).

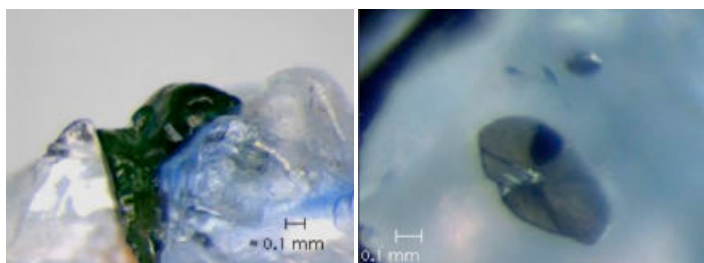


Figure 3. Some Kashmir sapphires collected at the mine hold unexpected inclusions: green spinel – often presented as typical of Sri Lankan sapphire - and hematite.

Another consequence is that some authentic Kashmir sapphires have a very light blue color, hence not have the expected appearance.

Chemical composition also cover a range of values for each deposits, and the key elements Fe and Ti are found in a larger-than-thought range of concentrations, leading to unavoidable overlaps between several reputed blue sapphire deposits.

In conclusion, there is not enough scientific documentation of blue sapphire deposits to assign a locality of origin to some blue sapphires. The current mode of attribution of origin to blue sapphires, from Kashmir and otherwise, is more akin to branding than to science. An increasing number of laboratories are developing policies nuancing or limiting geographical origin determination. This was the situation roughly a century ago for diamonds. The development of a diamond grading scale made geographical origin attribution for diamond obsolete.

Cultured pearl – Present situation and future prospect

Shigeru Akamatsu

Central Gem Laboratory Tokyo, Japan

The cultured pearl industry started one hundred and twenty years ago with Mr. Kokichi Mikimoto's Akoya hemi-spherical cultured pearl (Figure 1). In 1906, the culturing method for specific pearls was invented. Since then, the cultured pearl industry has greatly developed. Looking back at the history of cultured pearls, however, the present situation is not favorable. Rather, it seems to become more and more precarious. As the world pearl market began to head for lower price, the quality of the pearls produced began to decline accordingly. Consequently, it has become harder for pearl cultivators to cover the culturing costs with the income generated by the pearls produced. Therefore, they are forced to reduce the culturing cost by using low-quality mother oyster and nucleus, and hiring less skilled nucleus-inserting operators with low labor cost. This leads to further deterioration of pearl quality, and the vicious circle continues. In addition, in order to disguise the deterioration of the quality by improving the appearance, treatments have "developed" and become increasingly sophisticated. The concept of cultured pearl that forerunners such as Mikimoto aimed was "to make a pearl with human hands that will compete with natural pearls". However, pearl culturing of this day and age largely deviates from the original concept. In pursuit of profit, the culturing periods is shortened and pearls produced are heavily treated. Consequently, cultured pearls are further and further away from what can be called a gemstone. Not only Akoya cultured pearl but also all other cultured pearls come to a turning point.



Figure 1 (left): Akoya hemi-spherical pearl cultured by Mikimoto 120 years ago. Figure 2 (right): Newly harvested Akoya cultured pearls from the Aino-shima pearl farm.

Pearl culturing was so far "labor intensive". Namely it was mass production of middle to low quality pearls, and pearl culturing relied on cultivators experience and instinct. However, at present, mass production becomes harder since pearl farms, mother oysters and even nuclei are all limited in number. Under such circumstances, if the scale of culturing is expanded, immediately a big problem will arise. When pearl oysters are cultured beyond the capacity of self-purification of the pearl farm, the farm environment rapidly deteriorates because of the accumulation at the bottom of the sea of huge amounts of oyster droppings and wasted materials from shell cleaning. There are also subsequent emissions of toxic gas such as hydrogen sulfide. Mass culturing of pearl oyster causes food and oxygen shortage that weaken pearl oysters, consequently the production of good quality pearl will rapidly decrease. On the other hand, the farming environment has also greatly changed recently. For example, abnormally high water temperature is mea-

sured in the summer time while spells of extremely cold weather occurs. In Japan, massive mortality of Akoya oyster still continues. It resulted from the red tide caused by a new type of plankton -“Heterocapsa”- that suddenly appeared in 1992 and from an infectious disease in 1994. To cope with these calamities, experience and instinct are utterly useless. That is because pearl culturing is required to change from “labor intensive pearl culturing” to “technique intensive pearl culturing”.

The characteristics of “technique intensive pearl culturing” is to change the way of pearl production, while the pearl product remains the same. “Technique intensive pearl culturing” is to convert to the production of small amounts of high quality pearls possessing rarity value. In technique intensive pearl culturing, oysters are not cultured beyond the capacity of self-purification of the pearl farm, wastes resulting from the pearl culturing activity are not thrown at the bottom of the sea but to disposed of on land, thus promoting the preservation of a high quality farm environment. Conservation of oyster resources is also necessary. In order to keep the status of gem, cultured pearl should possess three requirements, namely rarity, durability and beauty. Such was the pearl that Kokichi Mikimoto, by throwing all his resources into it and Tokichi Nishikawa, at the risk of his life, wanted to make one hundred and twenty years ago. Now it is time to go back to the starting point of cultured pearl and to change culturing fundamentally. It is noticeable that K. MIKIMOTO & Co., has started pearl culturing in Aino-shima Island in Kyushu, in the southern part of Japan based on “technique-intensive pearl culturing”. This new pearl-culturing is operated by MIKIMOTO as follows.

1. Protection of oyster resources

Only pure Japanese Akoya oysters inhabiting the Aino-shima area are used for pearl culturing. Naturally-grown Akoya spats are collected by natural spawning. Once spats needed for pearl culturing are secured, the remaining oysters are returned to the sea, thus protecting the oyster resources.

2. Preservation of the pearl farming environment

All wasted materials resulting from pearl culturing are disposed of, not in the sea, but on land, following the “zero emission” policy. The number of pearl oysters actually used for pearl culturing is no longer beyond the self-purification ability of the sea.

3. Production of pearls with rarity value

The culturing period is two years or more, thus the pearls produced can truly qualify as gemstones, through their high nacre thickness and other quality factors. (figure 2)

4. Scientific management of the pearl farm

Using the latest available instrumentations, the farm environment is monitored every single day for useful indicators such as water temperature, salinity, biochemical oxygen demand (BOD) and the amount of chlorophyll. If such normal everyday environmental data are collected, prompt and accurate action can be taken when an abnormal situation occurs.

5. Promotion of pearl research and development

New knowledge and practices are developed through research, such as a red tide prediction system and ways to prevent infectious disease by keeping infected oysters in cold water (below 16°C) for a certain period of time. Thus former countermeasures based on experience and instinct will be replaced by such a new approach based on true scientific research.

It is our view that “technique-intensive pearl culturing” indicates the future direction for not only Japanese Akoya pearl culturing, but also all other types of pearl culturing.

Observations of natural pearls within freshly opened *Pinctada maculata* from Tongavera atoll, Cook Islands

Terrence S. Coldham

Gemmological Association of Australia, Sydney, Australia; terry@intogems.com.au

This presentation will detail observations made during the harvesting of pearl bearing *Pinctada maculata*, commonly known as the Pipi. The author was very fortunate to have the unique experience of being present at the harvesting of several hundred naturally-occurring pipi oysters at the remote Tongavera Atoll (also known as Penryhn Island), part of the Cook Island group situated in the Pacific Ocean. The atoll encloses a vast lagoon, which is home to a large population of *Pinctada maculata* growing naturally on coral heads. *Pinctada maculata* are known for occasionally carrying beautiful, mostly golden-coloured, natural pearls. (Figure 1).

To be able to open freshly harvested oysters and actually see natural pearls in-situ in their host oyster, provided an excellent opportunity to observe their position within the body of the animal. Of the six hundred or so oysters opened a dozen or so contained pearls. Details of the pearls, their position in the oyster and the host shells were logged, and the gems were photographed. (Figure 2).

The results are compared with a recent article published in *The Australian Gemmologist* titled "Natural pearls and cultured pearls: A basic concept and its variations" by Prof. D. H. A. Hänni (2012). The field observations are compared with explanations of natural pearl formation provided by Hänni (2012) with some interesting conclusions being drawn regarding the formation of blister pearls sometimes found in *Pinctada maculata*.



Figure 1. Natural pipi pearls as harvested. The largest is 6.50 mm in diameter.



Figure 2. A freshly opened *Pinctada maculata* with four pearls situated within the mantle tissue between the internal and external transparent mantle epithelium.

References

Hänni, H.A., 2012. Natural pearls and cultured pearls: A basic concept and its variations. *The Australian Gemmologist*, 24(11), 258-266.

Passfield K. 1997. Notes on 'pipi' pearl oyster, *Pinctada maculata*, fishing in Tongavera, Cook Islands, 1995. SPC Pearl Oyster Information Bulletin #10.

Pearl or gemstone? Galatea pearls: a 'new' pearl product from French Polynesia

Laurent E. Cartier¹, Michael S. Krzemnicki¹, John Rere²

¹ Swiss Gemmological Institute SSEF, Falknerstrasse 9, 4001 Basel, Switzerland (gemlab@ssef.ch)

² Rikitea, Gambier Islands, French Polynesia

Introduction

Cultured pearls can be produced both with and without a nucleus. The nucleus material used for these beaded cultured pearls is traditionally from freshwater Mississippi mussels. In recent years, there have been a number of attempts to use alternative pearl and shell materials as nuclei. This includes different types of shells, bironiteTM (processed dolomite, Snow 1999), laminated/powdered shell, freshwater cultured pearls, organic substances and even natural pearls (Superchi et al., 2008; Hänni et al., 2010; Cartier and Krzemnicki, 2013). An altogether different approach is to use gemstone beads as nuclei for pearls; these are subsequently artistically carved to show both a gemstone nucleus and surrounding mother of pearl (Figure 1). This type of pearl product - named Galatea Pearls - has been on the international market since 2007 and grown in importance in recent years (Roskin, 2007; Hänni, 2009; Strack, 2011). In 2012, CIBJO changed its Pearl Blue Book definition of a cultured pearl bead to accommodate other types of nuclei (e.g. turquoise bead cultured pearl) (CIBJO, 2012).



Figure 1: Carved Galatea cultured pearls from French Polynesia containing a treated turquoise nucleus. Photo: Laurent E. Cartier.



Figure 2: The pearl farm that currently produces Galatea cultured pearls from French Polynesia. Photo: Laurent E. Cartier

The Culturing Process

At present, all Galatea cultured pearls are produced at one farm in the Gambier Islands of French Polynesia (Figure 2) using indigenous *Pinctada margaritifera* oysters. In French Polynesia, all the necessary oysters can be obtained through wild spat collection by introducing spat collectors in selected areas of the lagoon twice a year (March-June, September-December). The oysters are nursed and may be placed in baskets to protect them from predating fish (Southgate and Lucas, 2008). At an age of around 3 years, the oysters usually reach a size (10-12cm in shell diameter) when they can be operated. In a first generation, a piece of donor mantle tissue ('saibo') along with a plastic nucleus (see Figure 3) are operated into the gonad of a host oyster. A plastic nucleus is chosen because of lower costs: the first generation pearl produced with these is not marketed. It has to be noted that French Polynesia export regulations

would not allow the export of pearls containing a plastic nucleus (JOPF, 2010).

After 6 months, the first generation cultured pearls containing the plastic nucleus can be harvested. A gemstone nucleus, for example turquoise, can then be inserted into the existing pearl sac. The pearl sac will secrete nacre covering the gemstone nucleus to form a cultured pearl; this can then be harvested 10-12 months later. Retention- and success rates are relatively high. Gemstone beads are not used in first generation because trials have shown that these can induce higher rejection rates and inconsistent nacre deposition, whereas they are fully suitable to a 2nd generation operation (pers. comm., John Rere 2012).

Production of Galatea is expected to reach 100,000 cultured pearls in 2014 (pers. comm., John Rere 2012). Galatea cultured pearls were previously also cultured in *Pinctada margaritifera* oysters in Vietnam, but no longer so. The manufacturing of associated pearl products remains there though: the pearls are carved and the Galatea jewellery is manufactured in Vietnam.

Studied Pearl Samples

Both carved and non-carved samples of harvested cultured pearls were studied. The non-carved samples have the same surface properties as can be expected of common Tahitian cultured pearls from *Pinctada margaritifera*. However, the SG of the samples is not the same as for normal cultured pearls because the nucleus material has a different SG (see also Hänni, 2009). An X-ray image of the non-carved samples will also show different absorption of the nucleus as is usually found for cultured pearls with a CaCO_3 nucleus derived from Mississippi freshwater shells. The carved samples can be clearly identified because the nucleus - of different colouration- is clearly visible.

We will present results on nacre thickness and internal structure of these samples using X-ray shadow images and X-ray luminescence. UV-vis and Raman spectrometer has been used to confirm the *Pinctada margaritifera* origin of these pearls. SG was determined for different pearl samples. The nucleus material was studied using FTIR and Raman spectrometry to determine the natural or artificial origin of the nucleus material and whether it is treated or not (see also Hänni, 2009). Depending on how the pearl is carved, it is more or less difficult to analyse the nucleus. In non-carved samples, it is not possible to conclusively identify the nucleus material using traditional methods.



Figure 3: Plastic nuclei used in first generation operation. The different colours correspond to different sizes. Photo: Laurent E. Cartier



Figure 4: Two harvested first generation cultured pearls that contain plastic nuclei are seen on the left. On the right are the nuclei that are used for insertion during a second operation and that produce the desired Galatea cultured pearls. Photo: Laurent E. Cartier

Conclusions

Nacre thickness of studied samples falls within the required 0.8 mm minimum limit set by Tahitian authorities. We will present a wide range of materials available as nucleus, which have been used in production, ranging from amethyst to emerald, topaz and turquoise. A number of samples have been examined to determine the origin of the nucleus material and determine if it is treated or not, to ensure correct disclosure according to CIBJO regulations. These pearls represent a niche market and an interesting innovation in cultured pearl production, and as production continues to increase their presence on the international market is set to become more important.

References

- Cartier, L.E., Krzemnicki, M.S., 2013. New developments in cultured pearl production: use of organic and baroque shell nuclei. *Australian Gemmologist*, 25 (1), 6-13.
- CIBJO, 2012. *The Pearl Book. Natural, Cultured, Composite & Imitation Pearls — Terminology & Classification*, 2012-01. www.cibjo.org
- Hänni, H.A., 2009. Engraved cultured pearls with an unexpected bead. *SSEF Facette*, 16, p.11, http://www.ssef.ch/en/news/facette_pdf/facette16_small.pdf
- Hänni H.A., Krzemnicki M.S., Cartier L.E., 2010. Appearance of new bead material in pearls. *Journal of Gemmology*, 32(1-4), 31-37.
- JOPF, 2010. L'arrêté n°297/CM du 9 mars 2010, JOPF n° 11, p.1235. http://www.servicedelaperliculture.pf/IMG/pdf/Arrete_no_1240_CM_du_30_aout_2007_modifie.pdf
- Roskin G., 2007. Black pearls have gemstone bead nuclei. *JCK*, 178(8), 50.
- Shor, R., 2007. From single source to global free market: the transformation of the cultured pearl industry. *Gems and Gemology*, 43(3), 200–226.
- Snow M. (1999) Bironite™: a new source of nuclei. *SPC Pearl Oyster Information Bulletin No. 13*, December 1999, pp. 19-21. http://www.spc.int/DigitalLibrary/Doc/FAME/InfoBull/POIB/13/POIB13_19_Snow.pdf
- Southgate P.C., Lucas J.S., 2008. *The Pearl Oyster*. Oxford: Elsevier.
- Strack, E., 2011. Le point sur les perles de culture Première partie - Les perles d'eau de mer. *Revue A.F.G.*, 176, 5-9.
- Superchi M., Castaman E., Donini A, Gambini E., Marzola, A. (2008) Nucleated Cultured Pearls: What is there inside? *Zeitschrift der Deutschen Gemmologischen Gesellschaft*, 57(1/2), 33-40.

Acknowledgments:

We thank Galatea Pearls (California, USA) for the donation of several samples for research purposes. Judith Braun (SSEF) is thanked for assistance in the analysis of studied samples. Finally, Laurent E. Cartier is grateful for travel funding from the Tiffany & Co. Foundation.

Current situation of the pearl cultivation at Guaymas (Sonora) Mexico

Stefanos Karamelas¹, Enrique Arizmendi², Douglas McLaurin², Manuel Nava², Pierre Hardy¹, Lore Kiefert¹

¹Gübelin Gem Lab, Maihofstrasse 102, Lucerne 6006, Switzerland

s.karamelas@gubelingemlab.ch, p.hardy@gubelingemlab.ch, l.kiefert@gubelingemlab.ch

²Perlas del Mar de Cortez, Bahía de Bacoachimambo SN Interior Tec Milenio, Fracc. Lomas de Cortez, Guaymas, Sonora 85450, Mexico; earizmendi@perlas.com.mx, dmclaurin@perlas.com.mx, mnavas@perlas.com.mx

For more than five centuries, natural pearls have been fished from the waters of Mexico (Carino & Monteforte, 1995; McLaurin & Arizmendi, 2002). The vast majority of the natural nacreous pearls are found in *Pinctada mazatlanica* (*P. mazatlanica*) and *Pteria sterna* bivalves, while the non-nacreous pearls are found in bivalves belonging to *Pectinidae* (a.k.a., «scallop pearls») and *Pinnidae* families (a.k.a. «pen pearls»). During the last fifty years, several experiments took place to cultivate nacreous pearls in *P. mazatlanica* and *Pteria sterna*. In 1993, a team of researchers from Instituto Tecnológico de Estudios Superiores de Monterrey (ITESM) at Guaymas (Mexico) started to cultivate such pearls and in parallel to develop a viable economical model which will help the region as well. Some years later, the first successful harvest of gem quality cultured pearls with bead, as well as of «mabés», from *Pteria sterna* came out. In 2000, a private company named «Perlas del Mar de Cortez» was established in connection with the ITESM. In 2005, after the closure of the local ITESM campus, the three original researchers (EA, DM and MN) with a private investor took over the company and changed their name to «Cultivadores Mexicanos de Perlas S.C.», keeping the name «Perlas del Mar de Cortez» as their brand-name. The present work will present an update on the situation of the pearl cultivation in Baco-chibampo Bay (Guaymas, Sonora) by this company as well as some spectroscopic and gemological results compared with already published data (see some examples in Kiefert et al., 2004; Reyjal, 2012).

Today about twelve people from the region are working for the company «Perlas del Mar de Cortez»; comparatively, about 30% more were employed back in 2007. This cut-down is mainly due to tourism decreasing in Mexico; however, in the last two years, tourism seems to start recovering. Moreover, 2007 and 2011 brought the coldest and warmest summer respectively, both of these had a negative effect on pearl cultivation.

Wild adult mollusks cannot be used for the cultivation process, as their fishing is still banned; for this purpose wild spats only are collected from the waters of the farm. The number of cultivated animals remains constant; about 250 000 are cultivated each year in order keep a balance in the bay. The cultivation processes for *Pteria sterna* and *P. mazatlanica* is different. For *Pteria sterna*, round beads (from about 6 to 10 mm diameter) from the freshwater shells belonging to *Unionidae* family are implanted into two-years old animals by simultaneous transplantation of a tissue from the same species as the host; note that *Pteria sterna* mollusks need to be completely opened for the operation and all animals are only operated once. Cultivation period lasts from 18 to 20 months; in average about 4 000 cultured pearls with bead of gem quality are harvested every year from *Pteria sterna*. Cultured pearls with bead from *P. mazatlanica* of gem quality are still not produced at present.

The success rate of *Pteria sterna* operations has increased over the years. The smallest samples collected from *Pteria sterna* are of 8 mm diameter; slightly bigger than in the past (7 to 7.5 mm). Their average size is today slightly above 9 mm diameter, whereas it was below 9 mm around 2004. They rarely yield pearls bigger than 12 mm in diameter (exceptionally up to 14 mm) and approximately one percent (1%) of the production consists of near-round samples. About 300 cultured pearls without bead of various shapes; i.e. «keshi» cultured pearls, are also collected each year. Their body color ranges from grey to black with various strong overtones. It is important to mention that from the last fourteen harvests only nine full necklaces have been assembled; this is mainly due to strong variations in body and secondary colors. The rest of the samples are sold either as individual samples (and/or jewelry pieces) or pairs. Most of the «mabé» pearls are mounted into hand-made jewelry pieces produced by Mexican silversmiths. More than half of

the samples/jewelry pieces are sold locally from the store located within the pearl farm to the tourists/visitors; more than 30% is sold directly from the owners of the farm at gem shows and finally less than 15% of the samples are sold via other gemstone dealers. The byproducts of the pearl cultivation are also used; e.g. the meat of the animals is sold as food locally and the inner part of the shells is fashioned into buttons.

For the present study ten saltwater cultured pearls (SWCPs) from *Pteria sterna* (7 with bead and 3 without bead) with various body-colors and overtones, five experimental SWCPs from *P. mazatlanica*, as well as their shells, colored from gray to yellowish gray to black with various overtones, were tested. All samples were collected at the pearl farm presented above. All samples were observed using a standard gemological microscope and their UV fluorescence using a standard 6 Watts gemological lamp. UV-Visible-NearIR spectra were acquired from 250 to 1500 nm using a DRA fitted to a Cary 5000 spectrometer (DI and SBW: 0.7 nm and scan rate: 60 nm/min). Photoluminescence (PL) spectra from 520 to 1000 nm were obtained with a Renishaw 1000 Raman spectrometer with microprobe (514 nm excitation with Ar+ laser, 50x magnification lens, 10 mW power, 10 seconds acquisition time, 0.1 nm resolution) and X-radiographs using a Comet X-ray unit and a Kodak 6120 digital sensor (voltage: from 60 to 65 kV, with current from 5 to 7 mA).

The samples are not polished after the harvest; thus they present very pronounced fingerprint-like structures due to the arrangement of aragonite crystals. All *Pteria sterna* samples, even light-colored ones, fluoresce strong (the light colored samples present weak fluorescence) red under LW-UV (365 nm) and are inert under SW-UV (254 nm). All *P. mazatlanica* samples are inert under LW- and SW- UV. All SWCPs with bead present a nacre thickness above 1mm (up to 1.5 mm) and the «keshi» SWCPs from *Pteria sterna* present cavities at their core, related to the transplanted tissue. Samples from *P. mazatlanica* present several absorption features in the visible range; a continuous band extending throughout the visible range, absorptions from the ultraviolet to the blue portion of the visible spectrum (330-460 nm, consisting of two bands at 330-385 nm and 385-460 nm), three others in the blue region at 405, 460 and 495 nm, three absorptions in the green-yellow-orange region at 530, 585, and 625 nm, and three in the red at 680, 700 and 745 nm. All bands are roughly Gaussian shaped having a moderately wide (width from about 30 to about 70 nm). The samples from *Pteria sterna* present bands at the same positions, with the exception of the band at 700 nm, which is not observed in these samples. PL spectra of samples from both mollusks present PL bands at around 620, 650 and 680 nm. These bands are more intense with *Pteria sterna* samples; the bands at 650 and 680 nm are barely seen on the PL spectra of *P. mazatlanica* samples.

Spectroscopic results from the *P. mazatlanica* samples are very similar to those from the *P. margaritifera* samples (Karampelas et al., 2011). These are in accordance with the results of phylogenetic studies which suggest the conspecificity of *P. margaritifera* and *P. mazatlanica* (Temkin, 2010; Cunha et al. 2011 and references therein). Compared with dark natural colored SWCPs from *P. maxima*, the samples from *P. margaritifera* (as well as *P. mazatlanica*) and *Pteria sterna* show an additional band at 405 nm (see Karampelas, 2012 and references therein). On the other hand, *Pteria sterna* SWCPs do not present the band at 700 nm as opposed to *P. margaritifera* (as well as *P. mazatlanica*) SWCPs of similar color (see Karampelas et al., 2011 and references therein). Additionally, *Pteria sterna* SWCPs present pronounced PL bands in the orange-red region, compared to samples from *P. maxima* and *P. margaritifera* (*P. mazatlanica*) where these bands are weak, when present. These also show a strong red luminescence under LW-UV radiation (see Hainschwang et al., 2013 and references therein). This makes it easy to identify SWCPs from *Pteria sterna* (as well as from *Pteria* sp. in general).

Cultivation of SWCPs using bivalve from *Pteria* sp. (*Pteria penguin*) is also taking place in Japan and China; the resulting samples are light brown to grey-brown with various overtones (see Southgate et al., 2008 and references therein). *Pteria sterna* is only successfully cultivated nowadays in Guaymas, Mexico. Cultivation of SWCPs using *P. mazatlanica* bivalve is not known today. In Guaymas, SWCPs production from *Pteria sterna* will gradually increase over the coming years (for environmental reasons, the upper limit will be set to 10 000 samples) and gem quality production from *P. mazatlanica* will hopefully start. The main purpose, however, is to maintain the quality of the cultured pearls samples as well as to preserve the environment and the collaboration with local inhabitants.

References

Carino M., Monteforte M., 1995. History of pearling in La Paz Bay, South Baja California. *Gems & Gemology*, 31 (2), 88-105.

- Cunha R.L., Blanc F., Bonhomme F., Arnaud-Haond S., 2011. Evolutionary patterns in pearl oyster of the genus *Pinctada* (Bivalvia: Pteriidae). *Marine Biotechnology*, 13 (2), 181-192.
- Hainschwang T., Karamelas S., Fritsch E., Notari F., 2013. Luminescence spectroscopy and microscopy applied to study gem materials: A case study of C centre containing diamonds. *Mineralogy and Petrology*, in press.
- Karamelas S., Fritsch E., Gauthier J-P., Hainschwang T., 2011. UV-Vis-NIR reflectance spectroscopy of natural-color saltwater pearls from *Pinctada margaritifera*. *Gems & Gemology*, 47 (1), 31-35.
- Karamelas S., 2012 Spectral characteristics of natural-color saltwater cultured pearls from *Pinctada maxima*. *Gems & Gemology*, 48 (3), 193-197.
- Kiefert L., McLaurin D.M., Arizmendi E.C., Hänni H.A., Elen S., 2004. Cultured pearls from the Gulf of California, Mexico. *Gems & Gemology*, 40 (1), 26-39.
- McLaurin D.M., Arizmendi E.C., 2002. Five centuries of Mexican pearls. *Australian Gemmologist*, 21(5), 190-201.
- Reyjal I., 2012. Perles de culture de la Mer de Cortez: les belles inconnues. *Revue de Gemmologie a.f.g.*, 179, 17-22.
- Southgate P.C., Strack E., Hart A., Wada K.T., Monteforte M., Carino M., Langy S., Lo C., Acosta Salmon H., Wang A., 2008. Exploitation and culture of major commercial species. In P.C. Southgate and J.S. Lucas, Eds., *The Pearl Oyster*. Elsevier, Amsterdam, 187-222.
- Temkin I., 2010. Molecular phylogeny of pearl oysters and their relatives (Mollusca, Bivalvia, Pterioidea). *BMC Evolutionary Biology*, 10 (342), 1-28.

The Pearl of Asia: examination of the pearl, a review of its history, and conjecture on its origin

Steve Kennedy

The Gem & Pearl Laboratory Ltd, Unit 23, 43 Kirby Street, London EC1N 8TE; info@thegemlab.co.uk



Pearl of Asia – front view

Additional data collected on natural and cultured pearls from *P. maxima* in Australian waters

Kenneth Scarratt

Gemological Institute of America; Ken.scarratt@gia.edu

This study follows on from the historic perspective and initial data published in *Gems & Gemology*, Winter, 2012 (Scarratt, 2012).

In the winter of 2012 additional *P. maxima* samples were collected from Australian waters. These included wild shell from the 80 mile beach that contained natural pearls, initially wild shell from the 80 mile beach that had subsequently been operated on for the culturing process that contained natural pearls, bead cultured pearls and non-bead cultured pearls and hatchery shell that has been operated on for the culturing process that contained natural pearls, bead cultured pearls and non-bead cultured pearls (Figure 1, 2 and 3).



Figure 1 (top left): One bead cultured and one non bead cultured pearl still in their 'pearl sacs' in a Hatchery Pinctada maxima shell.

Figure 2 (bottom right): One natural, bead cultured and one non bead cultured pearl still in their 'pearl sacs' in a Hatchery Pinctada maxima shell.



Figure 3: Two natural pearls still in their pearl sacs in a wild *Pinctada maxima* shell.

All pearls were recorded photographically while still in their pearl sacs to register the position for each within the mollusk. The pearls were catalogued, securely stored and examined for internal grown structures using Real-Time Microradiography and X-ray Computed Microtomography as well as trace element chemistry using Laser Ablation - Inductively Coupled Plasma - Mass Spectrometry.

Pearls located in the area of the mantle closest to the gills and the widest point of the adductor muscle, the area where natural pearls are likely to be found, revealed internal structures that are associated with natural pearls. The bead cultured pearls taken from the gonad revealed structures typical of this kind of pearl, with the bead center clearly defined. Other pearls found in the area of the gonad close to the 'heal' of the shell revealed two distinct grown structures that are now associated with non-bead cultured pearls.

Trace element chemistry, as well as visual observations, confirmed that the color and chemistry of the bead cultured pearls are linked with the sacrificial mantle tissue used in the culturing process as opposed to the mantle tissue of the host; although in many cases the trace element chemistry was similar.

References

Scarratt, K., Bracher, P., Bracher, M., Attawi, A., Safar, A., Saeseaw, S., Homkrajae, A, Sturman, N. (2012). Natural Pearls from Australian *Pinctada Maxima*. *Gems & Gemology*, 48(4), 236-261.

Digital SLR camera applied to investigation of X-ray luminescence of pearls

Sutas Singbamroong, Nazar Ahmed

Gemstone and Precious Metal Laboratory Unit, Dubai Central Laboratory Department, Dubai, United Arab Emirates; sutas.singbamroong@gmail.com

Investigation of pearls by X-ray luminescence is fast and useful to help differentiating between freshwater and saltwater environments (Hänni et al., 2005). Since freshwater pearls contain traces of manganese, freshwater pearls display weak luminescence under X-rays, whereas pearls from saltwater do not. The observation of X-ray luminescence could be made in the dark by naked eyes through a safety window of a conventional X-ray cabinet or with a special sensitive CCD camera system and a computer program, such as proposed by Hänni et al., 2005. However, instead of using the special sensitive CCD camera system and software, we propose the use of a commercially available and less expensive digital single-lens reflex (also named digital SLR or DSLR) camera without special software to record the luminescence pictures.

A Digital SLR Nikon D90 camera was preliminarily used for our experiment and has proved its validity. It has large and high quality CMOS image sensors offering lower noise, which is useful in low light and provides excellent pictures. The experiments were conducted under excitation in a Torrex cabinet X-ray system that is used for X-radiography, operating at 90 kV and 3 mA (Figure 1). The first reference picture can easily be taken with programmed auto mode of the camera under normal light conditions, via a Live View monitor. A second picture of the pearls under X-rays was taken in the same position with manual mode. The best results were obtained at the following settings: shutter speed = 30 seconds, aperture = f/3.2 and ISO sensitivity = 6400, which allows the low light of weak luminescence to enter the image sensors as much as possible.



Figure 1. The experiment set up for pearl investigation of X-ray luminescence by using a digital SLR Nikon D90 camera.



Figure 2. Chinese freshwater cultured pearl strand recorded under normal light (a), under X-ray radiation displaying distinct green-yellow luminescence (b).

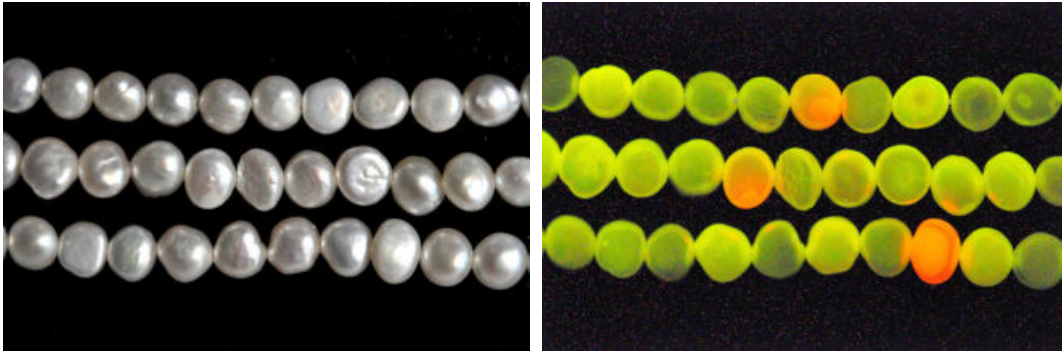


Figure 3. Chinese freshwater pearl strand recorded under normal light (a), under X-ray radiation, some displaying orange luminescence (b).

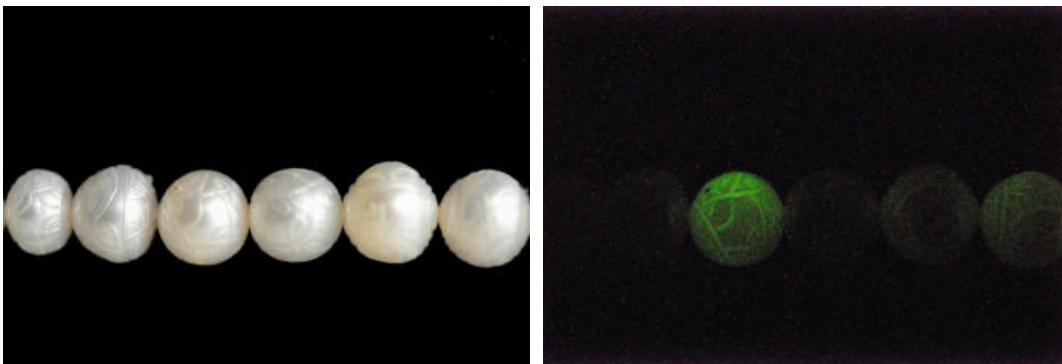


Figure 4. South Sea saltwater cultured pearl strand recorded under normal light condition (a), under X-ray radiation displaying variable luminescence reactions, depending on nacre thickness (b).

Chinese freshwater cultured pearls display a distinct green-yellow luminescence (Figure 2). Orange luminescence was also seen in some of them, especially on dull surface areas (Figure 3). The vast majority of beaded saltwater cultured pearls revealed variable luminescence reactions depending on nacre thickness and the amount of organic material on each bead that is apparently caused by the excitation of manganese in the freshwater mother-of-pearl core (Figure 4). Naturally dark-colored or dyed pearls with metallic compounds may inhibit luminescence since the coloring pigment or the metallic components of the dye mask or reduce the intensity of luminescence to such an extent that it cannot be observed.

This method is most useful in combination with radiography. Using the Digital SLR camera not only provides a quick way to identify a pearl strand that may contain a mixture of different types of pearls, but also delivers a permanent record for future reference.

References

Hänni, H.A., Kiefert, L. and Giese, P., 2005. X-ray luminescence, a valuable test in pearl identification. *Journal of Gemmology*, 29(5/6), 325-329.

Comparison of «cavities» in saltwater natural pearls and saltwater cultured pearls without bead

Abeer Tawfeeq Al-Alawi¹, Stefanos Karampelas², Osama Taqi¹

¹Gem & Pearl Testing Laboratory of Bahrain, Ministry of Industry & Commerce, PO Box 5479, Manama, Kingdom of Bahrain; atawfeeq@moic.gov.bh

²Gübelin Gem Lab, Maihofstrasse 102, Lucerne 6006, Switzerland

Difference in price of natural and cultured pearls is important; because of their separation is one of the major services of gemmological laboratories. A side product, result of the pearl cultivation improvement of the last twenty years, is some freshwater cultured pearls (FWCPs) as well as some saltwater cultured pearls (SWCPs) without bead which are sometimes difficult to identify (Scarratt et al., 2000; Akamatsu et al., 2001; Hänni, 2006; Sturman and Al-Attawi, 2006; Sturman, 2009; Karampelas et al., 2010; Krzemnicki et al., 2010; Scarratt et al., 2012). Separation of natural from cultured pearls is based mainly on (film or digital) X-radiography. Recently, X-ray computed tomography (micro-CT) was also started to be used for pearl identification by gemmological laboratories (see some examples in Karampelas et al., 2010; Krzemnicki et al., 2010; Scarratt et al., 2012 and references therein).

The samples which show «cavities/voids» cause sometimes difficulties to gemmological laboratories (see some examples at Sturman, 2009). Such internal structures when visualized could be very confusing. The formation of the voids or cavities depends on many factors including the environmental conditions in which the pearls have actually formed.

For this study ten SWCPs without bead from *Pinctada maxima* (*P. maxima*) and ten saltwater natural pearls (SWNPs) from *Pinctada radiata* (*P. radiata*), all from reputable sources (see acknowledgments), were pre-selected in order to study in details the «voids» using X-radiography and/or micro-CT. Some of the samples were cut in two pieces as well in order to check under microscope their internal structures. All samples were from white to white silver and white cream colour, having near round, oval, button and baroque shapes and sized from 3 to 8 mm.

Checking the results it was evident that the shape of the voids differs greatly from one sample to another (see some examples to Figure 1 to 4). Moreover, not only should the internal structure be taken into consideration but also the external appearance of the pearl. In figures 1 and 2, slices of micro-CT models of a SWNP from *P. radiata* are shown. The cavities observed in both samples are irregular and complex and to a degree flowed with the external appearance of the pearls. Externally, both pearls had a surface of medium lustre.

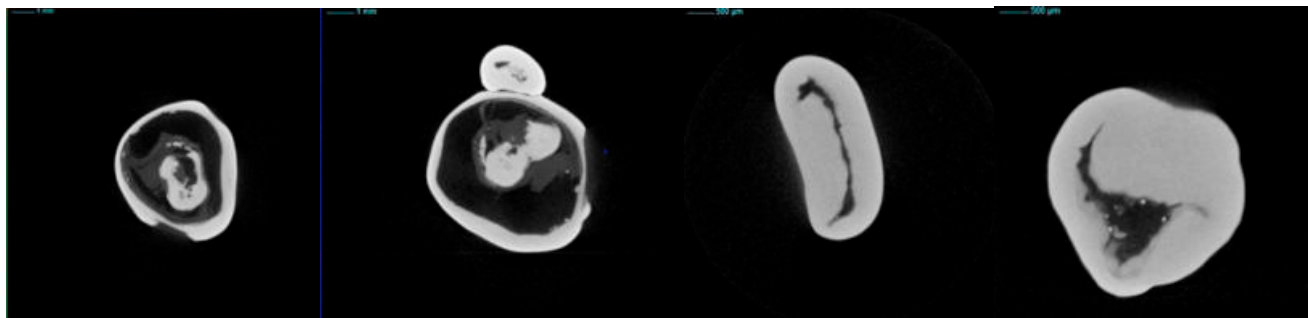


*Figure 1: Two dimensional slices of micro-CT models of a SWNP from *P. radiata*. The structures observed here can be misleading and easily mistaken with those observed in SWCPs without bead (see Figure 3).*

*Figure 2: Two dimensional slices of micro-CT models of a SWNP from *P. radiata*. The structures observed here can be misleading and easily mistaken with those observed in SWCPs without bead (see Figure 4).*

In figures 3 and 4, slices of micro-CT models of a SWCP from *P. maxima* are shown. The cavity visible has a sharp distinct outline and is not flowing much with the external shape of the pearl (figure 3) and has what looks like a curving ‘tail’ at one end with three central white spots. The linear cavity (figure 4) although central, tends to curve more at one end. Both samples have an extremely high and uniform surface lustre.

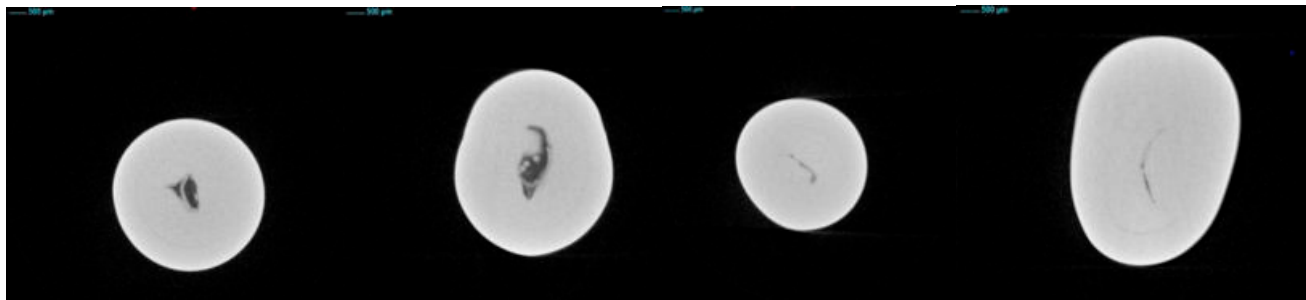


Figure 3: Two dimensional slices of micro-CT models of a SWCP from *P. maxima*.

Figure 4: Two dimensional slices of micro-CT models of a SWCP from *P. maxima*.

Comparing the organic material or voids of the natural and cultured pearls was noticed that there are much darker and more intense to the first. Moreover, different shades of grey were observed at the micro-CT images of natural pearls compared to those of cultured pearls (see Figure 1 vs Figure 3). The voids in natural pearls tend to show different opacity when observed in different directions when compared to the cultured pearls which are more pronounced. Externally, the difference in lustre between the two samples could be of help in their identification as the cultured pearls tend to be smoother and with a much higher surface lustre. However this is not always the case.

The linear structures observed in some natural pearls (see figure 2 left) can be sometimes misleading and confused with those observed in some cultured pearls (see figure 4). However, depending on the intensity and thickness of this structure it might appear different when observed from other directions (see figure 2 right). The linear structures observed in both samples relates to a certain limit to the external shape of the pearls as it is mostly observed in the elongated pearls. However, in the case of the samples studied such lines are always slightly thicker and denser in the natural pearls than cultured pearls.

Additionally, to better monitor these structures, it was very important to rotate the pearls (in the case of X-radiographs). Therefore, the interpretation of results given may vary from one laboratory to another as it is merely based on the opinion and experience of the gemmologist performing the tests. With all the new methods and technologies used in the culturing of pearls, the identification of natural saltwater pearls with cavities had become more challenging when comparing them to cavities visualised in saltwater cultured pearls without a bead.

References:

Akamatsu S., Zansheng T.L., Moses T.M., Scarratt K., 2001. The current status of Chinese freshwater cultured pearls. *Gems & Gemology*, 37 (2), 96-113.

Hänni H.A., 2006. A short review of the use of ‘keshi’ as a term to describe pearls. *Journal of Gemmology*, 30 (1-2), 51-58.

Karampelas S., Michel J., Zheng-Cui M., Schwarz J.-O., Enzmann F., Fritsch E., Leu L., Krzemnicki M. S., 2010. X-ray Computed Micro-Tomography Applied to Pearls: Methodology, Advantages, and Limitations. *Gems & Gemology*, 46 (2), 122-127.

Krzemnicki M.S., Friess D., Chalus P., Hänni H.A., Karampelas S., 2010. X-ray computed micro-tomography: Distinguishing natural pearls from beaded and non-beaded cultured pearls. *Gems & Gemology*, 46 (2), 128-134.

Scarratt, K., Moses, T.M., Akamatsu, S., 2000. Characteristics of nuclei in Chinese freshwater cultured pearls. *Gems & Gemology*. 36 (2). 98-109.

Scarratt, K., Bracher P., Bracher M., Attawi A., Safar A., Saeseaw S., Homkrajae A., Sturman N., 2012. Natural pearls from Australian *Pinctada maxima*. *Gems & Gemology*. 48 (4). 236-261.

Sturman N., 2009. The microradiographic structures on non-bead cultured pearls. GIA Thailand, Bangkok, www.giathai.net/pdf/The_Microradiographic_structures_in_NBCP.pdf.

Sturman N., Al-Attawi A., 2006. The "Keshi" pearl issue. *Gems & Gemology*, 42(3), 142.

Acknowledgements:

The authors wish to thank Bahrain Research Centre for supplying all the samples of natural pearls from *Pinctada radiata* (fished at «heirats» around the Kingdom of Bahrain on 2005 and 2012) as well as Stephen Arrow (Arrow Pearls, Broome, Western Australia) for supplying all the SWCPs without bead from *P. maxima*.

Itatiaia mine: a new emerald occurrence near Conselheiro Pena, Minas Gerais, Brazil

Jurgen Schnellrath¹, Ricardo Scholz², Dietmar Schwarz³, Stefanos Karamelas⁴, Ariadne Senna Azzaro⁵

- 1 Centro de Tecnologia Mineral, Rio de Janeiro, Brazil; jurgen@cetem.gov.br
 2 Universidade Federal de Ouro Preto, Brazil; r_scholz_br@yahoo.com
 3 Gübelin Gem Lab, Lucerne, Switzerland; drdietmarschwarz@hotmail.com
 4 Gübelin Gem Lab, Lucerne, Switzerland; s.karamelas@gubelingemlab.ch
 5 Universidade Federal do Rio de Janeiro, Brazil; lilikazaro@gmail.com

Brazil is one of the leading producers of emerald, together with Colombia and Zambia. Although non commercial emerald occurrences are known in Brazil since 1912, only in 1963 the first Brazilian emeralds from the State of Bahia got international attention. Still in the 1960's other important occurrences were found in that state, followed by new ones in the 1970's (State of Minas Gerais) and 1980's (State of Goiás and again Minas Gerais). Soon Brazil became one of the most important players in the emerald business. Since then other mines of economic importance were discovered in the vicinity of the already known sources, especially in the Itabira/Nova Era region in Minas Gerais. New occurrences, in places with no previous reports of emerald production, are also being sporadically found. Fazenda Bonfim in Rio Grande do Norte is one of the most recent discoveries reported in literature (Zwaan et al., 2012).

The Itatiaia Mine in Conselheiro Pena, Minas Gerais, is a medium sized pegmatite that begun its operation in 1942 for the production of industrial mica, quartz and beryl. Tourmalines of different colors (red, green and bi-colored), and slightly bluish, greenish or yellowish beryls of gemological quality are also found as byproducts. Although emeralds have never been mined at this location, rumors of small emerald crystals having been found in that area were reported (CPRM, 1998). In that same work, the authors already noticed that locally the pegmatite intersected amphibolitic layers present in the enclosing biotite schist, leading them to state that this was a favorable condition for the formation of this gem.



Figure 1. 1.88 ct cut emerald from the Itatiaia mine.



Figure 2. Cluster of emerald crystals in biotite-phlogopite schist from the Itatiaia mine.



Figure 3. Emerald in a wall of biotite-phlogopite schist.

In 2010 Geometa Ltda, the mining company that now owns the rights over the area, found the first emeralds when they were digging a shaft following a subvertical lense of a biotite-phlogopite schist with a proven chromium anomaly, in the search for the so long sought after emeralds. The crystals were analyzed by independent gemologists and a report was issued confirming them as emeralds. After a long period of legalization and research activities, the mine

entered production in 2012. Its economic feasibility has still to be proven, but the information so far are promising.

The Conselheiro Pena pegmatite district (CPPD) is one of the eleven metallogenic subdivisions of the Eastern Brazilian Pegmatite Province (EBP), which is inserted in the domains of the Araçuaí fold belt (Almeida, 1977). In the region of interest the predominant rocks are granitoids of different suites, such as Urucum and Palmital of Eocambrian to Paleozoic age, and Galiléia of Neoproterozoic age, as well as gneisses, schists, quartzites, and calcsilicate rocks of Neoproterozoic age (Tumiritinga and São Tomé formations of the Rio Doce group). Ages of the pegmatite bodies are about 580 My (Nalini, 1997), and are related to the granite G2 Supersuite (Pedrosa-Soares et al., 2001), which are intrusive in the metasediments. They consist mostly of S-type peraluminous granites and minor metaluminous granites, generated during the syn-collisional stage of the Araçuaí orogen.

The Itatiaia pegmatite is located in the southern portion of the CPPD, and is composed mainly by quartz, albite, and muscovite, with beryl, spodumene, tourmaline, and garnet as accessory minerals. The pegmatite body has a tabular shape, west-east elongation, and is both differentiated and zoned. The intermediate zone is composed of perthitic feldspar, with muscovite, black tourmaline, hyaline and milky quartz. The core is composed mostly of milky quartz. Huge altered spodumene crystals are found in the upper parts of the pegmatite. A high developed hydrothermal process was responsible for the introduction of Na in the system and the substitution of microcline by albite (cleavelandite) and muscovite. The pegmatite body, in general, is hosted by a quartz-biotite +- garnet schist with N-NW strike and an almost vertical dip. Intercalations of calcsilicatic and ultramafic rocks, mainly biotite/phlogopite schists of up to 4 m thickness, occur locally. The emerald mineralization occurs along the inferior discordant contact between the biotite/phlogopite schist and the pegmatite. Locally emerald crystals can also be found in a talc schist.

The emerald crystals are usually in the millimeter range, but a crystal with a diameter of 5.5 cm has already been found. The color of the emeralds varies from a light green to a saturated slightly bluish green. Unfortunately, up to now, most of the crystals show a colorless and included core, making it difficult to obtain bigger cut stones. Despite this, several stones of high clarity above the 2 ct range have already been produced.

The refractive indices of the emeralds lie in the normal range for natural emeralds, with n_o varying from 1.587 to 1.590 and n_e from 1.580 to 1.583, with a birefringence of 0.007. Specific gravity varied from 2.72 to 2.74 g/cm³.

Results of quantitative chemical analyses (XRF) performed so far are listed below:

Cr ₂ O ₃ : 0.05 to 0.55%	av.: 0.25%
V ₂ O ₃ : bdl to 400 ppm	av.: 150 ppm
Fe ₂ O ₃ : 0.32 to 0.99%	av.: 0.40%
MgO: 2.1 to 3.4%	av.: 2.4%
Na ₂ O: 1.4 to 1.9%	av.: 1.5%
Cs ₂ O: 0.15 to 0.3%	av.: 0.2%

It was also possible to detect traces of K, Ca, Mn, Zn, Ga, Rb. This chemical make-up is compatible with schist type emeralds, as are the Raman spectra.

The optical absorption spectrum (ordinary ray) revealed intense bands at around 440 and 600 nm, as well as less intense bands at around 640 and a doublet at 680 and 685 nm, all probably due to Cr³⁺. The bands at around 370 and 835 nm are probably due to Fe³⁺ and Fe²⁺ respectively.

In the FTIR absorption spectrum it is possible to observe a very intense broad band with total absorption from 3.900 to 3.400 cm⁻¹, as well as other quite intense bands at about 5.300 and 7.100 cm⁻¹, and a less intense band at 3.240 cm⁻¹, all probably due to various vibrations of water (and/or hydroxyl related) molecules. The sharp band at around 2.355 cm⁻¹

is most likely due to CO₂ vibrations.

As mineral inclusions we were able to identify, using MEV and Raman techniques, biotite/phlogopite, chlorite, apatite, zircon with Hf, pyrite with Ni, uraninite, thorianite(?), tourmaline, nickeline, gersdorffite, and quartz. Other types of inclusions are fluid inclusions, most of them two-phase liquid-gas inclusions, and growth phenomena. A very typical inclusion is a cloud like aggregation of tiny fluid (?) inclusions.

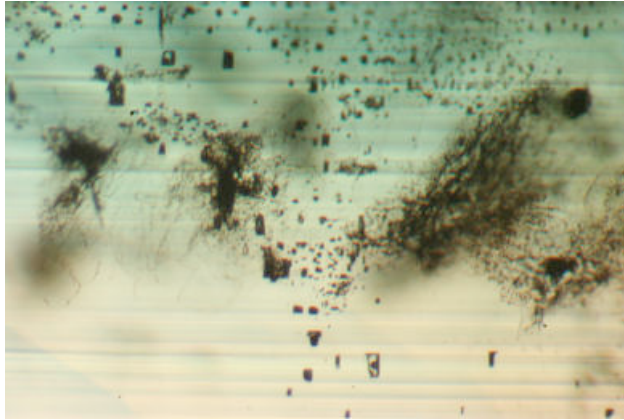


Figure 4. Typical inclusions in emeralds from the Itatiaia mine: two-phase liquid-gas inclusions, growth lines and cloud like aggregations of tiny fluid (?) inclusions.

References

- Almeida, F.F.M., 1977. O Craton do São Francisco. *Revista Brasileira Geociências*, 7, 349-364.
- Netto, C., Araujo, M.C., Pinto, C.P., Drumond, J.B.V., 1998. Projeto Leste: Cadastramento de Recursos Minerais, Pegmatitos. CPRM, Belo Horizonte, 197 pp.
- Nalini, H.A., 1997. Caractérisation dès suites magmatiques néoprotérozoïques de la region de Conselheiro Pena et Galiléia (Minas Gerais, Brésil). Saint Etienne, These de Docteur, Ecole Nationale Superieure dès Mines de Saint Etienne, 237 pp.
- Pedrosa-Soares, A.C., Noce, C.M., Wiedermann, C.M., and Pinto, C.P., 2001. The Araçuaí-West Congo orogen in Brazil: an overview of a confined orogen formed during Gondwanaland assembly. *Precambrian Research*, 110, 307-323.
- Zwaan, J.C., Jacob, D.E., Häger, T., Cavalcanti Neto, M.T.O., and Kanis, J., 2012. Emeralds from the Fazenda Bonfim Region, Rio Grande do Norte, Brazil. *Gems & Gemology*, 48(1), 2-17.

Identification of Maxixe beryls by EPR

Jean Marie Dereppe 1 and Claudette Moreaux 2

1 University of Louvain. Louvain La Neuve. Belgium. Jean-Marie.Dereppe@uclouvain.be

2 AGB. Court saint Etienne. Belgium. jefe@skynet.be

Maxixe beryls were discovered in 1917 in the Maxixe mine south of Aracuai, Minas Gerais, Brazil and first described by Wild (1933). This very rare type of beryl is characterized by a bright blue colour similar to the one shown by good quality sapphire. Around 1970 another kind of deep blue beryl appeared on the market and showed slightly different properties and was named Maxixe-type beryl (Nassau & Wood, 1973). Unfortunately both type of beryl faded relatively fast when exposed to intense light or temperature of the order of 100-150°C. Nevertheless original colour could be restored by artificial irradiation.

Maxixe beryl were studied by using Electron Paramagnetic Resonance (Anderson 1979 & 2010). Electron Paramagnetic Resonance (EPR) is a spectroscopic technique for studying chemical species that have one or more unpaired electrons. Every electron has a magnetic moment and spin quantum number $s=1/2$ with magnetic components $m_s=+1/2$ and $m_s=-1/2$. In the presence of an external magnetic field with strength B , the electrons the magnetic moments align either parallel or antiparallel to the field giving rise to two energy states separated by $\Delta E = g_e \mu_B B_0$. Where g_e is the Landé g factor and μ_B is the Bohr magneton. An unpaired electron can move between the two energy levels by absorbing or emitting radiation of energy $\varepsilon = h\nu = \Delta E$ which gives the fundamental equation of EPR as $h\nu = g_e \mu_B B_0$. Many measurements are made at 9-10 GHz in a magnetic field of 0.35T. Interaction of the electronic spin with the environment and with the other spins gives rise to "fine structures" which displace and broadens the resonance lines.

It was shown that the colour was due to a colour centre related to a NO_3 group for the Maxixe beryl and to a CO_3 group for the Maxixe-type. EPR can distinguish easily between Maxixe and Maxixe-type beryls. This can be useful as rate for colour fading is rather different for the two types of beryl.

References

- Andersson, L.O., 1979. The difference between Maxixe beryl and Maxixe-type beryl: an electron paramagnetic resonance investigation. *J. Gemm.*, 16, 213-217.
- Anderson, L.O., 2010. EPR investigation of NO_3 and CO_3 and other radicals in beryl. *Phys. Chem. Minerals* 37, 435-451.
- Nassau, K., Wood, D.L. 1973. Examination of the new Maxixe-type blue and green beryl. *Gems & Gemology*, 14, 130-133.
- Wild, G.O., 1933. Mitteilung über ein anscheinend neues Berylliumsilikat. *Zentralbl. Mineral. Geol. Paläont.* 1933A, 38-39.

New features to identify natural and synthetic emerald by vibrational spectroscopy

Le Thi-Thu Huong¹, Tobias Häger², Wolfgang Hofmeister², Stefanos Karamelas³,
Nguyen-Duc Trung-Kien⁴

¹Faculty of Geology, Hanoi University of Science, Hanoi, Vietnam; lethth@vnu.edu.vn

²Centre of Gemstone Research, University of Mainz, Germany

³Gübelin Gem Lab, Lucerne, Switzerland

⁴Advanced Institute for Science and Technology, Hanoi University of Technology, Vietnam

Raman and IR spectroscopy have been used in identifying natural and synthetic emerald based on the vibration features in the water range (Schmetzer & Kiefert, 1989; Huong et al., 2010). This abstract shows other possibilities to separate between natural and synthetic material based on other Raman and IR signals in the range of silicate structural vibration. We will focus on a Raman band at about 1070 cm⁻¹ generated by Si-O stretching vibration (Adams and Gardner, 1974) and an IR band (and its shoulder) around 1200 cm⁻¹, also generated by Si-O vibration (Aurisicchio et al., 1994).

In total, 326 samples, including 260 emerald crystals and 66 faceted synthetic emeralds were investigated with Raman, IR spectroscopy and EPMA. An Ar⁺ ion laser (514 nm emission), a grating of 1800 grooves/mm and a spectral acquisition time of 240 seconds were used with the Raman-spectrometer, resulting in a spectral resolution of 0.8 cm⁻¹. Samples were investigated with IR using powdered emerald mixed with KBr (KBr pellet technique) with 100 scans and 4 cm⁻¹ resolution.

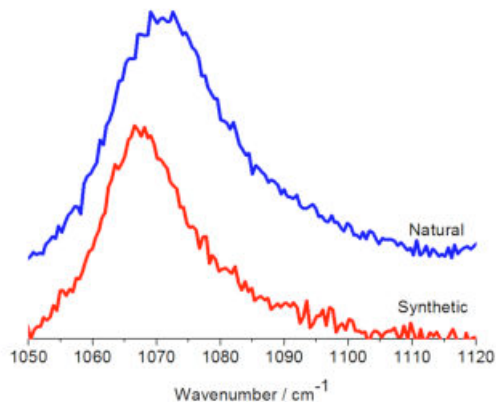


Figure 1. The Raman peak of a representative natural emerald is at a higher wavenumber than the Raman peak of a synthetic emerald.

The Raman band at about 1070 cm⁻¹:

In synthetic samples this band occurred at the position around 1067-1068 cm⁻¹ and its FWHM varied between 11 cm⁻¹ and 14 cm⁻¹. Whereas, in natural samples the band positioned at 1068 cm⁻¹ to 1072 cm⁻¹ and its FWHM varied between 12 cm⁻¹ and 26 cm⁻¹. The band obviously consisted of two Gaussian peaks fitted at about 1068 cm⁻¹ and 1072 cm⁻¹ (Figure 1). The shifting and broadening of the band could be attributed to different relative intensities of these peaks. Correlation diagrams of chemical data, Raman band positions and FWHMs showed that the band broadened and shifted to higher wavenumber when the content of silicon decreased (Figure 2). The shifting and broadening of the band are probably due to the results of chemical substitution. Trivalent and/or divalent ions substitute silicon in the crystal structure and charge compensators are served by alkali ions such as Na⁺, K⁺ which exist in structural channels. The correlation between Si- and alkali ion contents elucidated this fact as in samples with low Si amount, the alkali content

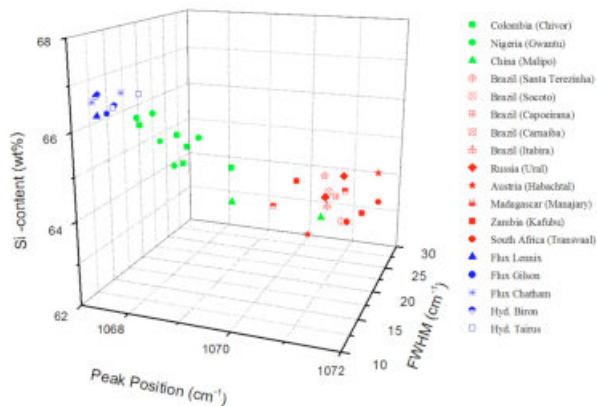


Figure 2. This diagram shows the correlation among position of the Raman peak, FWHM, and Si-content: The higher the position of the Raman peak, the higher the FWHM value, which corresponds to a lower silicon content

was high (Figure 3).

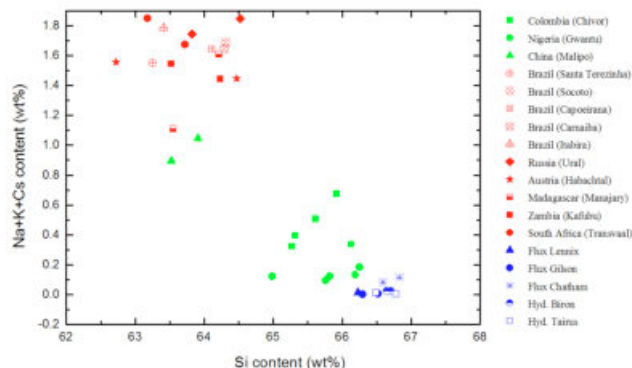


Figure 3. This diagram shows the correlation between silicon and alkalis content in natural and synthetic emeralds.

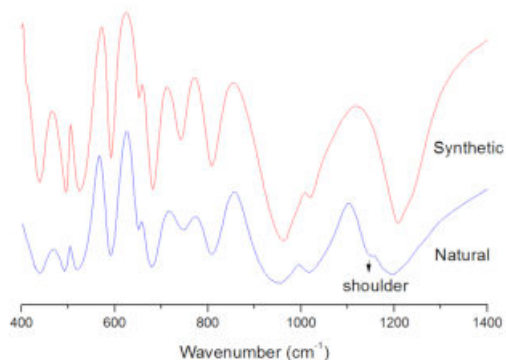


Figure 4. Natural and synthetic emerald show an IR band around 1200 cm⁻¹; in addition, natural emerald shows a shoulder around 1140 cm⁻¹. This shoulder did not appear in the synthetic emeralds studied.

The IR band at 1200 cm⁻¹ and its shoulder:

The band around 1200 cm⁻¹ in fact varies in its actual position from 1171-1207 cm⁻¹. All synthetic samples show the band around 1200 cm⁻¹ to about 1207 cm⁻¹, and natural emeralds show the band around 1171 cm⁻¹ to 1203 cm⁻¹. In addition, all emeralds of schist type show a shoulder at about 1140 cm⁻¹. Among non-schist type samples, this shoulder can be seen in Colombian (Chivor), Chinese emeralds but not in Nigerian emeralds. It is not observed in any of the synthetic samples (Figure 4). Correlating chemical data, it is found that the presence of the shoulder is also related to the alkali content. In the samples with high content of alkali ions (usually belonging to the schist type) the shoulder at 1140 cm⁻¹ is clearly present and also the position of the band at 1200 cm⁻¹ shifts backward to lower wavenumbers. In samples with low alkali content (usually synthetic samples), the shoulder disappears and the band at 1200 cm⁻¹ shifts towards higher wavenumbers.

Based on our results, in many cases natural and synthetic emeralds can be separated by Raman and IR spectroscopy. Not only the vibration signals in the range of water, but also in the range of the silicate, can be used to separate between natural and synthetic samples. Nevertheless, a larger number of samples, including synthetics with high alkali content and natural emeralds with low alkali content- have to be investigated before definitive conclusions can be drawn.

References

- Adams, D.M., Gardner, I.R, 1974. Journal of the Chemical Society - Dalton Transactions, 1502-1505.
- Auricchio, C., Grubessi, O., Zecchini, P., 1994. Infrared spectroscopy and crystal chemistry of the beryl group. The Canadian Mineralogist, 32, 55-64.
- Huong L.T.T., Häger T., Hofmeister W., 2010. Micro Raman spectroscopy: A powerful tool to identify natural and synthetic emerald. Gems & Gemology, 46(1), 36-41.
- Schmetzer K., Kiefert L., 1990. Water in beryl—A contribution to the separability of natural and synthetic emeralds by infrared spectroscopy. Journal of Gemmology, 22(4), 215-223.

Acknowledgment

This study is part of a PhD thesis of the first author at the University of Mainz, that still is continued at Vietnam National University, Hanoi, where now the first author works as a permanent researcher.

The role of vanadium and titanium in natural and synthetic chrysoberyl and alexandrite – coloration, chatoyancy and asterism

Karl Schmetzer¹, Michael S. Krzemnicki², Thomas Hainschwang³, Heinz-Jürgen Bernhardt⁴

¹ 85238 Petershausen, Germany, SchmetzerKarl@hotmail.com

² SSEF Swiss Gemmological Institute, CH-4001 Basel, Switzerland, gemlab@ssef.ch

³ GGTL Laboratories, Gemlab (Liechtenstein)/GemTechLab, FL 9496 Balzers, Liechtenstein/CH 1227 Geneva, Switzerland, thomas.hainschwang@ggtl-lab.org

⁴ ZEM, Institut für Geologie, Mineralogie und Geophysik, Ruhr-University, 44780 Bochum, Germany, Heinz-Juergen.Bernhardt@rub.de

Vanadium-bearing natural chrysoberyl is known from Tunduru, Tanzania (Johnson and Koivula, 1996; Bank et al., 1997; McClure, 1998), and vanadium-bearing synthetic chrysoberyl was also described (Krzemnicki & Kiefert, 1999; Schmetzer & Bosshart, 2010). Vanadium-bearing chrysoberyl crystals show weak pleochroism, but no colour change between daylight and incandescent light. Chrysoberyl with almost equal amounts of vanadium and chromium, e.g. from Orissa or Andhra Pradesh, India, are also bright green in daylight, but change their colour in incandescent light only to a pale grayish green, almost colourless (see again Schmetzer & Bosshart, 2010).

Titanium-bearing synthetic chrysoberyl crystals are known for technical use as laser materials, and faceted gemstones were briefly mentioned by Krzemnicki & Kiefert (1999). It is assumed that the pink coloration of these samples is caused by trivalent titanium. Furthermore, synthetic titanium-bearing alexandrite cat's-eyes as well as synthetic asteriated alexandrite is also known (Kane, 1987; Scarratt, 1988; Koivula et al., 1988; Schmetzer & Hodgkinson, 2011). Minute needle-like particles are found in three orientations with the alexandrite crystals, causing three different light bands which are inclined to each other at 60°.

Vanadium-bearing synthetic chrysoberyl (Figure 1) has been grown by Kyocera in Japan. Vanadium contents were found in the range of 0.11 to 0.13 wt% V₂O₃. Vanadium-bearing natural chrysoberyl in which the vanadium contents exceed the chromium contents of the samples were examined from four different sources, from Tunduru in Tanzania, from Ilakaka in Madagascar, from Sri Lanka and from Mogok, Myanmar (Figure 2). The samples from Ilakaka, Madagascar, revealed vanadium contents in the range of 0.02 to 0.15 wt% V₂O₃ with chromium being always below 0.01 wt% Cr₂O₃. Vanadium-bearing chrysoberyl from Tunduru, Tanzania, can be subdivided into two varieties. Some lighter bluish green samples are almost chromium-free (with Cr₂O₃ at or below 0.01 wt%) and vanadium contents in the range of 0.04 to 0.10 wt% V₂O₃. Some more intense bluish green chrysoberyls from Tunduru with vanadium contents of 0.16 and 0.18 wt% V₂O₃ showed chromium contents of 0.03 to 0.04 wt% Cr₂O₃. The somewhat more yellowish green vanadium-bearing chrysoberyls from Sri Lanka, in general, showed chromium contents in the range of or only slightly below the vanadium contents of the samples. One crystal, for example, showed vanadium contents of 0.08 wt% V₂O₃ with chromium contents of 0.05 wt% Cr₂O₃. The extremely intense bluish green gem chrysoberyls from Mogok, Myanmar, showed distinctly higher vanadium and chromium contents. For one faceted gemstone, the amounts of colour causing trace elements were determined as 0.38 wt% V₂O₃ and 0.24 wt% Cr₂O₃. A similar chrysoberyl from Mogok was already described by Payne (1956).

Absorption spectra of the synthetic vanadium-bearing chrysoberyls and the chromium-free or almost chromium-free natural samples show the known absorption maxima of trivalent vanadium in chrysoberyl (Bukin et al., 1980). Additional iron bands were recorded in natural samples from Tanzania, Madagascar, and Sri Lanka, the bright green samples from Myanmar were iron-free. According to the overlap of the absorption bands of trivalent vanadium and chromium in chrysoberyl (Figure 3), no separated absorption maxima for vanadium and chromium were recorded. There is, however, a shift observed for the main absorption maximum in the visible range. This maximum was recorded

for chromium-free, vanadium-bearing samples in the range of 608 nm, and shifts towards lower wavelengths with increasing chromium contents. For the chrysoberyl from Myanmar mentioned above, the maximum of this strong absorption band was observed at 589 nm.

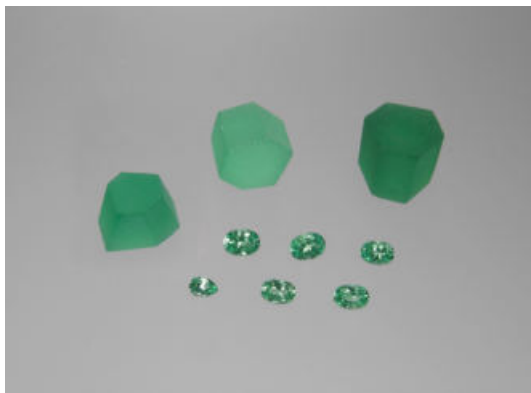


Figure 1. Rough and faceted vanadium-bearing synthetic chrysoberyls produced by Kyocera in Japan in daylight; size of the rough crystal above right 15.5 x 14.5 x 15.5 mm, weight 52.50 ct, the faceted sample below left weighs 0.49 ct and measures 6.0 x 4.0 mm. Photo by K. Schmetzer.



Figure 2. Natural and synthetic vanadium-bearing chrysoberyls; from left to right (a) three chrysoberyls from Sri Lanka, (b) chrysoberyl from Mogok, Myanmar, (c) three chrysoberyls from Tunduru, Tanzania, (d) two synthetic chrysoberyls produced by Kyocera in Japan; daylight, the triangular chrysoberyl from Tunduru weighs 0.38 ct and measures 4.3 x 4.2 mm. Photo by K. Schmetzer.

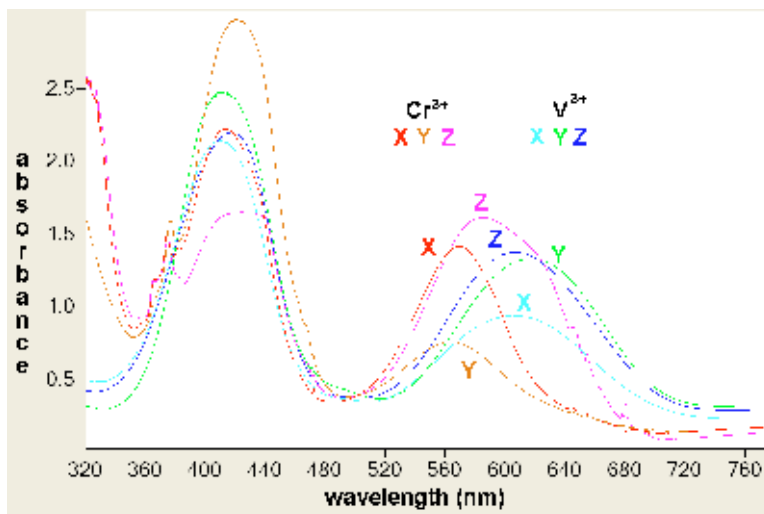


Figure 3. Plot of the polarized absorption spectra of chromium (Cr^{3+}) and vanadium (V^{2+}) in chrysoberyl; both transition metal ions show two strong absorption bands, a first absorption band at higher wavelength, and a second absorption band at lower wavelength. For all three directions (X, Y and Z) the absorption maxima for the first absorption band of vanadium are located at higher wavelengths than the maxima of the first chromium absorption band; for the second absorption band of vanadium the maxima are in the range of the maxima representing the second chromium band. Spectra were recorded from a synthetic alexandrite grown by Creative Crystals (for chromium) and from a synthetic chrysoberyl grown by Kyocera (for vanadium).

Titanium-bearing synthetic chrysoberyl (Figure 4) has been grown by Kyocera in Japan. Titanium contents were found in the range of 0.21 to 0.37 wt% TiO_2 . Synthetic alexandrites showing asterism or chatoyancy, on the other hand, revealed higher titanium-contents of 0.46 to 0.56 wt% TiO_2 , with chromium and vanadium contents of the range of 0.23 to 0.26 wt% Cr_2O_3 and 0.11 to 0.12 wt% V_2O_3 , respectively. This material (Figure 5) was also produced by Kyocera

in Japan. Chatoyancy and asterism are due to three series of minute needle-like inclusions, which are located in planes parallel to the a (100) pinacoid. These elongated particles (Figure 6) are oriented parallel to the c-axis of the chrysoberyl crystals and at angles of about $+60^\circ$ and -60° to this direction.

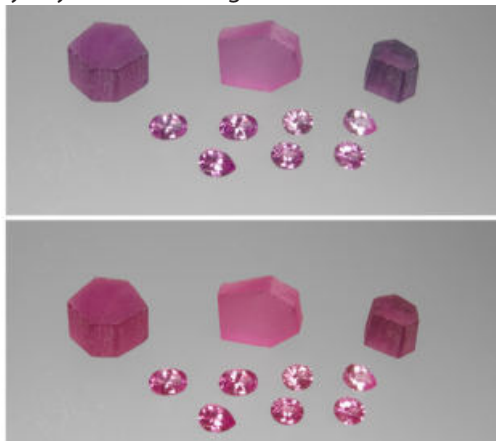


Figure 4. Rough and faceted titanium-bearing synthetic chrysoberyls produced by Kyocera in Japan in daylight (above) and incandescent light; size of the rough crystal above left 16.0 x 15.5 x 10.0 mm, weight 34.12 ct, the faceted sample below left weighs 1.08 ct and measures 7.8 x 5.7 mm. Photo by K. Schmetzer.

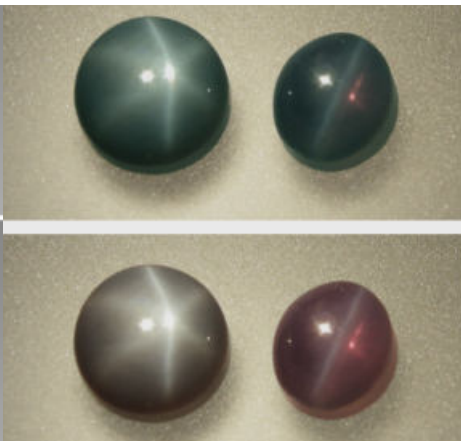


Figure 5. Synthetic asteriated alexandrite (left, 2.62 ct, diameter 8.0 mm) and synthetic alexandrite cat's-eye (1.55 ct, 7.0 x 6.0 mm) produced by Kyocera in Japan in daylight (above) and incandescent light. Photo by K. Schmetzer.

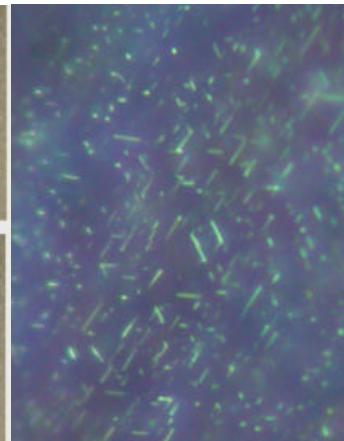


Figure 6. A thin section of an asteriated synthetic alexandrite from Kyocera oriented almost parallel to the a pinacoid shows three series of needles which form angles near 60° to each other. Reflected light, crossed polarizers, field of view 56 x 42 μm . Photo by H.-J. Bernhardt.

The production of synthetic chrysoberyl and alexandrite cat's-eyes is described in numerous Japanese and international patent applications, most of them published in the 1980s.

The production of alexandrite cat's-eyes involves a two-step growth and annealing process. The first step includes the production of homogeneous single crystals containing titanium oxide as dopant. Crystal growth is performed under neutral (e.g. argon or nitrogen) or reducing atmospheres and titanium is present in its trivalent state. In the second step annealing of the crystal at elevated temperatures in an oxidizing atmosphere is performed. During this second part of the process titanium is oxidized and elongated particles, most probably rutile needles, are precipitated. These exsolved particles are responsible for chatoyancy or asterism of the material when cut as a cabochon. The observation of one or three light bands in the center of the cabochon is only dependant of the orientation of the cut.

Absorption spectra of the synthetic titanium-bearing chrysoberyls and the chromium-free or almost chromium-free natural samples show the known absorption maxima of trivalent titanium in chrysoberyl (Segawa et al., 1987). Absorption spectra of the alexandrite cabochons showed a chromium spectrum with somewhat less transparency around 500 nm, i.e. in the area between the two strong chromium absorption bands. In this area, the known absorption maxima of trivalent titanium in chrysoberyl are located (Figure 7). Thus, the colour and pleochroism of the Kyocera synthetic chatoyant or asteriated alexandrites is understood if we assume the presence of various amounts of titanium in its trivalent state (in addition to chromium and vanadium as main colour causing trace elements). Most probably, not all titanium is exsolved by the heating step of production to form the minute rutile needles.

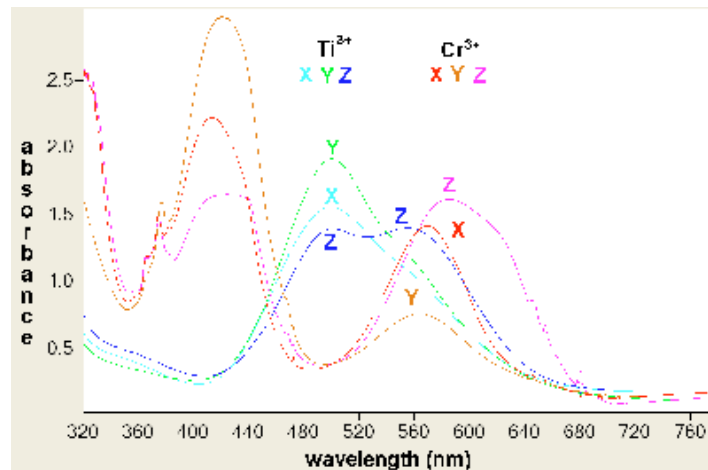


Figure 7. Plot of the polarized absorption spectra of chromium (Cr^{3+}) and titanium (Ti^{3+}) in chrysoberyl; for all three directions (X, Y and Z) the absorption maxima for the strong titanium band are located between the two strong chromium absorption bands; for samples which contain distinct amounts of chromium together with titanium in its trivalent state, only X is intense red orange, and Y and Z become very dark, almost non-transparent. Spectra were recorded from a synthetic alexandrite grown by Creative Crystals (for chromium) and from a synthetic chrysoberyl grown by Kyocera (for titanium).

References

- Bank, H., Henn, U., Milisenda, C.C., 1997. Mintgrüner Chrysoberyll aus Tansania. *Zeitschrift der Deutschen Gemmologischen Gesellschaft*, 46 (2), 63.
- Bukin, G.V., Eliseev, A.V., Matrosoy, V.N., Solntsev, V.P., Kharchenko, E.I., Tsvetkov, E.G., 1980. The growth and examination of optical properties of gem alexandrite. In: Sidorenko, A.V. et al. (Eds). *Inhomogeneity of minerals and crystal growth. Proceedings of the XI General Meeting of IMA, Novosibirsk 1978*, published Moscow 1980, pp. 317–28 (in Russian).
- Johnson, M.L., Koivula, J.I. (Eds.), 1996. Nonphenomenal vanadium-bearing chrysoberyl. *Gems & Gemology*, 32 (3), 215–216.
- Kane, R.E., 1987. Inamori synthetic cat's-eye alexandrite. *Gems & Gemology*, 23 (3), 158–62.
- Koivula, J.I., Fritsch, E., Fryer, C., 1988. The gemmological characteristics of Inamori synthetic cat's-eye alexandrite chrysoberyl. *Journal of Gemmology*, 21 (4), 232–6.
- Krzemnicki, M.S., Kiefert, L., 1999. Bluish green, light green, and pink synthetic chrysoberyl. *Gems & Gemology*, 35 (3) 175.
- McClure, S.F., 1998. Chrysoberyl, dark green. *Gems & Gemology*, 34 (3) 212–213.
- Payne, C.J., 1956. An alexandrite crystal from Burma. *The Gemmologist* 25 (296), 39–40.
- Scarratt, K., 1988. Kyocera synthetics. *Journal of Gemmology*, 21 (3), 136–9.
- Schmetzer, K., Bosshart, G., 2010. Colorimetric data of Russian alexandrite and yellowish green to green chrysoberyl. In: Schmetzer, K. *Russian alexandrites*. Schweizerbart Science Publishers, Stuttgart, 107–120.
- Schmetzer, K., Hodgkinson, A., 2011. Synthetic star alexandrite. *Gems & Jewellery*, 20 (3), 9–11.
- Segawa, Y., Sugimoto, A., Kim, P.H., Namba, S., Yamagishi, K., Anzai, Y., Yamaguchi, Y., 1987. Optical properties and lasing of Ti^{3+} doped BeAl_2O_4 . *Japanese Journal of Applied Physics*, 26 (4), L291–L292.

Acknowledgements

Natural vanadium-bearing chrysoberyls from different sources were obtained from the H.A.Hänni collection, which is housed as reference collection at the SSEF laboratory, Basel, Switzerland. Several natural and synthetic samples were submitted by private collectors, e.g. C. Cavey, S. Hanken, and A. Hodgkinson, which is greatly acknowledged. Synthetic vanadium- and titanium-bearing chrysoberyl were kindly loaned by R. Hochleitner from the Bavarian State Collection of Mineralogy, Munich, Germany.

A Comparative Overview of Inclusions in Spinel

Edward Boehm

Chattanooga, TN; Edward@RareSource.com

Spinel contains many interesting inclusions that reveal secrets about their host rocks and sometimes also their geographic origin. The primary spinel producing countries are Burma (Myanmar), Sri Lanka, Madagascar, Tajikistan, Tanzania, and Vietnam. Spinel host rocks vary but may also have much in common, particularly those from metamorphosed dolomitic limestones ($\geq 50\%$ Mg replacing Ca) commonly referred to as marble. During metamorphism calcic limestones become Magnesium rich which combines with silica to form spinel and silicates such as diopside, epidote, forsterite, garnet, zircon, etc. These same minerals may become characteristic inclusions within spinel. Other minerals that may be found in spinel include apatite, böhmite, diaspore, graphite, hercynite, högbomite, ilmenite, magnetite, various micas, rutile, sphene, and uraninite. These inclusions may be euhedral, subhedral, or corroded.

The most diagnostic and commonly seen inclusions in natural spinels are octahedral negative crystals (Figure 1) that are often aligned in rows or multiple rows within their host. These negative crystals may also be seen containing white dolomite, yellow phlogopite, or black hercynite. Some inclusions or combinations of inclusions may be considered diagnostic for particular geographic origins of spinel. Transparent to white rounded apatite crystals together with attached black hexagonal crystals of ilmenite or graphite form a diagnostic inclusion scene in spinels from Burma (Myanmar). Högbomite on twinning planes is unique to spinels from Morogoro, Tanzania. Sri Lankan spinels often have an assemblage of apatite (Figure 2), diopside, phlogopite, rutile, sphene, uraninite, and zircon.

Synthetic spinels are most often produced by the flame fusion process, which provides several diagnostic inclusions. Flux synthetic spinels may have typical flux inclusions but are often faceted into flawless gems, which require additional testing for conclusive identification. Inclusions in spinels are considered more useful for identifying their host than for origin determination, however, in some cases, diagnostic inclusions are evident.

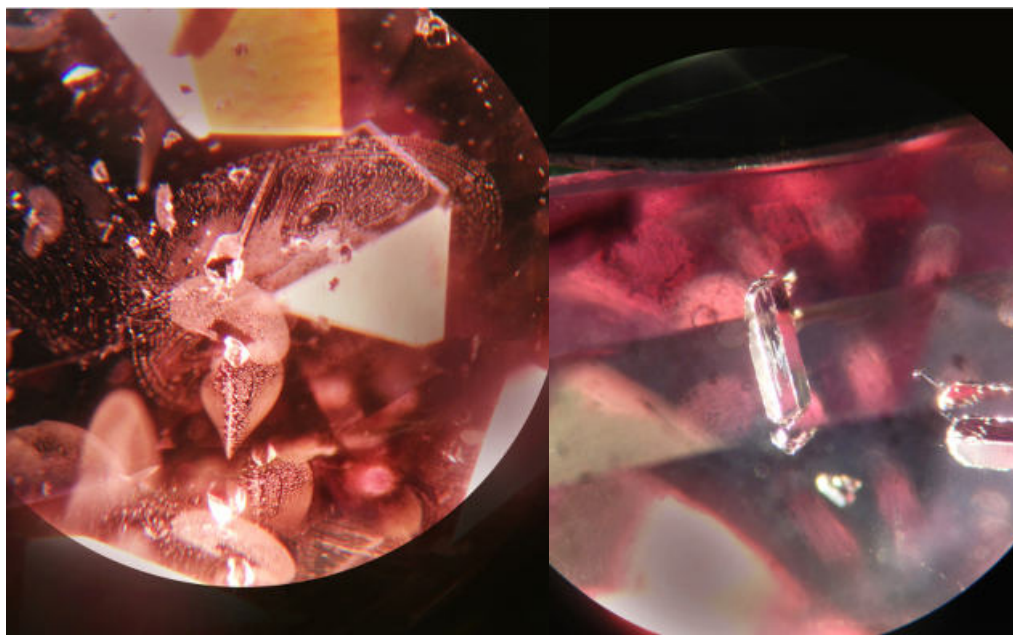


Figure 1. Octahedral negative crystals surrounded by fluid feathers in a rose colored spinel from Burma (Myanmar). From E. Gübelin collection at GIA. Photomicrograph by E. Boehm; magnified 40x, using a iphone 5.

Figure 2 (right): Growth tubes in an apatite crystal inclusion within a pink spinel from Sabaragamuwa, Sri Lanka. Photomicrograph by E. Boehm; magnified 60x, using a iphone 5.

Causes of colour of natural untreated spinels from Vietnam in comparison to flame fusion and flux grown synthetics

Häger, T.1, Hauzenberger, C.2, Lehmann, C.,1 Zimmer, D.1, Nguyen Ngoc Khoi 3,5, Duong Anh Tuan4,5, Le Thi-Thu Huong2 & Hofmeister, W.1

1 Centre of Gemstone Research, Johannes Gutenberg-University Mainz, 55099 Mainz, Germany
Tobias.Haeger@Uni-Mainz.de

2 Institute for Earth Sciences, Karl-Franzens-University Graz, A8010, Graz, Austria

3 Faculty of Geology, Hanoi University of Science, Hanoi, Vietnam

4 Inst. of Material Sciences, Vietnam Academy of Sciences & Technology, Hanoi, Vietnam

5 DOJ Gold & Gems Group, 44 Le Ngoc Han, Hai Bai Trung, Hanoi, Vietnam

In the last years spinel came more and more into vogue. Since 1987 spinel is found in the northern part of Vietnam in the Yen Bai area. Deposits are located near An Phu, Khoan Thong, Minh Tien, and Truc Lau in Luc Yen, and at Tan Huong in Yen Binh. In February 2010 a new occurrence of spinel has been detected near Lang Chap. This new mining area is famous for its vivid orange-red padparadscha-like stones (Khoi et al., 2011), but still today the most productive spinel deposit remains the Cong Troi mine in An Phu (Huong 2012).

Materials and methods

More than 34 natural samples have been selected, with colours ranging from blue to red via violet and from red to brown via orange (see Figure 1). Furthermore 7 blue flame fusion grown and 5 flux grown red and 3 flux grown blue synthetic spinels have been chosen (see Figure 2). The flux grown synthetics have been selected because of its inverse spinel amount (magnesium is on the aluminium position in the crystal structure and vice versa) and the flame fusion grown spinels, because of its defect spinel content (in defect spinels the Mg to Al ratio is not 1:2. Aluminium exceeds the 1:2 ratio and the additional charge is compensated by magnesium vacancies). Plane parallel plates have been produced. For major and minor elements the Electron Probe Micro Analysis (EPMA) have been selected and for minor and trace elements the Laser Ablation-Inductive Coupled Plasma-Mass Spectroscopy (LA-ICP-MS). Aluminium, determined with EPMA, was used as internal standard, NIST612 as standard glass and for drift correction and NIST 610 and BCR were analysed for quality check. The UV-Vis-NIR spectra were recorded with a Zeiss Axiolmager A2m microscope. Attached were two spectrometers from the company J&M (Germany).



Figure 1 (left): A selection of the analyzed natural, untreated samples from Vietnam.

Figure 2 (right): Selected flame fusion grown synthetic spinels (oval), 1 red flux grown and 3 blue flux grown synthetic spinels.

Unfortunately no natural sample with a single cause of colour has been found in the sample set. To eliminate the influence of V and Fe in red spinels a sample (sp1d) with the highest Cr/V ratio (48) and a sample (sp2c) with a lower Cr/V ratio (13.5) was chosen. Luckily these two samples contained a similar V/Fe-ratio, but unfortunately different V content. To solve this problem and to be able to compare the spectra of both samples, the following formula $AV_{\text{Vanadium_calc}} = (AV_{\text{Vanadium_meas}} * c_{\text{Vanadium_calc}} * t_{\text{calc}}) / (c_{\text{Vanadium_meas}} * t_{\text{meas}})$ was deduced from the Bouguer-Lambert-Beer-Law ($A = \text{absorbance}$, $c = \text{the amount of the element}$ and $t = \text{sample thickness}$). Due to the fact, that the absorption coefficient was used (absorbance divided by the sample thickness), the sp2c spectrum ($AV_{\text{Vanadium_meas}}$) was just multiplied by the factor 0.73 ($c_{\text{Vanadium_calc}} / c_{\text{Vanadium_meas}}$). The resulting spectrum displays the same V- and a quiet similar Fe-content in comparison to sp1d. This calculated spectrum was subtracted from spectrum sp1d. The difference shows a "pure" Chromium spectrum (Figure 3).

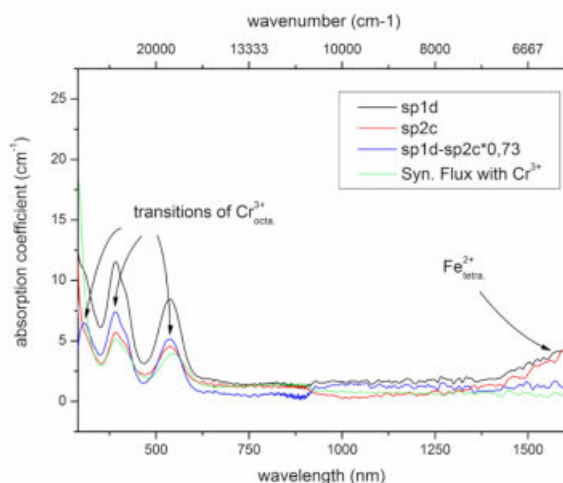


Figure 3. Spinel sp1d shows a spectrum dominated by Cr^{3+} . Sp2c has a similar V/Fe ratio as sp1d. To eliminate the V- and Fe-content out of the spectra sp2c was multiplied by the factor 0.73 and afterwards subtracted from sp1c. The difference displays the "pure" Cr^{3+} -Spectrum. Additionally a Cr^{3+} containing flux grown sample is shown.

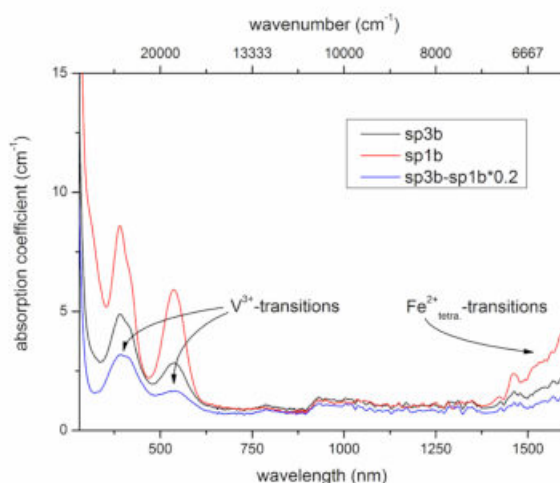


Figure 4. Sample 3b has the highest V/Cr-ratio and a similar Cr/Fe ratio as sample sp1b. To eliminate the Cr-content in the spectrum sp1b, it was multiplied by 0.2 and afterwards subtracted from spectrum sp3b. The resulting difference shows a "pure" V^{3+} spectrum in spinel.

The Peak maximum at 391 nm occurs in all spectra at the same position (see Table 2). The shoulder around 410 nm differs slightly for the V^{3+} spectrum and all three differ in the Peak around 540 nm. Only natural Cr^{3+} containing samples do show a shoulder around 307 nm. The shoulder around 307 nm, the Peak maximum around 540 nm and the Peak ratio of the maxima around 391 and 540 nm are therefore a useful tool to differentiate between natural and synthetic flux grown samples and to differentiate between Cr^{3+} and V^{3+} . In accordance to Reed (1971), the shoulder does not occur in flame fusion grown synthetic stoichiometric Cr^{3+} doped spinels. This study seems to indicate that with increasing inverse spinel content the shoulder at 307 nm disappears. Vanadium in small amounts is leading to an orange red, but with increasing V-content the colour turns to brownish red. Typical samples can be seen in Figure 1 in the third row from above, the first, second and third spinel from the left side.

Results – blue spinels

The spectrum "nat. Fe blue spinel" in Figure 5 displays only Fe^{2+} transitions in tetrahedral and octahedral sites (assignments Dickson & Smith, 1976). The spectrum "Co-Flame fusion" shows a pure Co^{2+} diagram without any calculation (because of its low Fe content, see Table 3), while in spectrum "nat. Co-spinel" and in the synthetic flux grown spinel the Fe content has been eliminated in the same way as described previously for V. All resulting cobalt spectra are identical. Just the peak intensity ratio of the peak at 580 nm / 594 nm shoulder seems to be different. In Figure 1, in

the upper first row, spinel 1, 2 and 3 from the left side, are coloured predominantly by Fe²⁺, while spinel 4, 5 and 6 are predominantly coloured by Co and the rest of the first row again by Fe²⁺.

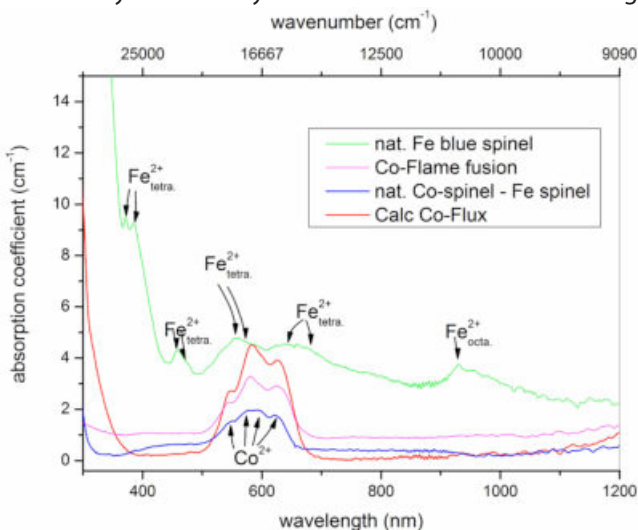


Figure 5. Spectra of a natural blue spinel with Fe, flame fusion grown synthetic with Co, Flux grown synthetic Co spinel corrected by the Fe content and nat. Co bearing spinel corrected by the Fe content.

Table 1: V, Cr, Fe content of sample sp1d, sp2c, sp3b and sp1b. All values in ppm by weight.

Sample	V	Cr	Fe
Sp1d	241	11724	3074
Sp2c	332	4502	3624
Sp3b	1894	1603	1050
Sp1b	243	8090	3679

Table 3: Fe content (EPMA ppm by weight FeO) and Co content (LA-ICP-MS ppm by weight Co) of the samples in Figure 5.

Sample no.	FeO	Co
Blue Flux 1	2280	643
	3090	396
Flame fusion	b.d	517
nat. Fe blue	39260	18
nat. Co blue	15160	81
sp7b	29180	24

Table 2: Peak maxima in nm determined by calc. Cr³⁺, calc. V³⁺ and the flux grown synthetic Cr³⁺ containing sample in Fig. 5.

Calc. Cr ³⁺	307	391	412	536
Calc. V ³⁺	-	391	408	539
Flux Cr ³⁺	-	391	413	547

Table 4: Approximated peak maxima (nm) of the respective cations:

Co ²⁺ in spinel:	550, 580, shoulder 594, 624, shoulder 635
Fe ²⁺ in tetra. site:	371, 386, 458, 475 shoulder, 515 shoulder, 555, 574 shoulder, 632, 661
Fe ²⁺ in octahedral site:	930

References

- Dickson, B. L., Smith, G., 1976. Low-temperature optical absorption and Mössbauer spectra of staurolite and spinel. *Canadian Mineralogist*, 14, 206-215.
- Huong, L. T.-T., Häger, T., Hofmeister, W., Hauenberger, C., Schwarz, D., Long, P.V., Wehrmeister, W. Khoi, N.N., Nhung, N. T., 2012: Gemstones from Vietnam: An update. *Gems & Gemology* 48 (3), 158-176.
- Khoi N.N., Sutthirat C., Tuan D.A., Nam N.V., Thuyet N.T.M., Nhung N.T., 2011. Ruby and sapphire from the Tan Huang-Truc Lau area, Yen Bai Province, northern Vietnam. *Gems & Gemology*, 47 (3), 182-195.
- Reed, J. S., 1971. Optical absorption spectra of Cr³⁺ in MgO * Al₂O₃ - 3.5 Al₂O₃ spinels. *J. of the American Ceramic Society*, 54, 202-204.

Henry A. Hänni

GemExpert, Basel, Switzerland
e-mail: h.a.haenni@gmail.com

Introduction

From 1975 on green grossular, Tsavolite, was found in N Tanzania and Tsavo National Park, Kenya (Bank et al., 1970; Bridges, 1974; Bank, 1975); Figure 1). The main colour-giving element was found to be vanadium (V) that is exceeding the Cr concentration by far, if there is Cr at all. The source of V is related to organic-rich meta-sediments. These former bituminous beds were transformed into graphite, and the V found the way into the growing grossular crystals.

The main reason to write this contribution, however, is a spectral particularity that became evident when the Raman spectra were created to assemble a data collection for the Gem Ram (Hänni & Hunziker, 2011). Comparing usual garnet spectra with spectra taken from Tanzanian grossulars showed significant differences at higher Raman shifts (1000-2400 cm^{-1}). My colleague Dr. Michael Krzemnicki drew my attention to this fact and I felt responsible to find an explanation. Similar peaks produced by a laser excitation are found in rare earths (REEs) doped synthetic crystals with garnet structure, such as GGG (Gallium Gadolinium Garnet), or YAG (Yttrium aluminium Garnet). Those peaks are photoluminescence (PL) features, caused by the dopant of REE. It was therefore of interest to find the reason for the high wave number peaks in East African grossulars. Similar peaks appear in apatites, e.g. from Durango (Mexico) and their contents of REE is well known by gemmologists as they produce the obvious absorption in the yellow part of the absorption spectrum (Rønsbo, 1989).



Figure 1. A mint green Tsavolite (V-grossular) crystal from Merelani area (N-Tanzania), seen at Idealgem (Chantaburi, Thailand), the source of all grossulars treated in this paper. Photo © H.A.Hänni.

UV-VIS spectrometry

Absorption spectroscopy is a common method to characterise gemstones. When the presence of REE is questioned, a glance into the spectroscope is always a good idea. Apatites containing REE (e.g. from Durango, Mexico) show the classical REE lines in the yellow part of the visible spectrum. These consist in a multitude of fine absorptions, forming a easily visible band. The sum of all REEs is about 1.3 wt% (Rønsbo, 1989). As this absorption feature is related to all elements, the relative contribution of single REE elements to the over all strength is not known.

Regarding mint green grossular of Tanzania the REE absorption feature is barely visible in the spectroscope. An absorption spectrum recorded with a Varian Cary 50 Spectrophotometer is shown in Figure 2.

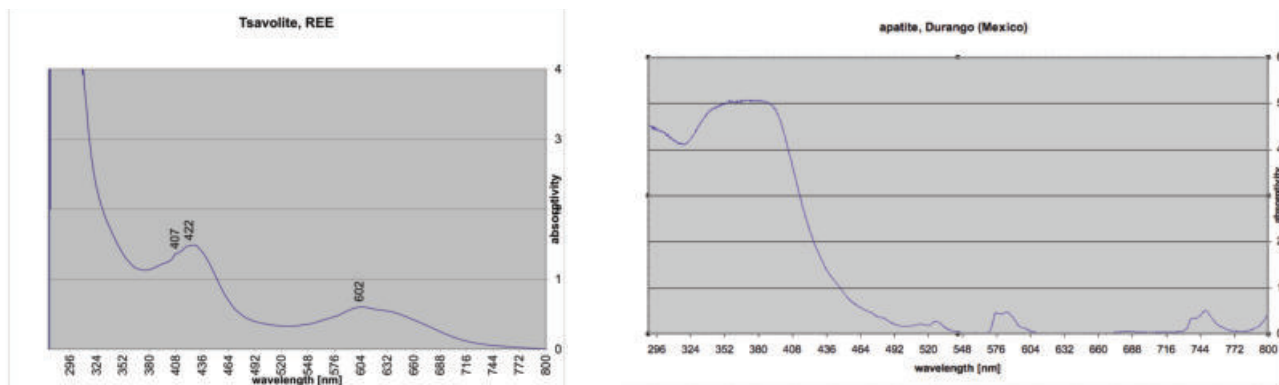


Figure 2. A Varian UV-VIS-NIR spectrometer Cary 500 Scan was used to record a UV-VIS-NIR spectrum of sample 1 Tsavolite crystal. In comparison, an absorption spectrum of apatite (Durango, Mexico) is shown, displaying the REE band in the yellow (580 nm).

Raman spectroscopy

Green grossular garnets have been characterised and identified with a Gem Ram portable Raman system produced by BWTek (Hänni & Hunziker, 2011). The GemRam utilizes a spectrum stabilized 785nm diode laser and high resolution TE cooled spectrometer to provide excellent performance and repeatability. It comes complete with a fiber optic probe, X-Y-Z positioning stage, and net book computer with preloaded software.

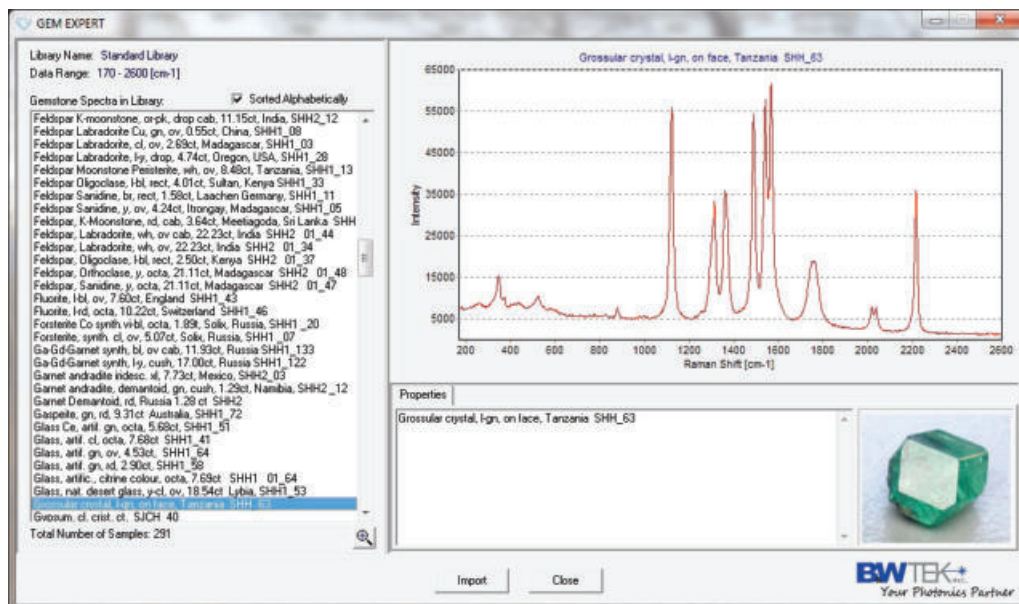


Figure 3. Screen print of a green grossular reference with the GemRam system. The peaks from 1100 to 2400 cm^{-1} are not Raman shift peaks of grossular, but PL peaks caused by REE traces.

LA-ICP-MS

In order to investigate the presence of REE in mint green grossulars from N-Tanzania, the REE contents were measured by LA-ICP-MS. Two samples (a crystal and a faceted stone) were analysed and the results are displayed in Table 1. Dysprosium with about 20 ppm is the REE found with the highest concentration.

	La	Ce	Pr	Nd	Sm	Eu	Gd
mass measured	139	140	141	143	147	151	157
	ppm	ppm	ppm	ppm	ppm	ppm	ppm
crystal surface	0.0021	0.0567	0.0569	1.008	2.9332	1.1758	10.9816
faceted stone	0.0588	1.0062	0.5597	7.0928	7.2174	3.3228	15.0424
	Tb	Dy	Ho	Er	Tm	Yb	Lu
	159	163	165	166	169	172	175
	ppm	ppm	ppm	ppm	ppm	ppm	ppm
	2.7014	19.6894	4.5634	13.6151	1.8083	13.3268	1.8554
	3.2051	24.7602	5.8704	18.2111	2.727	20.3991	3.1511

Table 1. REE contents in mint green grossulars from N-Tanzania, measured by LA-ICP-MS.

Conclusions

V-Grossular from Merelani (Tanzania) shows distinct PL peaks when excited with a 785 nm laser. These features are seen with the presence of REE, Dy with around 20 ppm being the highest in presence. It is common to find REE in Ca-rich minerals, as e.g., in apatite. But not all Ca-garnets, U-Gr-Andites, show PL peaks: in grossulars from Mali, Andradites from Russia, Namibia and grossulars from Mexico the PL feature is not seen. Tanzanites from Merelani, however, are displaying similar PL features. Further in-depth studies may show if the REE content is the true reason for the PL peaks seen with the analysed Tanzanian gemstones.

References

- Bank,H., Berdesinski,W. & Ottemann,J., 1970. Durchsichtiger smaragdgrüner Grossular aus Tansania.- Z. Dt. Gemmol. Ges. 19, 4-7.
- Bank,H., 1975. Grüne chrom- und vanadiumhaltige Granate (Grossulare) aus Kenya: Tsavolith - Möglichkeit einer neuen Benennung?. Z. Dt. Gemmol. Ges. 24, 13-15.
- Bridges,C.R., 1974. Green Grossular Garnets («Tsavorites») in East Africa. *Gems & Gemology*, 14(10), 290-295.
- Hänni, H.A. & J.C. Hunziker (2011) A portable Raman system for gemstone identification: The GemExpert Raman probe. in Abstract Proceedings, International Gemmological Conference IGC, 2011 Switzerland, www.igc2011.org/abstract-proceedings, 167-168.
- Kane, R.E., Kampf, A.R. & Krupp, H. (1990): Well-formed tsavorite gem crystals from Tanzania, *Gems & Gemology*, 26 (2), 142-148.
- Rønsbo, Jørn G., 1989. Coupled substitution involving REEs and Na in Si apatites in alkaline rocks from the Ilimaussaq intrusion, South Greenland, and the petrological implications. *Am.Mineral.*, 74, 896-901.

Acknowledgements

Thanks go to Werner Spaltenstein for his year-long support with information and stone samples from East Africa. Dr. M.S. Krzemnicki (SSEF, Basel) was the driving force to produce this paper. Dr. Alexey Ulianov, alexey.ulianov@unil.ch, University of Lausanne, Switzerland is acknowledged for his analytical work measuring the two samples by LA ICPMS.

Spectroscopic study of chrome pyropes from different sources

Jaroslav Hyrsl

Ke kurtum 383, CZ-14200 Prague 4, Czech Republic, email: hyrsl@hotmail.com

Pyrope is a well-known member of the garnet group, but gem-quality pyropes are quite rare and almost always very small. Their gemological boundaries are defined differently by various authors. Stockton & Mason (1985) define pyrope by a refractive index lower than 1.742, Webster (1994) gives a value 1.75, while Hanneman (1997) prefers limits of 1.747 for pyrope - almandine and 1.740 for pyrope - spessartine. Nevertheless, only Rouse (1986) took into account a high chromium content of pyropes from ultrabasic rocks, which can influence the refractive index very much. The Cr₂O₃ content in purple pyropes from Arizona can exceptionally reach 5.68 % (Wang et al., 1999) and from the Czech Republic 6.85 %, with a very high refractive index of 1.765 (Fiala, 1965). Seifert and Vrána (2005) found the Cr₂O₃ content in chrome pyrope from Podsedice (the most important garnet mine in the Czech Republic) to be 1.60 to 2.52 % in red garnet and 3.2 to 4.3 % in violet garnet, which corresponds to an uvarovite component of 4.6 to 11.8 %, the pyrope component of all of them gives a constant value of 73.8 to 75.0 %. For this reason, chrome pyrope should be considered in gemology as a separate garnet with refractive index between 1.740 and 1.765. Another reason is genetical – chrome pyropes are the only garnets that originate from peridotites in the mantle, while most others form in the Earth's crust.

The most popular chrome pyropes come from the Czech Republic (the famous “Bohemian garnets”, used in jewellery since the 7th century AC) but their size is limited to a diameter of 6 mm (aprox. 1 ct), larger stones being extremely rare. The largest chrome pyropes come probably from well-known localities on the Navajo reservation in north-eastern Arizona, where they are called „Anthill garnets“, with a diameter that can very rarely exceed 10 mm. Chrome pyropes are also mined in Tanzania and nice stones are known from Yakutia in Siberia. Because of high prices paid for exceptional chrome pyropes, it is important to determine criteria for their separation. Similar red pyropes, but with a very low Cr content, come from basaltic pyroclastic rocks in Nigeria, Mongolia, Thailand, etc.

As for absorption spectra, Cr-lines in the red part are only rarely seen with a hand spectroscope. Fortunately, the recent development of small and cheap spectrometers made them available to even small gemological labs. The author's study of chrome pyropes from different sources showed significant differences in their spectra (Figures 1–3). All chrome pyropes show a very small Cr peak at 685 nm. Stones from both of the important Czech sources (Podsedice in the České Středohoří Mts. and Vestřev in northern Bohemia) have just one peak with maximum at 575 nm, while chrome pyropes from Arizona, Tanzania and Yakutia have a very different spectrum with two peaks at 445 and 575 nm. Cr-poor pyropes from Nigeria, Mongolia and Thailand have just one peak with maximum between 510 and 540 nm and the Cr peak is missing.

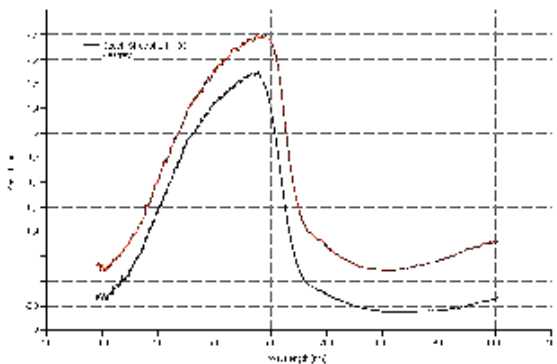


Figure 1. Absorption spectra of chrome pyropes from the Czech Republic.

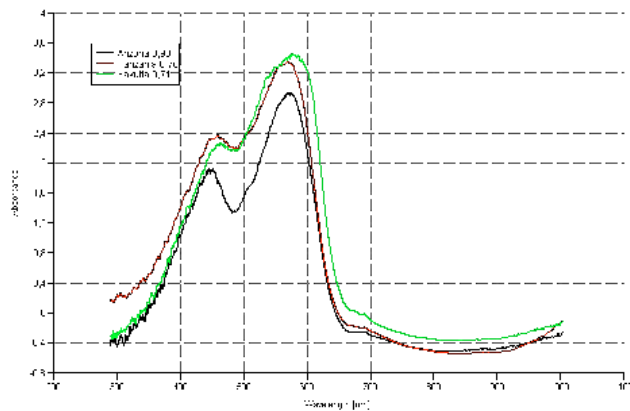


Figure 2. Absorption spectra of chrome pyropes from Arizona, Tanzania and Yakutia.

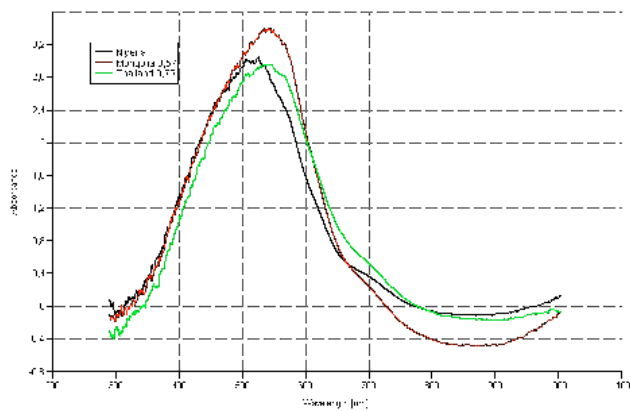


Figure 3. Absorption spectra of Cr-poor pyropes from Nigeria, Mongolia and Thailand.

Spectrum can be combined with study of inclusions, but chrome pyropes from all sources are usually very clean. Some typical inclusions follow :

- Czech Republic: strongly rounded anisotropic colorless crystals (forsterite or diopside) and multiple tension fractures around tiny colorless crystals (most probably zircon), never rutile.
- Arizona: very common three-dimensional net of very long fine rutile needles, strongly rounded colorless crystals (enstatite, forsterite or spinel), strongly rounded green chrome diopside crystals, black opaque flat ilmenite crystals, etc.
- Tanzania: very fine veils.
- Yakutia: all studied stones were clean.

References :

Fiala, J., 1965. Pyrope of some garnet peridotites of the Czech Massif. *Krystalinikum*, 3, 55-74.

Hanneman, W.W., 1997. A unified system for classifying garnets. *J. Gemm.*, 25(7), 471-473.

Rouse, J., 1986. *Garnets*. Butterworths, London.

Seifert, A.V., Vrána, S., 2005. Bohemian garnets. *Bull. of Geosciences*, 80, 113-124.

Stockton, C.M., Manson D.V., 1985. A proposed new classification for gem-quality garnets. *Gems & Gemology*, 21(4), 205 - 218.

Wang, L., Essene, E.J., Zhang Y., 1999. Mineral inclusions in pyrope crystals from Garnet Ridge, Arizona, USA: implications for processes in the upper mantle. *Contrib. Mineral. Petrol.*, 135, 164-178.

Webster, R., 1994. *Gems*, 5th edition (edited by P.G.Read). Butterworth-Heinemann, London, 1026 p.

Spectroscopic study of electron-irradiated OH-type topaz

Masaki Furuya

Japan Germany Gemmological Laboratory, Kofu, Japan email: jggl@sapphire.co.jp

The colouration of the orange-red variety of OH-type topaz, so-called «Imperial topaz» from Ouro Preto, Brazil is complex because it owes its colour both to transition metal ions and irradiation induced colour centers. Many spectroscopic studies about the colour of imperial topaz have been conducted. (Rloff, 1997; Taran et al., 2003) Also, alteration of its colour by X-ray or gamma-ray irradiation and annealing (Taran et al., 2003) or just heating (Nassau, 1994) has been examined. In this research, we tried electron irradiation on OH-type topaz to see the effect in its spectra. For the experiment, 29 pieces of yellow - orange - pink topaz from Ouro Preto, Brazil with sizes of 1 ct to 4 cts were prepared. 21 pieces were submitted to electron irradiation, though their details were not given and annealed at 350°C and 450°C by ourselves. 8 pieces were just heated together with the irradiated samples under the same conditions in order to compare them with the irradiated samples. Subsequently we examined their absorption spectra.

From the research of Taran et al. (2003), it has been known that there are three sets of absorption features in imperial topaz. Band set (i) refers to a pair of broad split bands with maxima around 25000cm^{-1} (400nm, with our test 393nm) and 18000cm^{-1} (556nm) caused by Cr^{3+} ion which is thermally stable. Band set (ii) refers to two types of UV absorptions. One is caused by a ligand-to-metal charge transfer which is thermally stable and the other is caused by some defect center(s) which are thermally unstable. Band set (iii) refers to two broad unstructured bands with maxima around 24000cm^{-1} (417nm) and 19000cm^{-1} (526nm) caused by Cr^{4+} which is thermally unstable from 300°C to be reduced to Cr^{3+} . Also, with the artificial X- or Gamma irradiation, 2Cr^{3+} (band set i) \rightarrow Cr^{4+} (band set iii) + Cr^{2+} occurs to give a dark red colour to the stone but this artificial Cr^{4+} absorption is unstable even at room temperature or daylight unlike natural Cr^{4+} .

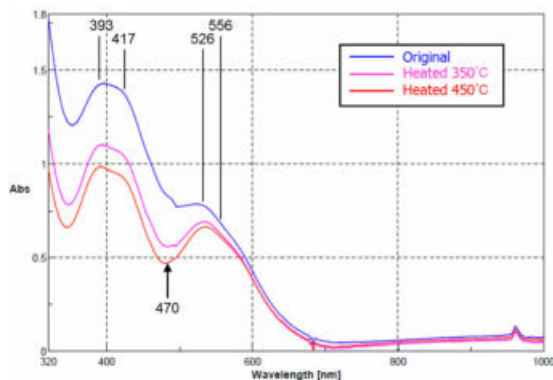


Figure 1. Change of absorption spectra of heated topaz (basal cleavage direction, not polarized).

By our heating experiment of the latter 8 pieces, above three band sets and their thermal alteration are detected as described by Taran et al. One alteration of spectra is the weakening of band set (iii) of 417nm and 526nm to cause the decrease of the absorption around 470nm (blue, middle of 417nm and 526nm) and it changes its colour from yellow-orange to violetish pink. The other alteration is the weakening of band set (ii) of the absorption in the UV (Figure1, from blue chart to pink to red one).

Electron irradiation itself caused two patterns of changes. (From the blue chart to the green one in Figure 2-4) First, yellow (Figure 4) to orange-red (Figure 2) topaz became less saturated pale pink topaz. In the spectra, the absorption of UV and yellow to orange (about 550-650nm) increased, and that of violet (370-450nm) decreased. Second, violetish pink (Figure 3) topaz darkened in colour. In the spectra, most absorption from UV to 650nm increased.

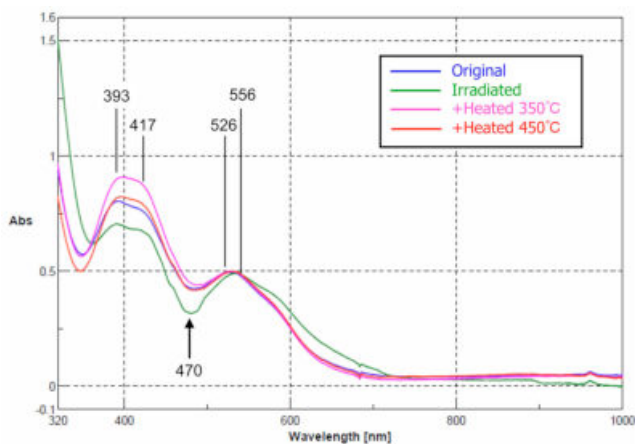


Figure 2. Change of absorption spectra of irradiated and annealed topaz of orange-red colour (basal cleavage direction, not polarized).

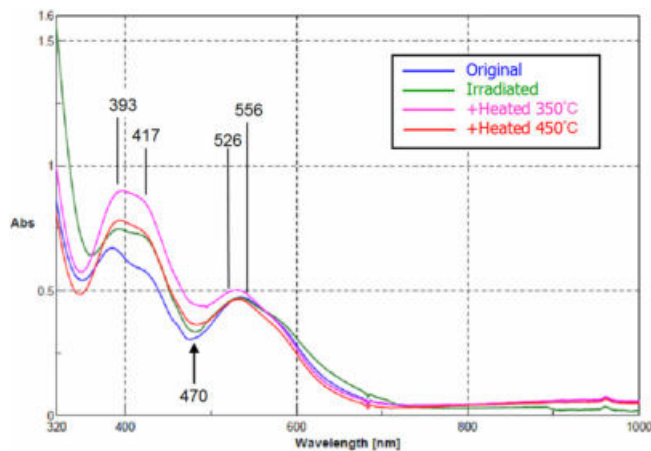


Figure 3. Change of absorption spectra of irradiated and annealed topaz of violetish pink colour (basal cleavage direction, not polarized).

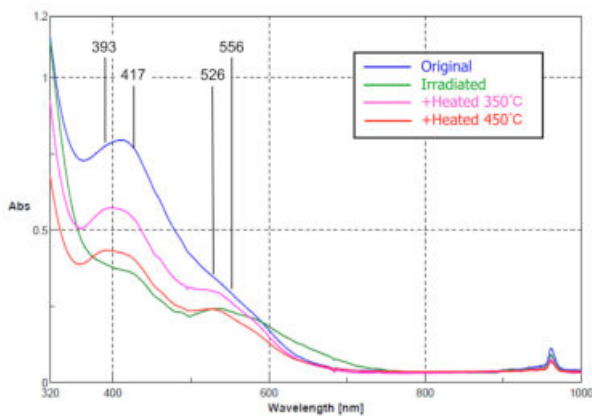


Figure 4. Change of absorption spectra of irradiated and annealed topaz of yellow colour (basal cleavage direction, not polarized).

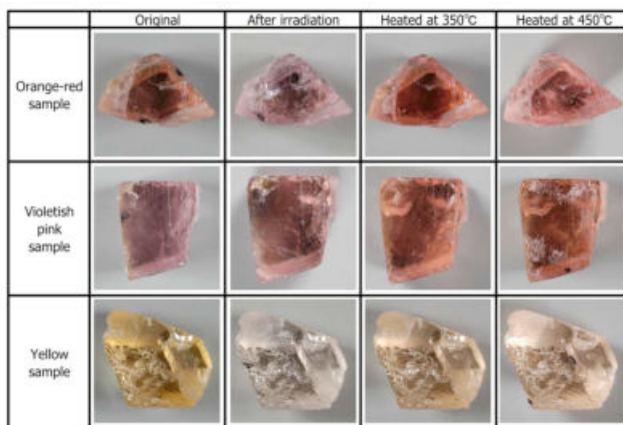


Figure 5. Photos of topaz at each step of electron irradiation and annealing at 350°C and 450°C.

However, by annealing at 350°C (pink chart in Figure 2-4) after this irradiating, the changes of UV and yellow to orange absorption caused by electron irradiation disappear in all samples and almost return to original spectra for these parts. It means that these two absorptions are unstable with heat, and may be related to some defect center. By continuous annealing up to 450°C, yellow (Figure 4) to orange samples without reddish tint do not enhance the colour and decrease the absorption of band set (i) or (iii) which are related to its colour at any temperature of annealing. On the other hand, orange-red (Figure 2) and violetish pink samples (Figure 3) enhanced the colour at some annealing temperature with an increase of the absorption in violet to blue which is related to its colour. These changes are shown in photos of Figure 5.

The change in violet to blue spectra caused by electron irradiation and annealing is inferred to be related to Cr^{4+} absorption. First, it is seen in samples with reddish or pinkish tint which have higher content of Cr and not seen in yellow samples with less Cr content. Second, because its absorption peaks are the same as in non-irradiated samples, it proves to be the same colouring mechanism as in natural topaz. Third, the photoluminescence of Cr^{3+} is identical in irradiated and non-irradiated topaz (Figure 6). It is known that the major emissions of Cr^{3+} (678.1 nm and 682.4 nm) have side lines which are related to different species of Cr^{3+} neighbouring O_4F_2 , $\text{O}_4\text{F}(\text{OH})$ and $\text{O}_4(\text{OH})_2$. Thus, it seems that the status of Cr^{3+} is the same despite irradiation. Considering these aspects, the change caused by electron irradiation and annealing is concluded to be caused by some change of Cr^{4+} .

As mentioned, in orange-red or violetish pink OH-type topaz, electron irradiation and adequate annealing can enhance its colour by increasing Cr⁴⁺ absorption at experimental level. But it does not have such effect on yellow to orange colour topaz without reddish tint.

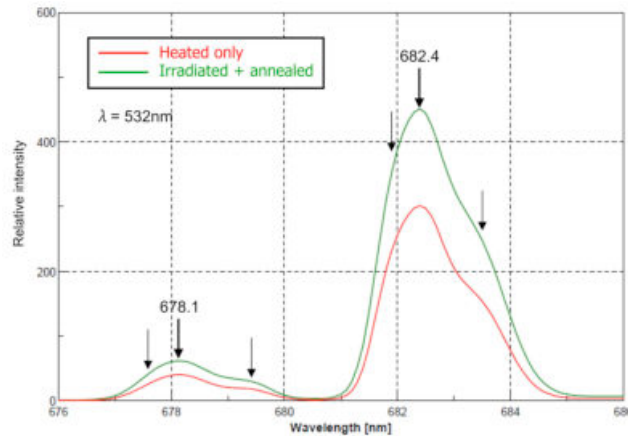


Figure 6. Emission lines in photoluminescence spectra of reddish orange topaz at 77 K: two major emissions (678.1 and 682.4) with side lines.

References

- Da Costa, G.M., Sabioni, ACS, Ferreira, C.M., 2000. Imperial topaz from Ouro Preto, Brazil: chemical character and thermal behavior. *Journal of Gemmology*, 27, 133-138.
- Gaft, M., Reisfeld, R., Panczer, G., 2005. *Luminescence spectroscopy of Mineral and Materials*. Springer, Germany.
- Nassau, K., 1994. *Gemstone Enhancement: History, Science and State of the Art*. 2nd ed. Butterworth-Heinemann, London.
- Rolff, A., 1971. Brazilian Imperial Topaz. *Lapidary Journal*, 25, 1556-1562.
- Taran, M.N., Tarashchan, A.N., Rager, H., Schott, S.T., Schürmann, K., Iwanuch, W., 2003. Optical spectroscopy study of variously coloured gem-quality topazes from Ouro Preto, Minas Gerais, Brazil. *Phys. Chem. Minerals*, 30, 546-555.

Zoisite from Pakistan

Claudio C. Milisenda¹, Kathrin Wehr², Michael Wild³

¹ DSEF German Gem Lab, Prof-Schlossmacher-Str. 1, D-55743 Idar-Oberstein, Germany, info@gemcertificate.com

² Guerickestraße 19a, D-80805, München

³ Hauptstr. 474, D-55743 Idar-Oberstein, Germany

The mineral species zoisite $\text{Ca}_2\text{Al}_3(\text{SiO}_4)(\text{Si}_2\text{O}_7)\text{O}(\text{OH})$ was originally called saualpite after its type locality in the Saualpe mountains in Carinthia, Austria. The name zoisite was introduced by Abraham Gottlieb Werner (1750-1817) in 1805 to honour Baron Sigmund Zois von Edelstein (1747-1819) who first realized that this was a new mineral (Faninger, 1985/86).

Zoisite is a dimorph of clinozoisite and the only orthorhombic member of the otherwise monoclinic epidote group. It has either a compact, massive morphology or occurs in transparent to translucent prismatic crystals often with distinct striations. Zoisite is an allochromatically coloured gem species and is colourless when chemically pure. Traces of iron, manganese, vanadium and chromium may produce yellow, brown, pink, green, blue and violet hues. The most famous zoisite variety is the blue to violet tanzanite, named after its occurrence in the Merelani Hills in Tanzania.

Gem-quality zoisites also occur in alpine-type clefts near Alchuri village in the Shigar valley, in the Baltistan region of Pakistan's Northern Areas. Recently the authors examined transparent, faceted, brown, brownish-green to green specimens weighing between 1.06 and 2.95 ct. (Figure 1) and a number of transparent greyish, brown and green zoisite crystals with a weight between 1.62 and 15.60 ct. Some specimens with matrix reportedly from the same mining area were also available for testing (Figure 2). The crystals showed a distinct trichroism with yellow-brown, green and greyish bluish-violet. The density varied between 3.33 to 3.34 g/cm³. Refractive indices were 1.700 – 1.705 for n_α and 1.709 – 1.710 for n_γ with $\Delta n = 0.005$ to 0.009. This is consistent with refractive indices of two green crystals reportedly from the same mining area (Koivula et al., 1992) and supports the observation that the refractive indices of zoisites from Pakistan are higher when compared to their Tanzanian counterparts.



Figure 1. Faceted Zoisites from Pakistan.

A distinct growth zoning and growth tubes, which are a common feature in zoisites, were observed under the microscope (Figure 3), in addition to fingerprint-type fluid inclusions.

Unpolarized absorption spectra taken on the cut stones showed bands with maxima at 390 nm, 426 nm and 451 nm, which can be attributed to ferric iron in octahedral coordination. Additional bands also typical of Fe^{3+} were observed at around 660 and 790 nm.

In addition to the major compounds of zoisite (calcium, aluminium and silicon) EDXRF analyses showed traces of strontium, vanadium and chromium as well as elevated iron contents up to 2 wt.% Fe_2O_3 . All the zoisites from Tanzania, by contrast have negligible iron concentrations (Barot & Boehm, 1992).

Heat treatment experiments are in progress in order to investigate possible changes in the absorption spectrum of the samples.



Figure 2. Zoisite crystals with matrix from Pakistan.

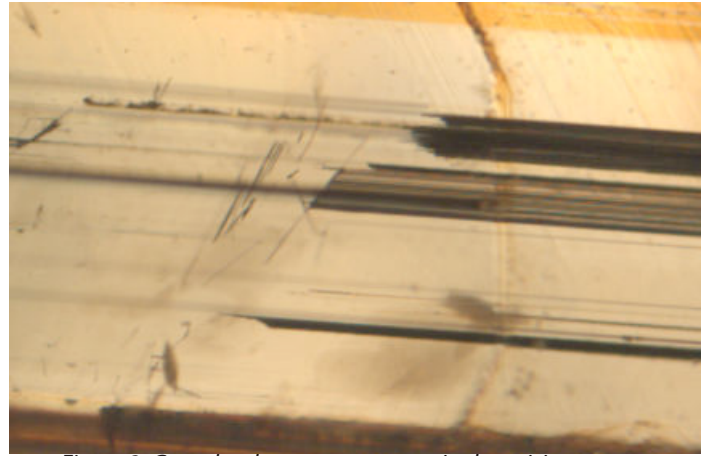


Figure 3. Growth tubes were common in the zoisites examined.

References

Barot, N. R., Boehm, E. W., 1992. Gem-quality green zoisite. *Gems&Gemology*, 28(1), 4-15.

Faninger, E., 1985/86. Die Entdeckung des Zoisits. *Geologija* 28/29, 337-342.

Koivula, J. I., Kammerling, R. C., Fritsch, E., 1992. Gem News: Green zoisites from Pakistan. *Gems&Gemology* 28(4), 275-276.

Canadian labradorite — classic colour

Willow Wight

Canadian Museum of Nature, Ottawa, Canada K1P 6P4, wwight@mus-nature.ca

Labradorite from Canada is a colourful mineral with a very colourful history. Its distinctive “labradorescence”, the vivid and varying colours that shift with the angle of light, captivated those who first saw it, and prompted its adoption in 1975 as the official gemstone of the province of Newfoundland and Labrador (NL). We consider this phenomenon of “labradorescence” to be the most distinctive feature of labradorite.

Members of the Moravian Brethren (or Unitas Fratrum) first took pieces of Labradorstein to Europe in 1775. This Protestant group from Eastern Europe sent missionaries to many parts of the world. In an effort to bring Christianity to the “Esquimaux” (now Inuit), they established a mission they called Nain on the northeast coast of Labrador in August, 1771.

The Moravians learned of this extraordinary colourful rock from the Inuit, whose chiefs wore “stones containing fire” as ornaments. Being curious about the Labradorstein, the Moravians showed it to experts in London. Some of the colourful pieces were polished, and there were hopes of developing a market for this new gem material. In 1777, a number of specimens were donated to the British Museum in London, including two large slabs, more than 30 polished pieces, and an unspecified number of “polished brooch stones”. These pieces show an amazing range of iridescent colours (Figures 1 to 4). One large slab is now on display in the Mineral Hall of the Museum of Natural History, and the other in the Gallery of Enlightenment in the British Museum. These seem to be the earliest mineral specimens from Canada on exhibit in any museum.



Figure 1. Polished slab showing schiller (~ 60 x 30 cm) donated by the Moravian Brethren in 1777 (#59890). On exhibit in the Mineral Gallery of the Natural History Museum, London.



Figure 2. Large slab showing green, yellow and bronze iridescence (#49552), Natural History Museum, London.



Figure 3. Polished piece showing dark blue, green, bronze, yellow and rare pink to purple iridescence, Natural History Museum, London.



Figure 4. Polished piece showing dark blue, turquoise and green iridescence, Natural History Museum, London.

Labradorite was the first new mineral described as coming from Canada (Werner, 1780). See Table 1 for the properties of labradorite, which are well documented in many reputable references.

Table 1. Properties of Anorthite var. Labradorite

CHEMICAL COMPOSITION: $(Ca,Na)Al_2Si_2O_8$: (An₅₀-An₇₀): a rock-forming mineral of the Feldspar group, plagioclase series

CRYSTAL SYSTEM: Triclinic, pinacoidal

OCCURRENCE: Found in mafic igneous rocks and anorthosites. The Nain, Labrador anorthosite (~1.3 billion years old) consists of plagioclase feldspar with minor olivine, pyroxene and magnetite.

LOCALITIES: In Canada, labradorite occurs over wide areas in the province of Newfoundland and Labrador (NL), with lesser localities in Quebec and Ontario. Paul Island and Tabor Island (NL) are often mentioned, and were the sources of the earliest specimens.

HABIT: Crystals typically thin, often tabular along {010} and rhombic in section, to 4 cm. Usually granular or massive. Twinning on {010} gives rise to lamellae that can be seen as grooves on the surface of a crystal face or on cleavage plane.

COLOUR: Colourless, white, greyish, pale yellow, bluish grey or greenish. Grey, massive, translucent to opaque material often shows labradorescence, especially on {010}: mostly blues and greens, but also yellow, bronze, and rarely red and purple.

LUSTRE: Vitreous, pearly on cleavages TRANSPARENCY: Opaque to transparent

HARDNESS: 6 to 6½

CLEAVAGE: Perfect on {001}, less perfect on {010}, intersecting at 90°; distinct on {110}

FRACTURE: Uneven to conchoidal TENACITY: Brittle

SPECIFIC GRAVITY: D(meas) = 2.68–2.72; D(calc) = 2.685–2.710

INCLUSIONS: Magnetite needles, zircon; exsolved black needle-like crystals of ilmenite are common along with platy magnetite (sometimes iridescent). Platy hematite crystals (often iridescent) are not uncommon.

OPTICAL PROPERTIES

REFRACTIVE INDEX: $\alpha = 1.555\text{--}1.565$; $\beta = 1.558\text{--}1.569$; $\gamma = 1.563\text{--}1.573$

Opaque 1.559–1.568 (0.009); Transparent 1.560–1.570 (± 0.001)

OPTIC SIGN: Biaxial (+) BIREFRINGENCE: 0.008–0.01

DISPERSION: $r > v$, weak; (CF) 0.010

Names and nomenclature

The geographical name “Labrador” is derived from that of Portuguese explorer, João Fernandes Lavrador (lavrador = landowner), who charted the coasts of southwestern Greenland and northeastern North America about 1500. “Terra do Lavrador” initially referred to Greenland, the first land sighted, but eventually the name became used only for Labrador.

In early literature, various terms are used for labradorite, depending on the year, and the language used: Labrador Stein or Labrador stone, Labrador Felspath, Labrador Feldspar, and Pierre de Labrador. Today, labradorite is considered a variety of anorthite, part of the plagioclase series of the Feldspar Group of minerals. Earlier, the plagioclase feldspar solid solution series was considered as six different species: the labradorite compositional range is 50-30% albite with 50-70% anorthite ($Ab_{50}An_{50}$ to $Ab_{30}An_{70}$).

Labradorescence

The most distinctive feature of labradorite is its iridescent schiller, an interference phenomenon called “labradorescence”. Labradorite is essentially a grey feldspar with a distinctive play of colours seen only on the more easy of the two cleavage surfaces, or on polished surfaces nearly parallel to this plane. The most common colours are blues and greens, but one also sees yellow, bronze, and (rarely) red and purple.

There are three regions in the plagioclase solid solution series in which a lamellar structure created by phase separa-

tion (exsolution) of fully ordered albite and anorthite is more stable than the solid solution structure (which consists of randomly distributed clusters of both phases). These regions are known as miscibility gaps. Two are important gemmologically, as they produce the effects seen in moonstone and labradorite.

Labradorescence occurs in the andesine-labradorite range (An_{45} - An_{60}), appearing as intense interference colours that vary with increasing anorthite content (blue $An_{48.5-52}$, green-yellow $An_{52-55.5}$, orange-red $An_{55-55.8}$) (Nissen et al., 1967). Both the physical properties and the chemical composition of the mineral control the observed colours. Labradorescence is an interference phenomenon of light, and the diffraction grating that causes the interference is produced by twin lamellae in the crystal structure. Secondly, the chemical composition affects the thickness of the lamellae and the refractive index, both increasing with Ca content. Increasing Ca content changes the iridescence through the visible spectrum from blue to red.

History and Early Literature

Because the Moravian Brethren had connections in Europe, pieces of labradorite made their way to researchers in parts of Germany as well as London. Werner (1780) described Labradorstein as almost always light or dark grey, but with certain directions that show a play of colour having different, usually very vibrant, bright colours.

Werner cites earlier publications on which he based his information. The English Naval Lieutenant Roger Curtis (1776) gave perhaps the first report on the beautiful blue-to-red sparkling rock. Schröter (1775) and Schreber (1776) described bright colours comparable to those of butterfly wings. In 1778, Leske indicated the way the colours changed at certain angles of the reflections to the eye, mentioning "stripes" in the rock, and with colours ranging from crimson red, leek green, and bright blue, often mixed. Brückmanns (1778) included Labradorstein in his Treatise on gems, describing it as true feldspar, belonging to the species of the cat's-eyes, and found as massive, grey, greenish, bluish, etc. pebbles. Layers of different colours could be seen even before polishing. Polished stones showed the most beautiful play of colour, like the feathers of the hummingbird or the peacock, especially when seen in the sun.

M. l'Abbé Haüy read a paper in Paris in 1784: "Observations on the crystal structure of feldspars" with geometrical descriptions of the crystal morphology by colour.

Commercial Uses

The development of the use of labradorite from quarries near Nain as decorative building stone began in the early 1960s, but success has been limited. Huge blocks from the Ten Mile Bay and Igiak Bay quarries have been shipped to Italy for finishing as dimension stone, with the main market in Europe. Labradorite is also used for table and counter tops, and other decorative pieces. Nain labradorite is used locally in jewellery, carvings, and other handicrafts, and is sold to rock shops outside of Labrador.

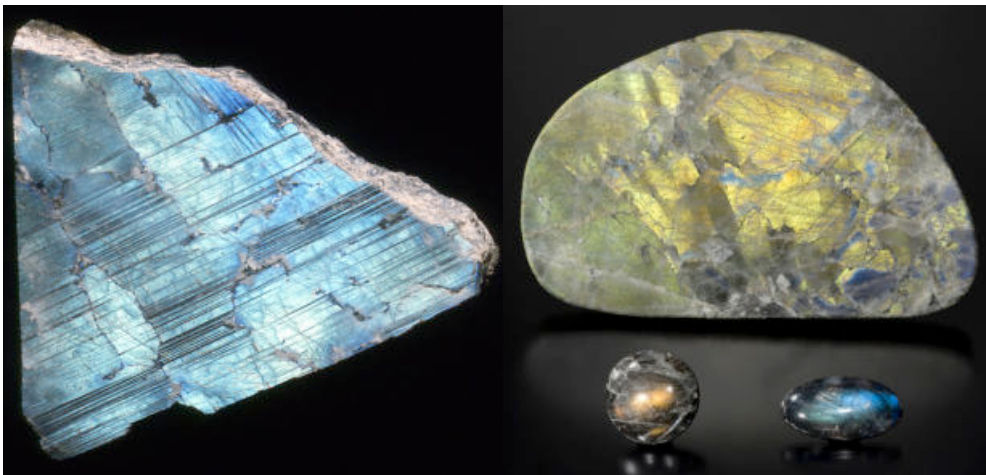


Figure 5 (left): Polished section showing twinning striations and bright blue iridescence. On exhibit in the Canadian Museum of Nature (CMNMC 41845) Photo ©CMN.

Figure 6 (right): Polished slab showing yellow, green and blue iridescence. On exhibit in the Canadian Museum of Nature (CMNMC 31151) with cabochons: bronze (CMNGE 20582; 52.54 ct) and blue (CMNGE 20583; 48.40 ct). Photo by M. Bainbridge for CMN

Large, colourful, polished slabs of Canadian labradorite are on exhibit in most major museums. (Figures 5 and 6). Advances in mineralogy have solved the mystery of the causes of the iridescence, but the phenomenal, vivid colours continue to fascinate us today, just as they first did in the 18th Century.

References

- Brückmanns, U.F.B., 1778. Gesammelte und eigene Beiträge zu seiner Abhandlung von Edelsteinen. Braunschweig: 250 pp.
- Curtis, R., 1776. Eine angenehme Nachricht von der Kuste Labrador. Göttingische Anzeigen, 29&30, 7-9 March, 1776 (Item 90, 244–245).
- Deer, W.A., Howie, R.A., and Zussman, J., 2001. Rock-Forming Minerals, Vol. 4A, 2nd ed. Framework Silicates. The Geological Society, London ,972 pp.
- Hauy, R.J., 1784. Mémoire sur la structure des cristaux de feld-spath, Mémoires de l'Académie Royale des Sciences, 273-286, Paris. Observations on the structure of crystals of feldspar (read 1784).
- Leske, N.G., 1778. Abhandlung von einigen sich wandelnden, zum Feldspat gehörigen Steinen aus Labrador. Der Naturforscher, 12, 145–163 plus plate (Figs 1-7).
- Nissen, H.-U., Eggman, H. and Laves, F., 1967. Schiller and submicroscopic lamellae of labradorite. A preliminary report. Schweiz. Min. Petr. Mitt., 47, 289-302.
- Schrebern, D.G., 1776. Nachricht von einem neu entdeckten schwärzlich und hochblau schielenden Steine aus Labrador. Beiträge zur Beförderung der Haushaltungskunde und anderer damit verwandter Wissenschaften, 289–300.
- Schröter, J.S., 1775. Von dem Changeant oder Schieler unter den Steinen aus dem Lande der Esquimaux. Journal für die Liebhaber des Steinreichs.ö Item 26, 397-406.
- Werner, A.G., 1780. Cronstedt's Versuch einer Mineralogie. S.L. Crusius, Leipzig, Germany, 354 pp. This is a German translation of Cronstedt (1758) 3rd ed. by Werner, with additional data by him.

Acknowledgements

The author is grateful for support from colleagues at the Canadian Museum of Nature, in particular Dr. Joel Grice. Alan Hart kindly provided access to labradorite specimens in the Natural History Museum, London, as well as the early catalogue entries. All photos are of labradorite from the Nain area of Labrador, NL, Canada. Thanks also to Karen Fox for many helpful discussions.

Special features in quartz colours

Ulrich Henn¹, Rainer Schultz-Güttler²

¹ DSEF German Gem Lab, Prof-Schlossmacher-Str. 1, D-55743 Idar-Oberstein, Germany, ulihenn@dgemg.com

² Instituto de Geociencias-USP, Sao Paulo, Brasil

Quartz shows an interesting variety of colours whose causes generally can be divided into three groups:

1. colour centers
2. inclusions
3. optical effects

Comprehensive descriptions of the colours of quartz have been published by Lehmann & Bambauer (1973), Rossman (1994) and Henn & Schultz-Güttler (2012).

The most common cause of colour in macro-crystalline quartz is due to colour centers which are associated with foreign ions. Among these ions, the most common ones are iron and aluminium and for this reason the colour center mechanisms are divided into two main groups of iron-bearing and aluminium-bearing quartz. Another type of colour centers is found in quartz with high water content.

Iron-bearing quartz is dominated by Fe⁴⁺-amethyst centers, which can be modified by temperature. At about 400-500°C iron particles (hematite) exsolve and produce a yellow to brown citrine colour. At similar temperatures particularly amethyst (from Montezuma, Brazil) changes to the green colour of prasiolite which is caused by Fe²⁺.

An unusual violetish-blue colour is produced by gamma irradiation and subsequent heat treatment of green prasiolite. Such quartz is called "blueberry quartz" in the trade. Both, prasiolite and "blueberry quartz" occur as non-transparent material, out of which these stones look very similar to chrysoprase and chalcedony (Figure 1).



Figure 1. Non-transparent "blueberry quartz" and prasiolite with an appearance similar to chalcedony and chrysoprase. Size of the pear-shape cut cabochons: 13.30 x 10.25 and 16.70 x 11.10 mm.



Figure 2. Gamma-irradiated green quartz. Size of the large geode fragment: 35 cm.

Heat treatment of amethyst above 500°C develops a milky turbidity and bleaching of the violet colour, and some stones of this type are called "neon quartz". The adularescent appearance is caused by light scattering at tiny water droplets as exsolution from silanol (-Si-OH) groups bound in the quartz.

In aluminium-bearing quartz AlO₄-centers produce a yellow citrine colour or the brown colour of smoky quartz.

Gamma irradiation changes colourless aluminium-bearing quartz into dark brown to black coloured morion which can be modified into smoky quartz or yellowish-green "lemon quartz" by heat treatment at approximately 140-280°C. Brown smoky quartz colour is produced in quartz with low lithium content while Li-rich material changes into yellowish-green.

In the case of lithium-rich quartz varying colour shades originate as a function of irradiation dose and temperature. In the gem trade such material is known as "greengold", "lemon", "oliva", "beer", "whiskey" or "cognac".

Colourless to pale yellowish quartz with high water content can be modified into a green colour by gamma irradiation (Figure 2). In the gem trade such material is called "green amethyst" or "greened amethyst". The cause of the green colour is due to NBOHC (non-bonding oxygen hole center).

Characterization and identification of quartz with colour centers is mainly based on absorption spectra. Additionally pleochroism and the presence of twinning as well as observation with a Chelsea colour filter can be helpful in the identification (e.g. gamma-irradiated green quartz turns red under the Chelsea filter, prasiolite keeps green).

Bi-coloured quartz is ascribed to different colour mechanisms in different growth sectors, e.g. in violet/yellow ametrine and colourless/yellow "lunasol" or brown/brownish-yellow material.

Inclusions as a cause of colour can be found in both, macro- and micro- to crypto-crystalline quartz.

In macro-crystalline quartz common colouring inclusions are iron oxides of syn- or epigenetic origin which cause the red colour of special gem material such as "strawberry quartz" or "raspberry quartz".

Such terms for special quartz varieties represent the tendency in the gemstone trade to create unusual names with the common reason to make material more interesting. By way of example, such terms are combined under the generic name "fruit quartz", including "lemon quartz", "blueberry quartz", "strawberry quartz" and "raspberry quartz" as well as "kiwi quartz", which is green jasper. Furthermore "cherry quartz" and "pineapple quartz" are provided, but both are ordinary glass.

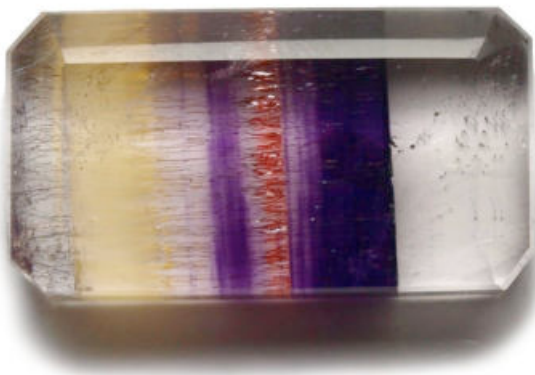


Figure 3. Multicoloured quartz with amethyst zones as well as yellow and brown bands with colouring iron oxide and iron hydroxide inclusions. Size of the faceted stone: 28 x 14 mm. Collection of Henry A. Hänni.

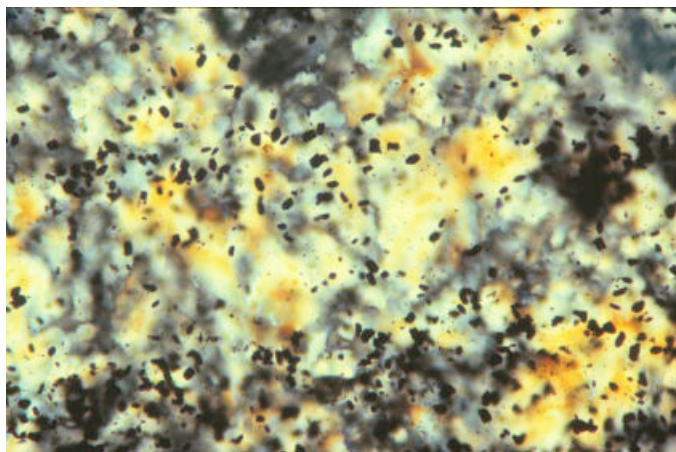


Figure 4. Manganese oxide inclusions in black jasper from India. Thin section, x 150.

An interesting feature in quartz colour is represented by multi-coloured material with different colour causes, e.g. colour centers combined with inclusions in zoned violet/yellow/brown specimens (Figure 3).

Colouring inclusions in quartz are of main importance in micro- to crypto-crystalline material (Henn, 2004). Particular attention is focused on the characterization of onyx as a dyed agate and naturally coloured black chalcedony or jasper (Henn et al., 2010). Determination is based on chemical analyses (e.g. EDAX) of the colouring agents, like cobalt in the case of dyed agate or manganese or carbon in black chalcedony or jasper.

The colour causes of most synthetic quartz varieties are comparable with those of natural quartz. An exceptional case is found in aquamarine blue synthetic quartz, which is coloured by cobalt. Co²⁺ dominated blue sectors are also

present in synthetic bi-coloured green/blue quartz, which was first described by Payette in 2012. The green sector is caused by bivalent iron as described in natural prasiolite.

References

- Henn,U., 2004: Zur Unterscheidung naturfarbener und künstlich gefärbter Chalcedone/Achate. Z. Dt. Gemmol. Ges. 53, 23-32.
- Henn,U., Schultz-Güttler,R., 2012: Review of some current coloured quartz varieties. J. Gemm. 33, 29-43.
- Henn,U., Häger,T., Milisenda,C.C., 2010: Ein Beitrag zum Thema Onyx. Z. Dt. Gemmol. Ges. 59, 83-94.
- Lehmann,G., Bambauer,H.U., 1973: Quarzkristalle und ihre Farben. Angew. Chem. 85, 281-289.
- Payette,F., 2012: Bicoloured quartz with unusual colour combination. Aust. Gemmol., 24, 11.
- Rossmann,G.R., 1994: Colored varieties of the silica minerals. Reviews in Mineralogy and Geochemistry 29, 433-463.

The Zonal Texture and Isomorphous Series in Fei Cui minerals

Prof. Mimi C. M. Ouyang, Dr. Miro F. Y. Ng

The Hong Kong Institute of Gemmology, Hong Kong, cmouyang@hkgemslab.com.hk

Abstract

From the researches over the decades, the authors discovered that zonal texture is very common and regular among the Fei Cui minerals (pyroxenes). According to the observations obtained from thin sections and electron microprobe chemical analyses we can deduce zonal textural characteristics among the pyroxene minerals as reflected by chemical composition changes. We can further visualize the zonal texture phenomenon by the use of cathodoluminescence technique. This on one hand reflects the environmental change during the mineral formation stages and also indicate the universality of isomorphous replacement in pyroxene minerals.

The zonal phenomenon is just looking at the composition of Burmese Fei Cui on its compositional relationship and change from textural point of view. The isomorphism between the three members is very clear just by observing the chemical and mineral composition characteristics. Jadeite and Kosmochlor forms homovalent isomorphous replacement while Jadeite and Omphacite forms heterovalent isomorphous replacement. The minerals that exhibit such an isomorphism should better be termed as "Fei Cui".

Colour change effects in gemstones: Causes and perception

1Krzemnicki M.S., 1Zhou W., 2J. Maizlan

1Swiss Gemmological Institute SSEF; gemlab@ssef.ch

2Institut für Geowissenschaften, Friedrich-Schiller-Universität Jena, Germany

Colour change, also known as “alexandrite effect” has been studied extensively since it first was described 1831 for alexandrite (chromium-bearing variety of chrysoberyl) from Russia (von Pott, 1842). Since then, numerous minerals or gemstones with colour change have been documented (Figure 1), including corundum, spinel, zircon, fluorite, monazite, bastnäsite, garnet, diaspore, kyanite, epidote and kornerupine, to name a few.



Figure 1: Colour changing gemstones in daylight (always left top of the pairs) and incandescent light (always right bottom). This picture has been combined from several pictures. The relative size of the stones is not maintained. The colours in daylight and incandescent light have been corrected (Adobe Photoshop®) to best match the observed colours. © M.S. Krzemnicki, SSEF

Traditionally, we speak of a colour change when the main hue of a mineral in daylight differs from that seen in incandescent light (LMHC 2010, Infosheet No. 9). With the advent of new light sources (fluorescent and LED lamps), and recently with the ban of incandescent tungsten bulbs, this definition may need further specification in the future. The main factors to observe a colour change in a gemstone/mineral are: a) two white light sources of distinctly different emission spectra (e.g. daylight versus incandescent light), b) a material that shows two transmission “windows” in its absorption spectrum separated by an absorption band at approximately 570 nm, c) an observer whose brain interprets the incoming residual light energies accordingly into a colour sensation (White et al., 1967; Schmetzer et al., 1980; Nassau, 1983; De Valois & Jacobs, 1984; Burns, 1993; Liu et al., 1999). Apart from colour change, there are further colour effects, which may considerably contribute to the colour perception of a mineral or gemstone, namely pleochroism (Liu et al. 1995) and the Usambara-effect (Halvorsen, 2006). Pleochroism describes the effect of different

colours due to different selective absorption along the two or three vibrational directions within an anisotropic mineral (very distinct in alexandrite), whereas the Usambara effect is a colour change effect related to the path length of light transmitted in a stone (Halvorsen & Jensen 1997).

In our study, we will summarize our findings on a number of colour changing minerals (Figure 1) that owe their colour change either to the presence of a broad absorption band due to a transition metal (commonly Cr or V, e.g. alexandrite, corundum, garnet, Krzemnicki et al. 2001 and references therein) or well-defined narrow absorption bands of rare earth elements (REE) in the 3+ valence state (e.g. zircon, fluorite, Nd-bastnäsité, Nd-monazite; Dieke & Crosswhite, 1963; Herzog & Krzemnicki, 2011)

We will further show how pleochroism may influence the perceived colours in anisotropic minerals, actually “reducing” the colour change especially in faceted alexandrite due to multiple internal reflections of the different plane polarised pleochroic colours (Figure 2) (see also Liu et al. 1995).

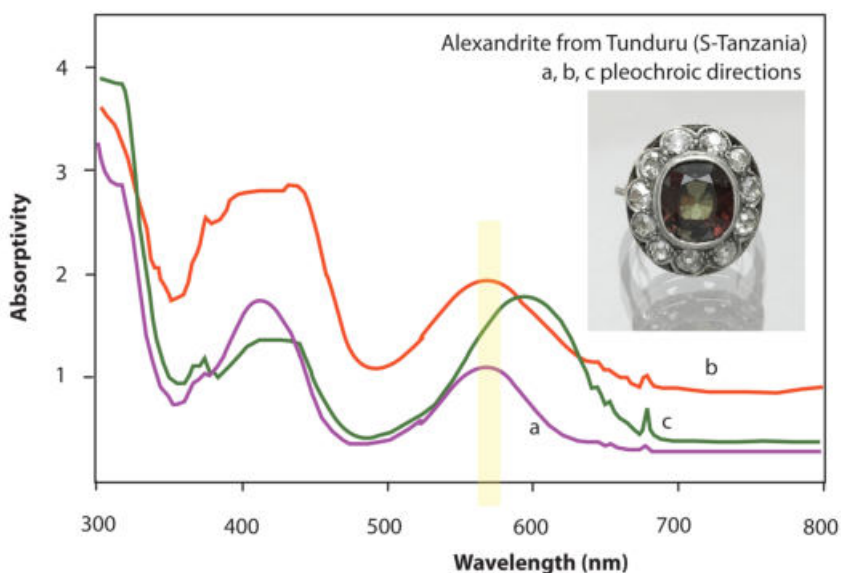


Fig. 2: Absorption spectra of alexandrite from Tunduru (S-Tanzania) for the three crystallographic directions a, b, c (pleochroic colours). The yellow bar indicates the 570 nm maximum criterion for a colour change which is not fulfilled for the c-direction. The photo shows a faceted alexandrite in daylight illustrating the effect of pleochroism. © M.S. Krzemnicki & L. Phan, SSEF

Furthermore we present data of some exceptionally large colour changing garnets (50-100 cts) from southern Tanzania which were recently analysed at SSEF. These chromium- and vanadium-bearing garnets of the pyrope-spessartine series show a distinct colour change (brownish green in daylight and red in incandescent light) combined with a distinct Usambara effect, resulting in reddish facet reflections around the girdle (Figure 3). This effect, first noted by Manson & Stockton (1984) as “colour-shift” on colour-changing garnets was only later fully described by Halvorsen & Jensen (1997) on Cr-bearing tourmaline from the Usambara mountain range, and thus named the Usambara effect. Normally this effect is best seen when two dark green Cr-tourmalines are superposed. The resulting red transmission colour is due to the near-doubling of the path length (see also Fig. 4). In the studied large faceted garnets, however, this effect is seen even without superposition of a second stone. In daylight these colour-changing garnets display a brownish-green colour in the main part below the table (\pm simple light transmission through the volume of the stone), and reddish facet reflections around the girdle as a result of increased path lengths of light by internal reflections.

Using colorimetric calculations based on computer generated absorption spectra, we will present spectroscopic criteria which are required to result in a colour change and Usambara effect in a mineral.

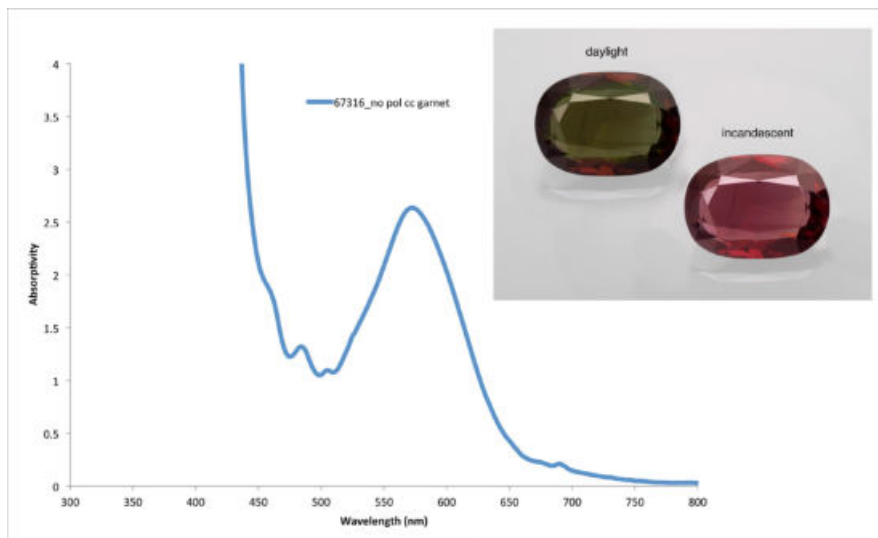


Fig. 3: Absorption spectrum of a large colour changing garnet from Tanzania, showing a marked absorption band due to vanadium and chromium at 570 nm. The inserted photo shows the colour change of this garnet from daylight (brownish green) to incandescent light (red). The reddish brown facet reflections around the girdle in daylight are the result of the Usambara effect. © M.S. Krzemnicki, SSEF



Figure 4. Usambara effect shown with two superposed colour changing garnets of 50+ ct each. © M.S. Krzemnicki, SSEF

References

- Burns R.G., 1993. Mineralogical Applications of Crystal Field Theory, 2nd edition Cambridge University Press, UK, 551 pages.
- Dieke, G.H., and Crosswhite, H.M., 1963. The spectra of the doubly and triply ionized rare earths. *Applied Optics*, 2 (7), 675-686.
- Halvorsen A., and Jensen B.B., 1997. A new colour-change effect. *Journal of Gemmology*, 25 (5), 325-330.
- Halvorsen A., 2006. The Usambara effect and its interaction with other colour change phenomena. *Journal of Gemmology*, 30 (1-2), 1-21.
- Herzog, F, and Krzemnicki M.S., 2011. Colour by rare earth elements (REE), as exemplified by colour-changing bastnäsite from Pakistan. Abstract volume of the 32nd IGC 2011, 169-171, <http://www.igc2011.org/-/abstract-proceedings/4540447685>

Krzemnicki M.S., Hänni H.A., Reusser E., 2001. Colour-change garnets from Madagascar: comparison of colorimetric with chemical data. *Journal of Gemmology*, 27 (7), 395-408

Liu Y., Shigley J.E., Fritsch E., Hemphill S., 1995. Relation between the crystallographic orientation and the « alexandrite effect » in synthetic alexandrite. *Mineralogical Magazine*, 59, 111-114

Liu Y., Shigley J.E., Fritsch E., Hemphill S., 1999. A colorimetric study of the alexandrite effect in gemstones. *Journal of Gemmology*, 26 (6), 371-385

LMHC (2010) Alexandrite and other colour-change gemstones. Laboratory Manual Harmonization Committee; Standardised Gemmological Report Wording, Infosheets No. 9, http://www.lmhc-gemmology.org/pdfs/IS9_23092010.pdf

Manson D.V., and Stockton C.M., 1984. Pyrope-spessartine garnets with unusual colour behavior. *Gems and Gemology*, 20 (4), 200-207

Nassau K., 1983. *The physics and chemistry of color - the fifteen causes of color*. John Wiley & Sons, New York
De Valois R.L., and Jacobs G.H. 1984. Neural Mechanisms of Color Vision. *Comprehensive Physiology, Supplement 3: Handbook of Physiology, The Nervous System, Sensory Processes*: 425-456. First published in print 1984, online published 2011. doi: 10.1002/cphy.cp010310

Von Pott H.A.G., 1842. Über den Alexandrit, oder uralischen Chrysoberyll, dessen Dichroismus und über die ungewöhnliche Grösse seiner Krystalle. *Schriften der in St. Petersburg gestifteten Russisch-Kaiserlichen Gesellschaft für die gesamte Mineralogie*, 1. Band, 1. Abtheilung, 116-126

Schmetzer K., Bank H., Gübelin E., 1980. The alexandrite effect in minerals: chrysoberyl, garnet, corundum, fluorite. *Neues Jahrbuch für Mineralogie - Abhandlungen*, 138, 147-164

White W.B., Roy R.R., and Crichton J.M.. 1967. The «alexandrite effect»: an optical study. *American Mineralogist* 52, 867-871

Optical spectroscopy of iron in sodium silicate glasses

Karen E. Fox

Waterloo, Canada N2T 2E5; k_e_fox@yahoo.com

Introduction

Mankind's fascination with gemstones is in large part inspired by the rich colours associated with transition metal ions captured within the crystal lattice of minerals. Similarly-coloured glass has also provided an important medium for faceted "gems".

Although glasses lack the long-range crystallographic order of minerals, they possess short-range order associated with glass-forming structural units. The present work illustrates the use of Raman, visible/infrared absorption, and luminescence spectroscopy to investigate changes in the structure of relatively simple binary alkali silicate glasses as a function of composition (Furukawa et. al., 1981), and to study the atomic environment of iron in these glasses (Fox et. al., 1982). These results can be applied to the analysis of more complex man-made and natural glasses used for gems.

Experimental

Varying compositions of sodium silicate glasses ($\text{Na}_2\text{O}\cdot x\text{SiO}_2$) were prepared both with and without the incorporation of iron. Samples are shown in Figure 1.

Optical absorption spectra in the visible and infrared range were measured on a Cary 14 Spectrophotometer. Raman and luminescence spectra were measured on a Spex Model 1401 double-grating spectrometer at a scattering angle of 90° to the exciting Ar-ion laser beam. Spectra were plotted versus wavenumber, ν , to provide a scale linear in energy, where wavenumber (cm^{-1}) = $107/\text{wavelength (nm)}$. It was possible to compare the intensities of different samples by using a standardized scattering geometry and optical alignment.

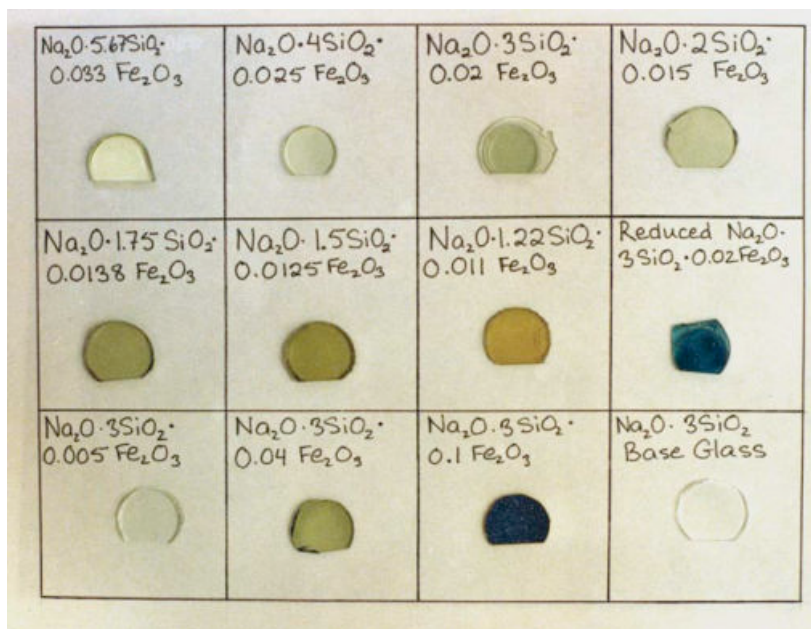


Fig. 1. Examples of the iron-doped sodium silicate glass samples used in this study.

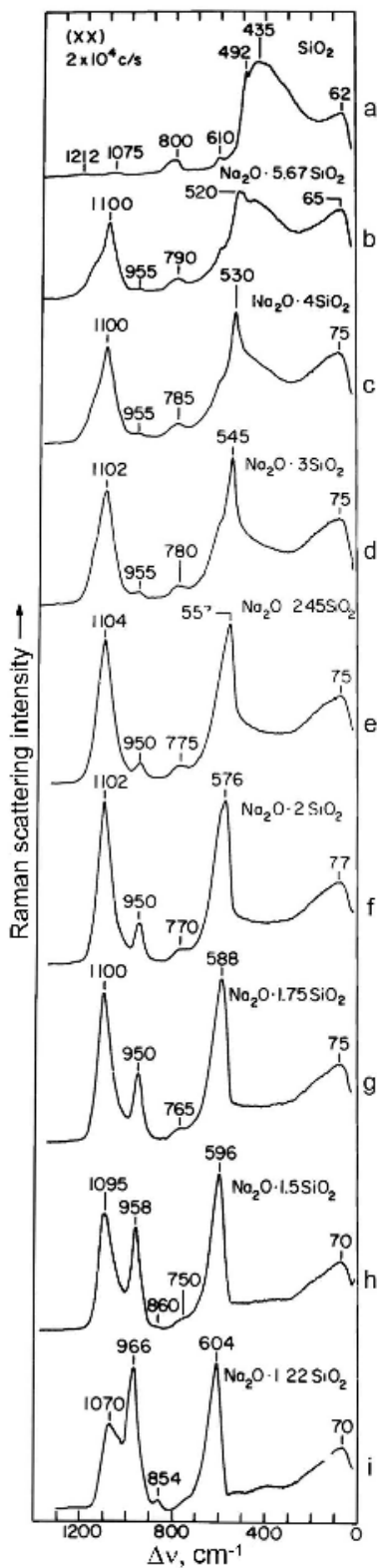


Figure 2. The Raman spectra of sodium silicate glasses show a continuous evolution as a function of silica content.

Raman spectroscopy and structure

Changes in the structure of $\text{Na}_2\text{O}\cdot x\text{SiO}_2$ glasses as a function of composition are reflected in the series of Raman spectra in Figure 2. Interpretation of these changes is guided by prior experimental and theoretical work (Brawer & White, 1975; Furukawa et al., 1981).

Just as silicate minerals are formed of silicon-oxygen tetrahedra linked into structures varying from 3-dimensional frameworks of tetrahedra, to pairs, chains, rings and sheet structures, so also is it generally accepted that silica glass consists of a three-dimensional somewhat non-uniform network of SiO_4 tetrahedra. Introduction of alkali oxides (M_2O) breaks the Si-O-Si bridging bonds, creating non-bridging oxygens (NBOs). The number of NBOs increases with increasing alkali oxide content and at the disilicate composition ($\text{M}_2\text{O}\cdot 2\text{SiO}_2$), SiO_4 tetrahedra have an average of one NBO, forming a sheet-like structure. Further addition of alkali oxide creates SiO_4 tetrahedra with two NBOs, and metasilicate glass ($\text{M}_2\text{O}\cdot\text{SiO}_2$) consists primarily of chain structure units with two non-bridging oxygens per SiO_4 tetrahedron.

The spectra of Figure 2 show that upon addition of Na_2O to silica, a band at 1100 cm^{-1} appears. This band has been assigned to a symmetric Si-O- non-bridging bond stretching within the disilicate structural unit. Its intensity increases up to the disilicate composition, beyond which it decreases with further increase in Na_2O . Another peak at about 950 cm^{-1} has been linked to a symmetric O--Si-O- stretching vibration of the metasilicate structural unit. In Figure 3, peak heights of these two bands are plotted as a function of the average number of NBOs per SiO_4 tetrahedron ($2/x$) as calculated from the chemical formula of the glass, $\text{Na}_2\text{O}\cdot x\text{SiO}_2$. The dependence of the Raman band intensity on number of non-bridging oxygens can be considered a plot of the relative numbers of tetrahedra with one and two NBOs making up the glass structure.

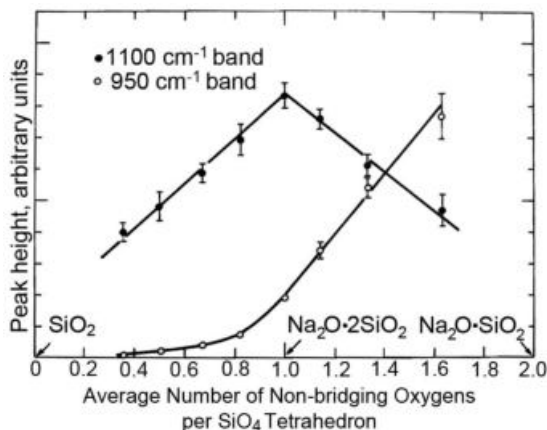


Fig. 3. Intensities of the 1100 cm^{-1} and 950 cm^{-1} Raman bands show a dependence on the number of non-bridging oxygens in the composition.

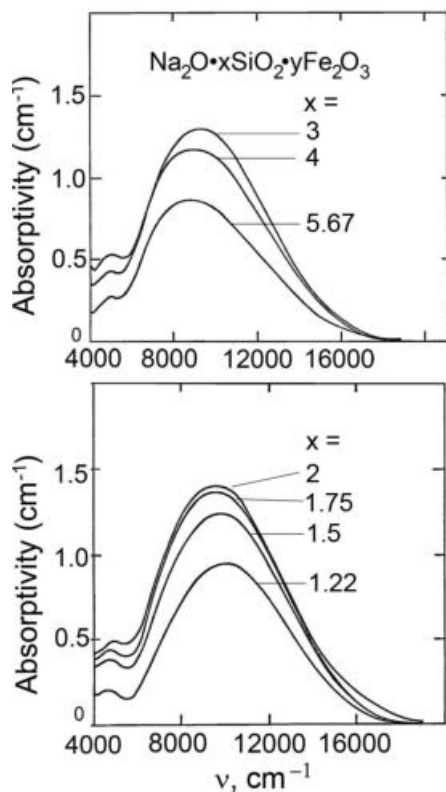


Fig. 4. Two absorption bands due to Fe^{2+} d-d transitions are observed in iron-doped sodium silicate glass.

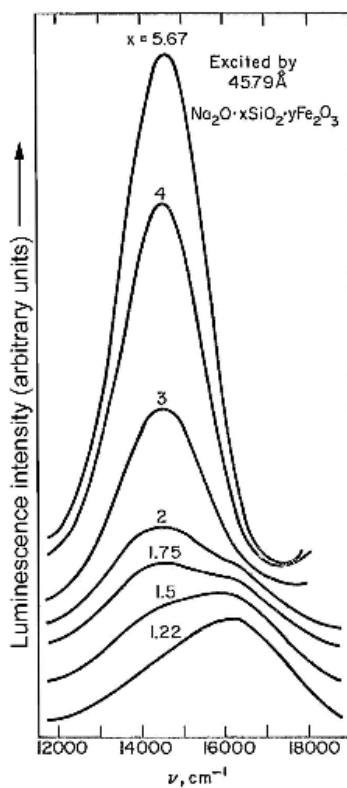


Fig. 5 Luminescence of sodium silicate glasses (nominal 0.50 mole% Fe_2O_3) excited by the 457.9 nm violet laser line suggests the presence of two kinds of tetrahedrally-coordinated Fe^{3+} .

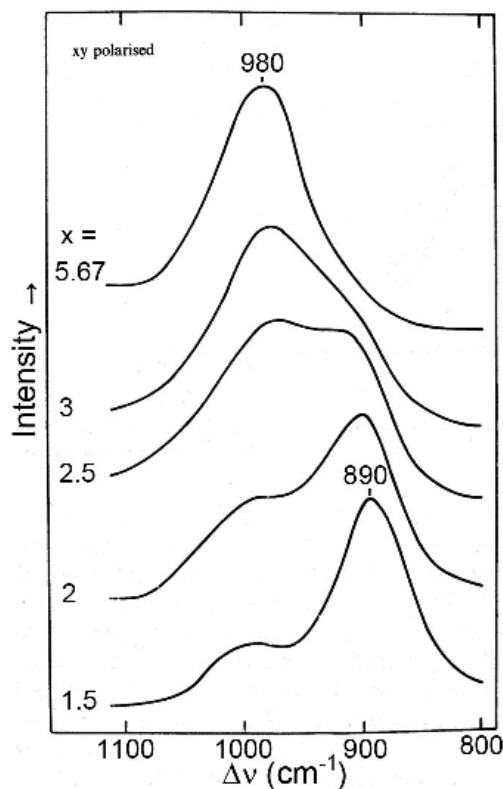


Fig. 6. Raman bands in sodium silicate glasses (2.4 mol% Fe_2O_3) suggest the presence of two different kinds of tetrahedrally-coordinated Fe^{3+} .

Iron in sodium silicate glasses

Ferrous iron

Two bands are observed in the infrared absorption spectra for the $\text{Na}_2\text{O}\cdot x\text{SiO}_2\cdot y\text{Fe}_2\text{O}_3$ (0.50 mol% Fe_2O_3) glasses, one at about 10,000 cm^{-1} , the other at about 5,000 cm^{-1} (Figure 4). The absorptivity of these bands is very high in the spectrum of a trisilicate sample prepared under reducing conditions, such that most of the Fe^{3+} has been reduced to Fe^{2+} , confirming that these bands are due to Fe^{2+} . The behaviour of these bands is consistent with d-d transitions for Fe^{2+} in six-fold (octahedral) coordination, as has been reported by other investigators (Goldman & Berg, 1980).

Ferric iron

Luminescence spectra support the presence of two distinct fourfold-coordinated sites for Fe^{3+} , whose concentrations change as the sodium content of the glass is varied. Excitation by the 21,839 cm^{-1} (457.9 nm) violet Ar-ion laser line gives rise to luminescence in the red at 14,600 cm^{-1} , as well as another band around 16,200 cm^{-1} (Figure 5). At low Na_2O concentrations, the low frequency band is most intense. At the disilicate composition, the higher frequency band makes its first appearance, and becomes most intense for the high sodium glasses.

Similarly, two sites are also indicated by the Raman spectra, which show a weak band around 980 cm^{-1} in glasses of low sodium content, while a second band appears at about 890 cm^{-1} as sodium is increased (Figure 6). The Raman spectrum of the reduced sample shows no matching bands in this region, confirming Fe^{3+} as their origin.

By analogy with orthoclase (Manning, 1970), Fe^{3+} is believed to take part in the glass-forming network in the low sodium glasses. Evidence suggests the FeO_4 tetrahedron is less polymerized in the high sodium glasses, and displays a

lower bond vibration frequency.

Conclusions

Raman, absorption and luminescence spectroscopy have been used to track the structure of glass-forming networks and the environment of iron ions in "simple" sodium silicate glasses. This work contributes to a fundamental understanding of silicate glass structure and can be applied to the interpretation of the spectra of glasses used as gemstones, an area which has received little attention in gemmological circles.

References

Brawer, S.A. & White, W.B., 1975. Raman spectroscopic investigation of the structure of silicate glasses. I. The binary alkali silicates. *Journal of Chemical Physics*, 63(6), 2421-2432.

Fox, K.E., Furukawa, T., White, W.B., 1982. Transition metal ions in silicate melts. Part 2. Iron in sodium silicate glasses. *Physics and Chemistry of Glasses*, 23 (5), 169-178.

Furukawa, T., Fox, K.E., White, W.B., 1981. Raman spectroscopic investigation of the structure of silicate glasses. III. Raman intensities and structural units in sodium silicate glasses. *Journal of Chemical Physics*, 75 (7), 3226-3237.

Goldman, D.S., Berg, J.I., 1980. Spectral study of ferrous iron in Ca Al borosilicate glass at room and melt temperatures. *Journal of Non-Crystalline Solids*, 38 & 39, 183-188.

Manning, P.G., 1970. Racah parameters and their relationship to lengths and covalencies of Mn²⁺- and Fe³⁺-oxygen bonds in silicates. *Canadian Mineralogist*, 10, 677-688.

Acknowledgements

This study was performed under the guidance of Toshiharu Furukawa and William B. White at the Materials Research Lab, Pennsylvania State University, Pennsylvania.

Gemmological examination of jewellery objects from the Veliki Preslav treasure in Bulgaria

Elisabeth Strack¹, Ruslan I. Kostov²

¹Gemmologisches Institut Hamburg, Poststr. 33 Business Center, 20354 Hamburg, Germany info@strack-gih.de

²University of Mining and Geology „St. Ivan Rilski“, 1700 Sofia, Bulgaria; rikostov@yahoo.com

The authors examined jewellery objects from the Treasure at the Veliki Preslav Museum in Preslav, Bulgaria. Preslav was the capital of the great Bulgarian empire between the late 9th and the early 10th century. Under Tsar Simeon the Great (893 – 927) the city became a centre for the new Bulgarian Christian culture. The Preslav Literary School included artistic workshops for painting, ceramics and jewellery making, supervised by artists from Constantinople (Jordanov, 2002).

In the year 971, the city was destroyed as a result of the wars between Kiev and the Byzantine emperor. In spring 1978, a treasure box, probably hidden since 971, was discovered near the former Preslav royal palace, after farmers had been ploughing the winter before. It is assumed that the stolen treasure was hidden by soldiers on their flight away from the capital (Totev, 1993).

11 out of a total of 15 jewellery objects were studied in detail, 3 of the objects are described here. Standard gemmological equipment was used, including a refractometer, a polariscope, a binocular optical microscope and a multispectral ultra violet lamp for 366 and 254 nm. Sizes were measured with a Leveridge gauge and a millimeter gauge.

Figure 1. Three gold pendants from a necklace



The 30 drilled emeralds in the two pendants shown in figure 1 all have hexagonal prismatic shapes, with crystal faces and/or their edges smoothed over by gentle polishing, 10 emeralds are polished all over. 6 emeralds were slightly to severely damaged. Sizes are below 10mm, length measurements are 2 to 6mm and width is from 4 to 7.2mm (Table 1). Colour varies from green to intense green and transparency is weakened by strong fracturing (Figure 2). Translucent areas in 5 emeralds made it possible to observe mica, tremolite and two-phase inclusions with the microscope. One emerald showed a weak yellow fluorescence under 366nm that was confined to a filling residue on fractures.



Figure 2. Detailed view of emeralds and pearls.

Discussion of origin

The inclusion evidence gathered allows to consider Egypt as a possible source. Characteristic inclusions of the type of deposit, formed by pneumatolytic contact metamorphism, consist of mica and amphiboles (usually actinolite and tremolite needles) and two-phase inclusions (Gübelin and Koivula, 1986; Grundman and Morteani, 1993). Fluid inclusions and healed fractures are frequently encountered.

The deposits in Upper Egypt have been known since Roman times (Plinius, translation of 1987) and remnants of Roman mining activity still exist (Sinkankas, 1981). The Egyptian origin of emeralds in Roman jewellery is to a certain extent verifiable (Auriscchio et al., 2005). Moreover, the similar, usually flawed appearance of emeralds used all over the Roman empire (as is evident from collections of major European museums) suggest a regular source of supply. After the fall of the Roman Empire, the Egyptian mines continued to be worked until the early 13th century (Sinkankas, 1981).

The Habachtal deposit in Austria belongs to the same genetic type as the Egyptian one (Gübelin, 1956; Morteani and Grundmann, 1977; Grundmann and Morteani, 1982). No written or other proof as to the use in antiquity or the early middle ages is available, the deposit can nevertheless not be excluded as a further possible source (Guilliani et al., 2001). It was first described in 1797 by C.M.B.Schroll (Leitmeier, 1937).

When Pliny mentions Scythian emeralds he may have referred to Theophrastus' report of 314BC on emeralds from Bactria (Plinius, translation of 1987 and Theophrastus, translation of 2008). The location of the deposit is open to debate as there is no evidence of mining between the 4th century BC and the 1970s when the present Panshir Valley deposits were discovered by the Soviet occupation (Giard, 1998).

The Scythians, a nomadic people of Persian origin, would have dwelled in a wide region including central Asia and the southern slopes of the Ural Mountains. No traces of ancient or medieval mining activity are so far known from the Ural emerald deposits that were discovered in 1830. As to the genetic type, the Ural deposit coincides with those of Egypt and Austria and inclusion evidence is similar (Gübelin and Koivula, 1986). By contrast, the Afghan deposit is of a different, middle to low temperature hydrothermal origin, yielding a dissimilar inclusion picture (Gübelin and Koivula, 1986).

All other known emerald deposits were discovered after the 10th century and are not further discussed.

Pearls

The drilled pearls in the two pendants measure between 3.5-4mm up to 6.8-7.2mm. They have barrel, button and high button shapes. Colours are an even dark grey, surfaces show distinct signs of decomposition. The pearls did not

fluoresce under ultra violet light.

As no method for origin determination is available for pearls, the origin of the Preslav pearls can only be supposed. They probably come from one of the classical finding places already known to the antique world: the Persian Gulf or the Red Sea. Pearls were still traded widely in the early medieval period when Constantinople was a main trading centre. The original colour of the pearls was probably white. Their present grey colour is an indication of a drying out process of the organic substance over a period of more than 1000 years. It was aided by temperature changes when the treasure was left in the soil during the winter of 1977/78.

Sapphires

The drilled purplish stones in the central pendant were identified as 10 purple sapphires and 1 garnet. They had previously been described as amethysts (Totev, 1993 and Antanansov, 1999a, 1999b). Shapes are irregular, with polished surfaces, measurements go from 5.5x4.2mm to 6.5x 6.8mm, transparency is fair to good. The sapphires yielded readings in the range of 1.76 – 1.77 with the spot method, showed rutile needles intersecting in three directions under the microscope and displayed a strong red fluorescence under long wave ultraviolet light (366nm) with a weaker one under 254nm. The authors suggest Sri Lanka as a place of origin (Gübelin and Koivula, 1986). A comparable example are purple sapphires in the 9th century altar of St. Ambrose Basilica in Milan, attributed to a Sri Lankan origin (Sperchi, 1988).

Garnet

One purplish stone was determined as single refractive, with a spot reading above the limit of the refractometer. It displayed no fluorescence and rutile needles were present in one direction.

The data observed would allow for the identification as a garnet but further testing might be advisable.

Conclusion

The objects described represented an opportunity to study examples of 10th century jewellery of within the sphere of medieval Byzantine influence. Testing with standard gemmological methods allowed the identification of all green stones as emeralds and of 10 purple gemstones as sapphires and 1 as possibly a garnet. All pearls were determined – under reserve of further testing – to be of natural marine origin.

References

Atanasov, G., 1999a. Insignia of the Medieval Bulgarian Rulers. Pleven, 291 p. (in Bulgarian with an English summary).

Atanasov, G., 1999b. On the origin, function and the owner of adornments of the Preslav treasure from the 10th century. *Archaeologia Bulgarica*, 3(3), 81-94, Sofia.

Aurisicchio, C., Corami, A., Ehrman, S., Graziani, G., Cessaro, S.N., 2005. The emerald and gold necklace from Oplontis, Vesuvian Area, Naples, Italy. *Journal of Archaeological Science*, 33(4), 725-734.

Giard, D., 1998. Le Bouzkachi des Emeraudes – Les Emeraudes de la Vallée du Panjshir. *Revue de Gemmologie – L'Emeraude*, AFG, Paris, 192 p.

Giuliani, G., 2001. L'exploitation des mines d'émeraude d'Autriche et de la Haute Egypte à l'Époque Gallo-romaine: mythe ou réalité? *Revue de Gemmologie*, 143, 20-24.

Grundmann, G., Morteani, G., 1982. Die Geologie der Smaragdorkommen im Habachtal (Land Salzburg, Österreich).

Archiv für Lagerstättenforschung der Geologischen Bundesanstalt A., 2, 71-107.

Grundmann, G., Morteani, G., 1993. Die Smaragdminen der Cleopatra: Zabara, Sikait und Umm Kabo in Ägypten. Lapis, Heft 7/8, 27.

Gübelin, E.J., Koivula, J.I., 1986. Photoatlas of Inclusions in Gemstones, ABC Edition, Zürich, 532 p.

Jordanov, I., 2002. Preslav. In: The Economic History of Byzantium: From the Seventh through the Fifteenth Century. Dumbarton Oaks, Trustees for Harvard University, Washington, D.C., p.667-671.

Kostov, R.I., 2008. Theophrastus. On Stones (translation, notes and comments). Publishing House „St. Ivan Rilski“, Sofia, 48 p. (in Bulgarian).

Leitmeier, H., 1937. Das Smaragdorkommen im Habachtal in Salzburg und seine Mineralien. *Tschermak's Mineralogische und Petrographische Mitteilungen*, 49(4-5), 245-368.

Morteani, G., Grundmann, G., 1977. The emerald porphyroblasts in the penninic rocks of the Tauern Window, Austrian Alps. *Neues Jahrbuch für Mineralogie Monatshefte*, 11, 509-516.

Plinius der Ältere, 1987 (translation into German), *Historia naturalis*, Franz Greno, Nördlingen, 406 p.

Preslav Treasure, The, 2007. Treasures of Medieval Bulgaria. Catalogue of the Exhibition (V. Pavlova). Regional Historical Museum, Varna, 4-15 (in Bulgarian).

Schwarz, D., Pardieu, V., 2009. Emeralds from the Silk Road Countries – A comparison with Emeralds from Colombia, *In Color*, Fall/Winter 2009, 12, 38-43.

Sinkankas, J. (1981). Emerald and other beryls. Chilton Book Company, Radnor, Pa., 665 p.

Strack E., Kostov, R.I., 2010. Emeralds, sapphires, pearls and other Gemmological materials from the Preslav treasure (X century) in Bulgaria. *Geochemistry, Mineralogy and Petrology*, Sofia, 48, 103-123.

Superchi, M., 1988. Volvinio's altar gems in St. Ambrose, Milan. *Gemmologia Europea II*, CIGEM, Milano, 72-99.

Totev, T., 1986. The Preslav Treasure. *Proceedings of the Varna Museum*, 22 (37), 81-107 (in Bulgarian).

Totev, T., 1993. The Preslav Treasure. Publishing House Altos, Sofia, 114p.

Gemstones of Greenland

Anette Clausen

Geology Department, Ministry of Industry and Mineral Resources, Government of Greenland, Imaneq 1A – 301, P.O. Box 1601, 3900 Nuuk, Greenland; ancl@nanoq.gl

Introduction

The many different geological environments in Greenland result in a vast variety of gemstones e.g. agate, almandite, amazonite, amethyst, beryl, chalcedony, cordierite, diamond, greenlandite, jasper, kornerupine, labradorite, lapis lazuli, moonstone, nummrite, peridot, ruby, sapphire, sodalite, spinel, topaz, tourmaline and tugtupite. Yet, both large scale and small scale exploration of gemstones has been limited. Introduced by legislation in 2012, small scale mining is a new term in Greenland. Gemstones have traditionally been collected in small quantities, fashioned as cabochons and sold locally as an addition to the main source of income. Only very few stones are faceted and the quality of the cuts is generally poor. Small scale exploration is targeted at ruby, sapphire, diamond, greenlandite, tugtupite, nummrite, topaz, opal, chrysoberyl, emerald, moonstone and quartz. Large scale exploration has focused mainly on diamonds, rubies and sapphires. Some of the most important Greenlandic gemstones are described below.

Ruby/Sapphire

Ruby and sapphire occurrences are known from many localities in Greenland, especially the area between Maniitsoq and Qeqertarsuatsiaat in West Greenland (Figure 1). The most well-known occurrences are located in the intrusive Fiskenaesset anorthosite complex near Qeqertarsuatsiaat. The complex comprises anorthosites, leuco-gabbros, gabbros and ultramafic rocks and is infolded with amphibolites and basement gneisses. The rubies and sapphires rest in a green tschermakite-rich anorthosite at the amphibolite contact zone (Figure 2, left).



Figure 1. Map of Greenland with the major cities.

One company exploring for rubies and sapphires at Qeqertarsuaasiaat is True North Gems Inc., which has explored the area for some years. The company has located several ruby and sapphire occurrences and expects to get an exploitation license this year over an area called Aappaluttoq. The main ore zone comprises three rock types: sapphirine-gedrite, leucocratic gabbro and phlogopitite. Whereas the sapphirine-gedrite is corundum barren and a key indicator of corundum mineralization, the gabbro and phlogopitite both contains corundum. The leucocratic gabbro is Al-rich and probably the primary source of aluminium to the corundum formation throughout the Aappaluttoq deposit. Pink sapphires are abundant in the gabbro in comparison to the amount of rubies. The opposite is the case with the phlogopitite which comprises the majority of the rubies in the deposit. The size of the rough corundum ranges from microscopic to 80 grams in weight, with the transparent rubies and sapphires typically ranging 1-10 grams in weight (Weston, 2009). The indicated resource is estimated to 189,100 tons with 313 g/t corundum equaling 59,300 kg corundum (296.5 million carats). The inferred resource is estimated to 77,200 tons with an average content of 283 g/t corundum, corresponding to 21,900 kg corundum (109.5 million carats). The amount of near gem and gem quality corundum is estimated to 31.3% rubies and 40.8% sapphires. Production is planned to start in 2014.



Figure 2. Green tschermakite-rich anorthosite with pink sapphires and rubies (left) and rubies and sapphires from Government prospect (right). Both are from the Fiskenaasset complex.

Another company working in the Qeqertarsuaasiaat area is Lone Wolf Documentary Group/Sixty Degree Resources. This company was granted permission to do prospecting in 2012 on an area with a known ruby and sapphire occurrence, which has been temporarily closed for license applications by the Government of Greenland based on a report from the Geological Survey of Denmark and Greenland (GEUS) (Kalvig & Keulen, 2011). The deposit forms a c. 1.5 km long belt of vast corundum-bearing units with lengths of more than 20 meters and up to 4.5 meters wide. A phlogopite-sapphirine-rich schist hosts the majority of the corundum and is in some places very rich in corundum, especially where the amount of sapphirine is high. The sampled material was submitted to the Government of Greenland in early 2013. A total of 42.5 g of ruby and sapphire rough were collected of 1-5 mm in size. Though most of the rough was not completely free of host-rock, it was apparent that the majority of the rough was transparent with color ranging from slightly purplish red to red-purple. Further studies are to be conducted on the material in 2013.

In 2011, the Government of Greenland and GEUS collected samples from eight localities in the Qeqertarsuaasiaat area to get material for studies aimed at characterizing rubies and pink sapphires from Greenland (Figure 2, right). The preliminary results from 32 samples tested by GEUS show that these are relatively high in chromium and iron and low in gallium and titanium. The results indicate that samples from the Qeqertarsuaasiaaq area can be distinguished from other Greenlandic ruby occurrences based on the values of the trace elements Fe, Cr, V, Ti, Ga and Si (Keulen & Kalvig, 2013). The government origin determination project on Greenlandic corundum will continue and more tests will be conducted by GEUS and by Dr. Pornsawat Wathanakul at the Gem and Jewelry Institute of Thailand.



Figure 3. From left to right: A 2.5 ct diamond from Sarfartoq (Photo courtesy: Hudson Resources Inc.), a 1.72 ct korerupine from the Fiskenaesset complex (Photo courtesy: Z. Fihl, Geological Museum), greenlandite from Isukasia, nuummite from Nuuk area and tugtupite from the Ilimaussaq complex.

Diamonds

Triggered by the diamond discoveries in Canada, diamond exploration intensified in West Greenland in the mid-1990's. The most prospective diamond area is in Central West Greenland between Nuuk and Sisimiut where the kimberlites are abundant (Figure 1). Canadian-based Hudson Resources Inc. has been exploring the area for several years and has extracted a total of 1,740 macro diamonds of more than 0.85 mm in three dimensions from a diamond bearing kimberlite dyke at Sarfartoq. To date, more than 100 carats have been recovered from the deposit with the largest diamond being 2.5 carat (Figure 3). Most of the diamonds are colorless, but pink, grey and amber colored diamonds also occur. The present recession of the diamond market has momentarily put the project on standby.

Korerupine

Korerupine is known from the Qeqertarsuatsiaat area where it appears in the Fiskenaesset anorthosite complex (Figure 1). The largest crystal found is 23 cm in length and has a dark green color. Kornerupine varies in color from non-transparent white and blue to the rarer transparent green (Figure 3). The gemstone is strongly pleochroic: from dark green to light blue or reddish blue (Petersen & Secher, 1993). A few of the large crystals have been faceted and are at display at the Geological Museum in Copenhagen. The largest faceted kornerupine is a transparent 5.88 ct of dark green color.

Greenlandite

Greenlandite is microcrystalline green to bluish green aventurine quartz mainly found in the Nuuk area, Central West Greenland (Figure 1). It was discovered at the Isukasia locality Northeast of Nuuk and its age of 3.8 billion years most probably makes it the oldest gemstone in the world (Figure 3). Greenlandite is one of the favorite gemstones for small scale miners and local gemstone cutters but no efforts have been made to exploit greenlandite commercially.

Tugtupite

Tugtupite is a mineral closely related to sodalite, found in hydrothermal veins at the Ilimaussaq Complex near Narsaq and Qaqortoq in South Greenland (Figure 1). The color varies from white to intense red with the red being the most praised (Figure 3). A light blue and a violet version also exist. Tugtupite shows intense yellowish orange fluorescence when exposed to long-wave ultraviolet light and strongly purplish red when exposed to short-wave ultraviolet light. It exhibits tenebrescence fading from red to pink or white and back to red again after being exposed to daylight. Tugtupite is very high in demand but unfortunately occurrences are scarce.

Nuummite

Nuummite is a mixture of the amphibole minerals anthophyllite and gedrite and is found at different localities in the Nuuk area (Figure 1). The gemstone exhibit iridescence of different colors, mainly yellow, golden, blue or blue-green, but red is also seen. Along with greenlandite and tugtupite, nuummite is a very popular gemstone which is almost

always sold as cabochons (Figure 3).

Conclusion

The few exploration companies searching for gemstones in Greenland have focused on diamonds, rubies and sapphires while small scale miners and locals are interested in a broad variety of gemstones. The gemstones are typically sold locally in Greenland and only exported in limited quantities. A more diverse and intense gemstone exploration in combination with more skilled local cutters might change this.

References

Kalvig, P., Keulen, N., 2011. Aktiviteter i Rubinprojektet, 2011. Danmarks og Groenlands Geologiske Undersoegelse Rapport 2011/138.

Keulen, N., Kalvig, P., 2013. Report on the activities in the ruby project 2012. Danmarks og Groenlands Geologiske Undersoegelse Rapport 2013/9.

Petersen, O. V., Secher, K., 1993. The Minerals of Greenland. The Mineralogical Record, 24(2), 3-65.

Weston, B., 2009. 2008 Report on Field Activities for the Fiskenaesset Ruby Project, Greenland. From www.truenorth-gems.com.

Gemstone mining in the United States in the previous decade

Michael Gray

Coast-to-Coast Rare Stones, rarestone.com; P.O. Box 1328, Ft. Bragg, California 95437 USA
mgray@rarestone.com

While the United States is not a major producer of gemstones, there are a number of important notes to be made in what is, and is not, being produced in recent years.

There is a renewed interest in gemstone mining in the United States, partly fueled by increased interest and prices in some mineralogical species, and by increased awareness brought about by the internet and television currently airing programs about gemstone mining. At the same time, it is getting increasingly more difficult and expensive to extract these minerals and gems, with stricter mining safety and environmental laws to contend with.

A number of previously closed gem localities are now being reworked, with a fair amount of success coming about with better mining equipment and techniques. A good example is the mine at Adams' Farm, near the town of Hiddenite, North Carolina. Some of the largest hiddenites, the chromium-colored variety of spodumene, ever faceted have been mined and cut in just the last few years.

On the other hand, a few world renowned mines have recently been permanently closed. As an example, there will be no more benitoite mined at the Benitoite Gem Mine in San Benito County, California, as that locality was not only closed due to exhaustion of the existing veins and alluvium, but all of the workings have been buried and «recovered» by bringing in other topsoil to cover whatever tailings were exposed and planted with ground cover.

These are just a couple of examples of the latest developments. There has been a lot of gemstone mining activity in the United States in the last decade, and there is no indication that it will slow down anytime in the future.

Further research into digital color analysis and communication of color in gems

Menahem Sevdemish, FGA D. Litt.

European Gemological Center, Ramat Gan, Israel; smenahem@gemewizard.com

Color is often the most important and the most influential attribute in the gem trade, both traditional and online. However, as the gem digital business is growing exponentially every year, the online buyer is struggling with color display and descriptive issues, which are lowering confidence in the trade. The need for gem-color analysis tools, enabling the users to better describe price and trade in gems, is growing.

The Gemewizard, a digital color analysis system, which we have been developing over the last decade, provides us with the power to scan, record, analyze and easily describe color data within gem images. We have also used the system to function as a research tool. The ability to inspect selected areas within the image has led us to new insights regarding the ratio of and relationship between the colors composing the gem. This allowed us to record and measure the effect of multi-colored, strongly pleochroic, and unevenly color-zoned crystals, on the overall polished gem appearance. For example, color image analysis makes it possible to accurately describe the different colors seen in a multi-colored tanzanite (Figure 1). Another application is to provide a more accurate and measurable description of distinctly pleochroic gems, such as gem tourmalines (Figure 2)

We are also able to use the data in order to give pre-cutting consultation to colored diamond and colored stone's cutters.

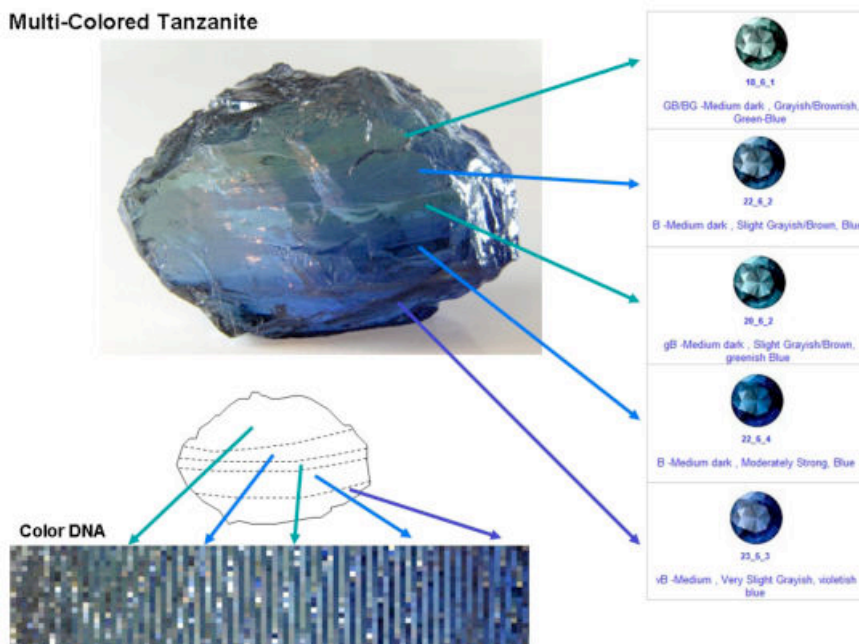


Figure 1. A color analysis by the Gemewizard system of multi-colored tanzanite. The analysis identifies the color zones within the rough crystal and their color values, using the «color DNA» method.

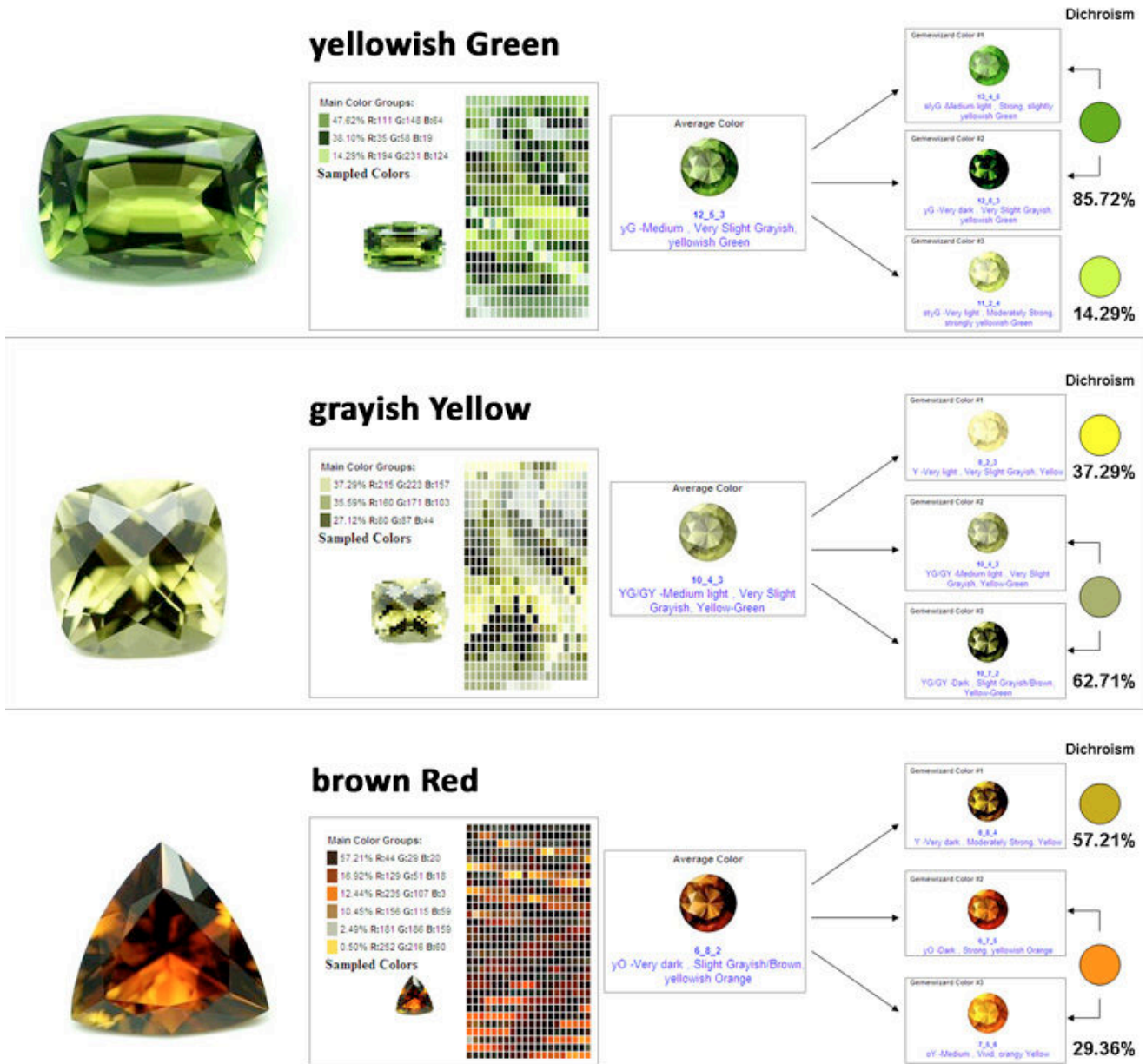


Figure 2. Color analysis by the Gemewizard system of three strongly dichroic tourmaline gems. The analysis maps the gems' color makeup and extracts the resultant polarized colors.

Establishing a uniformly accepted digital visual color language and analysis systems, will allow labs, educational institutes and the trade to use the same standards when describing color.

Digital Microscopy applications in gemmology

Yuri Shelementiev¹, Sergey Sivovolenko²

¹MSU Gemmological Center, Moscow, Russia; yuri@gem-center.ru

²OctoNus Software, Tampere, Finland; sivovolenko@octonus.com

Binocular microscope is the common tool used by gemologists worldwide to solve a number of problems, including challenges of gemstone identification, distinguishing natural and synthetic stones, identifying indications of treatment and color origin, etc. Conventional binoculars offer a way to witness beautiful and exciting interior scenes in gemstones.

In order to record an image observed under such microscope, nowadays photo and video cameras are applied. Apart from the certain advantages, such cameras also have the certain limitations, and one of them is mono image: only a single photo or single movie is obtained while recording an initial stone.

Stereo image has some advantages in comparison with mono: on the base of stereo human brain divides objects by the depth of their location, for example, it easily distinguishes a scratch on the stone's surface from inclusions under the surface. In some cases a stereo image provides a qualitatively different and critical information for making a decision than its equivalent mono image.

For receiving stereo information, Octonus Software Company developed Digital Microscope (DM), enabling to record images by using two video cameras, respectively for the left eye and for the right eye. It makes possible to record real time immersive 3D movies with high image quality. Independent video signals are compressed and transmitted for the left and right eyes, so that high-resolution 3D images can be recorded and viewed on 3D-capable TVs or 3D computer monitors. Using special software for stereo films viewing one can watch movies in 3D-version, and these movies have the same properties as the images observed under a binocular microscope.

Technical parameters and possibilities of DM:

- controlling and monitoring the microscope by multi-button computer «mouse»
- regulating the gemstone's position by using a manipulator.
- observing internal "pictures" on the monitor by using stereo glasses.
- a Leica microscope head, providing the optical zoom up to 115 X magnification.
- real-time recording of movies,
- various types of lighting, automatic adjustment of brightness when enlargement (zoom) changes.
- 3D viewing software with the function of distant simultaneity (synchronization)

After recording several dozens of movies with gems (colored gemstones and faceted diamonds) we've learn that this technology can be a useful teaching tool for gemologists and jewelers, because it has the following properties and features:

1. 3D effect mentioned above.
2. Recording of internal features in gemstones, which passed through a laboratory and were returned back to their owners.

3. Demonstration of the process of gemstones observation and examination, as gemstones are usually seen and observed by a well-experienced, skilled specialist. It helps to avoid the stage of training the newcomers (non-skilled users) in installing and tuning the microscope, lighting, image (image properties and conditions) and looking for the necessary details and focusing on them.

4. The possibility of simultaneous viewing (watching) a certain movie by two or more observers, located in different countries (the observer can play it manually – moving it by the computer “mouse”- and point to the discussed area by the “mouse”). Each participant can see the “mouse” cursors of all the observers.

Demonstration movies, produced by us, enable to learn how to analyze inclusions, to identify natural or synthetic origin of colored gemstones, indications of treatment, and also to observe luminescence. Recording of internal features for cut diamonds allows creating a database of various clarity grades, with various schemes of inclusions in diamonds. Such database doesn't require buying a great amount of real diamonds, and makes it possible to reduce subjectivity in clarity grading, and also to provide training in clarity grading of polished diamonds.

Such stereo movies can make the educational process (process of teaching and process of learning) significantly more effective. A database of such movies, classified and systematized properly, makes it possible to improve effectiveness of distance education.

A remote operator may control and monitor the microscope at a distance, and that enables to observe a stone, located in another place, under the microscope. We see the potential of such a technology: in fact it is a new method of cooperative shared work and learning, as gemologists can share 3D scenes, details and excitement with others.

As imaging technologies are developing from year to year, stereo images technology and 3D movies viewing will become more available in the future. Nowadays it is already available, for example, on the stereo computer monitors with the certain video cards (display cards), 3D projectors (projection devices) and 3D TV-s.

Structural and chemical analysis of Thai ivory from Lampang Province using SEM/EDS and LA-ICP-MS

Chakkrich Boonmee¹, Natthapong Monarumit ¹, Sermrak Ingavanija¹, Somruedee Satitkune¹, Pornsawat Wathanakul^{1,2*}

¹ The Gem and Mineral Sciences Special Research Unit, Department of Earth Sciences, Faculty of Science, Kasetsart University, Bangkok 10900, Thailand

² The Gem and Jewelry Institute of Thailand, Bangkok, Thailand; *pwathanakul2@gmail.com

Introduction

Ivory is a valuable and beautiful material. It is made for jewelry and other decorations around the world. The ivory is demanded in the jewelry market, many elephants have been hunted for dominating their ivories. Today, elephants and their ivories are protected under the Convention on International Trade in Endangered Species (CITES). The ivories are, therefore, illegal to import and/or export for commercial purposes. The Asian elephant (*Elephas maximus*) was listed in CITES Appendix I since 1975 (Banerjee et al., 2008 and Reifsten et al., 2008). The main composition of ivory caused by biomineralisation is hydroxylapatite ($\text{Ca}_{10}(\text{PO}_4)_6(\text{OH})_2$). African and Asian ivories have been identified by using advanced scientific instruments such as FTIR, XRF, TEM, and DNA analysis. The Thai ivory data from previous research are scarce, thus, this study serves the purpose of creating a database of SEM/EDS and LA-ICP-MS data of Thai ivory samples from Lampang Province, northern Thailand.

Materials and Methods

Twenty-two samples of Thai ivory (Figure 1) were collected from the Timber Center, Lampang Province. The samples were registered and prepared for analyses of their structures and chemical compositions, with the help of advanced scientific instruments.



Figure 1. Examples of Thai ivory samples

SEM produces a highly focused electron beam to excite and interact with a sample contained in a high vacuum environment in order to form a high resolution image of hydroxylapatite. EDS was applied to measure the chemical composition semi-quantitatively. The LA-ICP-MS technique is used for analyzing the element composition on the parts per million and parts per billion scales.



Figure 2. SEM/EDS (JEOL JSM-6335F) at Science and Technology Service Centre, Faculty of Science, Chiangmai University (Left) and LA-ICP-MS (Agilent Technology-7500 Series) at The GIT- Thailand (Right)

Results and Discussion

The fibrous pattern of hydroxylapatite in the Lampang ivory samples could be magnified by SEM. Besides, the chemical compositions were observed by EDS as shown in Figure 3. There are Ca, C, O, Na, Mg, Si, Al, and P.

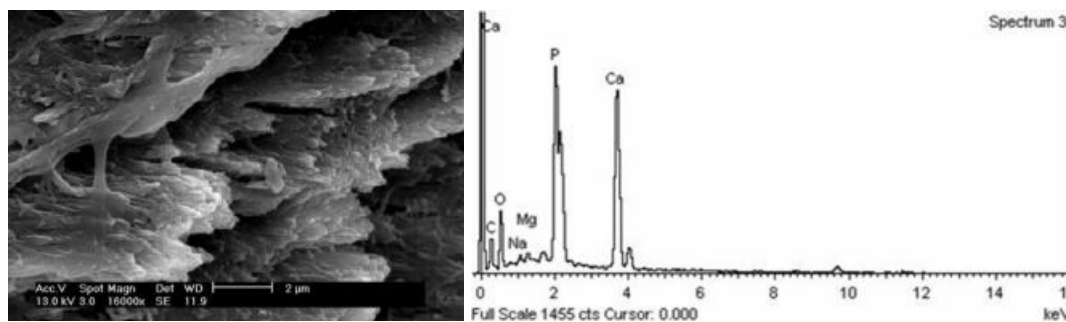


Figure 3. SEM image showing fibrous pattern (Left), and EDS spectrum (Right) of ivory samples.

The trace elements of twenty two Lampang ivory samples were analysed by LA-ICP-MS. The samples are characterised by Cl, Mn, Fe, Cu, Zn, Rb, Sr, Sn, Ba, La, Ce and Pb (Figure 4) (Wathanakul et al., 2010). The Cl concentration is higher than those reported in both African and forest elephants by Jacob et al., 2008.

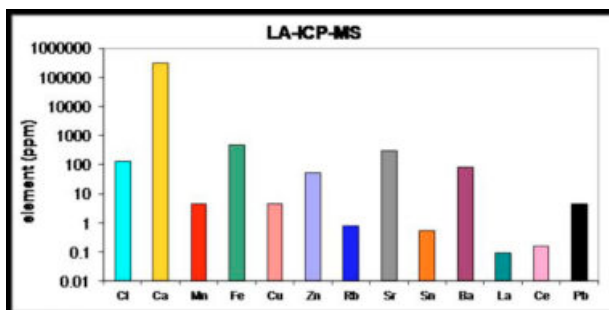


Figure 4. LA-ICP-MS result of Thai ivory samples from Lampang Province.

Conclusion

This study described fibrous patterns of Thai ivories under the SEM. The chemical compositions of hydroxylapatite in Thai ivory samples from Lampang Province were detected by EDS. LA-ICP-MS is applied for trace element analyses. The specific characteristics of Lampang ivory can be used in a database that is built for distinguishing ivory samples from other origins.

References

- Banerjee, A., Bortolaso, G., Dindorf, W., 2008. Distinction between African and Asian Ivory. In Proceedings of INCENTIVS-meeting (2004-2007), 37-49.
- Reifenstein, V., Kitschke, C., Ziegler, S., 2008. Elephant Conservation and the Ivory Trade. In Proceedings of INCENTIVS-meeting (2004-2007), 13-25.
- Banerjee, A., Bortolaso, G., Hofmeister, W., Petrovic-Prelevic, I., Keiwisch, B., , 2008. Investigation of quality of commercial mammoth ivory by means of X-ray Powder Diffraction (Rietveld method) and FTIR Spectroscopy. In Proceedings of INCENTIVS-meeting (2004-2007), 51-63.
- Jacob, D.E., Stracke, A., Wiegand, B., Dindorf, W., Tracing ivory by its chemical and isotopic composition. In Proceedings of INCENTIVS-meeting (2004-2007), 93-99.
- Wathanakul, P., Vetayaprasit, W., Boonmee, C., Ingavanija, S., 2010. Identifications of Thai Elephant Ivory. Final report submitted to Kasetsart University Research and Development Institute (KURDI), 58 pp.

Acknowledgements

The authors appreciate various supports from the Department of Earth Sciences, Faculty of Science, Kasetsart University; The Forest Industry Organization, Ministry of Natural Resources and Environment, Johannes Gutenberg University Mainz, Germany, and The Convention on International Trade in Endangered Species (CITES) of Thailand. Special thanks are due to The Gem and Jewelry Institute of Thailand (Public Organization)-GIT for LA-ICPMS analyses; Kasetsart University Research and Development Institute (KURDI) for the research fund, and The Science and Technology Service Centre, Faculty of Science, Chiang Mai University for the SEM facility.

Inclusions in Indian rubies

Gagan Choudhary¹ and Shyamala Fernandes²

¹Gem Testing Laboratory, Jaipur, India; gagan@gjepcindia.com

²SF Gem Labs, Bardez, Goa, India; sflabs@gmail.com

India is homeland for many fabulous historic diamonds, especially from the Great Golconda diamond field in central-southeast India, now known as Andhra Pradesh and many exquisite blue sapphires from Kashmir (e.g. Durlabhji et al., 2003). In addition, India is also known to produce some extraordinary sizes of star rubies from Mysore in the Karnataka state, along with fine qualities of various types of gemstones (e.g. Choudhary, 2012).

Ruby deposits in India are located in the following states (Fernandes & Choudhary, 2010):

- Tamil Nadu: Karur, Salem, Manvadi, Kambam, Coimbatore, Madurai and Tiruchirapalli
- Andhra Pradesh: Khammam, Guntur, Anantpur, Warangal, Vishakhapatnam and Hyderabad
- Karnataka: Mysore, Ramannahalli, Dughahalli, Coorg, Mercara, Tumkur, Hassan and Chikmangalur
- Chhattisgarh: Raipur and Bastar
- Odisha (Orissa): Kalahandi and Bolangir
- Maharashtra: Bhandara (e.g. Indian Bureau of Mines, 2010)

Most of the deposits are being worked out by local villagers, as small-scale mining operations at Raipur in Chhattisgarh, in Odisha, at in Andhra Pradesh; in Karnataka and districts in Tamil Nadu.

Due to the diverse geological setting, ruby deposits in India are mainly associated with complex rock types comprising gneisses and schists, exhibiting a great deal of variation in mineralogical composition and grade of metamorphism (see e.g. Sarkar & Guru, 2005).

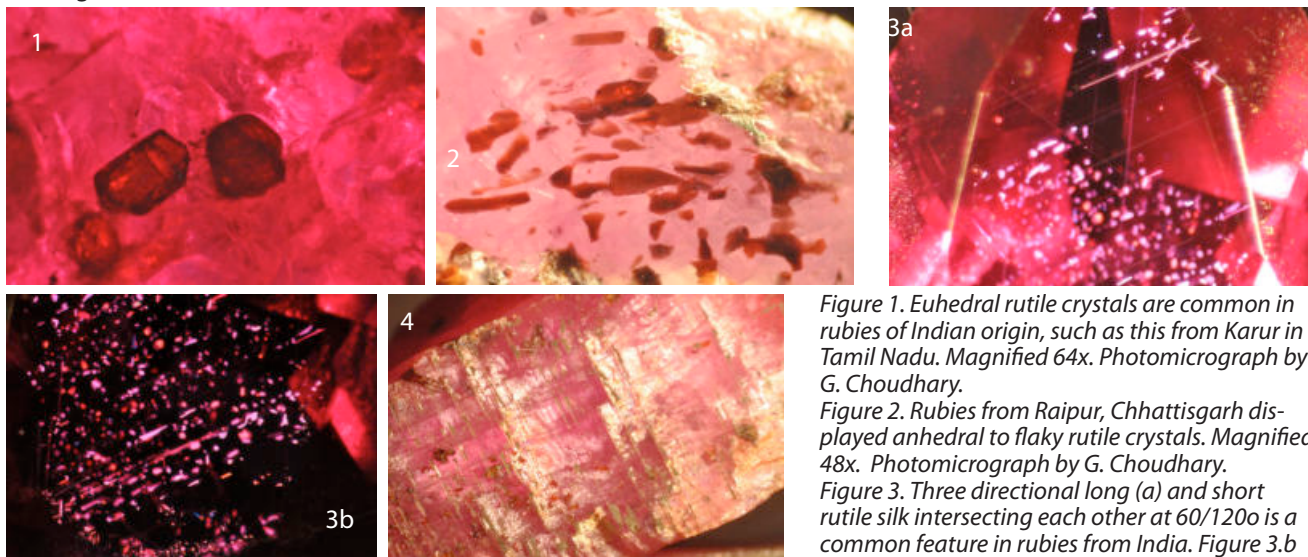


Figure 1. Euhedral rutile crystals are common in rubies of Indian origin, such as this from Karur in Tamil Nadu. Magnified 64x. Photomicrograph by G. Choudhary.

Figure 2. Rubies from Raipur, Chhattisgarh displayed anhedral to flaky rutile crystals. Magnified 48x. Photomicrograph by G. Choudhary.

Figure 3. Three directional long (a) and short rutile silk intersecting each other at 60/120o is a common feature in rubies from India. Figure 3.b shows short rutile silk/platelets with re-entrant angle. Long as well as short silk can be present in the same specimen such as this. Magnified 80x (both). Photomicrographs by G. Choudhary.

Figure 4. Twinning planes coated with layers of diasporite in a ruby from Andhra Pradesh, India, producing bright iridescent colours as well as whitish appearance. Also note scattered brownish rutile crystals. Magnified 48x. Photomicrograph by G. Choudhary.

In this paper, an attempt has been made to correlate the types of inclusions observed in rubies from various Indian states and their associated rock types. The common inclusions observed in Indian rubies and the rock types are given in table 1.

Table 1: Common types of inclusions observed in Indian rubies and their associated rock types

States	Features Rock Type [Fernandes et al (1999), Panjekar J. (1997, 1999, 2002)]	Inclusions	
		Solid	Fluid / Structural / Others (common for all locations)
Tamil Nadu	Basic holocrystalline granitoid gneiss (Charnockites) with orthopyroxene	Crystals Apatite: Colourless, euhedral, prismatic Rutile: Brown, euhedral to sub-rounded (Figure 1) Zircon: Colourless, elongated and rounded, with stress cracks Spinel: Yellowish, rounded octahedron	Exsolved inclusions: Rutile in form of <ul style="list-style-type: none"> Long and short silk in three directions, oriented along the basal plane and intersecting at 60/120°. Short silk often displaying twinning (re-entrant) angles at the broader end (Figure 3). Fine discs / dust concentrated along the hexagonal zones / bands of the host ruby, often iridescent. Boehmite / Diaspore in form of <ul style="list-style-type: none"> Whitish needles along the edges of twinning planes Films along the surface of twinning planes (appear iridescent in reflected light and whitish in transmitted light) (Figure 4)
Karnataka	Contact zones of ultramafic rocks and pegmatite veins, within pelitic schists; gabbroic anorthosite, permeated by magnesite	Crystals Rutile: Brown, euhedral to sub-rounded to anhedral	Fingerprints: In the form of veils they are common in most of the Indian rubies. However, their visibility is not very pronounced as in some other deposits, due to the presence of large number of twinning planes, which tend to overlay the fingerprints Films: Iridescent films are visible only in ruby from Raipur, Chhattisgarh Phase: No distinct phase inclusion is visible
Andhra Pradesh	Quartz, feldspar, mica and hornblende rich gneiss, associated with sillimanite gneiss and schists, along with nepheline, corundum and zircon syenites	Crystals Rutile: Brown, sub rounded to anhedral Black, rounded with metallic lustre	
Odisha	Highly foliated gneiss, closely associated with schists of variable composition. The gneiss is often dioritic owing to larger proportions of plagioclase feldspar. Corundum occurs along the contact of the gneiss and limestone. Another rock type is gneiss and sillimanite schist (Khondalite)	Crystals Chromite: Black, sub-rounded granular Flakes / Platelets: Greenish mica flakes randomly oriented	Growth / Colour Zoning: Very common in most of the rubies (especially the star varieties) forming hexagonal to pseudo-hexagonal patterns typically associated with corundum. These zones typically contain rutile discs, dust, and / or short needles Twin Planes: Indian rubies are characterized by the twin planes with intervals varying from very dense to broad. However, this is not consistent with the location.
Chhattisgarh		Crystals Rutile: Anhedral and flaky (Figure 2) Hematite: Black, metallic, platy, elongated and sub-hedral	Others: Iron stained fractures / films are present in many rubies. Some whitish cloudy crystal of unknown nature is visible in rubies from Raipur, Chhattisgarh

This study revealed a range of inclusions found in Indian rubies, which were of more or less similar type, pattern and appearance. No consistency was observed in the type and pattern of inclusion, restricted to a specific locality (states) and the associated rock types, although some of the minerals were identified only in specific locality such as hematite (in Chhattisgarh), chromite and green mica (in Orissa), and apatite and yellow spinel (in Tamil Nadu).

References

Choudhary, G., 2012. An overview of inclusions in Indian gemstones. 3rd International Gem & Jewelry Conference (GIT 2012), Bangkok, Thailand, proceeding volume, pp 149- 152.

Durlabhji, M., Fernandes, S., Choudhary, G., 2003. ICA Mining Report.

Fernandes, S., Joshi, V., Schwarz, D. & Bharadwaj, R., 1999. Indian Ruby - Deposits & Characterization. XXVI International Gemmological Conference, Goa, India.

Fernandes, S. & Choudhary, G., 2010. Understanding Rough Gemstones. Indian Institute of Jewellery, Mumbai.

Indian Bureau of Mines 2010. Indian Minerals Year Book 2011, 50th ed. Indian Bureau of Mines, Nagpur, India (http://ibm.nic.in/IMYB%202011_Corundum%20&%20Sapphire.pdf; accessed 03-05-2013).

Panjikar, J., 1997. Comparative study of corundum from various Indian occurrences - Corundum from Orissa. Indian Gemmologist, 7(1-2), 12 – 17.

Panjikar, J., 1999. Comparative study of corundum from various Indian occurrences - Corundum from Karnataka. Indian Gemmologist, 8(1-2), 3-8.

Panjikar, J., 2002. Comparative study of corundum from various Indian occurrences - Corundum from Tamil Nadu. Indian Gemmologist, 10(1-2), 3-8.

Sarkar, S.K. & Guru, A.I., 2005. Review of gemstone belts of eastern and southern India and guidelines for the search of gemstone deposits. Indian Gemmologist, 13(1-2), 41-49.

XVII - XVIII century garnet-garnet doublets imitating rubies

Arunas Kleismantas

Department of Geology and Mineralogy, Faculty of Natural Sciences, Vilnius University, M.K. Čiurlionio 21/27, LT-03101, Vilnius, Lithuania; arunas@kleismantas.eu

Introduction

In the past, clear gemstones of rich red colour such as rubies, garnets, spinels, tourmalines and others were often used in jewellery. As far as liturgical supplies are concerned, garnets, rubies and artificial materials like red glass, doublets made up of colourless material glued together with a red substance in between, were predominant (Kleismantas, 2011). Amongst all mentioned gemstones, rubies are the most brilliant ones. People were always fascinated by the red colour and particularly by the brilliance of gemstones. Transparent rubies of high quality and sizes bigger than a pea are rarely found in nature; hence in liturgical supplies combined gemstone-doublets were often used. In Western Europe in the XVII - XVIII century, skilful gem grinders produced garnet-garnet doublets with special bright brilliance similar to the one of rubies.

Research material and methods

11 garnet-garnet doublets from the Lithuanian Church Heritage Museum and from three liturgical supplies of Lithuanian churches were identified and described: 2 doublets in the monstrance of the Lithuanian Church Heritage Museum (hereinafter referred to as the Museum monstrance) (Figure 1), 7 doublets from the Church of St Matthew the Apostle and Evangelist in Rokiskis in a free-standing altar small cross and 2 doublets from the Church monstrance (currently it is not known in which one as the monstrance has been researched in the Pranas Gudynas Restoration Centre of Lithuanian Art Museum (hereinafter referred to as the Church monstrance).

In order to identify the gemstones, microscopic, physical and optical methods have been used. To carry out those examinations, the following devices have been used: reconstructed immersion microscope, refractometer, duo-tester of thermal conduction, loupe, and callipers for calculating the measurements. The age of the examined liturgical supplies is referred to in the references (Goldsmith's art, 2006; 2007).



Figures 1a and 1b. Garnet-garnet doublets in the Museum monstrance (the second figure shows two larger gems).

Research data of garnet-garnet doublets

From the examined ninety-nine museum exhibits and liturgical supplies from the XVI – XX century, 6862 gems were identified and described. Out of these 120 XVI – XIX century doublets of different structure were determined. A particular interest was caused by the combined gemstones made out of two garnets within empty spaces. 11 garnet-garnet doublets were identified in three liturgical supplies. They were produced in the XVII-XVIII century.

In the examined liturgical works of art with garnet-garnet doublets, the majority of red gemstones turned out to be rubies – 105 units (26 units – in the Church monstrance and 89 units – in the Museum monstrance). These rubies are small – up to 3mm and only some of them are bigger – up to 5mm. Also, these works of art contain other red gemstones, that are – garnets (10 units in the Church monstrance) and glass, artificial material (5 units in the Museum monstrance).

The examined garnet-garnet doublets are of unusual composition. They are special because two garnets are glued together in such a way that there is an empty space between them (Figure 2). Due to this space and a particular cut, these doublets shine more than usual. In the doublets with an empty space, light beams break several times at different angles. A light beam passes through the doublet's upper half and reaches the concaved wall of the bottom half through the empty space. Then, it reflects and comes back (Figure 3). Then it leaves again through the crown of the garnet-garnet doublet. In this way, the light beam provides a special brilliancy to the stone.

The shape of these doublets is oval or irregular round. The upper parts of the doublets have cut facets. The crown areas of two doublets are surrounded by 16 cut facets, seven doublets – 12 facets and the facets of two doublet's crowns are not very clear. The upper and bottom parts of the garnet-garnet doublets are distinctively cut. The lower part of the doublet's upper half is not flat as it is usually known in doublets but it is cut with a slight leaning towards the centre with five or six wedged facets (Figure 4). The bottom parts of the doublets are similar to a barrel, their inner part is gouged into the depth but their external part is only slightly polished.



Figure 2. Scheme of a garnet-garnet doublet with an empty space.

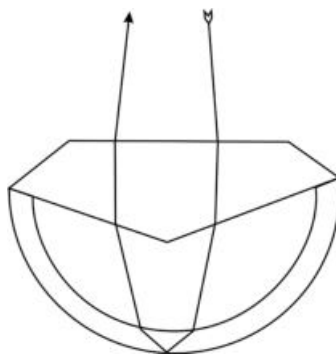


Figure 3. Scheme of the light beam in a garnet-garnet doublet.

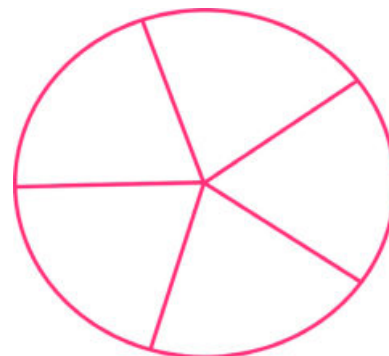


Figure 4. Scheme of a pavilion of a garnet-garnet doublet's upper part.

Discussion

Having examined 120 doublets of the XVI – XIX century in fourteen liturgical works, it was proved that in different periods different material was used for making doublets and doublets were cut in the shapes typical only for that particular period (Kleismantas, 2011). In the production of doublets, the most popular material was transparent quartz and glass, cemented together with coloured glue. However, in the XVII – XVIII century, garnets cut in a particular shape and cemented with an empty space were also used in the production of doublets. It is claimed that the examined garnet-garnet doublets were used for imitating rubies because they are the most brilliant amongst all red gemstones. Polishers, having made the garnet-garnet doublet with an empty space, managed to obtain brilliancy similar to the one of a ruby. In my opinion, garnet-garnet doublets were produced due to the lack of rubies in Europe and also it was an attempt to make cheaper jewellery.

Conclusion

According to the examination, composite stones, imitating valuable gemstones, were skilfully produced a few centuries ago. The examined garnet-garnet doublets were made in the XVII-XVIII century. They are unique as they stand out due to an extremely bright brilliancy similar to the one of rubies. Brilliancy emerges due to a particular shape of cut and due to an empty space close to the glue. Having passed through the gas space and reflected from another surface in the glued gem, a light beam breaks several times at different angles providing the gem with a special brilliance.

References

Goldsmith's art, 2006. Sacred Art of Lithuania. Volume IV. Book One. 320 p

Goldsmith's art, 2007. Sacred Art of Lithuania. Volume IV. Book two. 232 p.

Kleismantas A. 2011. Ruby in Monarchs' Crowns and Ecclesiastical Liturgical Appliances. Baltic Jewellery News. March 2011 (21). 66-67.

Kleismantas A. 2011. XIIth century doublets in liturgical items. Abstract proceedings. 32nd International Gemmological Conference IGC. Interlaken, Switzerland. 172-174.

Causes of colour in natural and irradiated green spodumene

Liu Shang-1,2, George Bosshart³ †, Peng Ming-sheng¹

1 Institute of Gems and Minerals Material, Sun Yat-sen University, Guangzhou, China;

2 Gemmological Association of Hong Kong, Hong Kong SAR; gemedward@hotmail.com

3 Horgen-Zurich, Switzerland

Green spodumene has long been of interest to mineralogists and gemologists by its “tenebrescent” behavior, that is the colour of some samples may fade under sunlight or heat, but the colour may be restored with irradiation (Bosshart et al., 2011; Esther, 1953). This study is an extended work of the second author (George Bosshart) in investigating the causes of colour of stable and unstable shades of green in spodumenes. Three spodumene specimens were selected (Figure 1, top) and believed to come from different localities with different colour origins: a natural hiddenite from Adams Mine, North Carolina (sample no. #1), one laboratory-irradiated yellowish green spodumene from Afghanistan (sample no. #2) and one naturally irradiated bluish-green spodumene from Northern Pakistan (sample no. #3) .



Figure 1. Green spodumene specimens #1-#3 (from left to right), a) before (upper row) and b) after strong light and UV exposure (lower row). Specimens #2 and #3 exhibit clear colour fading. Photos by Edward Liu S.I.

UV-Vis spectroscopy and chemical analysis by XRF showed similar results to previous studies (Bosshart, 2011). The North Carolina natural spodumene sample contains Cr and V which exhibited no tenebrescence and retained its original colour after x-ray irradiation and exposure to sunlight. The Cr³⁺ absorption band at 621 nm and a doublet at 688 and 692 nm were found. The 540 nm band which usually appears in irradiated green spodumene was absent in this natural green specimen.

Two irradiated (natural and treated) green spodumene samples showed similar absorption spectra which are related to colour centre(s). Their unstable colour can be easily bleached (from green to colourless) under daylight, ultra-violet, or moderate heat (<250°C), with a decrease in the corresponding absorption band at 637 nm.

The laboratory-irradiated spodumene from Afghanistan partially appeared light purplish red after exposure to x-ray. This colour faded rapidly within a few seconds under visible light.

EPR spectroscopic studies of all samples revealed that their colour may probably be caused by different mechanisms:

1. EPR spectra indicated that hiddenite sample from NC contains Cr³⁺ (in the 6-coordinated Al³⁺ site) with three fine structure lines. No signal of colour centre can be observed. V⁴⁺ fine structure lines signal has also been detected (Figure 2 and 3).
2. The EPR spectra of laboratory-irradiated green spodumene specimen showed the Cr³⁺ signal overlapping with a related colour centre.
3. The naturally-irradiated green spodumene sample displayed a different EPR spectrum which contains a simple signal of colour centre (with anisotropic g-factor) only.

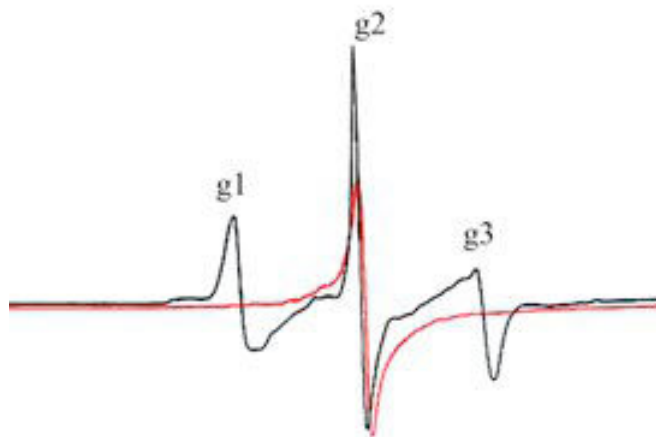


Figure 2. EPR spectra of Cr³⁺ fine structure of Hiddenite (sample no. #1) at different orientations (g//:black line; g-/: red line). g-factor (black line): g1=3.671, g2=2.953, g3=1.595. [H (Magnetic field): 3350 ±1000G].

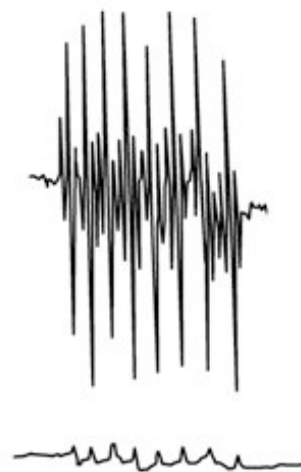


Figure 3. EPR spectra of V⁴⁺ hyperfine structure of Hiddenite (sample no. #1) (experimental spectrum (below) and spectrum after data processing (above)) from Adams Mine, North Carolina [H: 3350 ±1000G].

According to Hasson and Libib (1978) and Nassau (1983), the green colour of spodumene can be created by irradiation which induced electron hole(s) to transform (oxidize) Mn²⁺ (colourless) to Mn³⁺ (purple) and further to rather unstable Mn⁴⁺ (green). XRF analysis also revealed that both irradiated green spodumene samples have higher MnO contents than the natural hiddenite sample. However, no distinct Mn EPR signal can be observed in this study. The discovery of these colour centres may indicate that the defects in the naturally- and artificially-irradiated green spodumene samples are different and other colouring mechanisms may also exist. Owing to the limited samples, further study is needed to investigate these colour centres and the possibility to use them for characterization.

References

Bosshart, G., Tay, Y.K., Hainschwang, T. Krzemnicki, M., Dressler, R., 2011. Colorimetric investigation of unstable and stable spodumene colours. IGC 2011 proceedings, Interlaken, Switzerland, 26-30.

Esther, W. Claffy, 1953. Composition, tenebrescence and luminescence of spodumene minerals, American Mineralogist, 38, 919-931.

Hassan & Labib, 1978. Induced color centers in alpha spodumene called kunzite Neues Jahrbuch fur Mineralogie Abhandlungen 110, 128-141.

Nassau, K., 1994. Gemstone Enhancement. Butterworth-Heinemann, Oxford, English. ISBN 0-7506-1797-7.

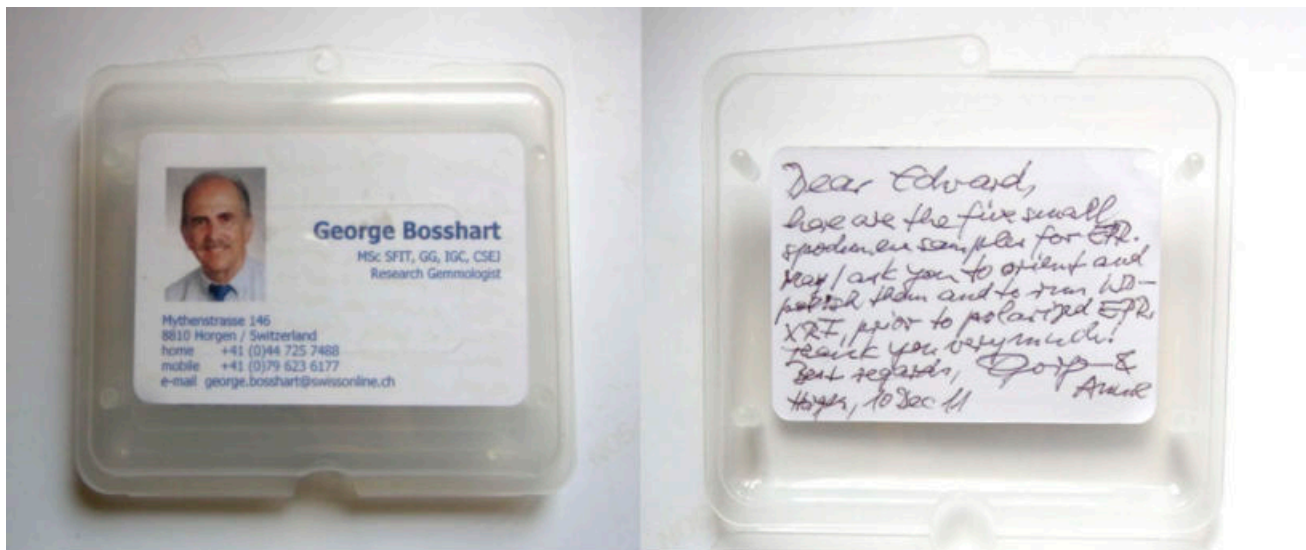
Liu, S.I., Peng, M.S., 2012. A reinvestigation of hackmanite and its tenebrescent properties, J. The 3rd International Gem & Jewelry Conference (GIT2012) Proceedings, 145-148.

Acknowledgements

The authors are grateful for support from Lau Chun Kit and Tsui Kin Wah Tommy of China Gems Laboratory Limited. Special thanks are also extended to Prof. Emmanuel Fritsch of Institut des Matériaux Jean Rouxel (I.M.N.) for his valuable suggestions and guidance.

Extending Bosshart's latest research

This extended study is to pay homage to the second author – George Bosshart, an honoured research fellow, for his many contributions to the field of gemology.



The box in which was sent spodumene samples by the second author (GB) before he passed away.

Sapphire deposits of Sri Lanka - past & present

Gamini Zoysa

Sri Lanka; gaminigz@hotmail.com

Almost all the sapphire producing deposits in Sri Lanka are alluvial-type. In recent time more of eluvial deposits have been discovered and also evidence for primary occurrence for sapphires have been noted.

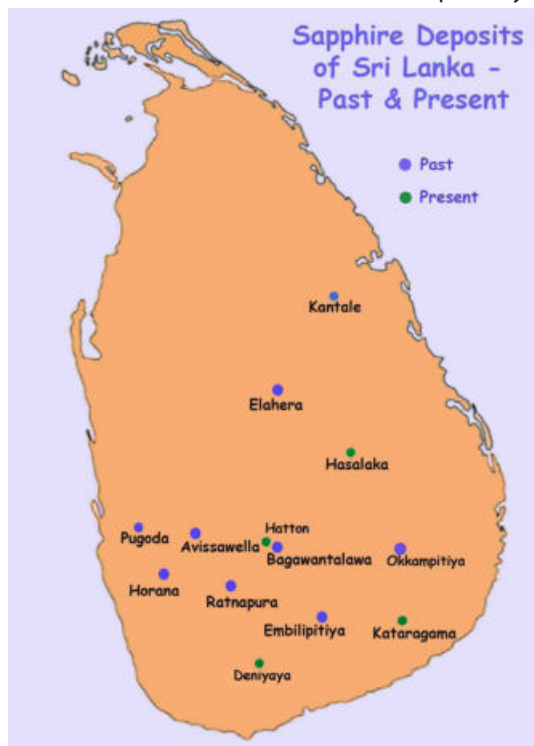


Figure 1. Sapphire deposits in Sri Lanka.



Figure 2. Gem Mining in Welgaha Wadiya, Thorapitiya.

Since blue Sapphire was declared as the national gemstone of Sri Lanka a great enthusiasm for sapphire mining could be observed. As a result more gem potential areas were identified.

Hasalaka

Located near the town of Mahiyangana in the central part of the island. There are 3 mining locations which are as follows:

1. Welgaha Wadiya
2. Thorapitiya
3. Eke Ela

As usual, all the three areas are alluvial gem pits & produce sapphires from 1 gram to 20 grams mainly in yellow-blue and Geuda types of corundum. Each area extends up to about 1-2 km. In Welgaha Wadiya sapphires mined are mostly yellow in colour and sizes vary up to about 15 mm. In Eke Ela, in addition to sapphires, purplish spinels are also encountered. The production is about 50 carats per day.

As accessory minerals, rhodolite garnet, spinel and goethite were common in the heavy fractions. The gemmology, chemistry and their inclusions will be described in detail. Spinel usually show purple to lavender colours and sizes vary from 5 mm to 10mm. The rough fragments are partially worn. Most of the spinels are largely transparent.



Figure 3. Gem mining in Eke Ela.



Figure 4. Mining on a public road by the villagers.



Figure 5. Excavation at the mining site in Tammanawa, Kataragama.

Tammanawa village in Kataragama which is in the extreme south of Sri Lanka became known as a new mining area since April 2012. (Zoysa & Rahuman, 2012). In April 2013 the mining rights have been extended for another period of 1 year by the National Gem & Jewellery Authority.

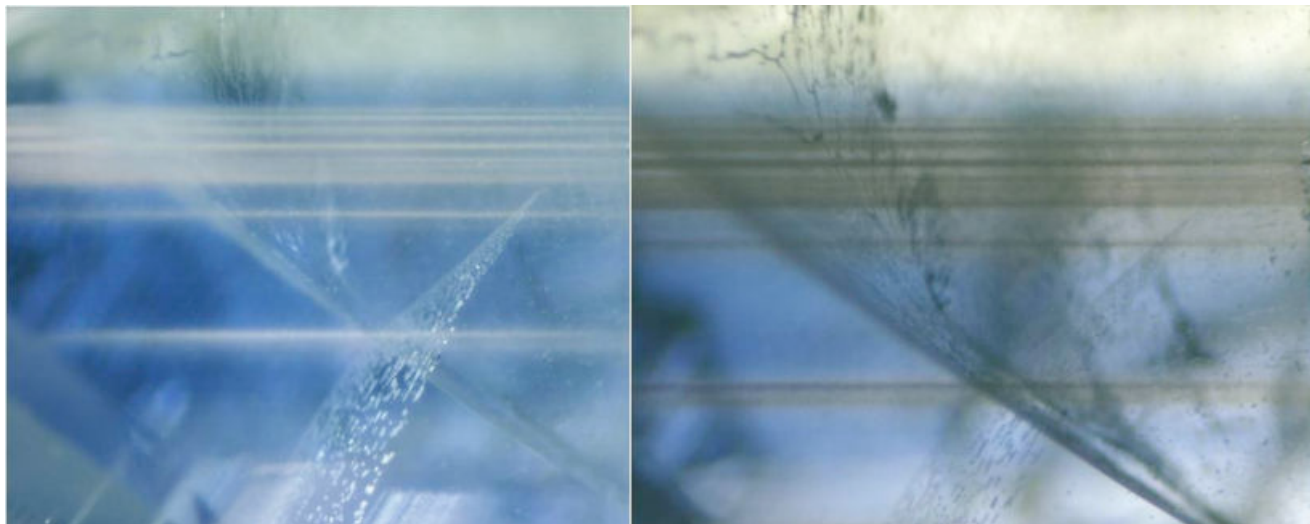
Properties – Sapphire's from Kataragama

Properties were described by Pannipitiye et al. (2012), Pardieu et al. (2012) and Zoysa & Zwaan (2012). The crystal fragments showed high transparency, although some were heavily included, and largely showed slightly violetish blue to blue, light to medium tones. R.I. values showed 1.760-1.763 to 1.769-1.771, with birefringence of 0.008-0.009. Specific gravities of 3.97 to 3.98 g/cm³ were measured (low values probably due to the presence of inclusions). The sapphires generally remained inert under long wave (LW) and short wave (SW) UV radiation.

Inclusions

Colour zoning is prominent. Parallel to the colour zoning, bands were present, consisting of tiny particles ('dust') and very short needles, oriented at angles of 120° in three directions. The bands appeared milky in dark field illumination but turned brownish in transmitted light (Figure 6, 7). Rutile needles could not only be found associated with these milky bands, but also occurred in nests. Long rutile needles were not common and when present, located in small

areas, in otherwise clean and transparent crystals. Furthermore, partially healed fissures and negative crystals were among the most prominent internal features. The voids present in the 'fingerprint' fissures appear dark in transmitted light and the ones that could be measured with micro-Raman contained CO₂. Negative crystals showed a high relief and many of them showed a clear hexagonal outline with barrel shapes, typical of corundum rough. The ones that were close enough to the surface to be measured with Raman micro spectroscopy contained CO₂ as well. Apart from the described rutile inclusions, the sapphires did not contain many other solid inclusions. Rounded and transparent plagioclase inclusions were present in two samples, but were hard to spot with a normal gemmological microscope, in between the many negative crystals.



Milky bands running parallel to colour zoning consisted of tiny particles and short needles. Figure 6 (left): in darkfield illumination; Figure 7 (right): in transmitted light.

Chemistry

26 spot chemical analyses were performed on 7 crystal fragments, resulting in similar compositions, with FeO content varying between 0.20 and 0.40 wt.%, with an average of 0.29 wt.%, very low to low TiO₂, below detection limit up to 0.03 wt.%, and Ga₂O₃ showing 0.02-0.03 wt.%. Additionally, in one sample, only 3 spot analyses on milky bands, showed elevated TiO₂, 0.05-0.06 wt.%, supporting the presence of rutile in the milky bands.

UV-VIS and FTIR spectroscopy

In the UV-visible region, a characteristic absorption spectrum of the measured samples (along the ordinary ray) showed a shoulder at 328 nm, a broad band with a maximum around 578 nm, caused by intervalence charge transfer (IVCT) taking place between Fe²⁺ and Ti⁴⁺, and bands with peaks around 375, 388 and 450 nm, related to absorptions due to Fe³⁺.

In the mid-infrared, all the specimens showed strong peaks at 2359 and 2339 cm⁻¹, indicating the presence of CO₂, a weak feature around 3310 cm⁻¹.

Also peaks near 3697, 3669, 3654 and 3622 cm⁻¹ occurred in 5 samples, indicating the presence of kaolinite-group minerals (Beran & Rossman, 2006). These samples contain dense, milky zones. It may show that the milky zones not only contain rutile, but include extremely fine grained hydrous minerals, such as kaolinite, as well (Zoya & Zwaan, 2012).

Discussion

The crystals studied were not only a pure blue, as stated by Pannipitiye et al. (2012), but also showed slightly violetish to violetish blue. Although not common, long rutile needles were found, which also contradicts the findings of Panni-

pitiye et al. (2012). Solid inclusions, other than rutile needles, were uncommon. Spinel, biotite (at the rim), zircon, and graphite inclusions, such as reported by Pardieu et al. (2012), were not found, but instead, small grains of plagioclase, and a rutile fibre in a fluid inclusion, were positively identified.

Although the inclusions of sapphires from Thammannawa may appear similar to those in light blue sapphires from another Sri Lankan primary deposit in Wellawaya, also found in granulitic gneiss, the chemistry is significantly different, with sapphire from Thammannawa showing moderate iron content, but sapphires from Wellawaya showing much lower FeO (0.07-0.15 wt.%) but substantially higher TiO₂ (0.03-0.12 wt.%; Zwaan and Zoysa, 2007).

The UV-VIS spectra showed a pattern that is similar to spectra of sapphires from metamorphic regions, in that there is no contribution of absorption related to Fe²⁺/Fe³⁺ IVCT. However, there is less dominance of the Fe²⁺/Ti⁴⁺ IVCT absorption, relative to the absorption peaks caused by Fe³⁺, than commonly seen in 'metamorphic' sapphires (compare, e.g., Smith, 2010, and Schwarz et al., 1996). This appears to be consistent with the low Ti contents in these sapphires.

References

- Beran A., Rossmann, G.R., 2006. OH in naturally occurring corundum. *European Journal of Mineralogy*, 18, 441-447
- Pannipitiye, G.R., Dharmaratne, H., Ranjith Premasiri, H.M., Dillimuni, D., 2012. Sapphires from Thammannawa, Kataragama area, Sri Lanka. *Gems & Gemology*, 48(2), 98-107.
- Pardieu, V., Dubinsky, E.V., Sangsawong, S., Chauviré, B., 2012. Sapphire rush near Kataragama, Sri Lanka (February-March 2012). *GIA News from Research*, May 2012, <http://www.giathai.net>.
- Schwarz, D., Petsch, E.J., Kanis, J., 1996. Sapphires from the Andranondambo region, Madagascar. *Gems & Gemology*, 32(2), 80-99.
- Smith, C.P., 2010. Inside sapphires. *Rapaport Diamond Report*, 33(6), 123-132.
- Zoysa, E.G and Rahuman S., 2012. Sapphire Rush in Kataragama, *InColor*, 19, 56-62.
- Zoysa, E. G., Zwaan, J.C., 2012. Gemmological update on the Sapphire Deposit from Tammannawa, Kataragama, Sri Lanka. *GIT Conference, Thailand*, 52-59.
- Zwaan, J.C. and Zoysa, E.G., 2007. New primary gem occurrences in Sri Lanka. *Zeitschrift der Deutschen Gemmologischen Gesellschaft*. 57 (1/2), 23-32.

Application of dielectric constant values on identifying ruby samples from Myanmar and Mozambique

Natthapong Monarumit¹, Thitinun Chantrakul¹, Pongsakorn Jantaratana², Pornsawat Wathanakul^{1,3*}

¹The Gem and Mineral Sciences Special Research Unit, Department of Earth Sciences, Faculty of Science, Kasetsart University, Bangkok 10900, Thailand

²Department of Physics, Faculty of Science, Kasetsart University, Bangkok 10900, Thailand

³The Gem and Jewelry Institute of Thailand, Bangkok, Thailand; *pwathanakul2@gmail.com

Introduction

Ruby, a variety of corundum (Al_2O_3) with Cr^{3+} impurity, is a precious and popular gemstone due to its properties such as beauty, rarity and durability. At present, ruby samples are obviously rare to collect in some localities. There are some potential sources to discover them; Mong Hsu and Mogok (Myanmar), Luc Yen (Vietnam), Montepuez (Mozambique) (Hughes, 1997; Sutherland et al., 1998). The ruby samples from different sources show various characteristics that can be distinguished by microscope, chemical analysis and spectroscopic instruments (e.g., Rossman, 1988; Smith, 1995). Moreover, advanced techniques in terms of physical chemistry have been tried to apply in gemstone research; for example, x-ray absorption spectroscopy (XAS), x-ray diffraction (XRD), and photoluminescence (PL). Nevertheless, this research will focus on the dielectric property of gem-material, especially applied on ruby samples from different geological sources.

Materials and Methods

Rough ruby samples from Mong Hsu, Myanmar and Montepuez, Mozambique were selected in this study, ten samples from each locality (Figure 1). Samples were registered and basic gemstone properties were measured, such as specific gravity (SG) and refractive indices (RI). Then dielectric constant values were measured.



Figure 1. Rough ruby samples from (a) Myanmar and (b) Mozambique; scale bar = 1 cm

The dielectric insulating materials between two plates of capacitors can be divided into two types, i.e. polar dielectrics and non-polar dielectrics. In this case, we have concentrated on non-polar dielectrics which are caused by a non-permanent electric dipole moment.

Electric dipole moments can be induced by placing the samples in an externally applied electric field. The space

between the plates is filled with dielectric material, the capacitance (C) of a capacitor calculates by the equation below.

$$C = \frac{\kappa \epsilon_0 A}{d}$$

Where κ is the dielectric constant, ϵ_0 is the vacuum permittivity, A is the area of the electrode and d is the distance between electrodes (assumed as sample thickness). In this study, the dielectric constant was measured 3 times for each sample by a precision LCR meter (HP 4284A) equipped with a dielectric test fixture (HP 16541B) using 1 MHz frequency and 1 V signal level (Figure 2).



Figure 2. (left) A precision LCR meter model HP 4284 and (right) a dielectric test fixture model HP 16541B

Results and Discussion

The dielectric constant values of ruby samples from Myanmar (MS) and Mozambique (MZ) are reported in table 1. Figure 3 shows the variation of K average in each sample. Dielectric constants of ruby samples from Myanmar are mostly higher than the Mozambique ones. The average K values measured for Myanmar and Mozambique rubies are significantly different; approximately higher than 20, and on average lower than 12, respectively.

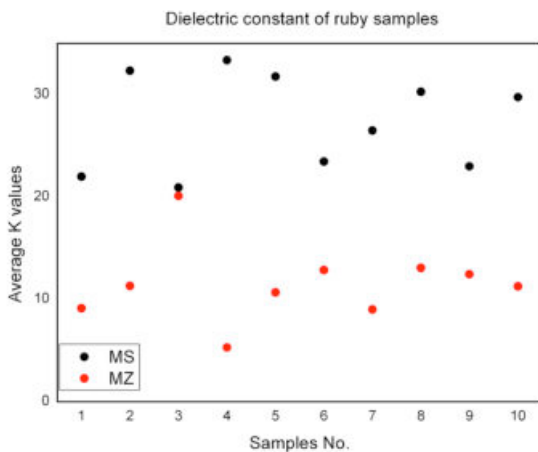


Figure 3. Comparison of dielectric constant values between Myanmar (MS) and Mozambique (MZ) ruby samples.

Samples	K 1	K 2	K 3	Average K values
MS01	21.946	22.035	21.999	21.993 ±0.04
MS02	32.361	32.295	32.314	32.323 ±0.03
MS03	20.920	20.921	20.901	20.914 ±0.01
MS04	33.362	33.383	33.320	33.355 ±0.03
MS05	31.752	31.708	31.785	31.748 ±0.04
MS06	23.453	23.484	23.416	23.451 ±0.03
MS07	26.468	26.475	26.494	26.479 ±0.01
MS08	30.232	30.264	30.275	30.257 ±0.02
MS09	22.931	22.985	23.036	22.984 ±0.05
MS10	29.716	29.775	29.721	29.737 ±0.03
Average MS				27.124
MZ01	9.229	9.071	9.064	9.121 ±0.09
MZ02	11.443	11.372	11.102	11.306 ±0.18
MZ03	20.212	20.118	19.930	20.087 ±0.14
MZ04	5.333	5.225	5.300	5.286 ±0.06
MZ05	10.545	10.756	10.698	10.666 ±0.11
MZ06	12.763	12.779	13.007	12.850 ±0.14
MZ07	8.963	9.075	8.994	9.011 ±0.06
MZ08	13.024	12.986	13.168	13.059 ±0.10
MZ09	12.444	12.520	12.377	12.447 ±0.07
MZ10	11.340	11.230	11.210	11.260 ±0.07
Average MZ				11.509

Table 1: The dielectric constant values of unheated ruby samples collected from Myanmar (MS) and Mozambique (MZ) localities

Conclusion

The dielectric constant values can be applied to specify the ruby samples from the different sources chosen (Myanmar vs Mozambique). Therefore this non-destructive technique offers potential for testing rubies from other localities (e.g., Vietnam), and for gemstone identification and mineral science research in general.

References

- Hughes, R.W., 1997. Ruby & Sapphire. RWH Publishing, USA, 511 p.
- Rossmann, G.R., 1988. Optical Spectroscopy. In Spectroscopic Methods in Mineralogy and Geology: Reviews in Mineralogy, 18, 207-254.
- Smith, C.P., 1995. A Contribution of Understanding the Infrared Spectra of Rubies from Mong Hsu, Myanmar. Journal of Gemmology, 24(5), 321-335.
- Sutherland, F.L., Hoskin, W.O., Fanning, C.M., Coenraads, R.R., 1998. Model of Corundum Origin from Alkali Basaltic Terrain: Reappraisal. Contribution of Mineralogy and Petrology, 133, 356-372.

Acknowledgements

The authors appreciate the Department of Earth Sciences, the Department of Physics, Faculty of Science, Kasetsart University and the Gem and Jewelry Institute of Thailand (Public Organization) for supporting research facilities and funding.

Gemstones from Luc Yen pegmatite in Vietnam

Nguy Tuyet Nhung^{1,2}, Le Thi Thu Huong², Nguyen Thi Le Quyen¹, Tran Thi Duyen², Dinh Thi Hue², Tran Thi Lan²

¹ Gemmological Center, Vietnam Gemstone Association, Hanoi. Email: nguytuyetnhung@yahoo.com

² Faculty of Geology, University of Science, Vietnam National University, Hanoi

Introduction

LucYen is a district of Yen Bai province located in the North of Vietnam, approximately 270 km away from Hanoi. Since ancient times people have found gems in this area, there was gemstone trade and exchange. However, the exploitation and trade in gemstones had been stopped for a long time. Gem mining started again only in 1987 and since then up to now many gem occurrences were discovered and different kinds of gemstones such as ruby, sapphire, spinel, tourmaline, humite, quartz, pargasite, amazonite, lazurite and tectite have been found there. Gemstones may be gathered from secondary deposits in Quaternary sediments or from primary deposits in metamorphic rocks as marble, gneiss, migmatite and pegmatite. This research presents the characteristics of some gemstones found in pegmatite.



Figures 1a and 1b: Tourmaline from Luc Yen pegmatite.



Figure 3. Amazonite from Luc Yen pegmatite.

Geology

The study area is located on the eastern side of the Chay river belonging to the Lo Gam tectonic zone which consists of moderately to highly metamorphosed (amphibolite-facies) schists, gneisses and marbles. These metamorphic rocks are intruded by many pegmatite bodies, some of which discovered to bear gemstones. Gem-bearing pegmatite bodies are granitic with main minerals including quartz, feldspars, mica scattering in Luc Yen from the north in the

Khai Trung to the south in the Minh Tien and Tan Lap communes. The gemstones include tourmaline, green feldspar and lepidolite and quartz. The age of this pegmatite formation is about 30 Ma.

Materials and methods

Many pegmatite samples which consist of tourmaline, feldspar, mica with different colours were collected in several fieldworks carried out during a period from 2004 to 2012. Some other samples were bought from local people. Different methods including gemmological, mineralogical, LA- ICP-MS, EPMA, X- ray powder diffraction were implemented to study in different surveys at the Gemmological Center of the Vietnam Gemstone Association, the Faculty of Geology of Hanoi University of Science, the Institute of Geology in the Institute of Science & Technology of Vietnam and the Centre of Gemstone Research, University of Mainz, Germany.

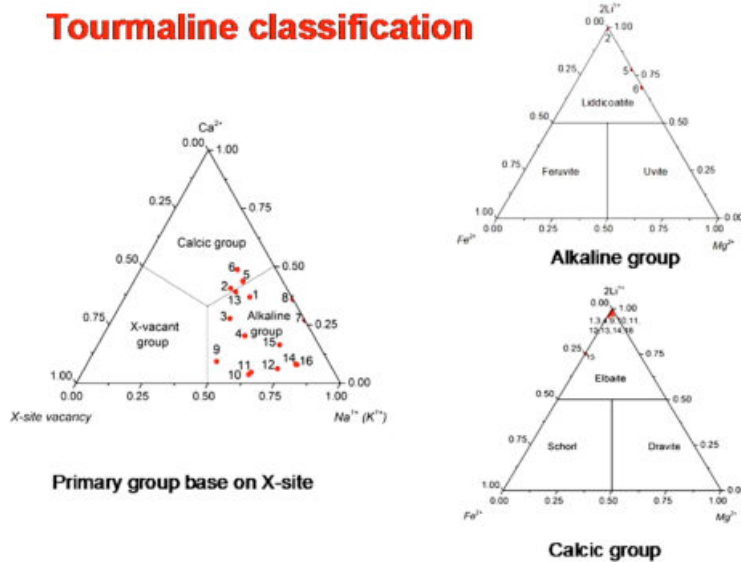


Figure 2. Compositional plot for 16 samples from Luc Yen pegmatite.

Results and discussion

Tourmaline.

Luc Yen tourmaline displays plentiful colour which varies from nearly colourless to green, yellow, orange, brown, pink, greyish blue and black. Colour zoning is fairly common and may be parallel to the prism faces or the basal plane. The crystal length may reach ten centimeters or more. The transparency is rather low due to inclusions and fracture appearances. The result of 18 chemical analyses for 13 tourmaline samples with variety colour revealed that:

- All samples contain Li ranging from 0.004 to 5.2 wt% Li_2O with lowest values in greyish blue and black samples (< 0.01 wt%)
- The relative contents of Na and Ca show that most samples have ratio $\text{Na}/\text{Ca} > 1$ and belong to elbaite, while the rest belongs to liddicoatite (see Figure 1b)
- Two samples are rich in Mg (11.83 and 13.75 wt% MgO). The X-ray powder diffraction analysis identified them as dravite while chemical analysis revealed the ratio $\text{Na}/\text{Ca} < 1$, so these samples belong to liddicoatite and could be named magnesium liddicoatite
- The colour of tourmaline depends on transition metal content. The orange samples are rich in Mn (6.4-6.5 wt% MnO), the brown and black samples are rich in Fe (2.0 to 5.8 wt% FeO) and the green samples are rich in Cr or Fe.

Green feldspar.

Green feldspar was found in the Minh Tien pegmatite with big sizes up to tens of centimeters in vivid green to grey green or bluish green colours. The transparency is low in most samples. Pb causes the green colour of feldspar (Thuyet

et al., 2010). The X- ray powder diffraction analyses determine that some samples are orthoclase similar to the results from other works (Ponahlo et al., 2001, Laurs et al., 2005, Le et al., 2012). Besides that, some other samples are intermediate microcline and could be named amazonite after Thuyet et al. (2010).

Lepidolite.

Mica in Luc Yen pegmatite may display brown, white and violet colour. The crystal plate may reach one centimeter or more. The X- ray powder diffraction analyses indicate that white and violet mica are lepidolite, while brown mica could be zinnwaldite. However, the mica refractive index (Table 1) reveals all of them belong to lepidolite, the brown one may be rich in Fe. The chemical analyses (Table 2) show the high Li contents of 3.79, 6.0, 9.0 wt% Li₂O according to violet, white and brown samples respectively. Besides that, brown lepidolite is richer in Fe, Mg, Ti and Rb than the others whereas violet one is richer in Cs and white one is richer in Ta.

Luc Yen pegmatite containing minerals rich in Li, Cs and Ta such as Li tourmaline and lepidolite may be classified to a Rare- Element pegmatite and LCT (Lithium, Cesium, Tantalum enrichment) type.



Figure 4. Lepidolite from Luc Yen pegmatite.

Table 1. Refractive index of different coloured lepidolites

colour	Nm	Ng
white	1.547	1.549
violet	1.548	1.550
brown	1.560	1.562

Table 2. Chemical composition (wt.%) of different coloured lepidolites

Colour	Li	Na	Mg	K	Ca	Ti	V
white	6.006	1.587	0.091	0.101	0.143	0.012	0.000
violet	5.747	nd	0.061	0.093	0.127	0.014	0.000
brown	3.972	0.072	0.818	nd	0.101	0.385	0.001
Colour	Cr	Mn	Fe	Rb	Cs	Ta	Pb
white	0.002	0.011	0.237	0.001	0.000	0.015	0.002
violet	0.001	0.102	0.138	0.000	0.372	0.011	0.002
brown	0.003	0.012	9.288	0.583	0.079	0.007	0.002

Current mining and using

All gem-bearing pegmatite bodies in Luc Yen were discovered by local people and spontaneously and perfunctorily exploited without Government permission from 2000 up to now. Tourmalines gathered from pegmatites also from placers were polished and carved. Green feldspar was polished in a small amount. Until now lepidolite is almost not being used. However, many gem-bearing pegmatite blocks with the size reaching 1 to 2 m³ or bigger were mined for display purpose.

Conclusion

Luc Yen pegmatite contains tourmaline, green feldspar, lepidolite which could be used for jewellery, ornament or collection and display purpose.

The widely distribution of pegmatite bodies and the regular existence of tourmaline together with other gemstones such as ruby, sapphire, spinel in many placers, eluvials in Luc Yen indicate a significant gem potential of that pegmatite type in the area.

References

- Henry D.J., Novak M., Hawthorne F.C., Ertl A., Dutrow B.L., Uher P., Pezzotta F., 2011. Nomenclature of the tourmaline-supergroup mineral. *Amer.Miner*, 96, 895-913.
- Le T.T.H, Hager T., Hofmeister W., Hauzenberger C., Schwarz D., Pham V.L, Wehmeister U., Nguyen N. K., Nguy T. N., 2012. Gemstones from Vietnam: An Update. *Gem & Gemology*, 48(3), 158-176.
- Nguy T.N., Nguyen T.M.T., Vu N.A., Nguyen V.N., 2005. Gem tourmaline in Luc Yen rare metal pegmatite. *Proceeding of The International Workshop on: Gem-Materials and Modern Analytical Methods*, Hanoi, 2005, 135-145.
- Nguy T.N., Nguyen T.L.Q., Nguyen T.M.T, 2010. Mineral assemblage of rubellite- bearing pegmatite from Khai Trung, Luc Yen, Yen Bai. *Proceeding of The International Workshop on: Provenance and Properties of Gems and Geo- Material*, Hanoi, 2010, 34-39.
- Nguy T.N., Nguyen T.M.T., Hofmeister W., Hager T., LeT.T.H., 2012. Gem tourmaline from Luc Yen: Species determination on the basis of the chemical composition using Clastour software. *GIT 2012 Conference*, Bangkok, Thailand.
- Nguyen T.M.T., Nguy T.N., Hofmeister W., Hager T., 2010. Amazonite from Luc Yen mining, Yen Bai, Vietnam. *Proceeding of The International Workshop on: Provenance and Properties of Gems and Geo- Material*, Hanoi, 2010, 40-51.
- Yavuz F., Gultekin A.H., Karakaya M.C., 2002. CLASTOUR: a computer program for classification of minerals of the tourmaline group. *Computers & Geosciences* 28,1017-1036.
- Wilson W.E., 2007. Tourmaline from the Minh Tien pegmatite, Luc Yen Mining District, Yenbai Province, Vietnam. *Mineralogical Record*, 38(6), 453-457.

Acknowledgements

The authors thank Prof. Wolfgang Hofmeister and Tobias Hager for support on LA-ICP.MS analyses in the Institute of Geology at Johannes Gutenberg University, Mainz, Germany. The research is part of a project supported by the Vietnam National Foundation for Science and Technology Development (NAFOSTED, project 105.02-2011.01).

The alteration of structural OH group in FTIR spectra on ruby samples from Mong Hsu, Myanmar and Montepuez, Mozambique

Aumaparn Phlayrahan¹, Natthapong Monarumit¹, Luksika Loetwanitsakul¹, Somruedee Satitkune¹, Pornsawat Wathanakul^{1,2*}

¹Department of Earth Sciences, Faculty of Science, Kasetsart University, Bangkok 10900, Thailand

²The Gem and Jewelry Institute of Thailand, Bangkok, Thailand; *pwathanakul2@gmail.com

Introduction

Ruby is one of the most popular gemstones in the world market. However, their beautiful colour and/or clarity are commonly enhanced by heat.

FTIR spectra provide information about chemical composition and crystal structure of the samples. The structural OH group is the most significant region in FTIR spectra of heated ruby, especially from MongHsu origin (Smith, 1995). In addition, this region likely indicates the relationship with internal features and the temperature of heating. There are many studies that used the peak in this region to confirm heat-treatment of rubies (e.g., Volynets et al., 1972, 1974; Beran and Rossman 2006; Wathanakul et al., 2013). Consequently, this research has been focused on the alteration of the structural OH group, related to internal features of ruby samples from MongHsu, Myanmar and Montepuez, Mozambique.

Materials and Methods

Ruby samples with polished faces perpendicular to the c axis, from MongHsu, Myanmar and Montepuez, Mozambique, were collected for the experiments. The samples were registered and the specific gravity (SG) and refractive index (RI) were measured. The MongHsu ruby samples were heated in oxidizing atmosphere at 800, 1200 and 1650 °C, while intermediate temperature steps of 1000 and 1450 °C were set for ruby samples from Montepuez.



Figure 1. The polished ruby samples from Mong Hsu, Myanmar (left) and Montepuez, Mozambique (right)

Internal features of the collected samples were recorded with a Nikon dark field illuminator gemological microscope. All FTIR spectra (before and after heat treatment) were acquired by a NEXUS 470 FTIR spectrometer in transmission mode within the range of 4000-400 cm^{-1} . The parameters were employed with a spectral resolution of 4 cm^{-1} and 128 scans.

Results and Discussion

The internal features of Mong Hsu and Montepuez ruby samples (before and after the heating experiment) are shown in Table 1.

Type of inclusion	Ruby samples from MongHsu, Myanmar				Ruby samples from Montepuez, Mozambique			
	Before heating	After heating (°C)			Before heating	After heating (°C)		
		800	1200	1650		800	1200	1650
blue zones and blue core	xxx	xx	x	-	-	-	-	-
hydrous aluminum phase (i.e. diaspore, boehmite and gibbsite)	xxx	xx	x	-	-	-	-	-
fluid inclusion	xx	x	-	-	xx	x	-	-
crystal inclusion	x	x	-	-	xxx	xx	x	-
negative crystal	x	-	-	-	xx	x	-	-

Table 1: Summary of inclusion features in ruby samples from MongHsu, Myanmar and Montepuez, Mozambique. Note: - = absent, x=weak, xx = moderate, xxx =strong

The ruby samples from MongHsu obviously show blue zones and blue cores, as well as inclusions of hydrous aluminium phases (i.e. boehmite, diaspore and gibbsite), whereas these inclusions were absent in ruby samples from Montepuez, Mozambique. These inclusions were slightly decreased after heating and disappeared at high temperatures. Furthermore, the other inclusions found in ruby samples are fluid inclusions, crystal inclusions and negative crystals. These inclusions were not significantly different between the two origins.

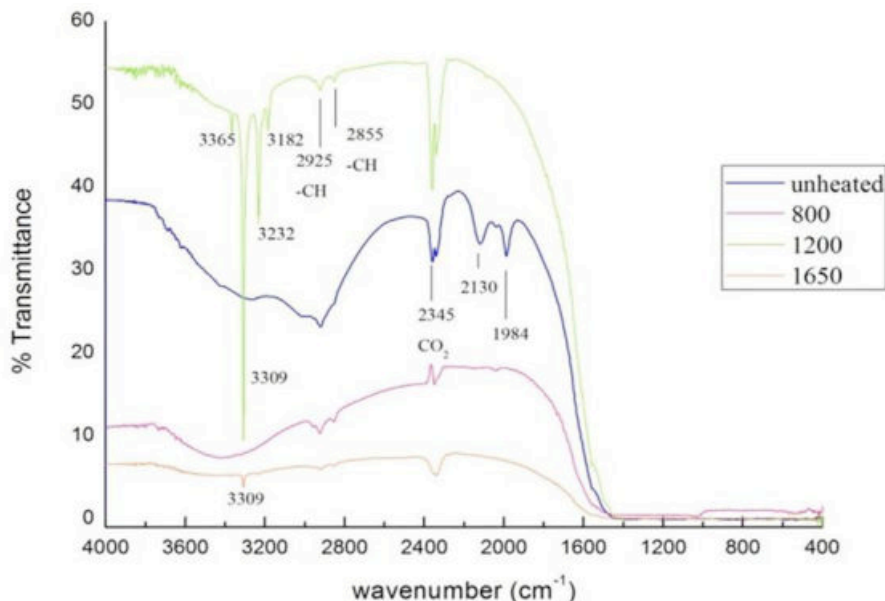


Figure 2. FTIR spectra of ruby samples from Mong Hsu, Myanmar at different heating temperatures; unheated (blue line), 800 °C (pink line), 1200 °C (green line) and 1650 °C (orange line).

The FTIR spectra of unheated ruby samples from MongHsu, Myanmar shown in Figure 2 indicated the absorption peak of a hydrous aluminum phase (i.e. boehmite, and diaspore at 1984 and 2130 cm^{-1} ; Smith, 1995). These peaks tend to decrease when heating at higher temperatures. Simultaneously, a number of peaks were collected in the 3100-3400 cm^{-1} region in heated samples, which are attributed to the structural OH group. Noteworthy, these peaks are obviously increasing in intensity while the peaks of hydrous aluminum phases (1984 and 2130 cm^{-1}) are slightly disappearing, as a result of dehydration of the hydrous aluminum phase. This process produced hydrogen atoms in the host structure. Then, the hydrogen atom formed a structural OH group, bonding with a certain trace element in the corundum structure, i.e., Ti, Fe, V, Cr, Mg, etc. that is shown in the 3100-3400 cm^{-1} absorption region (Beran and Rossman, 2006).

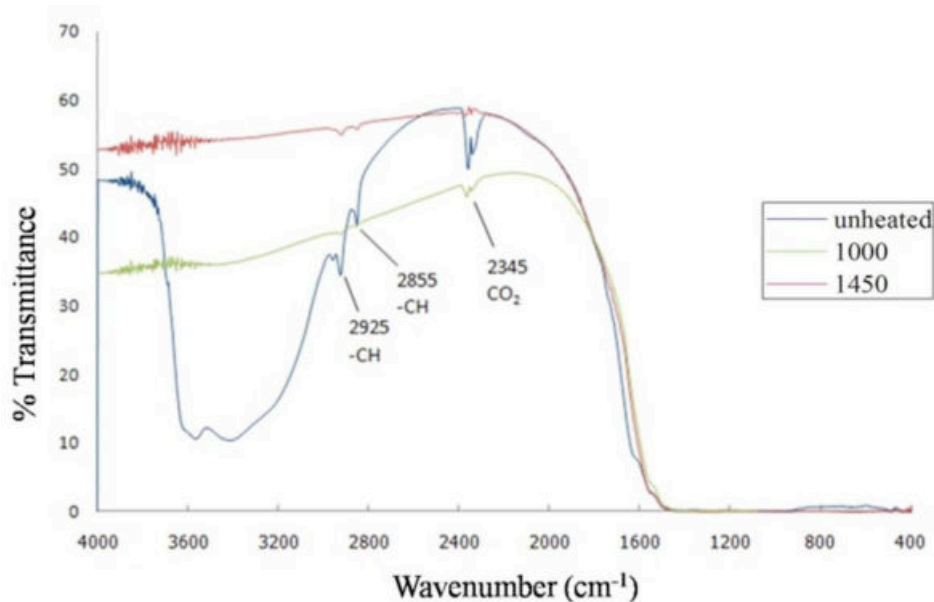


Figure 3. FTIR spectra of ruby samples from Montepuez, Mozambique at different heating temperatures; unheated (blue line), 1000 °C (green line) and 1450 °C (pink line); E//c.

FTIR spectra of unheated and heated ruby samples from Montepuez, Mozambique are compared in Figure 3. The spectrum of unheated samples shows the broad absorption at 3200-3600 cm^{-1} , corresponding to molecular water absorption. However, these peaks are diminished at 1000 °C and disappeared at 1450 °C. The absorption peaks detected at 2925 and 2855 cm^{-1} probably indicate the presence of contamination of -CH from oil, used during polishing, and/or the composition in the structure (Beran and Rossman, 2006). As a consequence, the heated samples did not show the absorption peak at approximately 3100-3400 cm^{-1} of structural OH; because the H-bond of water molecules was broken in the heating process and decayed at high temperature. Besides, after dissociation, the H^+ and OH^- ions disappeared the samples of this source. Accordingly, either the H_2O or structural OH cannot be formed in the structure of heated samples. Also according to the internal features, the samples from Mozambique did not contain the hydrous aluminum phases as well.

Conclusion

The comparison of FTIR spectra between ruby samples from MongHsu, Myanmar and Montepuez, Mozambique, revealed differences in the 3100-3400 cm^{-1} range, where peaks related to a structural OH group can be recorded. Alterations of the peaks in this region during heating likely coincide with the dehydration of hydrous aluminum phase inclusions, in the presence of certain trace elements in the structure of the samples.

References

Beran, A. and Rossman, R.G., 2006. OH in naturally occurring corundum. *European Journal of Mineralogy*. 18(4), 441-447.

Smith, C.P., 1995. A Contribution of Understanding the Infrared Spectra of Rubies from Mong Hsu, Myanmar. *Journal of Gemmology*, 24(5), 321-335.

Volynets, F.K., Vorob'e, V.G. and Sidorova, E.A., 1972. Infrared absorption bands in corundum crystals. *Journal of Applied Spectroscopy*. 10, 665-667. Translate from *Zh. Prikl. Spekr.* 1969, 10(6), 981-984.

Volynets, F.K., Sidorova, E.A., and Stsepuro., N.A., 1974. OH group in corundum crystals which were grown with the Verneille technique. *Journal of Applied Spectroscopy*. 17, 1626-1628. Translate from *Zh. Prikl. Spekr.* 1972, 17(6), 1088-1091.

Wathanakul, P., Monarumit, N., Leelawatanasuk, T., Ingavanija, S., Sriprasert, B., Atichat, W., and Hauzenberger, C. 2013. Infrared spectra for indicating heating extents of ruby samples from Mong Hsu, Myanmar, and Luc Yen, Vietnam. (submitted).

Acknowledgements

The authors gratefully acknowledge supports from Department of Earth Sciences, Faculty of Science, Kasetsart University, the Gem and Jewelry Institute of Thailand (GIT) for instrumental supports and the Graduate School Kasetsart University for the research fund.

Heat treatment of zircon samples from Kanchanaburi, Thailand and Ratanakiri, Cambodia

Somruedee Satitkune¹, Bhuwadol Wanthanachaisaeng², Krit Won-in¹, Wiwat Wongkokau³, Pongsakorn Chantararat³, Thanong Leelawattanasuk⁴, Pornsawat Wathanakul^{4*}

¹Department of Earth Sciences, Faculty of Science, Kasetsart University, Bangkok 10900, Thailand

²Gems Enhancement research unit, Faculty of Gems, Burapha University, Chanthaburi, Thailand

³Department of Physics, Faculty of Science, Kasetsart University, Bangkok, Thailand

⁴The Gem and Jewelry Institute of Thailand, Bangkok, Thailand; *pwathanakul2@gmail.com

Introduction

Zircon is a valuable and beautiful gemstone. The favourite colour of zircon in the gem market is blue, which is commonly obtained by heating the reddish brown variety. Heat treatment of zircon is the most conventional method to improve their colour. The famous locality of heated blue zircon is Ratanakiri Province, North Eastern Cambodia. Nowadays, the amount of gem quality rough zircon is decreasing because mining areas are mainly replaced by rubber plantations. Then, zircon samples from another source have been investigated for heat treatment. Kanchanaburi Province, Thailand is an important source of blue sapphire; besides, zircon has also been found in sapphire mining areas. Zircon samples from Kanchanaburi are also reddish brown in colour, similar to those of from Ratanakiri, but are smaller in size. The aim of this study is to examine and compare the heat treatment results of zircon samples from Ratanakiri and Kanchanaburi.

Materials and Methods

Some reddish brown zircon grains from Kanchanaburi, Thailand and Ratanakiri, Cambodia, were sampled for heat treatment experiments. They were polished as flat surfaces before further investigations. The physical properties and spectroscopic characteristics (UV-Vis-NIR and FTIR) of the samples were observed, measured and recorded before and after each step of the heating experiment. Heating experiments were carried out in a reducing atmosphere. For each experiment, three maximum temperatures, 800 °C, 900 °C and 1000 °C, were set for one hour soaking time.

Results and Discussion

After heating at 800 °C, zircon samples from both localities lost their reddish brown colour. The samples from Kanchanaburi changed from reddish brown to light yellow and near colourless. The blue shade in the Cambodia samples was intensified after heating at 900 °C and 1000 °C, respectively (Figure 1).

Most reddish brown zircon samples from Ratanakiri deposit have a potential to reach the best colour when thermal enhancement is applied under the proper conditions. Dark reddish brown samples appear to become dark blue after heat treatment at 1000°C.

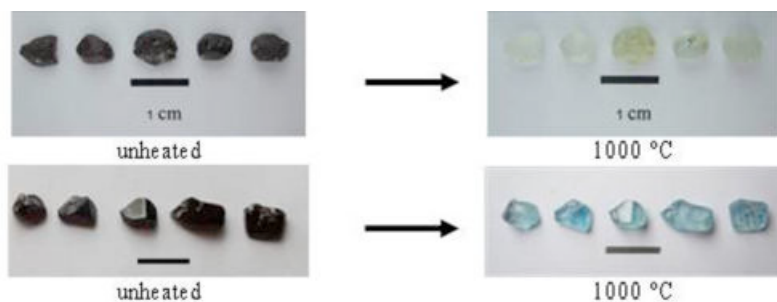


Figure 1. Zircon samples from Kanchanaburi, Thailand (top) before and after heat treatment in a reducing atmosphere at 1000 °C, compared to those of from Ratanakiri, Cambodia (bottom).

In this study, the FTIR spectra of zircon samples from Kanchanaburi and Ratanakiri are unique and clearly applied to separate unheated samples from the heated ones. The appearances of absorption peaks at 4072 and 4262 cm^{-1} , which are due to OH-stretching, are found only in unheated samples. After heating these peak positions disappeared, while an absorption peak at 4833 cm^{-1} became visible (Zhang et al., 2003).

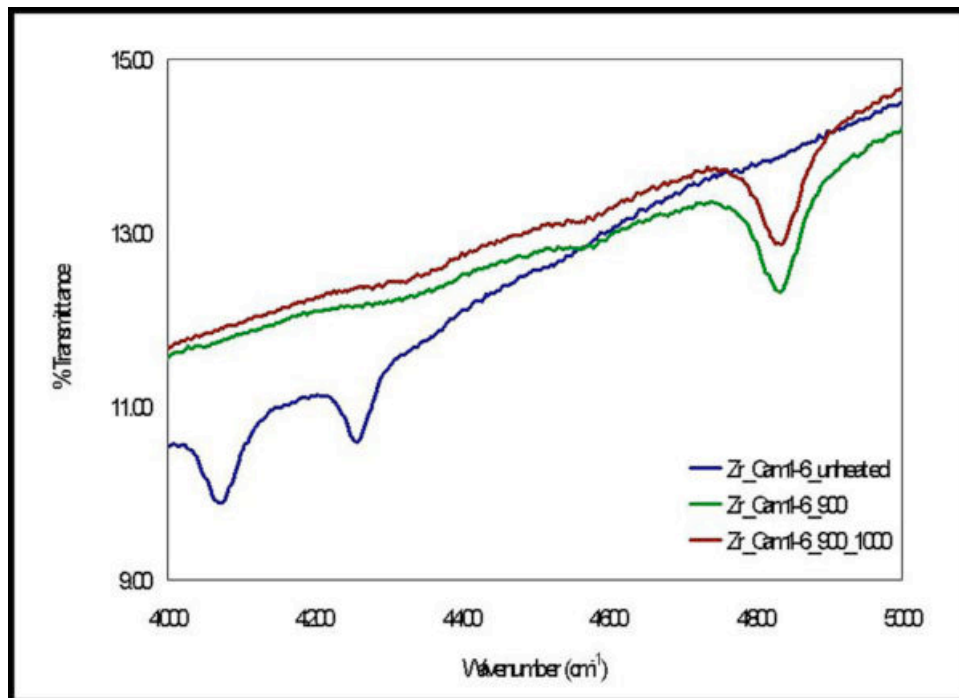


Figure 2. FTIR results of zircon samples before and after heat treatment.

The UV-Vis-NIR absorption spectra (Figure 3) show that the change of colour after heat treatment is mainly caused by a change of valence state of uranium. The transition of U^{5+} to U^{4+} at 653 nm (Zhang et al., 2003) occurred during heating and this phenomenon produced the blue colour in the samples from Ratanakiri. In contrast, this absorption was not found in the heated samples from Kanchanaburi, which showed the near colourless and light yellow colour.

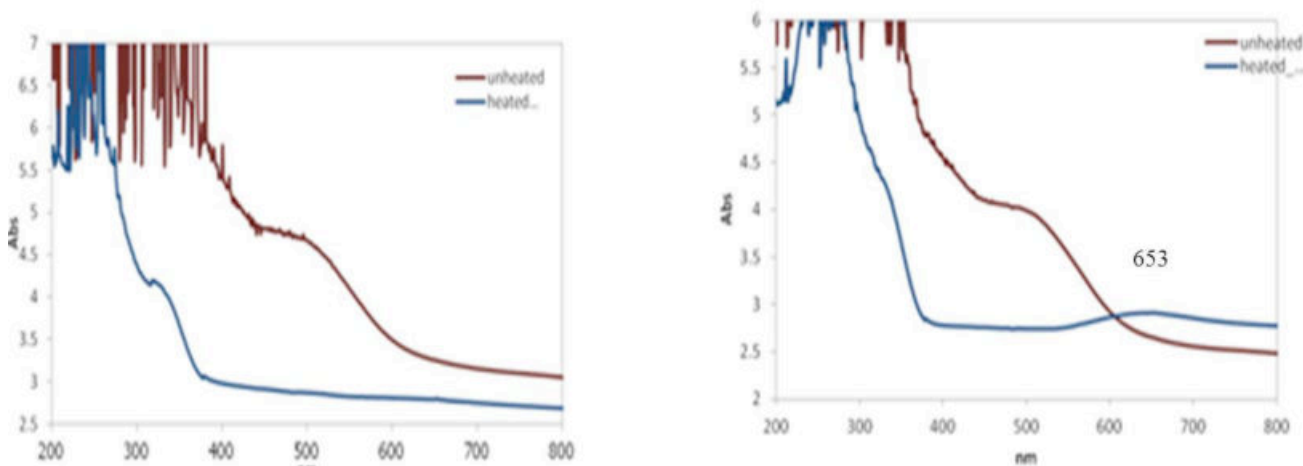


Figure 3. UV-Vis-NIR spectra of zircon samples from Kanchanaburi, Thailand (left) and Ratanakiri, Cambodia (right). Blue spectra: unheated samples; Purple spectra: heated samples.

Conclusion

Results of this study clearly indicate that the zircon samples from Ratanakiri, Cambodia have a potential for thermal enhancement. They can be changed from reddish brown to blue. The suitable condition for heat treatment is 1 hour soaking time at 1000 °C, in a reducing atmosphere. However, the tested samples from Kanchanaburi deposit, Thailand, turned colourless after heating. The blue colour is obviously caused by the absorption of U^{4+} at 653 nm in UV-Vis-NIR spectra. FTIR spectra can be used to distinguish unheated from heated samples.

References

Zhang, M., Salje, E. K. H. and Ewing, R. C., 2003. Oxidation state of uranium in metamict and annealed zircon: near-infrared spectroscopic quantitative analysis. *Journal of Physics: Condensed Matter*, 15, 3445-3470.

Acknowledgements

The authors would like to thank the National Research Council of Thailand (NRCT) and Faculty of Science, Kasetsart University, for granting the research project. Heating and spectroscopic analysis facilities at Department of Earth Sciences, Faculty of Science, Kasetsart University and The Gem and Jewelry Institute of Thailand (Public Organization) are gratefully acknowledged.

Effect of electron irradiation on diamond surfaces using Atomic Force Microscope

Chanikarn Sanguanphun,¹ Natthapong Monarumit,¹ Thanapong Lhuaamporn,² Wiwat Wongkokua,³ Somruedee Satitkune¹, Pornsawat Wathanakul^{1,2*}

¹The Gems and Mineral Sciences Special Research Unit, Department of Earth Science, Faculty of Science, Kasetsart University, Bangkok, Thailand

²The Gem and Jewelry Institute of Thailand (GIT), Bangkok, Thailand

³Department of Physics, Faculty of Science, Kasetsart University, Bangkok, Thailand; *pwathanakul2@gmail.com

Introduction

Diamond is one of the valuable and popular gemstones for many centuries. Colorless to pale yellow stones are classified as a colorless diamond group. According to popularity, this group is the most desirable in the gem market. Red, blue, green, brown, black, pink, orange and strong yellow diamonds are classified as fancy color diamonds. Because of its rarity, the fancy diamond is more expensive than the colorless ones. Generally, natural diamonds are obviously yellow to brown in low quality. Irradiation is one of the techniques to improve their color quality and value. Electron irradiation is the method to produce a green, dark green and bluish green color, depending on the type of diamond, duration and dose of irradiation (Campbell et al., 2002 and Collins, 2007). The Atomic Force Microscope (AFM) is the technique applied to distinguish natural and irradiated diamond considering with the morphology in nanometer scale (Giessibl, 2003).

Materials and Methods

Seven untreated diamond samples of the brilliant cut (Figure 1) were selected from an entrepreneur. The samples were analyzed by AFM. The sample preparation included meticulously clean and dry. The samples were then fixed on a glass slide by placing the table surface on the top. The AFM model is MFP-3D-BIO placed at the Scientific Equipment Center, Faculty of Science, Kasetsart University, Bangkok. The sample surfaces were measured in micro-nanometer scale by the tapping mode AFM; the surface features have been measured and recorded. The diamond samples were then irradiated with electrons by an electron accelerator at the Nuclear Research Center, Ongkarak, Nakhon Nayok Province, Thailand. After the irradiation process without annealing, the irradiated samples were repeatedly studied on their surface features by AFM. For the final step, the images of the diamond surfaces were recorded and compared before and after irradiation.



Figure 1. Seven brilliant cut untreated diamond samples used for the experiment (Scale = 5 mm).

Results and Discussion

In the electron irradiation process without annealing, the dose of electrons increased to 30,000 KGy with 62.5 hrs soaking time. The diamonds were changed to green and bluish green (Figure 2). Their colors are still stable and consistent.

According to Collins (2007), the colors of irradiated diamonds can be become to blue, bluish green, green, and dark green. After irradiation and annealing at 600-900°C, it would exhibit possible varieties of colors from strong yellow to brownish orange, greenish yellow, brown, pink and purple based on types of diamond.

The study of diamond surface features before and after electron irradiation was considered in the 3D AFM topographic images which appear in parallel long stripes or in steps that were caused by rearranging of the atomic steps (Figure 3 and 4). Calculation of the values of step height and Root Mean Square (RMS) roughness indicated that the electron irradiated diamonds have shown the average step height and RMS roughness higher than those in the untreated ones (Figure 5).



Figure 2. Seven electron irradiated diamond samples (Scale = 5 mm).

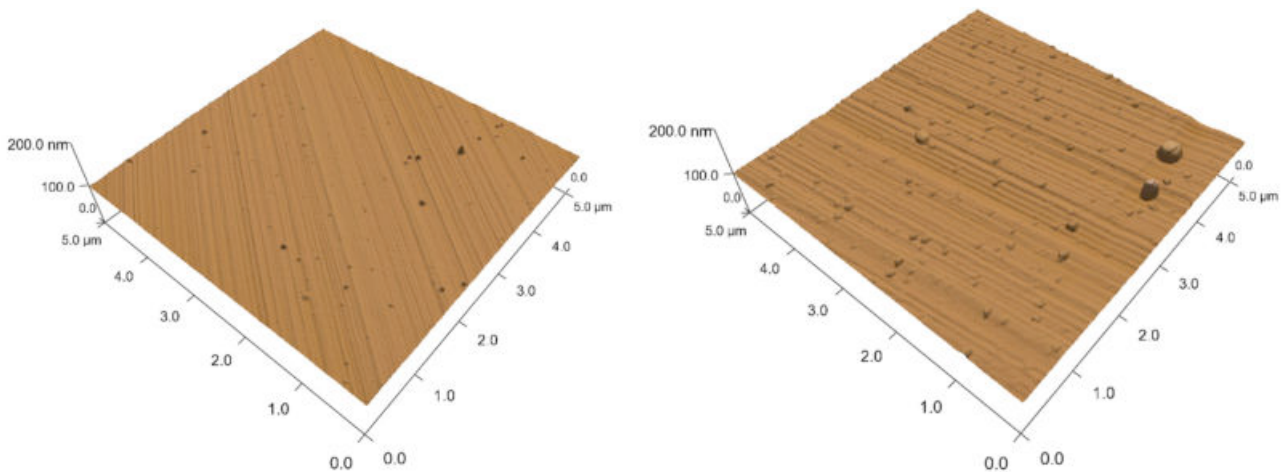


Figure 3 (left): The 3D image surface features of an untreated diamond sample. Figure 4 (right): The 3D image surface feature of an electron irradiated diamond sample.

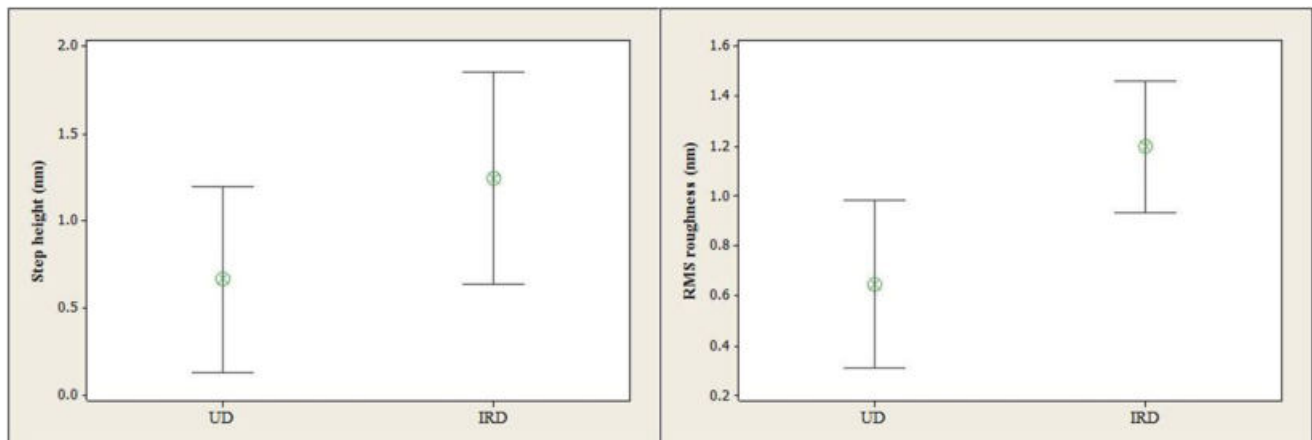


Figure 5. The average step height and RMS roughness of seven untreated diamond samples (UD) compared with those of the electron irradiated ones (IRD).

Conclusion

It can be concluded that the result of electron irradiation at 30,000 KGy dose without annealing on the diamond samples is the change of their colours to green and bluish green. Spot damages were possibly observed in the treated samples. AFM images show that the step height and RMS roughness of electron irradiated diamonds obviously increased compared to the untreated ones.

References

Campbell, B., Choudhury, W., Mainwood, A., Newton, M., Davies G., 2002. Lattice Damage caused by the Irradiation of Diamond. *Nuclear Instruments and Methods in Physics Research. A*(476), 680–685.

Collins, A.T., 2007. Optical Centres Produced in Diamond by Radiation Damage. *New Diamond and Frontier Carbon Technology*. 17(2), 47-61.

Giessibl, F.J., 2003. Advances in Atomic Force Microscopy. *Reviews of Modern Physics*. 75, 949-983.

Acknowledgements

This project was supported by the Gem and Jewelry Institute of Thailand, and partly by the Gems and Mineral Sciences Special Research Unit, Department of Earth Sciences, Faculty of Science, Kasetsart University. The Scientific Equipment Center, Faculty of Science, Kasetsart University and the Nuclear Research Center, Ongkarak, Nakhon Nayok Province, Thailand provided AFM equipment and electron irradiation facility.

Gemstone occurrences, “organic” odors, and a circular structure in the collision zone between East and West Gondwana

John M. Saul

ORYX, Paris, France; john.saul@wanadoo.fr

Observations

In SE Kenya/NE Tanzania, the host rocks of transparent gemstones emit a strong foul odor when struck or crushed. Varieties of gemstones found in these deposits include sapphire, ruby, tsavorite, tanzanite, diopside and tourmaline. Hydrogen sulfide, sulfur (S₈), some methane, and traces of nitrogen have been identified in fluid inclusions within crystals of tanzanite during recent studies (Olivier, 2006; Giuliani, 2010). Older, unreplicated reports from samples obtained from substantially higher in the tanzanite deposit found ethane and perhaps propane and butane (Malisa et al., 2006; Malisa, 1998). Skatole (C₉H₉N) has been reported from the rocks in the Mogok Gem Tract of Burma (Iyer, 1953) and judging by the distinctive odor, might be present in Kenyan and Tanzanian deposits.

The gemstone deposits in question are all situated in sediments metamorphosed in Pan-African times, c.550Ma, or in ultrabasic (ophiolitic?) intrusions into these metasediments.

Large quantities of graphite are present at all these gem deposits. This is also the case in Madagascar and in Sri Lanka where “the extent of the deposits has inspired significant study, and although the resulting literature is extensive, little is known about the origin of the vein graphite” (Taylor, 2006; also see <http://www.asbury.com/Vein-Graphite.html>).

The association of gases with transparent gems is due to the existence of small 3-D zones of locally low pressure in which gases and fluids accumulated, and where crystals grew with locally low constraining pressure. On Mgama Ridge, tsavorite-bearing horizons are capped by impervious roof rocks whose irregularities act as traps (Bridges, personal communication). At Merelani, tsavorite “crystallized in tension zones within and in proximity to... boudins”, and tanzanite hosted in calc-silicate layers occurs “in various types of low-pressure sites within and adjacent to... boudins” (Olivier, 2006). SE Kenya/NE Tanzania lie within the contact zone between East & West Gondwana. The five most important primary gem deposits in SE Kenya/NE Tanzania are all situated on the rim of a nearly perfect geometric circle approximately 260 kms in diameter (Figure 1).

The two next most important gem deposits in the region, plus some twenty less important primary occurrences of gems, are located on two tangents to the circular area (Figure 1). These tangents, and at least two additional mineralized fractures, are all oriented parallel to the join between East & West Gondwana.

Elements of an interpretation

An ancient (3-D) plug of resistant rock with a (2-D) circular outline was trapped during the collision of the two halves of Gondwana. Highly localized low-pressure zones were produced around its perimeter and along two tangent fault-zones, and fluids accumulated in these zones of low pressure. The low constraining pressure also favored the growth of fine-quality crystals.

The geological literature contains no reports of circular patterns this large other than 1) vestiges of the Late Heavy Bombardment (c.4100-3800 Ma), as favored by the author (Saul, 1978), and 2) vestiges of more recent meteorite impacts. In consequence, if the reality of the circular pattern is accepted, it is necessary to accept one of these two possibilities, or to devise a novel idea applicable to these occurrences, or to attribute the circular pattern to a geographical accident without geological significance, which seems unlikely in the light of its position at the join of East and West Gondwana. In all cases, we are in the domain of extraordinary, or at least unusual, claims, but the Merelani and John Saul occurrences are indeed geologically unusual, as is the alignment along Penny Lane.

Three origins for the gases seem possible: 1) materials of primordial origin, 2) mobilization of evaporites that had acted as fluxes during the crystallization of the gems, and 3) serpentinization of ophiolites, producing H₂ and hydro-

carbons. One origin for some of the gas does not preclude another origin for a different fraction of the gases present.

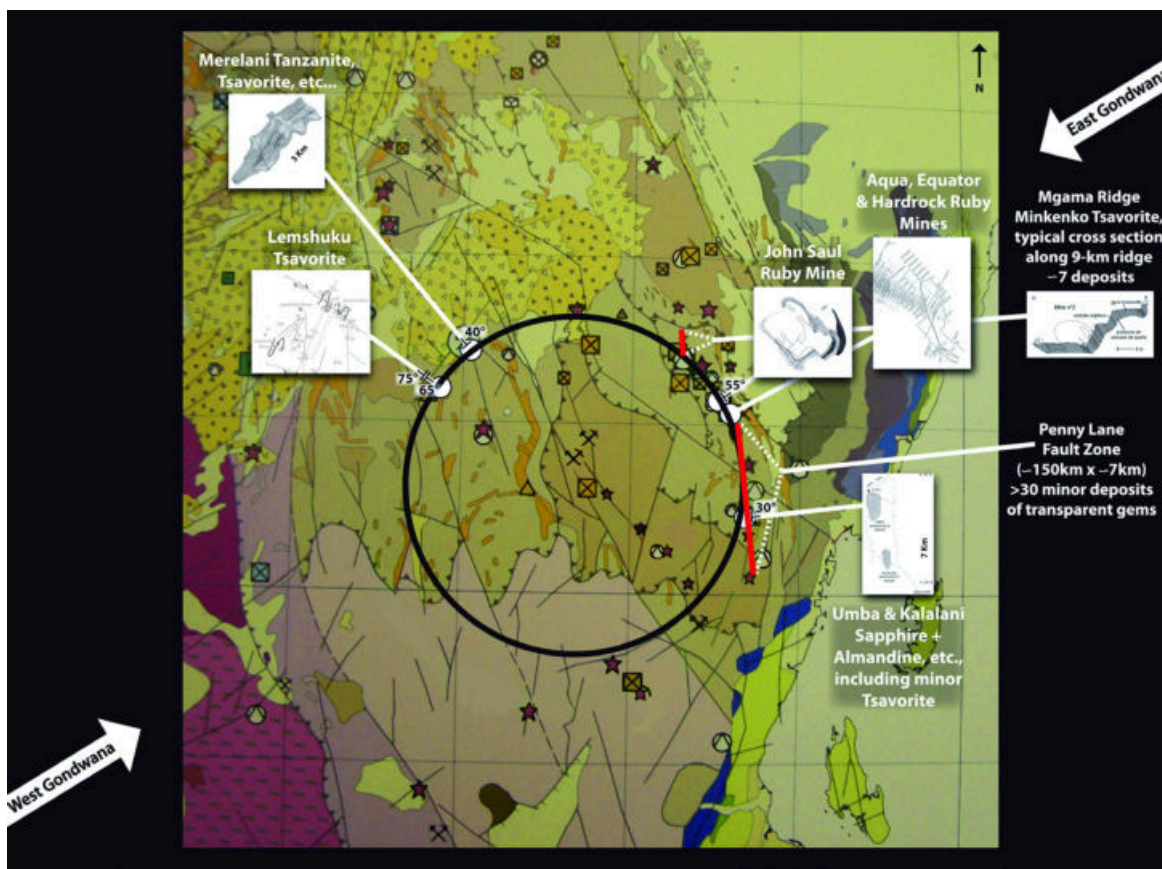


Figure 1. Geological Sketch Map of SE Kenya and NE Tanzania. Work that has been done on the several gem deposits and geological features, going clockwise, commencing in the NW:

Lemshuku (tsavorite): Feneyrol (2012); Mark Saul, personal communications (2013);

Merelani (tanzanite; tsavorite, magnesio-axinite, diopside): Olivier (2006); Wilson et al. (2009); Čílek (1980);

Mgama Ridge deposits (tsavorite): Pohl & Niedermayr (1978); Campbell Bridges (personal communications);

John Saul Ruby Mine (ruby, minor tourmaline): Simonet (2000); personal observations;

Aqua, Equator, Hardrock and Jongor (ruby): Austromineral (Oct. 1978); personal observations;

Penny Lane occurrences (ruby, sapphire, tourmaline, tsavorite, almandine, rhodolite, Cr/V kornepurine): "Règne Minéral" (2013);

Austromineral (Oct. 1978); personal observations;

Umba and Kalalani (sapphire, almandine, rhodolite): Solesbury (1967); Seifert & Hyrsl (1999);

Angle of collision between East and West Gondwana: Chatterjee et al. (2013); Feneyrol (2012)

References

Austromineral G.m.b.H., Vienna (Oct. 1978). Geological Prospecting and Economic Assessment of the Gemstone Belt in Southeastern Kenya. Kenya-Austria Mineral Exploration Project, 2nd Report to the Ministry of Natural Resources, Mines and Geological Department, Nairobi.

Chatterjee, S., Goswami, A. and Scotese, C.R., 2013. The longest voyage: Tectonic, magmatic, and paleoclimatic evolution of the Indian plate during its northward flight from Gondwana to Asia, *Gondwana Research*, 23(1), 238-267.

Čílek, V., 1980. The geology of the Merelani tanzanite deposit. *Sbornik Geologického Ústavu, Ložisková Geologie Mineralogie*, 21, 183-185.

Feneyrol, J., 2012. Pétrologie, géochimie et genèse des gisements de tsavorite associés aux gneiss et roches calco-silicatées graphiteux de Lemshuku et Namalulu (Tanzanie). Thesis, Institut National Polytechnique de Lorraine, Vandoeuvre-lès-Nancy, 617 pp.

Feneyrol J., Ohnenstetter D., Giuliani G., Fallick A.E., Rollion-Bard C., Robert J.L. and Malisa E.P., 2012. Evidence of evaporites in the genesis of the vanadian grossular 'tsavorite' deposit in Namalulu, Tanzania. *Canadian Mineralogist*, 50(3), 745-769.

Garnier, V., 2003. Les gisements de rubis associés aux marbres de l'Asie Centrale et du Sud-Est: genèse et caractérisation isotopique". Thesis, Institut National Polytechnique de Lorraine, Vandoeuvre-lès-Nancy, 373 pp.

Giuliani, G., 2010. Les gisements de tsavorite associés aux gneiss graphiteux de Tanzanie, Madagascar et du Kenya: genèse et caractérisation isotopique. Rapport CESSUR, AO INSU, pp.1-10.

Iyer, L.A.N., 1953. The Geology and Gem-Stones of the Mogok Stone Tract, Burma. *Mem. Geol. Surv. India*, 82, p.35.

Malisa, E.P., 1998. Application of graphite as a geothermometer in hydrothermally altered metamorphic rocks of the Merelani-Lelatema area, Mozambique Belt, Northeastern Tanzania. *Jour. African Earth Sci.*, 26(2), 313-316.

Malisa, E.P., Kinnunen, K. and Koljonen, T., 1986. Notes on fluid inclusions in vanadiferous zoisite (tanzanite) of the Merelani area, Tanzania. *Bull. Geol. Soc. Finland*, 58, 53-58.

Olivier, B., 2006. Geology and Petrology of the Merelani Deposit, NE Tanzania. Thesis, Stellenbosch.

Pohl, W. and Niedermayr, G., 1978. Geology of the Mwatate Quadrangle and the vanadium grossularite deposits in the area. *Rep. Geol. Surv. Kenya*, 55, 51 pp.

"Règne Minéral", 2013. Les Gemmes du Gondwana, Cahier No. 2.

Saul, J.M., 1978. Circular structures of large scale and great age on the Earth's surface. *Nature*, 271 (5643) 345-349.

Simonet, C., 2000. Géologie des gisements de saphir et de rubis – l'exemple de la John Saul Ruby Mine, Mangare, Kenya. Thesis, Nantes, 350 pp.

Seifert, A.V. and Hyrsl, J., 1999. Sapphire and Garnet from Kalalani, Tanga Province, Tanzania, *Gems & Gemology*, 35(2), 108-120.

Solesbury, F.L., 1967. Gem corundum pegmatites in NE Tanganyika. *Eco. Geol.*, 62(7), 983-991.

Taylor, H.A., Jr., 2006. In J.E. Kogel, N.C. Trivedi and J.M. Barker, Eds., *Industrial Minerals and Rocks: Commodities, Markets, and Users*. Society for Mining, Metallurgy and Exploration, 7th ed., 507-518.

Acknowledgments

The author thanks the Richard Lounsbery Foundation for backing this project.

Fancy colored diamonds cut optimization technology

Sivovolenko S.1, Serov R.2, Shelementiev Y.2

1 - OctoNus Software, Moscow, Russia

2 - Moscow State University Gemmological center, Moscow, Russia

Introduction

Theoretical foundations of Fancy colored diamonds cut optimization technology were announced in 2006 (Sivovolenko S, 2006) in IV Gemological Symposium, San Diego. The main goals of the Fancy colored diamonds cut optimization technology are high saturation, lightness, good color distribution of polished diamond along with high yield. Those goals could be achieved using the developed Process Flow of rough diamond processing.

Technology is based on the obtaining the correct optical absorption spectrum of fancy diamond through the windows. That spectrum is used to predict and optimize future diamond color at the stage when the diamond itself is still in the form of rough, and there are numerous cutting opportunities. Spectrum, the cut and the size of the stone, as well as the observation conditions determine the color of fancy colored diamond. Computer simulation is used to predict and optimize the cut takes into account all these factors.

The oral presentation Sivovolenko S, 2006 was released theoretical Process Flow of Fancy colored diamonds cut improvement technology, which consists of 7 points:

1. Scanning rough diamond and recording absorption spectrum through pairs of parallel windows
2. Selecting few prospective shapes on the base of spectrum
3. Rough allocation plans
4. Color and contrast optimization by proportions
5. Expert evaluation of photorealistic images and calculated color metrics in different lighting and viewing conditions
6. Rough optimization with found proportions
7. Final decision

The technology was implemented into diamond polishing factories during last 7 years. And now polishing factories in Surat, India and Smolensk, Russia use the Fancy colored diamonds cut optimization technology to deal with fancy colored diamonds.

This thesis is focused on the problems that were solved during the practical implementation of the technology. In addition, the results of cut optimization technology in comparison with conventional cutting technology will be shown.

The problems that were solved during the practical implementation of the technology

With the implementation process set of tools have been created to ensure the obtaining of qualitative input data and further acceleration of the cut creation process. Also the methods to achieve the projected girdle shape and facets angles/azimuths of the polished diamond were developed.

1. Creation and implementation of algorithms for automatic setting of pairs of parallel windows for spectroscopy, so they did not effect on the future stones
2. Using a modified Avalon tool for the accurate control of polished windows parallelism
3. Using the Light Table for verification and correction of the optical spectrum of the stone
4. Creation and implementation of algorithms for automatic baseline correction of the spectrum, using data from an optical spectrometer and the Light Table
5. Creation of a Cut Designer. It is a tool that allows creation of cutting 3D parametric models, which can be

automatically optimized for the particular stone size and spectrum. The cut creation process in Cut Designer is not complicated than in GemCad, but allows creation the cutting with variable angles and proportions. Automatic variation of cutting parameters is one of the basics to find the cut parameters with high performance – color saturation and distribution.

6. Desired girdle contour for fancy cut can be made using an automated Aqua system, allowing reproduction exactly the predicted girdle shape.

7. Comparative reports are used to compare actual polished diamond and the forecasted on semi-polished or full polished stages and show deviations in azimuths and angles of the facets. This tool also allow the cutter adjust the facets and azimuths of the cut during the cutting process to achieve better forecast reproduction. In addition, comparative reports is useful to control repetition of girdle shape.

Implementation of the improvements described above significantly helped to increase the quality of the spectral data and the accuracy of the forecast (see Fig. 1). Also the automatic processing of cuts selection decreases the operators manual work time.



Fig. 1. Diamonds polished using fancy colored diamonds cut optimization technology in Lemon TechnoMist factory, Surat, India.

Comparison between conventional and Fancy colored diamonds cut optimization technology

Rough diamond 3.60 ct with distorted octahedral shape was sawn into two halves. First half was polished according to conventional technology. The other half was processed using a Fancy colored diamonds cut optimization technology. Optical absorption spectrum shows N3-center related absorption. The color of the rough diamond was light yellow.

In both cases, cushions have standard brilliant crown and pavilion with four main facets. Conventional technology meant the distortion of known cushion pattern to achieve the higher yield. As a result 1.25 ct polished cushion with 1.22 ratio.

Cushion optimized with Fancy colored diamonds cut optimization technology were processed following the shown above Process Flow. Optimized cushion was 1.15 ct with ratio 1.15. Total yield for two cushions was 65.8%.

Conventional cushion though had 0.10 ct bigger weight, but was less color saturated under the table. Its color could be estimated as Fancy Light Yellow.

Color of the polished optimized cushion had a good match with forecast and could be estimated as Fancy Yellow (Fig. 2 and 3).

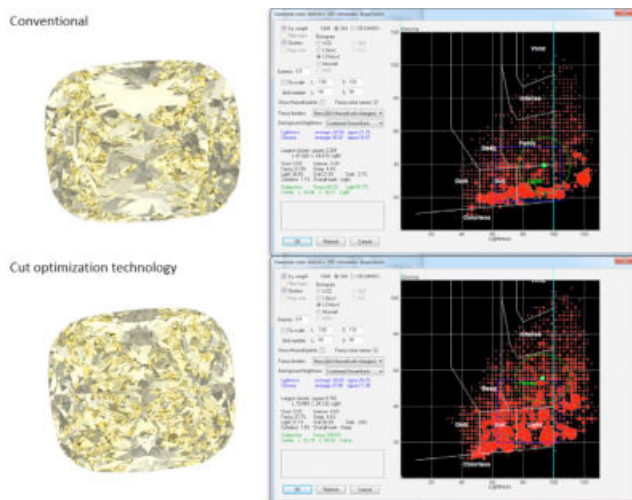


Fig. 2. Photoreal images for conventional and optimized cushions with Corresponding diamond color statistics.



Fig. 3. Photo of conventional and optimized cushions in Gretag Macbeth Judge II.

Conclusion

Development and implementation of fancy colored diamonds cut optimization technology in cutting factories confirmed the theoretical thesis, published by Sivovolenko S, 2006 that such optimizing technology can be created and the predicted diamond colors can be achieved. Automation of the most time-consuming parts of the technology (related with the windows polishing, spectrum and cut optimization), as well as the introduction of additional control methods (windows parallelism control, control of the predicted cut polishing) leads to significant quality and stability improvements and reduce the time to work with each individual stone. Comparison of the conventional and Fancy colored diamonds cut optimization technology results (see Table 1) shows that for conventional stone it is not possible to accurately predict color and appearance of negative optical phenomena. That is why conventional polished stone may be the bigger one for the rough, but can not be the most costly one.

Fancy colored diamonds cut optimization technology allows to precisely predict the color and appearance of the stone while the diamond is in rough and avoid possible negative phenomena. Also technology has the methods not only to predict, but to achieve the predicted shape and color for real diamond.

	Conventional		Cut optimization technology
Cut type	Known cut (previously polished) with fixed proportions	Distorted known cut (modified cut depth, ratio, girdle shape) for higher yield	Optimized cut created by Cut optimization technology
Result prediction	Medium Based on already polished stones with exactly same cut proportions. Can not really consider the color and size of diamond.	Low to Medium Inaccurate, based mainly on polisher experience	High Based on computer modeling technology. Taking in account rough spectrum and cut proportions
Color Saturation	Medium to High	Inconsistent from Low to Medium	Highest possible
Color distribution	Good	Inconsistent from Good to Poor	Good
Negative phenomena	Can be avoided	May appear	Can be avoided
Yield	Low to Medium	Highest	High

Table 1: Comparison of the conventional and Fancy colored diamonds cut optimization technology results

References:

Sivovolenko S, Shelementiev Y, Fancy-Color Diamonds: Better Color Appearance by Optimizing Cut, Oral Presentation at IV Gemological Symposium, San Diego, Ca, USA 27-30 Aug 2006.

Classifications of Jadeite

Elizabeth Su

Gemsu Rona, Shanghai, China; esu_gems@yahoo.com

As a jadeite dealer and gemologist working with affluent clients mostly in mainland China and Hong Kong, buying and selling all kinds of jadeite raw materials and jewelry, I am researching the classification of jadeites by different criteria.

Classification of Jadeite

1. By deposit

- Primary ore: discovered in Dou Maw district, Burma, in 1875, no weathered shell on the new-mined jadeite, so people can see the texture, color and transparency clearly.
- Secondary ore: already found in the 13th century in alluvial deposits of the Wu Lu River, Burma. The secondary deposit jadeites have different kinds of weathered shells with different colors and thicknesses. In jadeite business we call these weathered shells the «skin». The skin color appears pale yellow, yellow, grayish yellow, brownish yellow, gray, grayish green, deep gray, black and so on. Normally the finer the grain of the «skin» is, the finer the texture of jadeite, and vice versa.

2. By color

- Green: the best green has a strong to vivid saturation, with an even color distribution, and without a gray or blue component.
- Yellow-orange-red-brown: the best colors have a strong to vivid saturation, with an even color distribution, without a gray or blue hue; a colour with a brown tint is less valuable than yellow and orange ones. The jadeites that have a real red hue are very rare, most of them are reddish orange.
- Lavender-violet-purple: the best colors have a strong to vivid saturation, with an even color distribution, without a gray or blue shade.
- Black: inky jadeite, under transmitted light it shows deep green, and under incident light it shows black.
- Colorless: glassy or icy jadeite shows its special color with all kinds of hues, gray and yellow tints have lower value than others. Pure colorless jadeite and with a violet shade have extremely high value.

3. By crystal grain

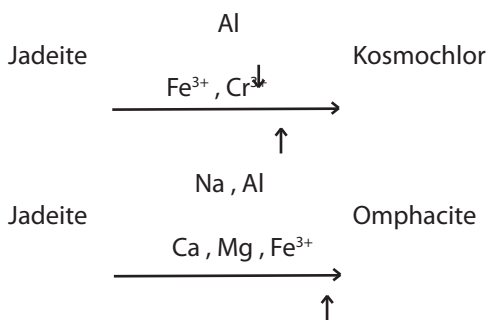
- Old mined (glass) species: contains a very fine texture, the crystal grains are very hard to see even under a 10x loupe; it has few or no inclusions. Most of them are fully transparent like glass, we can see the texts below through it .
- Icy species: compared with glassy jadeite, its texture is a little coarser, with a 10x loupe some crystal texture can be seen, which still cannot be observed with the unaided eye.. This type of jadeite shows good transparency and minor inclusions.
- Hibiscus species: the size of the crystal grains is similar to icy jadeite, with a fine texture, but it is translucent rather than transparent; when it has violet or light green colors, it's quite attractive to buyers.
- Sticky rice species: shows a very fine texture, normally crystals cannot be seen under a 10x loupe. But compared with glassy jadeite, it has much lower transparency just like the « sticky rice», and all kinds of colors distributed in many patterns.
- Bean species: the size of the grains is mixed, with bigger and smaller crystals, the texture is coarser and not even, and the crystal grains can easily be seen with the unaided eye.
- Oil green species: this species also has a fine texture, combined with a good translucency, but the color is not too saturated, always strongly grayish, and it has a low value too.
- Dry green species: the texture is coarse, it has a poor translucency, and although the color is even, it has a low value.

4. By transparency

When viewing larger pieces of rough, the material is called

- fully transparent: >10mm jadeite material can be seen through;
- transparent:6-10mm jadeite material can be seen through;
- translucent:3-6mm jadeite material can be seen through;
- slightly translucent: 1-3mm jadeite material hardly can be seen through;
- opaque: jadeite material cannot be seen through and light does not pass.

5. By mineral composition

**References**

- Bosshart G., 2006. Old and new Jade roads from the Jadeite jade mines in Upper Burma to the vast market-places of Chinese cities. Proceedings 1st International Gem and Jewelry Conference, Gem and Jewelry Institute, Bangkok, 43.
- Hughes R.,W., Galibert O., Bosshart G., Ward F., Thet Oo, Smith M., Tay T.S., Harlow G.E., 2000. Burmese Jade – The inscrutable gem. *Gems & Gemology* 36 (1), 2-26.
- Lam, C., 2005. *Jade*. ISBN 962-86332-5-2
- Ma Baozhong, 2008. *Research of jadeite trading in Yunnan*. ISBN 962-450-319-2
- Zhang Zhifang, 2006. *Jadeite book*. ISBN 7-222-04824-3.

Differentiation of the colorless gemstones: phenakite, petalite, pollucite and goshenite

Sora Shin¹, Jingyo Seo¹, Yongkil Ahn¹, U. Tin Hlaing², Jongwan Park¹

¹Department of Materials Science and Engineering, Hanyang University, 17 Haengdang-dong, Seongdong-gu, Seoul, 133-791, Republic of Korea; jwpark@hanyang.ac.kr

²Centre Department of Geology (retired), Panglong University, Myanmar

We investigated the colorless gemstones are phenakite, petalite, pollucite, and goshenite mostly silicate minerals found in pegmatite deposits.

As a lithium aluminium tectosilicate mineral, petalite has a three-dimensional network and its formula is $\text{LiAlSi}_4\text{O}_{10}$. Phenakite Be_2SiO_4 is a beryllium nesosilicate. Pollucite and colorless beryl, goshenite, are cyclosilicate of compositions $(\text{Cs},\text{Na})\text{AlSi}_2\text{O}_6 \cdot n\text{H}_2\text{O} (\text{Cs}+n=1)$ and $\text{Be}_3\text{Al}_2(\text{Si}_6\text{O}_{18})$, respectively. Their spectra were investigated by ultraviolet-visible, mid-infrared, and wavelength-dispersive X-ray fluorescence (WD-XRF)..

The physical properties of colorless gemstones are summarized in Table 1. There was weak UV-Vis fluorescence in all samples. Furthermore, all showed birefringence except the pollucite, which is cubic. They showed refractive indices spanning 1.500-1.670 with a birefringence ranging between 0.005 and 0.018. Specific gravity values extend from 2.39 to 3.00. Phenakite has the highest specific gravity as 3.00, whereas petalite appeared the lowest at about 2.38. Phenakite showed a medium red to long- and short-wave UV radiation. Goshenite beryl appeared with a medium red fluorescence to short-wave UV radiation but was inert to long-wave UV.

As shown in Table 2, there were large differences in the trace-element chemistry of colorless gemstones, but all the samples contained lots of SiO_2 as a main oxide (silicates). Especially, they had virtually no transition elements except for a small amount of Fe_2O_3 . They do not offer an octahedral coordination in their crystal structure with the exception of goshenite so that they are not expected to gain color through d-d transitions or charge transfer absorptions, as most gems, colored by transition metal ions, do. Pollucite contains 16.45 wt % Cs_2O . This element is rare in gemstones.

Table 1. Physical properties of the investigated colorless gems. RI: refractive indices, DR: birefringence, SG: specific gravity, UVF-LW: long wave UV, UVF-SW: short wave UV.

Sample	RI	DR	SG	UVF-LW	UVF-SW
petalite	PEM-1 1.500-1.510	0.010	2.39	Weak red	Weak red
petalite	PEM-2 1.500-1.511	0.011	2.38	Weak red	Weak red
petalite	PEM-3 1.500-1.512	0.012	2.38	Inert	Weak red
petalite	PEM-4 1.500-1.514	0.014	2.36	Weak red	Weak red
phenakite	PHM-1 1.651-1.668	0.018	3.00	Inert	Weak red
phenakite	PHM-2 1.653-1.670	0.017	2.95	Weak red	Weak red
phenakite	PHM-3 1.654-1.671	0.017	2.92	Weak red	Weak red
phenakite	PHM-4 1.653-1.670	0.017	3.00	Weak red	Weak red
pollucite	POM-1 1.510	-	2.87	Weak red	Medium red
pollucite	POM-2 1.489	-	2.87	Weak red	Medium red
pollucite	POM-3 1.510	-	2.72	Weak red	Medium red
pollucite	POM-4 1.507	-	2.80	Weak red	Medium red
goshenite beryl	GM-1 1.568-1.574	0.006	2.60	Inert	Medium red
goshenite beryl	GM-2 1.576-1.582	0.006	2.62	Inert	Medium red
goshenite beryl	GM-3 1.576-1.581	0.005	2.60	Weak red	Medium red
goshenite beryl	GM-4 1.577-1.582	0.005	2.67	Inert	Medium red

Sample	SiO ₂	Al ₂ O ₃	CaO	Cs ₂ O	Na ₂ O	Rb ₂ O	MgO	Fe ₂ O ₃	SO ₃
petalite	75.77	24.11	-	-	-	-	0.06	0.01	-
phenakite	94.44	5.43	0.05	-	-	-	-	0.03	-
pollucite	50.73	29.63	0.15	16.45	1.89	0.67	0.23	0.06	0.19
goshenite beryl	70.16	28.99	-	0.061	0.23	0.02	0.03	0.11	0.36

Table 2. Chemical composition of four colorless gemstones by WD-XRF. (Unit: wt %).

Figure 1 shows the UV-Vis absorption spectra of the colorless gemstones. No absorption band occurs in the visible region, as the samples are colorless. We obtained mid-infrared spectra in the range 4000 – 2000 cm⁻¹. Petalite showed a strong and broad absorption band between 3500 and 3000 cm⁻¹ before irradiation, although it does not contain water. However, this band nearly disappeared after irradiation. Other colorless samples did not show any remarkable change by irradiation. Based on mid-infrared results, the change of petalite with irradiation will be discussed in more detail.

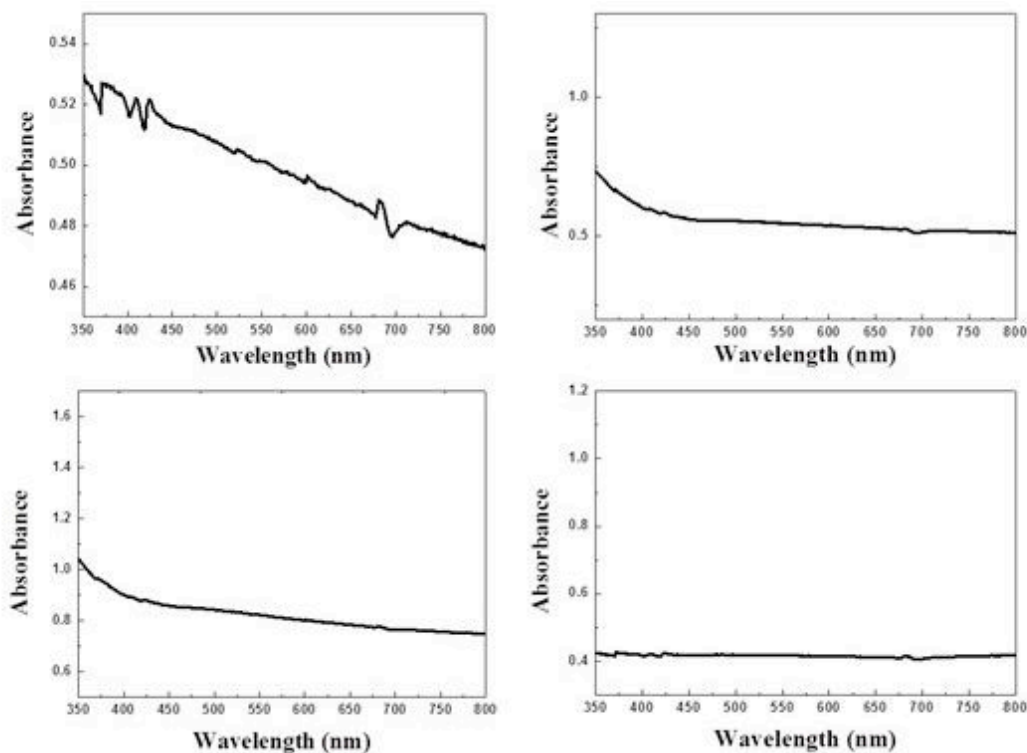


Figure 1. UV-Vis absorption spectra of the colorless gemstone samples in the region of 300 to 750 nm: (a) petalite, (b) phenakite, (c) pollucite, and (d) goshenite.

References

- Fleischer M., Ksanda C. J., 1940. Dehydration of pollucite, *American Mineralogist*, 25, 666-672.
 Win K. K., Themelis T., 2003. Gem quality petalite from Myanmar (Burma), *Australian Gemmologist*, 21(10), 407.
 Aurisicchio C., Fioravanti G., Grubessi O., Zanazzi P.F., 1988. Reappraisal of the crystal chemistry of beryl. *American Mineralogist*, 73, 826-837.

Heat treatment of coloured beryl from Madagascar

Panjawan Thanasuthipitak, Chawalit Chankhantha, Theerapongs Thanasuthipitak

Gemmology Program, Department of Geological Sciences, Faculty of Science, Chiang Mai University, Chiang Mai 50200, Thailand; panjawan.t@cmu.ac.th

One hundred rough beryl samples from Madagascar were characterized using basic gemmological methods and several spectroscopic techniques including: UV-Vis-NIR absorption; FTIR; Photoluminescence; and X-ray absorption spectroscopy. Chemical analyses using electron microprobe (EPMA) were also carried out. The samples, ranged from 1.312 to 4.745 ct, were classed into four groups on the basis of their original colour: greenish blue (20), greenish yellow (25), yellowish green (35), and orangish pink (20). They were heat treated in an electric furnace to try to enhance their appearance. The heating atmosphere of reducing condition was created through continuous purging of Ar gas into the heating chamber, by which the oxygen content in the chamber decreased from approximately 21% down to 0.5 mol%. The heating experiments show that optimum heating temperature for enhancing the samples of the first three groups into purer aquamarine blue is 400°C, while 350°C is sufficient to produce morganite pink from samples of the last group (Figure 1).

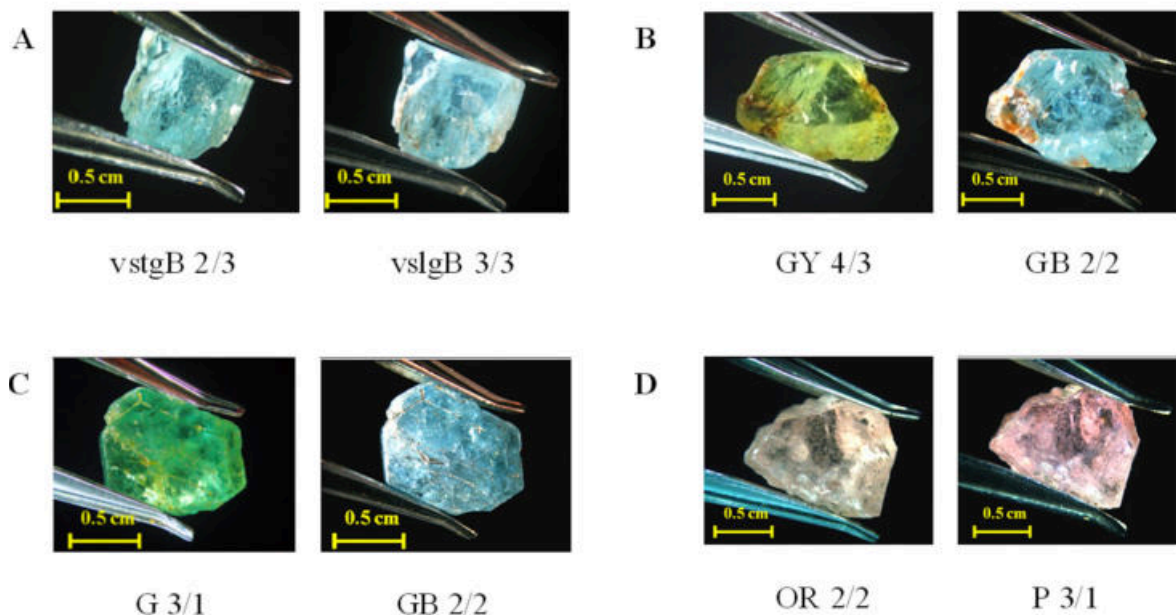


Figure 1. The samples before and after heat treated at 400°C of group greenish blue (A), group greenish yellow (B), and group yellowish green (C), and after heating at 350°C of group (D) under reducing atmospheres. (GIA Gem Set codes are described to compare the changing of colour).

UV-Vis-NIR absorption spectra show a decrease in intensity of octahedral Fe^{3+} peaks at 370 and 427nm, and a slight increase in intensity of a broad band, centred at 8720 nm, of octahedral Fe^{2+} , after heat treatment (Figure 2). X-ray absorption near edge structure (XANES) spectra indicate that Fe^{3+} at the octahedral site was converted to Fe^{2+} after heating. The elimination of an unfavourable yellow tint in the samples can hence be attributed to the conversion of yellow-causing Fe^{3+} at the octahedral site (e.g., Eeckhout et al., 2005; Nassau, 1994) into Fe^{2+} , which only causes slight absorption at the red end of the visible spectrum.

This study also shows that after heat treatment, FTIR spectra (Figure 3) reveal a marked decrease in intensity of a shoulder due to O-H stretching, between 3200 and 3000 cm^{-1} (Wood & Nassau, 1968). The PMA results show a rather

low Fe content in the greenish beryl from Madagascar being studied, 0.21 to 1.23 wt% FeO(total) compared to those of similar coloured beryl from other localities (e.g. 4.96 – 5.04 wt% FeO(total) in Canadian aquamarine from Yukon Territory (Adamo et al., 2008); 1.37 – 1.50 wt% FeO(total) in beryl from Vietnam (Huong et al., 2011); and up to 2.19 wt% FeO(total) in beryl from Brazil (Viana et al., 2002).

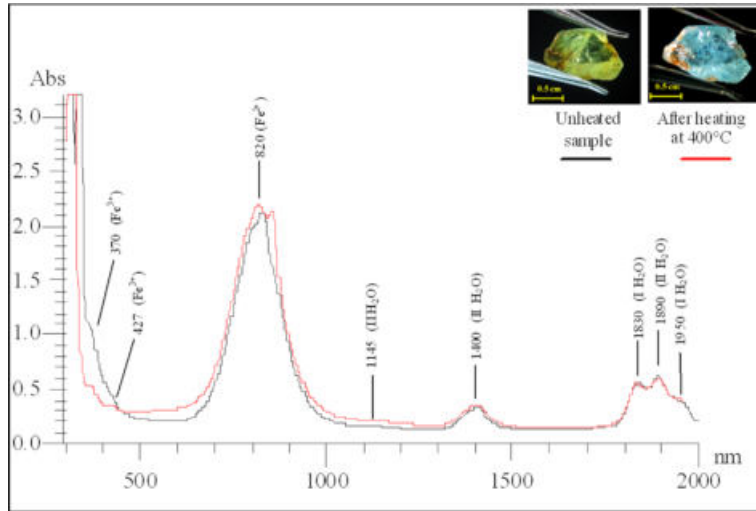
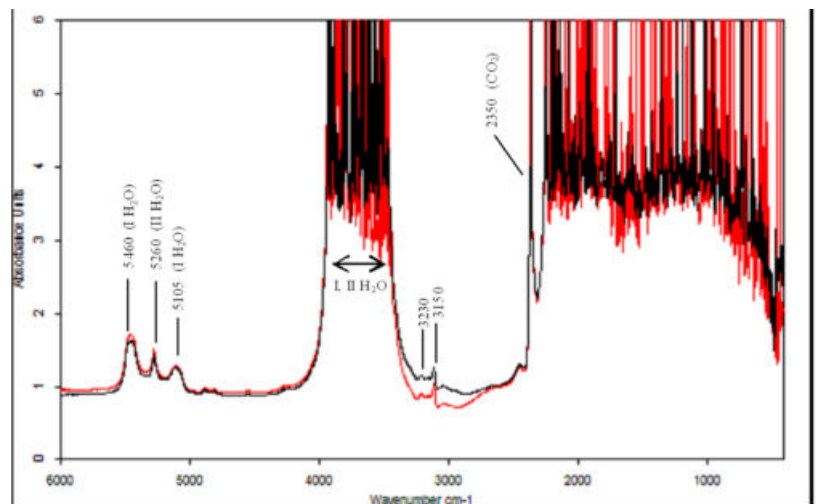


Figure 2. UV-Vis-NIR absorption spectrum of unheated greenish yellow aquamarine sample (black line) compared with spectrum of blue aquamarine (red line) after heat treated at 400°C.

Figure 3. Infrared spectrum of unheated yellowish green aquamarine sample (black line) compared with infrared spectrum of blue aquamarine sample after heated at 400°C (red line).



References

- Adamo, I., Pavese, A., Prospero, L., Diella, V., Ajo, D., Gatta, G.D. and Smith, C.P., 2008, Aquamarine, Maxixe-type beryl, and hydrothermal synthetic blue beryl: analysis and identification. *Gems & Gemology*, 44 (3), 214-226.
- Eckhout, S.G., Neisius, T. and Castaneda, C., 20. Oxidation effects in beryl induced by synchrotron radiation. *Nuclear instruments and methods in physics research*, 299, 73-77.
- Huong, L.T.T., Hofmeister, W., Hager, T., Khoi, N.N., Nhung, N.T., Atichay, W. and Pisuta-Arnond, V., 2011. Aquamarine from the Thuong Xuan district, Thanh Hoa province, Vietnam. *Gems & Gemology*, 47(1), 42-48.
- Nassau, K., 1994. *Gemstone Enhancement – History, Science and State of the Art*. 2nd Ed., Butterworth-Heinemann Ltd., Oxford, 252 p.
- Viana, R.R., Jordt-Evangelista, E.H., Magela da Costa, E.G. and Stern, W.B., 2002, Characterization of beryl (aquamarine variety) from pegmatites of Minas Gerais, Brazil. *Physics and chemistry of minerals*, 29 (10), 668 – 679.
- Wood, D.L., Nassau, K., 1986. The characterization of beryl and emerald by visible and infrared absorption spectroscopy. *American mineralogist*, 53, 777-800.

Some gemmological characteristics of peridot from South Vietnam

Nguyen Thi Minh Thuyet¹, Nguyen Ngoc Khoi^{1, 2}, Christoph Hauzenberger³, Nguyen Hoang⁴, Duong Anh Tuan²

¹Hanoi University of Science, 334 Nguyen Trai str., Thanh Xuan dist., Hanoi, Vietnam; nmthuyet@vnu.edu.vn

²DOJI Gold & Gems Group, 44 Le Ngoc Han, Hanoi, Vietnam

³Karl-Franzens-University of Graz, A – 8010, Graz, Austria

⁴Institute of Geological Sciences, Vietnam Academy of Science & Technology, 84 Chua Lang, Dong Da, Hanoi, Vietnam

Introduction

Peridot was discovered in Vietnam in the 1990s (Kammerling et al., 1995). From that time gem quality peridot has been produced in three provinces (Gia Lai, Dak Lak, and Lam Dong) in Tay Nguyen Highlands. Up to now, mining activity remains only in the Gia Lai province, where two main mines (Ham Rong and Bien Ho) yield more than 100 kg monthly. Mining here mostly is done on a small scale by individual diggers, where the gem material has been extracted either from alluvial gravels or from peridot nodules (Figure 1a). In some places, miners must dig pits 3-5 m deep to reach the peridot-bearing alluvial layers. Vietnamese peridot occurs in spinel lherzolite xenoliths found within basalt flows (Quoc et al., 1995; Toan et al., 1995).

Samples and Methods

For this study gem-quality peridot nodules and 3 lots of rough peridot, as well as 15 faceted stones were examined by the authors (Figure 1). We used standard gemological equipment to record optic character, refractive indices and birefringence, pleochroism, absorption spectra, and UV fluorescence. Specific gravity was measured by the hydrostatic method using an electronic balance. Various gemological microscopes (vertical and horizontal, incorporating different lighting techniques) were used to observe internal features. Two peridot grains of low quality (right side in Figure 1b), 9 grains of a medium to good quality batch (middle lot in Figure 1b) and 9 samples from the best quality samples (left side of Figure 1b) from Ham Rong area were mounted and embedded in resin, polished and then analyzed by microprobe and LA-ICPMS.

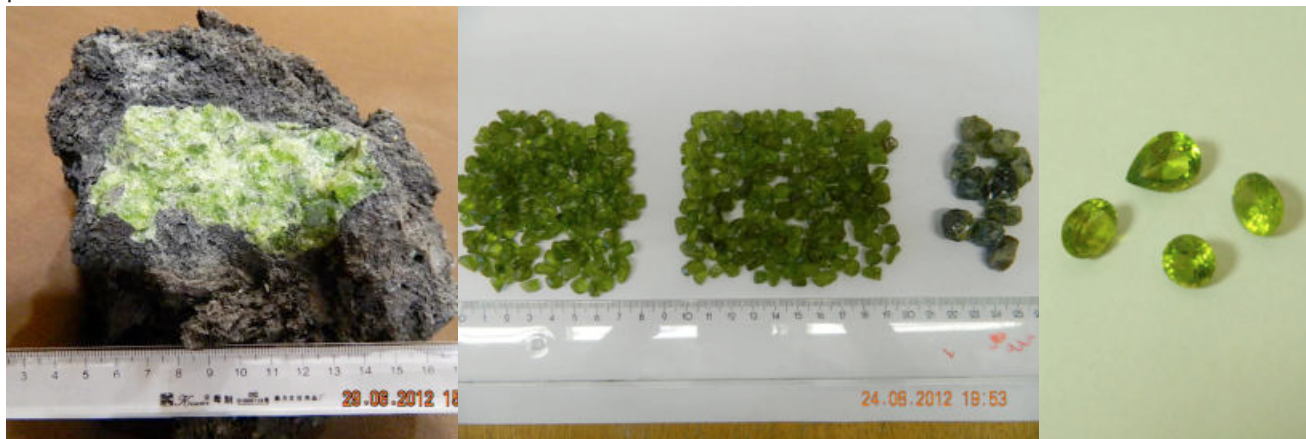


Figure 1. Peridot nodule (a), 3 lots of rough stones (b) and some cut stones from 0.98 to 1.63 ct (c) used for this study.

Results

Crystal Morphology

The peridot is found as gemmy nodules (xenoliths) in extrusive vesicular alkali basalt lava flows (Keller & Wang, 1986).

Like the peridot found in Zhangjikou-Xuanhua area of Hebei Province (China) and in San Carlos of Arizona (United States), which also occurs in basalt (Koivula, 1986), no idiomorphic single crystals of rough peridot have been found in Vietnamese deposits and occurrences.

Visual Appearance

The peridot samples examined ranged in color from a light yellowish green to a darker, richer yellow green, "olive" green and brownish green. Faceted stones show an attractive yellowish green color (Figures 1c). Diaphaneity ranges from translucent (due to high fracturing) to transparent. The dimensions of most Vietnamese peridot vary from several millimeters to 1.5 cm in diameter (Figure 1b). Pieces as large as 4-6 cm are occasionally discovered.

Optical Characteristics and Specific Gravity

Refractive index readings on 15 faceted stones were almost identical: biaxial positive with indices of $x = 1.650-1.667$, $y = 1.665-1.669$, and $z = 1.686-1.703$; $\Delta n = 0.036-0.038$. The visible-light absorption spectra of Vietnamese stones showed pattern, typical for peridot. All the stones are inert to both LW and SW ultraviolet radiation. The specific gravity determined by the hydrostatic balance was 3.36 ± 0.02 .

Internal Features

The internal features of Vietnamese peridot are similar to those formed in an alkali basalt. Most prominent inclusions are round, flat (dislike) healing planes ("lily pads") with a small opaque black crystal near the center (Figure 2a), black opaque octahedral crystals of chromite surrounded by a tension halo (Figure 2b). Partially healed secondary fractures with iridescence could be seen in most of Vietnamese peridot.

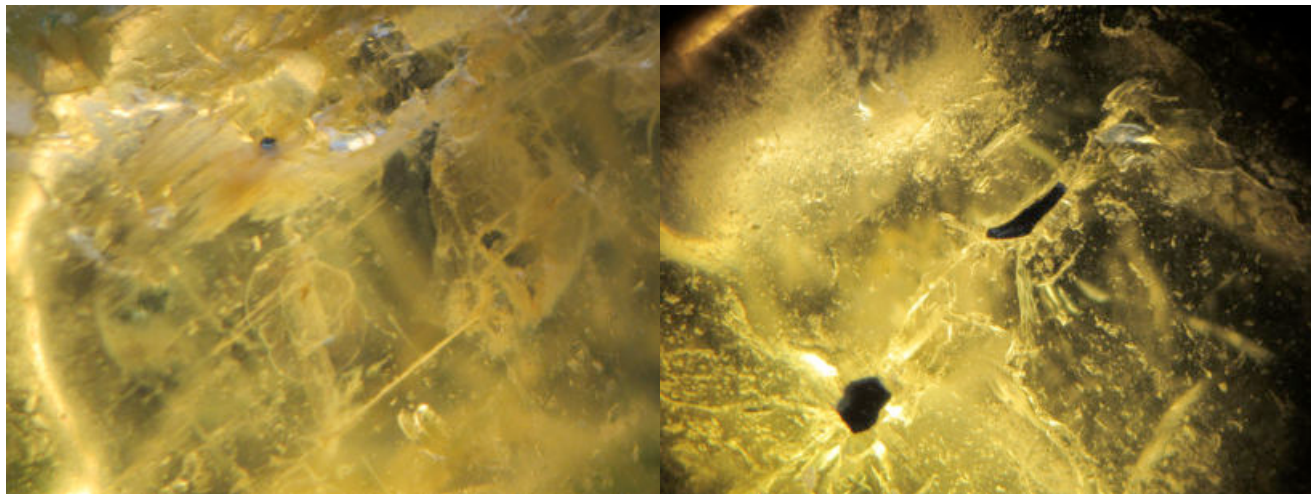


Figure 2. Some internal characteristics of Vietnamese peridot: (a). Healing planes; (b). Chromite crystal surrounded by a tension halo.

Chemical Analysis

The olivine samples have a very narrow X_{Mg} range with forsterite ranging from 90 to 91.5 mol. % and fayalite from 8.5 to 10 mol.%. Ni is the most important trace element with values between 2750 and 3200 ppm. X_{Mg} and Ni contents are typical values for an average mantle composition (Figure 3b). Trace amounts of Li (1-2ppm), Al (45-80ppm), Ca (240-380ppm), Ti (9-17ppm, and one sample with ~35ppm), Cr (90-120ppm), Mn (900-1100ppm), Co (138-149ppm), and Zn (48-63ppm) were detected by LA-ICPMS. Using the Al in olivine and Cr in olivine single grain thermometer from De Hoog et al. (2010), temperatures between 910 and 1000°C can be calculated, assuming a pressure of 2.0 GPa, which corresponds to a depth of around 60 km and is within the stability field of a spinel-lherzolite. The Cr in Ol ther-

momometer gives consistently a 20°C higher temperature compared to the Al in Ol values (Figure 3a). Mn concentrations are high with values around 1000 ppm, which is typical for olivine which was derived from a spinel-lherzolite source.

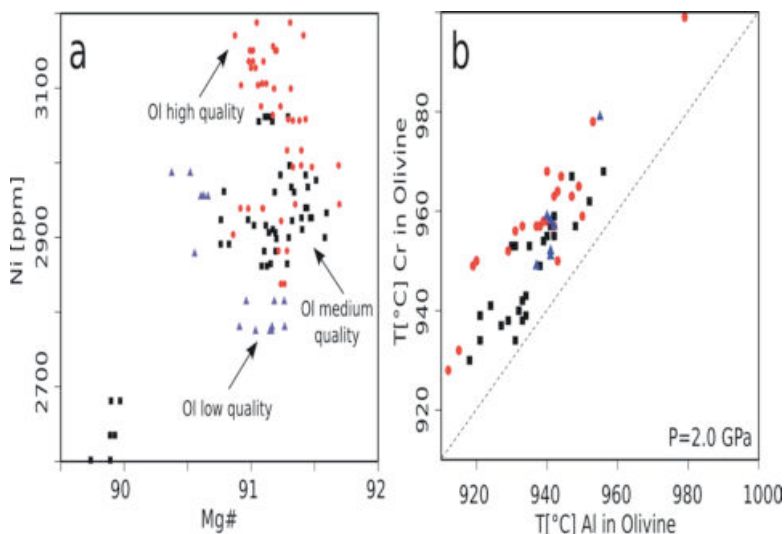


Figure 3. (a) Mg# against Ni [ppm] plot. Mg# is slightly higher than for primitive mantle (=89.5), Ni content in olivine is typical for the mantle (2900 ± 300 ppm). (b) Al in olivine and Cr in olivine calculated for 2.0 Gpa. Calculated temperatures are 910°C to 1000°C. Mg# = magnesium number = $100 \times X_{Mg}$ (mole fraction of Mg over Mg+Fe).

Discussion

No systematic differences were noted in the gemological characteristics or chemical composition of Vietnamese peridot from different sources in the country. The Vietnamese peridots examined show the gemmological properties similar to and within the range noted for peridot from any other source found in xenoliths within basalt flows.

Acknowledgements

This research is funded by Vietnam National Foundation for Science and Technology Development (NAFOSTED) under grant number 105.01-2012.01. The Austrian Academy of Sciences is thanked for financial support for chemical analysis.

References

- De Hoog, J.C.M, Gall, L., Cornell, D.H. 2010. Trace-element geochemistry of mantle olivine and application to mantle petrogenesis and geothermobarometry. *Chemical Geology* 270, 196–215.
- Kammerling R.C. and Koivula J.I., 1995. A preliminary investigation of peridot from Vietnam. *J. Gemmology*, 24, 5, pp. 355-361.
- Kane, R.E., McClure, S.F., Kammerling R.C., Khoa, N.D., Mora, C., Repetto, S., Khai, N.D., and Koivula, J., 1991. Rubies and fancy sapphires from Vietnam. *Gems & Gemology*, 27, 136-155.
- Keller, C., Wang, F., 1986. A survey of the gemstone resources of China. *Gems & Gemology*, 22 (1), 3-13.
- Koivula J.I., Fryer C.W., 1986. The gemological characteristics of Chinese peridot. *Gems & Gemology*, Vol. 22 (1), 38-40.
- Le Thi-Thu Huong, Tobias Häger, Wolfgang Hofmeister, Christoph Hauzenberger, Dietmar Schwarz, Pham Van Long, Ursula Wehmeister, Nguyen Ngoc Khoi, and Nguy Tuyet Nhung, 2012. Gemstones from Vietnam: An Update. *Gems & Gemology*, 48 (3), 158–176.
- Long P.V., Giuliani G., Garnier V., Ohnenstetter D., 2004. Gemstones in Vietnam - A review. *Australian Gemmologist*, 22 (4), 162–168.
- Quoc N.K., Hieu H.H., Luong P.T., and Trung N.D., 1995. Gemstones potential of Vietnam. *Proceedings of the National Conference on Geology of Vietnam*, Hanoi, October 4-10, pp. 143-152.
- Toan T.X. and Ty N.H., 1995. Geology and gemstones resources in South Vietnam. *Proceedings of the National Conference on Geology of Vietnam*, Hanoi, October 4-10, pp. 153-160.
- Webster R., 1992. *Gems, Their sources, Description and Identification*, Butterworth, London.

Differentiation of African and Asian elephant dentine by FT-Raman spectroscopy and chemometric methods

U. Wehrmeister,^a* T.M. Gluhaka, H. Götz and D.E. Jacobc

^a Department of Geosciences and Earth System Science Research Centre, Johannes Gutenberg-Universität, D-55128 Mainz, Germany

^b Institute of Applied Structure- and Microanalysis, Department of Medicine, Johannes Gutenberg-Universität, D-55128 Mainz, Germany

^c Department of Earth and Planetary Sciences, Macquarie University, North Ryde, NSW 2109 Sydney, Australia

* Correspondence to: wehrmeis@uni-mainz.de

The term ivory summarizes teeth and tusks of different animals, which are of any commercial interest and large enough to be processed (Espinoza and Mann, 1991). Traditionally, the tusks (second upper incisors) of elephants and mammoths are referred to as the only "true" ivory. It is relatively soft and strongly favoured by artists for its carvability. The desire for elephant ivory has been one of the major factors in the reduction of the world's elephant population. The family of elephants (Elephantidae) within the order Proboscidea contains two genera: *Loxodonta* – the African and *Elephas* – the Asiatic elephant, including three different species. Ivory trade is a politically highly sensitive matter and a considerable proportion of the trade is illegal resulting in ivory to be found in different markets around Asia and Africa, but also in the US and Europe. Because of illegal ivory trade elephant populations declined in massive numbers in the 1970s and 1980s before the international trade was banned by CITES in 1989, when also the African elephant was uplisted from Appendix II ("managed commercial trade") to Appendix I ("no commercial trade") joining the Asian elephant already listed there. In 1997 Botswana, Namibia, Zimbabwe and later South Africa (in 2000) received limited trade rights for controlled sales of ivory stockpiles and their elephant populations were "downlisted". Many scientists oppose these stockpiles sales, because they suspect further increase of poaching (Wasser et al., 2010) which seems to be supported by the latest news in the media.

From the viewpoint of forensic science a non-destructive determination of the various ivories is very important in order to detect illegal imported ivory samples. Visually, ivories can be differentiated by observing the Schreger lines (Espinoza and Mann, 1991) which are natural growth features characteristic for elephant ivory. However, most samples are carved, and for these samples this method is often not applicable. Various Raman spectroscopic investigations provide rapid and non-destructive methods that do not require sample preparation. However, the organic materials intrinsic to ivory often cause fluorescence which dominates the characteristic Raman signals. Reducing fluorescence is therefore of great importance for successful Raman analysis of ivory. The aim of the present study is to further improve non-destructive analysis of ivories by use of FT-Raman spectroscopy and chemometric methods.

Materials and Experimental Methods

Analyses were carried out on 22 ivory samples of *Loxodonta africana* from different African localities, one sample of *Loxodonta cyclotis* from Congo and 16 samples of *Elephas maximus* from different provenances in Asia. FT-Raman spectra were collected with a NXR FT-Raman Module for FT-IR spectrometers (Nicolet 5700, Thermo Scientific) at the Medical Faculty, Johannes Gutenberg-University, Mainz. A near-infrared Nd : YAG laser operating at 1064 nm, a liquid nitrogen-cooled germanium detector (NXR Genie, Thermo Scientific) with a near-constant noise level over a very wide frequency range and a CaF₂ beam splitter were used. Spectra were recorded with a laser power of 0.5 - 1.0 W in order to avoid damage to the material. In order to improve S/N ratio 256 spectra were collected at a resolution of 4 cm⁻¹ with Happ-Genzel apodization from (250-3700) cm⁻¹. For each sample 3 to 5 FT-Raman spectra were acquired at different locations. A MicroStage FT-Raman Microscope focuses the Laser Beam to a spot size of 50µm. To obtain the best comparability, all spectra were normalized to the highest Raman peak at 960 cm⁻¹. For each sample group, master

spectra were calculated from all data points of Raman spectra. In order to collate the results we followed the essential studies of Edwards et al. (2006) and Brody et al. (2001) with only minor changes in dividing the spectra into different wavenumber areas (labelled with letters),

Vibrational assignment of the FT Raman spectra of elephant ivory

Master spectra of five different sample groups are discussed according to both the different wavenumber regions and the mineral and organic components. A general view of an ivory FT-Raman spectrum is given in Figure 1 and shows the main vibrational bands according to the organic and mineral phases.

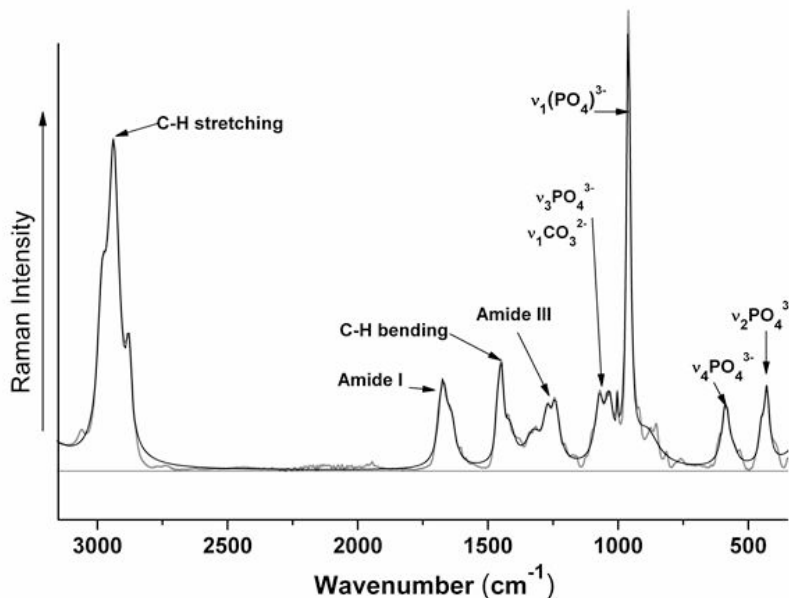


Figure 1: Vibrational bands according to the organic and mineral phases of elephant ivory. The letters A-K below the baseline define the wavenumber areas, used especially for chemometric methods.

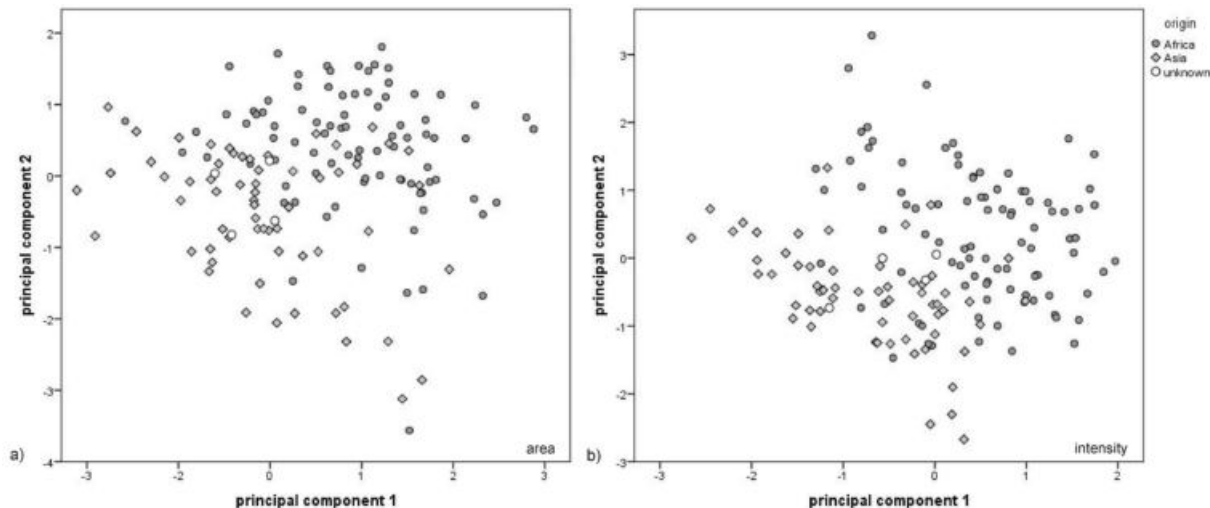
Main diagnostic differences between African and Asian ivory are reported at 1721 cm^{-1} and 1504 cm^{-1} (areas B, C) for African, as well as at 720 cm^{-1} and 453 cm^{-1} (areas J, K) for Asian ivory (Edwards et al., 1997; Carter and Edwards, 2001). However, we show here, based on our much larger data base, that differences of Raman band positions of inorganic and organic modes are not diagnostic nor statistically significant for both Asian and African ivory. The areas under the bands within the different wavenumber areas (A-K), as well as the maximum height of peaks in every one of these are calculated and collated. Comparison of Box- and Whisker-plots of the peak area and their intensity-values shows that, in general, the intensity values show less overlap than the corresponding peak area-values, especially the intensities in B, C, and D characterised by organic modes.

Statistical data evaluation

Hierarchical cluster (CA)-, principal component (PCA)-, and discriminant analyses (DA) are applied to the peak area-data as well as to the intensity-data to test if and, if yes, which one of the approaches achieves an adequate separation into African and Asian ivory. Furthermore, four samples of identical origin were treated as being of "unknown provenance" to test the statistical models. Outliers and extreme values are deleted from the statistical evaluation. Normal distribution was checked by the Kolmogorov-Smirnov-test.

The CA (average linkage, city block distance) shows that clustering based on the intensity-values affiliates 86.2% of all samples correctly to their respective group; the application of the area-values resulted in 81.9% correct grouping. However, both approaches came to concordant results for the test-group of unassigned origin: The CA of the intensity- as well as the area-values resulted in an affiliation to the Asian ivory group.

Figure 2 shows the principal component scores for the PCAs. Neither the PCA of the area-, nor of the intensity-values results in a clear separation of African from Asian samples. Furthermore, including our test samples of “unknown provenance” into the PCAs shows that, although they plot in a field dominated by the Asian ivory samples, it is not possible to affiliate them unequivocally to either Africa or Asia.



The Discriminant Analysis (stepwise method) showed that, when based on the intensity-values, higher percentages of correct classifications were achieved in cross validation than based on the area-values (88.2% in comparison to 84.6%). Anyway, DA based on the intensity-values failed to affiliate the “unknown provenance” test samples correctly, whereas DA based on the area-values assigned them correctly to the Asian ivory-group, which is in accordance with the results from the CA. As results of DA have to be interpreted with caution, we recommend to calculate a CA and PCA as first steps, then to study the general data structure, in order to be able to judge the classification by DA with the results of CA and PCA in the background.

The statistical evaluation shows that preference can be given neither to area- nor to intensity-values in deciding on the provenance of elephant ivory. We recommend always including both values into the statistical evaluation.

References

- R. H. Brody, H. G. M. Edwards, A. M. Pollard, 2001. Chemometrics Methods Applied to the Differentiation of FT-Raman Spectra of Ivories. *Anal. Chim. Acta*, 427, 223-232.
- H. G. M. Edwards, N. F. Nik Hassan and N. Arya, 2006. Evaluation of Raman spectroscopy and application of chemometric methods for the differentiation of contemporary ivory specimens I: elephant and mammalian species. *Journal of Raman Spectroscopy*, 37 (1-3), 353-360
- E.O. Espinoza and M.J. Mann in cooperation with the CITES Secretariat, WWF and Traffic, 1992. Identification Guide for Ivory and Ivory Substitutes. WWF Publications, Baltimore.
- S. Wasser, J. Poole, P. Lee, K. Lindsay, A. Dobson, J. Hart, I. Douglas-Hamilton, G. Wittemyer, P. Granli, B. Morgan, J. Gunn, S. Alberts, R. Beyers, P. Chiyo, H. Croze, R. Estes, K. Gobush, P. Joram, A. Kikoti, J. Kingdon, L. King, D. Macdonald, C. Moss, B. Mutayoba, S. Njumbi, P. Omondi, K. Nowak, 2010. Elephants, Ivory, and Trade. *Science* 327, 1331-1332.



www.igc-gemmology.org